

Ministry of Education and Science of Russian Federation
Pacific National University

**NUCLEAR THEORY
IN THE SUPERCOMPUTING ERA
(NTSE-2012)**

**International Workshop
PROCEEDINGS**

Khabarovsk, June 18–22, 2012

Khabarovsk
Pacific National University
2013

УДК 539.14
ББК 38я43
N 338

Editors A. M. Shirokov and A. I. Mazur

N 338 **Nuclear** Theory in the Supercomputing Era (NTSE-2012): International Workshop. Proceedings. — Khabarovsk: Pacific National University, 2013. — 195 p.
ISBN 978-5-7389-1266-5

The primary motivation for the first International Workshop “Nuclear Theory in the Supercomputing Era (NTSE-2012)” hosted by the Pacific National University, Khabarovsk, Russia (June 18-22, 2012) was the rapid growth of supercomputers and the impact they, along with theoretical and algorithmic developments, are having on nuclear theory. These proceedings include invited talks and contributed papers presented at the Workshop which are also available online at <http://www.ntse-2012.khb.ru/>.

УДК 539.14
ББК 38я43

ISBN 978-5-7389-1266-5

©Pacific National University, 2013

Preface:

The first International Workshop on “Nuclear Theory in the Supercomputing Era (NTSE-2012)” was held at Pacific National University in Khabarovsk, Russia, June 18–22, 2012. The primary motivation for the meeting was the rapid growth of supercomputers and the impact they, along with theoretical and algorithmic developments, are having on nuclear theory. Manuscripts of the invited talks and contributed papers presented at the meeting constitute these proceedings.

It is a great pleasure for me, and I believe I speak on behalf of my fellow attendees, to thank our gracious Russian sponsors and hosts, the Pacific National University and its President, Professor Sergey Nikolaevich Ivanchenko. The consensus view among all participants is that the sponsorship and hosting of the meeting was indeed first class in all respects. We offer a special thanks to Prof. Alexander Mazur for his thorough planning and guidance in all aspects of the meeting.

It is important to note that the workshop was organized according to the Pacific National University Strategic Development Program for 2012–2016 and this Program provided financial support for which we are grateful.

The sponsors and hosts assembled for this meeting many of the world’s top experts in this forefront area of physics with strong links to applied mathematics and computational science. During the meeting we learned the latest developments and explored research opportunities for the coming decade in areas of basic science important to the security of fissionable materials, to advanced nuclear reactor designs, to fusion energy research as well as to astrophysical phenomena such as supernovae and neutron stars.

It is a great pleasure for me to mention that last year Pacific National University and Iowa State University signed an agreement launching an ambitious framework for growing collaborations, exchanging students and faculty, and jointly sponsoring research programs. During this meeting we discussed enhancing this framework with further program development.

All participants anticipated and were rewarded with an exciting meeting and productive discussions about recent developments in our field. We also discussed the potential for further developing our international collaborations with the region of East Asia represented by Pacific National University. It was especially valuable to have participants from other countries in the region. Finally, we also learned a great deal about the far-reaching vision for Pacific National University and its ambitious plans for the future.

I sensed that while this was the first time for the international attendees to visit Pacific National University, we all left with the anticipation to return again for another very productive scientific meeting in the future.

James P. Vary,
Iowa State University,
Vice Chair of the NTSE-2012 Organizing Committee.
June 2012

International Workshop

**NUCLEAR THEORY
IN THE SUPERCOMPUTING ERA
(NTSE-2012)**

**INVITED TALKS
AND CONTRIBUTED PAPERS**

Ab Initio Nuclear Structure – Recent Developments

James P. Vary

Department of Physics and Astronomy, Iowa State University, Ames, IA 50011, USA

Abstract

The goals of *ab initio* theory of nuclear structure and nuclear reactions are to preserve the predictive power of strong interactions based on QCD, to test fundamental symmetries with the nucleus as laboratory and to develop new understandings of the vast array of nuclear phenomena. Recent progress includes the derivation, within chiral perturbation theory (ChPT), of the leading terms of the nucleon-nucleon (NN), three-nucleon ($3N$) and four-nucleon ($4N$) potentials. Additional substantial progress includes using these ChPT interactions to solve nuclear structure and reactions in light nuclei and some heavier nuclei around closed shells and closed subshells. Advances in theoretical frameworks (renormalization and many-body methods) as well as in computational resources (new algorithms and leadership-class supercomputers) signal a new generation of theory simulations that will yield valuable insights into origins of nuclear shell structure, collective phenomena and complex reaction dynamics. I outline some recent achievements that, with additional research, will strengthen the links between nuclear theory and nuclear experiment, between nuclear physics and astrophysics, and between nuclear physics and its practical applications.

Keywords: *Nuclear theory; microscopic many-body theory; chiral interactions; light nuclei*

1 Introduction

A long-standing goal of nuclear theory is to predict nuclear structure and nuclear reactions from knowledge of the underlying strong interactions based on the accepted theory of the strong interactions, Quantum Chromodynamics (QCD). With this foundation, we may address many fundamental questions of nuclear physics such as:

1. What controls nuclear saturation?
2. How do the nuclear shell and collective models emerge from the underlying theory?
3. What are the properties of nuclei with extreme neutron/proton ratios?
4. Can we predict useful cross sections that cannot be measured?
5. Can nuclei provide precision tests of the fundamental laws of nature?
6. Under what conditions do we need explicit quark and gluon degrees of freedom to describe nuclear properties?

Traditionally, we pursued this goal with meson-theoretical nucleon-nucleon (NN) interactions that were tuned to provide high-quality descriptions of the NN scattering phase shifts and the deuteron bound state properties. We also employed three-nucleon forces ($3NF$ s) that were derived from meson theory and then tuned to the properties of $A = 3$ nuclei and/or other nuclear properties. The Argonne V18 [1] NN interaction

plus the Tucson–Melbourne [2, 3] 3NF or Urbana IX [4] 3NF represent popular choices of this genre and we continue to use these interactions.

More recently, concerted efforts have led to the development of realistic NN and 3NF based upon QCD. Chiral perturbation theory (ChPT) within effective field theory (EFT) [5] provides us with a promising bridge between QCD and the hadronic systems [6]. In this approach one works consistently with systems of increasing nucleon number [7, 8, 9] and makes use of the explicit and spontaneous breaking of chiral symmetry to systematically expand the strong interaction in terms of a dimensionless constant, the ratio of a generic small momentum divided by the chiral symmetry breaking scale (about 1 GeV/ c). The resulting NN and 3NFs [10, 11, 12] provide a high-quality fit to the NN data and the $A = 3$ ground state properties. Continuing world-wide efforts are expected to provide next-generation interactions within the coming year or two.

To solve for the properties of finite nuclei with these realistic microscopic Hamiltonians, one faces immense theoretical and computational challenges. Recently, *ab initio* approaches have been developed that preserve all the underlying symmetries and they converge to the exact result. If we limit our discussions to nuclei heavier than $A = 6$, there are two main approaches that have proven successful with these realistic interactions. The first approach, called No-core Shell Model (NCSM) [13, 14] or No-core Full Configuration (NCFC) [15], diagonalizes the Hamiltonian in a suitable basis. The second approach, called Coupled Cluster (CC) [16, 17] solves coupled equations that emerge from a representation of the nuclear eigenstate as a correlation operator acting on a representative Slater determinant (SD). The primary advantages of these *ab initio* no core methods are their flexibility for choosing (1) the Hamiltonian; (2) the method of renormalization/regularization; and (3) the single-particle basis. These advantages also support the adoption of these same techniques in light-front quantum field theory [18].

Recent developments in other *ab initio* approaches show additional promise for addressing fundamental questions posed above. These include the Green’s Function Monte Carlo (GFMC) approach [19, 20, 21, 22] using meson exchange interactions and a lattice-simulation approach with nucleons using effective field theory [23].

Additional notable advances attempt to retain advantages of a configuration interaction (CI) basis while overcoming the explosion in the basis space that occurs with the original *ab initio* NCSM when one addresses collective modes such as clusters or proceeds to heavier systems. These advances include the “Importance-truncated” NCSM [24], the “Symmetry-adapted” NCSM [25], the “Monte-Carlo” NCSM [26], and the NCSM with a core [27] (based on ideas presented in Ref. [28]). For a more complete recent review of the *ab initio* NCSM and its connections with some of these other methods one may consult Ref. [29].

2 *Ab initio* No-core Shell Model (NCSM) and Full Configuration (NCFC) methods

The starting point of *ab initio* nuclear theory is the non-relativistic many-body Hamiltonian:

$$H_A = T_{\text{rel}} + \mathcal{V} = \frac{1}{A} \sum_{i < j} \frac{(\vec{p}_i - \vec{p}_j)^2}{2m} + \sum_{i < j} V_{ij} + \sum_{i < j < k} V_{ijk} + \dots, \quad (1)$$

where m is the nucleon mass, V_{ij} is the NN interaction including the Coulomb interaction between protons, V_{ijk} is the three-nucleon interaction, and we allow for higher-body interactions as well. Note that the Hamiltonian does not involve the nuclear center of mass (CM) motion.

We obtain solutions in a basis of Slater determinants (SDs) constructed with single-particle states, usually from the harmonic oscillator (HO) but not exclusively. To force the many-body eigenstates to factorize into a CM component times an intrinsic component, we add the “Lawson projection term” [30] $\beta(H_{\text{CM}} - \frac{3}{2}\hbar\Omega)$ to the Hamiltonian (1) to shift the spurious CM excitations. The center-of-mass Hamiltonian can be written as $H_{\text{CM}} = T_{\text{CM}} + U_{\text{CM}}$, where $U_{\text{CM}} = \frac{1}{2}Am\Omega^2\bar{R}^2$, $\bar{R} = \frac{1}{A}\sum_{i=1}^A\vec{r}_i$, and Ω the HO frequency. With β chosen large and positive (a typical value is 10) the eigenenergies of physical states are the low-lying solutions and are independent of the parameter β . When a basis other than the HO is used or a many-body truncation other than the preferred N_{max} truncation is used within the HO basis, this factorization may not be precise to within numerical precision. In that event, additional investigation is needed to measure the extent of the factorization in each eigenstate.

Realistic nuclear NN interactions, such as those mentioned in the Introduction, fit the NN phase shift data and deuteron properties to high precision. This implies that these NN interactions have components that strongly couple low nucleon momentum regions (regions typical of the nuclear Fermi momentum $\approx 1 \text{ fm}^{-1}$ with higher momentum regions $\approx 3 \text{ fm}^{-1}$ and above. This strong coupling, which is a likely feature of $3NF$ s as well, requires us to “soften” these interactions using renormalization techniques that preserve the exact many-body solutions in suitable limits that are achievable with current computational methods and resources. An outline of selected renormalization methods is presented in Section 5.

Refs. [13, 14, 31, 32, 33, 34, 35] and [15, 36, 37, 38] provide examples of the recent advances in the *ab initio* NCSM and NCFC, respectively. The NCSM adopts a renormalization method that provides an effective interaction dependent on the chosen many-body basis space cutoff (N_{max} for example discussed below). The NCFC either retains the un-renormalized interaction or adopts a basis-space-independent renormalization so that the exact results are obtained either by using a sufficiently large basis space or by simple extrapolation to the infinite matrix limit. For a more complete discussion of nomenclature and relationships to other methods, see Section 3 below.

Recent results for the NCSM employ realistic NN and $3NF$ s derived from ChPT to solve nuclei with atomic numbers 10–13 [31]. Recent results for the NCFC feature a realistic NN interaction that is sufficiently soft that binding energies and spectra from a sequence of finite matrix solutions may be extrapolated to the infinite matrix limit as in the case of results for the Li isotopes [38]. Experimental binding energies, low-lying spectra, magnetic moments and Gamow–Teller transitions are well-reproduced in both the NCSM and NCFC approaches. Convergence of long range observables such as the rms charge radius and the electric quadrupole moment are more challenging. A sample of recent results is presented in Section 6 below.

In a NCSM or NCFC application, one typically adopts a 3D HO for all the particles in the nucleus (with harmonic oscillator energy $\hbar\Omega$) as mentioned above, treats the neutrons and protons independently, and generates a many-fermion basis space that includes the lowest oscillator configurations as well as all those generated by allowing up to N_{max} oscillator quanta of excitations. Alternatives to the HO basis space such as a Woods–Saxon basis [39] and a Coulomb–Sturmian basis [40] have recently been investigated with promising results. The single-particle states specify the orbital angular momentum projection and the basis is referred to as the m -scheme basis. For the NCSM one also selects a renormalization scheme linked to the basis truncation while in the NCFC the renormalization is either absent or of a type that retains an infinite matrix problem.

It is important to note three recent analytical and technical advances. First, non-perturbative renormalization has been developed to accompany these basis-space methods and their success is impressive. Several schemes have emerged and current research focuses on understanding the scheme-dependence of convergence rates (differ-

ent observables converge at different rates) [36]. For an introduction to two of these methods see Section 5. Second, impressive new extrapolation tools have emerged [41, 42] with indications they are the forerunners of even more powerful tools based on improved theory of the infra-red and ultra-violet properties of the interactions and basis spaces. Third, large scale calculations are performed on leadership-class parallel computers to solve for the low-lying eigenstates and eigenvectors and to evaluate a suite of experimental observables. Low-lying solutions for matrices of basis-space dimension 10-billion on 215,000 cores with a 5-hour run is the current record. However, one expects these limits to continue growing as the techniques are evolving rapidly [33] and the computers are growing dramatically. Matrices with dimensions in the several tens of billions will soon be solvable with strong interaction Hamiltonians. It remains to be seen if the higher degree of parallelism offered by the newest technological advances, Graphics Processor Units (GPUs) adapted for numerical simulations, can be efficiently exploited by the many-body methods described here.

Additional advances in physics and algorithm developments are well underway and offer additional promise. One of the current ambitious undertakings seeks to develop a symmetry-adapted no core shell model approach [25]. In this approach, called the Symplectic No-core Shell Model (Sp-NCSM), one augments the conventional spherical harmonic oscillator basis with the physically relevant symplectic $Sp(3,R)$ symmetry-adapted configurations of the symplectic shell model that describe naturally the monopole–quadrupole vibrational and rotational modes, and also partially incorporate α -cluster correlations. The potential savings in basis space dimensions are enormous but there is a price — increased complexity of the Hamiltonian matrix elements. Current projections indicate a net large gain in the scope of physics problems that may be addressed with the Sp-NCSM.

Another ambitious program extends the Monte Carlo Shell Model (MCSM) to the no-core regime and greatly increases the number of active shells [26]. Since the MCSM has superior scaling properties with the number of nucleons, once validated, we envision this will be a very fruitful avenue for addressing heavier nuclei — possibly the entire periodic table. However, there are daunting challenges to overcome such as developing a load-balanced and scalable code.

3 Relationships among many-body methods

There are several quantum many-body methods that are closely related to the methods we have developed and applied. The associated nomenclatures require some discussion as well.

The term Configuration Interaction (CI) is the broadest term that seems widely recognized across physics disciplines. In general any method that uses a basis space developed from Slater Determinants (SDs) of single-particle wave functions (configurations) is referred to as a CI method. It covers all the methods discussed here except the Coupled Cluster, Greens Function Monte Carlo and lattice simulation methods mentioned above.

The term Full Configuration Interaction (FCI) was introduced by the quantum chemists and used widely by them. FCI signifies the use of all many-body configurations consistent with a chosen set of symmetries and a defined finite set of single-particle states. Most often there is an inert core of filled single-particle states in these calculations. An FCI calculation is considered the “gold standard” in quantum chemistry to which, for example, Coupled Cluster and Density Functional Theory (DFT) approaches are often benchmarked.

The use of no-core model spaces for solving light nuclei in Hamiltonian matrix formulations has a long history. Some of that history is summarized, including the distinction between the FCI truncation and the N_{max} truncation in Ref. [43]. For a more recent summary, see Ref. [29].

The term “No-core Shell Model” (NCSM) first appeared in the title of a paper in Ref. [44] where the renormalization scheme was the Brueckner G -matrix approach adapted to the no-core basis. Limitations to this approach included the presence of spurious CM motion in the effective NN interaction, the G -matrix, and in the occurrence of a free parameter, the “starting energy”. While the first limitation remains to this day, the starting-energy dependence of this approach could be removed by including sufficiently large sets of higher-order processes formed with the G -matrix as building block, including effective 3NFs and beyond.

To accurately preserve all the symmetries of the underlying strong interactions and include sufficient renormalization to achieve accurate results, we developed the “*Ab Initio* No-core Shell Model” [13, 14]. Indeed, the terminology “*Ab Initio* No-core Shell Model” first appeared in a title in Ref. [14] while the term “*ab initio* no-core nuclear shell model” appears in the first sentence of the abstract of Ref. [13]. At the time of its introduction, we adopted the “Okubo–Lee–Suzuki” (OLS) method [45, 46] of renormalizing the Hamiltonian (see Section 5 below for an introduction) since it enabled us to preserve the factorization of the CM and internal motion which is important especially in light nuclei.

It is important to note that both the Brueckner G -matrix and the OLS approaches evaluate effective Hamiltonians specific to the many-body basis space for that application. That is, they are dependent on the many-body basis truncation and may also have dependence on the atomic number. More importantly, there is no variational upper bound property of the resulting eigensolutions and this limits the ability to extrapolate to the infinite matrix limit.

As a guide to our recent papers where a more extensive presentation of the methods and results may be found, it is useful to note that we have used the following terminology:

1. No-core Shell Model (NCSM) — follows the original NCSM papers where the interaction is derived for the chosen many-body model space. This could be any renormalization scheme such as the Brueckner approach or the OLS approach that has a dependence on the model space cutoff. It is “*ab initio* NCSM” if it respects all the symmetries of the original nuclear Hamiltonian so this includes OLS renormalization but not Brueckner G -matrix applications.
2. No-core Full Configuration (NCFC), first introduced in the title of Ref. [15], — signifies we use interactions independent of the basis space and achieve converged eigenenergies within numerical error estimates or we extrapolate to the infinite matrix limit with error estimates. The interactions may be either the “bare” interactions of Eq. (1) or interactions softened via methods that are independent of the many-body basis space. Thus, the NCFC results are independent of all basis parameters (N_{max} , N_{shell} (number of HO shells), $\hbar\Omega$, Woods–Saxon parameters, Coulomb–Sturmian parameters, etc). This newer terminology emerged in response to the criticism that the NCSM was not so much of a “Shell Model” as a CI approach which did not assume a shell model structure for the solutions. In other words, the approach was general and should, if successful, be able to derive the “Shell Model” from first principles. One colleague even refers to the NCSM as the “no-core no-shell no-model” approach to underscore that criticism. Additionally, quantum chemists have adopted the terminology of CI and FCI which are widely understood in physics so we should include the term “Configuration” as we do with NCFC.
3. No-core Configuration Interaction (NCCI), introduced in the text of Ref. [40], — for a more general case where the variational upper bound is obtained for an arbitrary finite basis (i. e. includes FCI, N_{max} truncation, N_{shell} truncation, Coulomb–Sturmian, etc.) — i. e. without the extrapolation and error estimation of the NCFC.

With this newer terminology, results from basis-space independent interactions, therefore allowing for some forms of renormalization, with extrapolation and error estimates would be called NCFC calculations. Without extrapolation and error estimates, they would be called NCCI calculations according to our current usage.

This usage has evolved since we earlier used NCSM more liberally (prior to introducing “NCFC” in early 2009) to include both truncated calculations preserving variational limits as well as extrapolations with error estimates in Ref. [36].

Due to the flexibility of renormalization procedures, choice of truncations, choice of basis, etc., it may be that the above nomenclature does not cover all cases uniquely. That is, it is easy to see there are possible overlaps in the use of these terminologies.

4 Realistic Hamiltonians

We began our no-core investigations in the 1980s and 1990s with the best available interactions that were meson-theoretical nucleon-nucleon interactions, tuned to provide high-quality descriptions of the NN scattering phase shifts and the deuteron bound state properties. For example, we introduced and employed no-core spectral distribution methods [47, 48, 49] with realistic NN interactions in advance of the current era where direct diagonalization in large basis spaces became feasible. Those early results produced favorable comparisons with Coupled Cluster results [50] for total binding energies.

As mentioned earlier, we also employed 3NFs that were derived from meson theory and then tuned to the properties of $A = 3$ nuclei and/or other nuclear properties such as the binding energy of nuclear matter. The Argonne V18 [1] NN interaction plus the Tucson–Melbourne [2, 3] 3NF or Urbana IX [4] 3NF represent popular choices of this class of interactions. Many current investigations continue to use these interactions. When these interactions are employed, it is possible to include a consistent treatment of meson-exchange currents in the development of effective operators for other observables such as electromagnetic moments and transition rates. There is an increasing trend to using these theoretically consistent operators.

More recently, concerted efforts have led to the development of realistic NN and 3NF based upon QCD using chiral perturbation theory (ChPT) within effective field theory (EFT) [5]. This EFT approach provides us with a promising bridge between QCD and the hadronic systems [6]. In this approach one works consistently with systems of increasing nucleon number [7, 8, 9] and makes use of the explicit and spontaneous breaking of chiral symmetry to systematically expand the strong interaction in terms of a dimensionless constant, the ratio of a small momentum (characteristic of the low-energy application such as nuclear structure) divided by the chiral symmetry breaking scale of QCD (taken to be about 1 GeV/ c). The resulting NN and 3NFs [10, 11, 12] have the appearance of a pion-exchange theory (no higher mass mesons appear explicitly nor do baryon resonances) and they provide a high-quality fit to the NN data and the $A = 3$ ground state properties. The ChPT is characterized by the appearance of low-energy constants (LECs) which are, in principle, calculable with non-perturbative methods from QCD itself. However, since they are not calculable with current computer resources, these constants are fit to NN data and three-nucleon systems (for the new constants that appear in the 3NFs). One hallmark of this approach is the natural hierarchy that places NN interactions at lower order than 3NFs. In addition, a cross check that ChPT is producing a convergent series, i. e. one that is “under control”, is that these LECs all turn out to be of order unity. The appearance of an LEC of order 10, for example, would signal the potential need to rearrange the series. Such a rearrangement is under development with a “deltafull” version of ChPT where the delta-resonance is included explicitly as intermediate state excitations with the ChPT graphs.

At present we employ NN interactions complete through “next-to-next-to-next-to

leading order” (N3LO). However, the 3NFs we use are only available in the useful partial-wave decomposed form through N2LO. Fortunately, world-wide efforts are expected to provide ChPT interactions for both NN and 3NFs complete through N3LO within the coming year or two. At about the same time, we expect the deltafull versions of ChPT to become available.

We also adopt the NN interaction JISP16, a realistic NN interaction initially developed from NN data using inverse scattering techniques [32, 51, 52]. It is then adjusted with phase-shift equivalent unitary transformations to describe light nuclei without explicit 3NFs. One major advantage of JISP16 is that it is considerably softer (reduced high-momentum components) relative to the meson-exchange or ChPT NN interactions. Since JISP16 incorporates some of the 3NF effects of the other interactions, and is sufficiently soft, we can achieve NCFC results in light nuclei and the results are in remarkably good agreement with experiment [15, 37, 38, 41, 53].

With all these interaction developments, we can expect an era of vigorous scientific activity testing these improved interactions in nuclear structure and nuclear reactions. With the emerging predictive power, we expect to be able to reliably predict quantities that cannot be measured directly in the laboratory but have practical significance such as in the design of advanced nuclear reactors.

5 Renormalization and regularization

Given that the NN interaction and 3NFs couple strongly the low-momentum regions of phase space with the high-momentum regions, we require methods to soften these interactions (reduce those couplings) while maintaining the full predictive power of the microscopic theory. This leads to the introduction of renormalization and regularization methods. When properly used, these methods allow the exact results (results from the original input interactions) to be obtained in a systematic and controllable approach. Different methods have been introduced and each has its advantages and disadvantages. Here, I will summarize two of those methods that we have been using extensively. The first is the Okubo–Lee–Suzuki (OLS) method [45, 46] and the second is the Similarity Renormalization Group (SRG) method [54, 55, 56, 57, 58, 59]. There is considerable freedom in each of these renormalization methods and there is ongoing research that investigates the potential utility of these freedoms. For the subsections of this section, I will follow our descriptions presented in Ref. [29] that should be consulted for additional details and key references.

The topic of regulators is one that requires its own discussion. For the present paper, I will simply mention that regulators appear at all levels of the development of effective Hamiltonians. These occur in the choices of form factors regulating vertices in the underlying interactions all the way up to the choice of basis space parameters such as N_{max} and $\hbar\Omega$. Ultimately, the test of a good theory is to obtain converged results that agree with experiment as regulators are removed. These challenges are addressed, at least in part, by the ChPT approach of EFT and by the NCFC method discussed above.

5.1 Okubo–Lee–Suzuki method

For pedagogical purposes, we outline the OLS approach with NN interactions alone and point the reader to the literature [29] for the extensions to include 3NFs. We begin with the simplified purely intrinsic Hamiltonian for the A -nucleon system, i. e. we retain only the first two terms of Eq. (1) to write

$$H_A = T_{\text{rel}} + \mathcal{V} = \frac{1}{A} \sum_{i < j}^A \frac{(\vec{p}_i - \vec{p}_j)^2}{2m} + \sum_{i < j}^A V(\vec{r}_i - \vec{r}_j), \quad (2)$$

where m is the nucleon mass and $V(\vec{r}_i - \vec{r}_j)$, the NN interaction, with both strong and electromagnetic components. Note the absence of a phenomenological single-particle potential. We may use either coordinate-space or momentum-space NN potentials. They may also be non-local interactions.

Next, we add the center-of-mass HO Hamiltonian to the Hamiltonian (2) $H_{\text{CM}} = T_{\text{CM}} + U_{\text{CM}}$, where $U_{\text{CM}} = \frac{1}{2}Am\Omega^2\vec{R}^2$, $\vec{R} = \frac{1}{A}\sum_{i=1}^A\vec{r}_i$. In the full Hilbert space the added H_{CM} term has no influence on the intrinsic properties. However, when we introduce our cluster approximation below, the added H_{CM} term facilitates convergence to exact results with increasing basis size. The modified Hamiltonian, with a pseudo-dependence on the HO frequency Ω , can be cast into the form

$$H_A^\Omega = H_A + H_{\text{CM}} = \sum_{i=1}^A \left[\frac{\vec{p}_i^2}{2m} + \frac{1}{2}m\Omega^2\vec{r}_i^2 \right] + \sum_{i<j=1}^A \left[V_{\text{N}}(\vec{r}_i - \vec{r}_j) - \frac{m\Omega^2}{2A}(\vec{r}_i - \vec{r}_j)^2 \right]. \quad (3)$$

In the spirit of Da Providencia and Shakin [60] the OLS method [45, 46] introduces a unitary transformation, which is able to accommodate the short-range two-body correlations in a nucleus, by choosing an antihermitian operator S , acting only on intrinsic coordinates, such that

$$\mathcal{H} = e^{-S}H_A^\Omega e^S. \quad (4)$$

In our approach, S is determined by the requirements that \mathcal{H} and H_A^Ω have the same symmetries and eigenspectra over the subspace \mathcal{K} of the full Hilbert space. In general, both S and the transformed Hamiltonian are A -body operators. Our simplest, non-trivial approximation to \mathcal{H} is to develop a two-body ($a = 2$) effective Hamiltonian, where the upper bound of the summations “ A ” is replaced by “ a ”, but the coefficients remain unchanged. The next improvement is to develop a three-body effective Hamiltonian, ($a = 3$). This approach consists then of an approximation to a particular level of clustering with $a \leq A$,

$$\mathcal{H} = \mathcal{H}^{(1)} + \mathcal{H}^{(a)} = \sum_{i=1}^A h_i + \frac{\binom{A}{2}}{\binom{a}{2}} \sum_{i_1 < i_2 < \dots < i_a} \tilde{V}_{i_1 i_2 \dots i_a}, \quad (5)$$

with

$$\tilde{V}_{12\dots a} = e^{-S^{(a)}} H_a^\Omega e^{S^{(a)}} - \sum_{i=1}^a h_i, \quad (6)$$

and $S^{(a)}$ is an a -body operator; $H_a^\Omega = h_1 + h_2 + h_3 + \dots + h_a + V_a$, and $V_a = \sum_{i<j}^a V_{ij}$. Note that there is no sum over “ a ” in Eq. (5). Also, we adopt the HO basis states that are eigenstates of the one-body Hamiltonian $\sum_{i=1}^A h_i$.

If the full Hilbert space is divided into a finite model space (“ P -space”) and a complementary infinite space (“ Q -space”), using the projectors P and Q with $P + Q = 1$, it is possible to determine the transformation operator S_a from the decoupling condition

$$Q_a e^{-S^{(a)}} H_a^\Omega e^{S^{(a)}} P_a = 0, \quad (7)$$

and the simultaneous restrictions $P_a S^{(a)} P_a = Q_a S^{(a)} Q_a = 0$. Note that a -nucleon-state projectors (P_a, Q_a) appear in Eq. (7). Their definitions follow from the definitions of the A -nucleon projectors P, Q . The net effect of the OLS renormalization procedure is to develop a finite P -space effective Hamiltonian decoupled from the infinite complementary Q -space as illustrated in Fig. 1.

The unitary transformation and decoupling condition, introduced by Suzuki and Okamoto and referred to as the unitary-model-operator approach (UMOA) [61], has a solution that can be expressed in the following form

$$S^{(a)} = \text{arctanh}(\omega - \omega^\dagger), \quad (8)$$

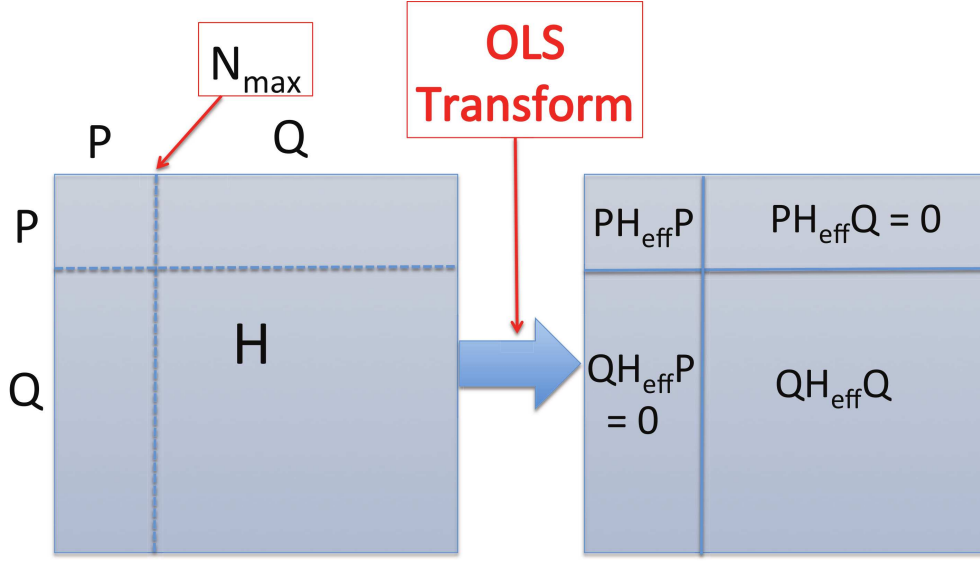


Figure 1: Schematic illustration on how Okubo–Lee–Suzuki (OLS) similarity transformation yields an \bar{H}_{eff} in a finite model space P decoupled from the infinite complementary Q -space.

with the operator ω satisfying $\omega = Q_a \omega P_a$, and solving its own decoupling equation,

$$Q_a e^{-\omega} H_a^\Omega e^{\omega} P_a = 0. \quad (9)$$

Let us also note that $\bar{H}_{\text{a-eff}} = P_a e^{-S^{(a)}} H_a^\Omega e^{S^{(a)}} P_a$ leads to the relation

$$\bar{H}_{\text{a-eff}} = (P_a + \omega^\dagger \omega)^{-1/2} (P_a + P_a \omega^\dagger Q_a) H_a^\Omega (Q_a \omega P_a + P_a) (P_a + \omega^\dagger \omega)^{-1/2}. \quad (10)$$

Given the eigensolutions, $H_a^\Omega |k\rangle = E_k |k\rangle$, then the operator ω can be determined from

$$\langle \alpha_Q | \omega | \alpha_P \rangle = \sum_{k \in \mathcal{K}} \langle \alpha_Q | k \rangle \langle \tilde{k} | \alpha_P \rangle, \quad (11)$$

where we denote by tilde the inverted matrix of $\langle \alpha_P | k \rangle$, i. e., $\sum_{\alpha_P} \langle \tilde{k} | \alpha_P \rangle \langle \alpha_P | k' \rangle = \delta_{k,k'}$ and $\sum_k \langle \alpha'_P | \tilde{k} \rangle \langle k | \alpha_P \rangle = \delta_{\alpha'_P, \alpha_P}$, for $k, k' \in \mathcal{K}$. In the relation (11), $|\alpha_P\rangle$ and $|\alpha_Q\rangle$ are the model-space and the Q -space basis states, respectively, and \mathcal{K} denotes a set of d_P eigenstates, whose properties are reproduced in the model space, with d_P equal to the dimension of the model space.

With the help of the solution for ω (11) we obtain a simple expression for the matrix elements of the Hermitian effective Hamiltonian

$$\begin{aligned} \langle \alpha_P | \bar{H}_{\text{a-eff}} | \alpha'_P \rangle &= \sum_{k \in \mathcal{K}} \sum_{\alpha''_P} \sum_{\alpha'''_P} \langle \alpha_P | (P_a + \omega^\dagger \omega)^{-1/2} | \alpha''_P \rangle \langle \alpha''_P | \tilde{k} \rangle E_k \langle \tilde{k} | \alpha'''_P \rangle \\ &\quad \times \langle \alpha'''_P | (P_a + \omega^\dagger \omega)^{-1/2} | \alpha'_P \rangle. \end{aligned} \quad (12)$$

For computation of the matrix elements of $(P_a + \omega^\dagger \omega)^{-1/2}$, we can use the relation

$$\langle \alpha_P | (P_a + \omega^\dagger \omega) | \alpha''_P \rangle = \sum_{k \in \mathcal{K}} \langle \alpha_P | \tilde{k} \rangle \langle \tilde{k} | \alpha''_P \rangle. \quad (13)$$

We note that in the limit $a \rightarrow A$, we obtain the exact solutions for d_P states of the full problem for any finite basis space, with flexibility for choice of physical states subject to certain conditions [62].

On account of our cluster approximation a dependence of our results on N_m and on Ω arises. For a fixed cluster size, the smaller the basis space, the larger the dependence on Ω . The residual N_m and Ω dependences can be used to infer the uncertainty in our results.

The model space P_2 is defined by the maximal number of allowed HO quanta of the A -nucleon basis states N_m from the condition $2n + l \leq N_m - N_{\text{spsmin}}$, where N_{spsmin} denotes the minimal possible HO quanta of the spectators, i. e., nucleons not affected by the interaction process. For example, ^{10}B , $N_{\text{spsmin}} = 4$ as there are 6 nucleons in the $0p$ -shell in the lowest HO configuration and, e. g., $N_m = N_{\text{spsmin}} + 2 + N_{\text{max}}$, where N_{max} represents the maximum HO quanta of the many-body excitation above the unperturbed ground-state configuration. For ^{10}B , $N_m = 12$ for an $N_{\text{max}} = 6$ or “ $6\hbar\Omega$ ” calculation.

In order to construct the operator ω (11) we need to select the set of eigenvectors \mathcal{K} . We select the lowest states obtained in each two-body channel. It turns out that these states also have the largest overlap with the model space for the range of $\hbar\Omega$ we have investigated and the P -spaces we select. Their number is given by the number of basis states satisfying $2n + l \leq N_m - N_{\text{spsmin}}$.

We input the effective Hamiltonian, now consisting of a relative 2-body operator and the pure H_{CM} term introduced earlier, into an m -scheme Lanczos diagonalization process to obtain the P -space eigenvalues and eigenvectors. At this stage we also add the term H_{CM} again with a large positive coefficient (referred to as β above) to separate the physically interesting states with $0s$ CM motion of the HO from those with excited CM motion according to the Lawson method [30]. We retain only the states with pure $0s$ CM motion when evaluating observables.

All observables that are expressible as functions of relative coordinates, such as the rms radius and radial densities, are then evaluated free of CM motion effects. In addition, all observables that are not spherically symmetric such as electromagnetic multipole operators receive no contribution from the $0s$ CM motion component of state vectors so they are correctly dependent only on the internal motion though they may be evaluated within the full SD basis.

We close our presentation on the theoretical framework with the observation that all observables require the same transformation as implemented on the Hamiltonian. To date, we have found rather small effects on the rms radius operator when we transformed it to a P -space effective rms operator at the $a = 2$ cluster level [13, 14]. On the other hand, substantial renormalization was observed for the kinetic energy operator when using the $a = 2$ transformation to evaluate its expectation value [63].

5.2 Similarity Renormalization Group method

The Similarity Renormalization Group (SRG) method also develops effective two-, three- (and even higher-) body forces (induced many-body interactions) while reducing the strong couplings of the available initial interactions across large regions of momentum space. This will also aid convergence in many-body calculations provided the induced interactions are retained to the level needed. One perceived advantage of SRG is that it retains the effective interactions in the full (infinite) Hilbert space. With a given SRG-evolved effective Hamiltonian, the variational principle allows smooth extrapolations to the ground state energy from above as a function of the many-body truncation. Thus NCFC results are, in principle, obtainable with SRG-evolved effective Hamiltonians. This advantage is absent in the OLS approach.

The SRG is a continuous unitary transformation of the free-space Hamiltonian H (2) ($H \equiv H_{\lambda=\infty}$),

$$H_\lambda = U_\lambda H_{\lambda=\infty} U_\lambda^\dagger, \quad (14)$$

labeled by a momentum parameter λ that runs from ∞ toward zero, which keeps track of the sequence of Hamiltonians ($s = 1/\lambda^4$ has been used elsewhere [54, 64, 65]). These

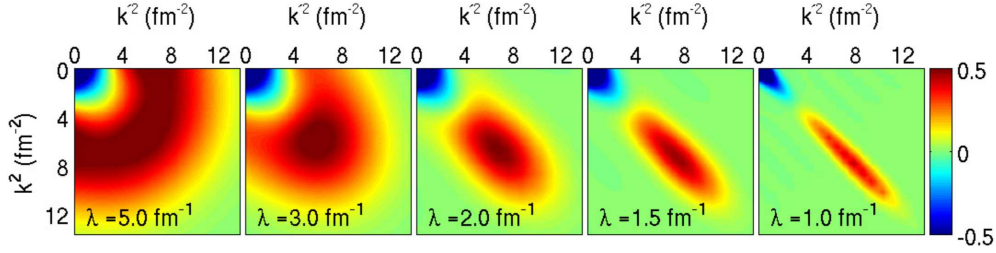


Figure 2: Illustration of how the SRG procedure [64, 66, 65, 67] weakens the strong off-diagonal couplings of the 1S_0 chiral N^3LO NN potential [11, 12] in momentum space as the flow proceeds to smaller values of λ (left to right panels). The flow increasingly concentrates the non-vanishing potential strength to an attractive region near the origin and a repulsive region at higher momenta with both regions lying along the diagonal.

transformations are implemented as a flow equation in λ (in units where $\hbar^2/M = 1$),

$$\frac{dH_\lambda}{d\lambda} = -\frac{4}{\lambda^5} [[T_{\text{rel}}, H_\lambda], H_\lambda], \quad (15)$$

whose form guarantees that the H_λ 's are unitarily equivalent [54, 55, 56, 66].

The utility of the nucleon relative kinetic energy T_{rel} in Eq. (15) is that it reduces the coupling of the high- and low-momentum parts of H_λ , which means softer and more convergent many-body calculations [36, 57]. This is evident in a partial-wave momentum basis, where matrix elements $\langle k|H_\lambda|k' \rangle$ connecting states with (kinetic) energies differing by more than λ^2 are suppressed by $e^{-(k^2-k'^2)^2/\lambda^4}$ factors and, therefore, the states decouple as λ decreases. (Decoupling also results from replacing T_{rel} in Eq. (15) with other generators [54, 56, 58, 59] where the common feature is a generator having diagonal or nearly diagonal structure in the relative HO basis.) The decoupling between the high-momentum and low-momentum parts of the NN interaction is illustrated in Fig. 2.

To see how the two-, three-, and higher-body potentials are identified, it is useful to decompose H_λ in second-quantized form. Schematically (suppressing indices and sums),

$$H_\lambda = \langle T \rangle a^\dagger a + \langle V_\lambda^{(2)} \rangle a^\dagger a^\dagger a a + \langle V_\lambda^{(3)} \rangle a^\dagger a^\dagger a^\dagger a a a + \dots, \quad (16)$$

where a^\dagger , a are creation and destruction operators with respect to the vacuum in some (coupled) single-particle basis. This defines $\langle T \rangle$, $\langle V_\lambda^{(2)} \rangle$, $\langle V_\lambda^{(3)} \rangle$, ... as the one-body, two-body, three-body, ... matrix elements at each λ . Upon evaluating the commutators in Eq. (15) using H_λ from Eq. (16), we see that even if initially there are only two-body potentials, higher-body potentials are generated with each step in λ . Thus, when applied in an A -body subspace, the SRG will “induce” A -body forces. But we also see that $\langle T \rangle$ is fixed, $\langle V_\lambda^{(2)} \rangle$ is determined only in the $A = 2$ subspace with no dependence on $\langle V_\lambda^{(3)} \rangle$, $\langle V_\lambda^{(3)} \rangle$ is determined in $A = 3$ given $\langle V_\lambda^{(2)} \rangle$, and so on.

While it may seem natural to solve Eq. (15), in momentum representation, it is an operator equation, so we can use any convenient basis. In our applications, we evolve in a *discrete* HO basis, where spectators are handled without a decomposition and induced many-body forces can be directly identified. Having chosen such a basis, we obtain coupled first-order differential equations for the matrix elements of the flowing Hamiltonian H_λ , where the right side of Eq. (15) is evaluated using simple matrix multiplications.

Calculations may be performed in the Jacobi coordinate HO basis. We start by evolving H_λ in the $A = 2$ subsystem, which completely fixes the two-body matrix

elements $\langle V_\lambda^{(2)} \rangle$. Next, by evolving H_λ in the $A = 3$ subsystem we determine the combined two-plus-three-body matrix elements. We can isolate the three-body matrix elements by subtracting the evolved $\langle V_\lambda^{(2)} \rangle$ elements in the $A = 3$ basis [68]. Having obtained the separate NN and NNN matrix elements, *we can apply them unchanged to any nucleus*. We are also free to include any initial three-nucleon force in the initial Hamiltonian without changing the procedure. If applied to $A \geq 4$, four-body (and higher) forces will not be included and so the transformations will be only approximately unitary.

Once the evolved interactions are determined in the Jacobi HO basis, transformations to the SD basis are performed, in particular, when nuclei with $A > 4$ are studied. The transformations of two-body interactions are standard. The correspondent $3NF$ transformations were derived and implemented in Refs. [69, 70] with recent advances presented in Ref. [71], where a JT -coupled representation was developed with a highly efficient storage scheme, which allows us to handle $3NF$ matrix-element sets up to $N_{\max} = 12$ model spaces for p -shell nuclei.

6 Recent NCSM and NCFC results

In this section, I present a selection of NCSM and NCFC results. First, recall that in the NCFC case [15], one extrapolates to the continuum limit (infinite matrix result) illustrated in Fig. 3.

Here, I show results for the ground state (gs) of ^{12}C as a function of N_{\max} obtained with the realistic NN interaction, JISP16 [32, 51, 52]. The smooth curves portray exponential fits that achieve asymptotic independence of N_{\max} and $\hbar\Omega$. The NCFC gs energy (the common asymptote) of -94.5 MeV indicates overbinding of $\sim 2.5\%$ leading us to conclude that $3NF$ s must play a role. The assessed uncertainty

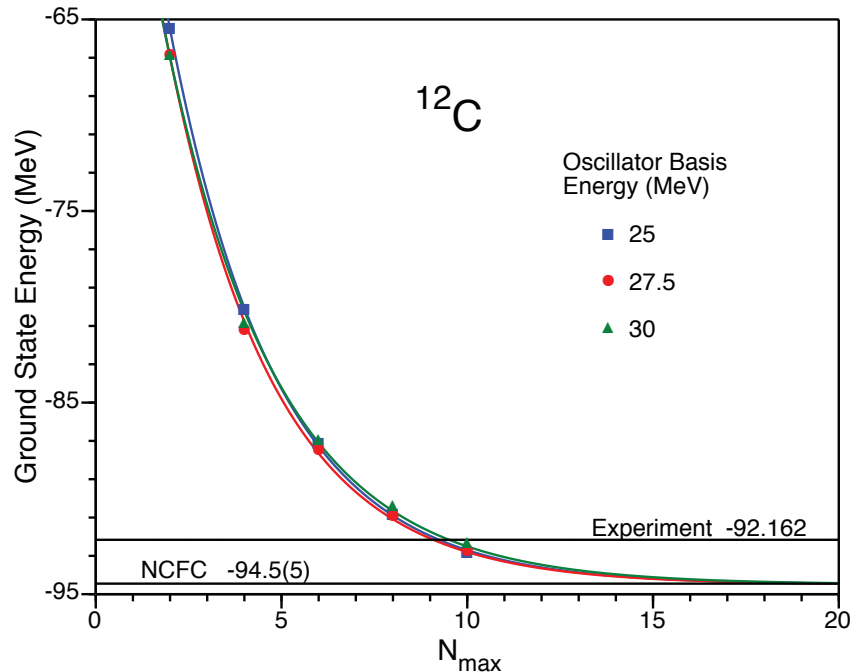


Figure 3: Calculated ground state (gs) energy of ^{12}C for $N_{\max} = 2-10$ (symbols) at selected values of $\hbar\Omega$. For each $\hbar\Omega$, the results are fit to an exponential plus a constant, the asymptote, constrained to be the same for all $\hbar\Omega$ [15]. Horizontal lines indicate the experimental gs and the NCFC result (uncertainty = 0.5 MeV).

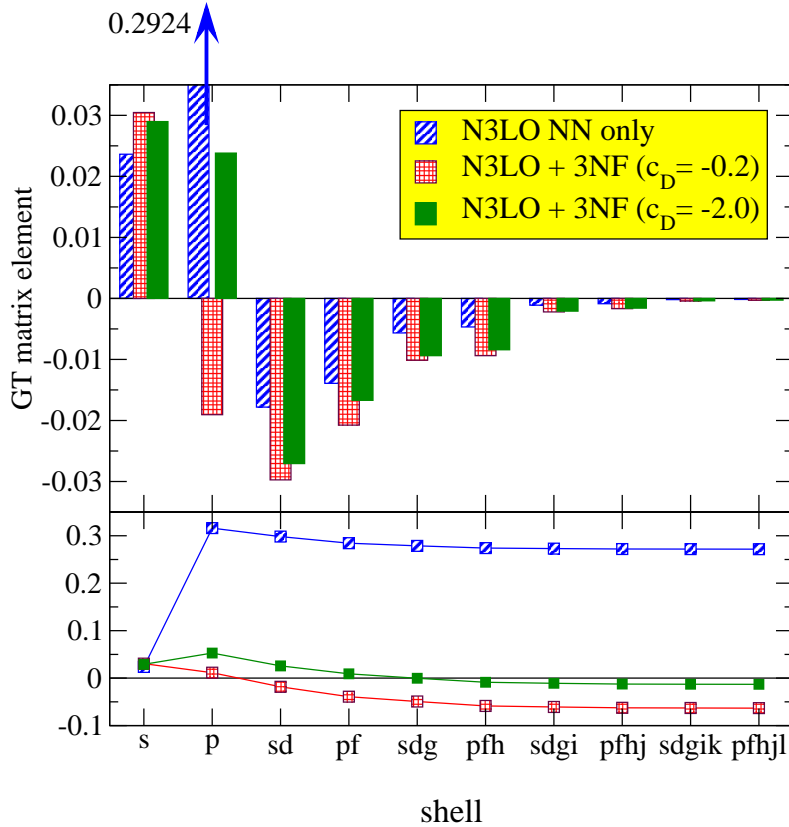


Figure 4: *Ab-initio* NCSM calculations the Gamow–Teller (GT) matrix element for the beta decay of ^{14}C [34]. Contributions to the ^{14}C beta decay matrix element are displayed as a function of the HO shell in the $N_{max} = 8$ basis space using interactions from ChPT. The top panel displays the contributions without and with the 3NF with two reasonable choices for the 3NF parameter c_D . Contributions are summed within each shell to yield a total for that shell. The bottom section displays the running sums of the GT contributions over the shells. Two choices for c_D in the 3NF lead to similar strong suppression of the GT matrix element where the final sums are closer to zero. $c_D = -2.0$ yields the final sum closest to zero. Note, in particular, the order-of-magnitude suppression of the $0p$ -shell contributions arising from the 3NF.

in the NCFC result is 0.5 MeV shown in parenthesis in the figure. The largest calculations correspond to $N_{max} = 10$, with an m -scheme matrix dimension near 8 billion. $N_{max} = 12$ produces an m -scheme matrix dimension near 81 billion which we hope to solve in the future.

A particular example of the recent NCSM accomplishments stands out and that is the demonstration that the anomalous long half life of ^{14}C is a consequence of ChPT 3NFs strongly quenching the Gamow-Teller (GT) matrix element [34]. The results without and with 3NFs are shown in Fig. 4. In the top of Fig. 4 one observes that, without 3NFs there is a large contribution to the GT matrix element coming from the $0p$ -shell single particle spin flip as a neutron converts to a proton. This is the conventional shell-model single-particle GT transition and it leads to a “normal” beta decay half-life of a light nucleus which is not suppressed.

Inclusion of 3NFs shows little effect on the contribution of most shells to the GT matrix element. However, the contribution of the $0p$ -shell terms becomes strongly suppressed — by more than an order of magnitude in the two examples shown. The two examples differ by changes in the LECs of the 3NF that are allowed within the

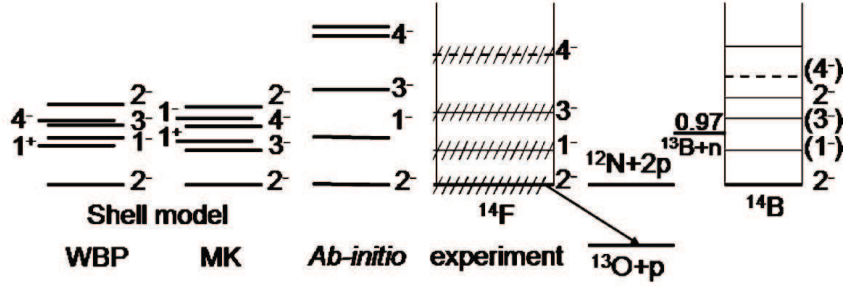


Figure 5: Comparison of the ^{14}F theoretical spectra with the Texas A&M Cyclotron experiment showing excellent agreement between *ab initio* predictions of Ref [37] and experiment [53]. This figure also shows comparisons with predictions of traditional phenomenological shell model calculations with a core labelled by “WBP” and “MK” (see Ref [53] for details).

range that is “natural” as discussed above. The conclusion is that one may easily fit the exact experimental halflife with an allowed adjustment of the LECs for the 3NFs . However, we did not carry out this fine tuning since there remain additional corrections from enlarging the basis and including ChPT corrections to the weak decay matrix element. These additional small corrections will not change the main conclusion (large suppression due to 3NFs) but will effect the fine tuning of the LECs.

As another example of NCFC achievements, we successfully predicted the spectra for the proton unstable nucleus ^{14}F [37] before it was measured using JISP16 [32, 51, 52] as shown in Fig. 5. This figure is adapted from the paper [53] reporting the experimental results and presenting the comparison with our published *ab initio* NCFC predictions.

As a final example illustrating recent NCSM progress in light nuclei, I select the example of ^7Li calculated with $NN + 3\text{NFs}$ from ChPT. The resulting excitation spectra is shown in Fig. 6 at $N_{\text{max}} = 4-6-8$ [35] and compared with experiment shown in the leftmost column. The HO energy is chosen, where the g.s. energy of ^7Li is a minimum in the $8\hbar\Omega$ basis space. Note that our $NN + 3\text{NF}$ (also referred to as “ NNN ” in the legend) spectral ordering is in agreement with experiment for the 9 lowest states in ^7Li and the excitation spectra is rather stable with increasing N_{max} . We also obtain theoretical excitation spectra showing comparable agreement with experiment for ^7Be .

7 Summary

The *ab initio* NCSM and NCFC approaches treat all A nucleons equally with modern $NN + 3\text{NF}$ interactions and successfully describe properties of nuclei throughout the $0p$ -shell. Collaborations with computer scientists and applied mathematicians as well as the use of supercomputers is critical to the progress achieved to date. Several investigations are underway to extend these *ab initio* methods to nuclei with $A > 16$ and to more completely unify these *ab initio* structure approaches with a corresponding predictive theory of nuclear reactions [72]. The outlook is very promising for resolving many long-standing problems in microscopic nuclear theory.

8 Acknowledgements

I would like to thank my collaborators who have worked diligently over many years to accomplish the key results summarized here. They are most easily identified by the papers I have cited in this work. I also thank the sponsors of this workshop, Pacific

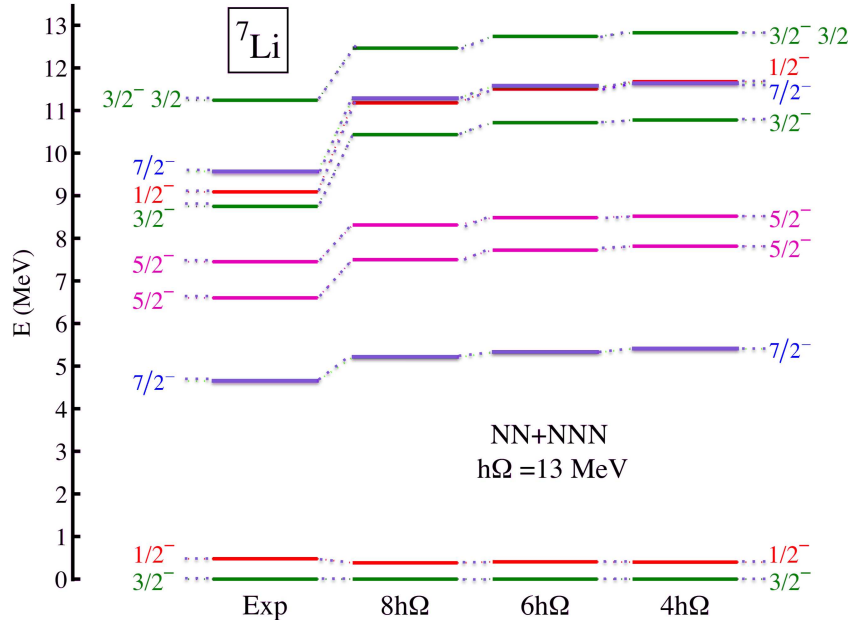


Figure 6: Calculated and experimental excitation energies of ${}^7\text{Li}$ from Ref. [35]. Dependence on the size of the basis is presented. The chiral EFT NN and NNN interaction was used and $\hbar\Omega = 13$ MeV. The isospin of the states is $T = 1/2$ unless shown otherwise as in the example of the highest lying experimental state which is $T = 3/2$.

National University, for their generous support. I also acknowledge partial support from DE-FG02-87ER40371, DE-FC02-09ER41582 (SciDAC/UNEDF) and by the US NSF grant 0904782. Computational resources were provided by the National Energy Research Supercomputer Center (NERSC), which is supported by the Office of Science of the U.S. Department of Energy. Computational resources were also provided by a “Petascale Early Science Award” and an INCITE Award on the Jaguar supercomputer at the Oak Ridge Leadership Computing Facility at ORNL which is supported by the DOE Office of Science under Contract DE-AC05-00OR22725.

References

- [1] R. B. Wiringa, V. G. J. Stoks and R. Schiavilla, *Phys. Rev. C* **51**, 38 (1995).
- [2] S. A. Coon, M. D. Scadron, P. C. McNamee, B. R. Barrett, D. W. E. Blatt and B. H. J. McKellar, *Nucl. Phys. A* **317**, 242 (1979).
- [3] S. A. Coon and H. K. Han, *Few Body Syst.* **30**, 131 (2001); *nucl-th/0101003* (2000).
- [4] B. S. Pudliner, V. R. Pandharipande, J. Carlson and R. B. Wiringa, *Phys. Rev. Lett.* **74**, 4396 (1995).
- [5] S. Weinberg, *Physica A* **96**, 327 (1979); *Phys. Lett. B* **251**, 288 (1990); *Nucl. Phys B* **363**, 3 (1991).
- [6] V. Bernard, N. Kaiser and U.-G. Meißner, *Int. J. Mod. Phys. E* **4**, 193 (1995).
- [7] C. Ordonez, L. Ray and U. van Kolck, *Phys. Rev. Lett.* **72**, 1982 (1994); *Phys. Rev. C* **53**, 2086 (1996).

-
- [8] U. van Kolck, *Prog. Part. Nucl. Phys.* **43**, 337 (1999).
- [9] P. F. Bedaque and U. van Kolck, *Annu. Rev. Nucl. Part. Sci.* **52**, 339 (2002); E. Epelbaum, *Prog. Part. Nucl. Phys.* **57**, 654 (2006).
- [10] E. Epelbaum, W. Glöckle, and U.-G. Meißner, *Nucl. Phys. A* **637**, 107 (1998); **671**, 295 (2000).
- [11] D. R. Entem and R. Machleidt, *Phys. Rev. C* **68**, 041001 (2003)
- [12] R. Machleidt and D. R. Entem, *Phys. Rep.* **503**, 1 (2011); arXiv:1105.2919 [nucl-th] (2011).
- [13] P. Navrátil, J. P. Vary and B. R. Barrett, *Phys. Rev. Lett.* **84** 5728 (2000).
- [14] P. Navrátil, J. P. Vary and B. R. Barrett, *Phys. Rev. C* **62** 054311 (2000).
- [15] P. Maris, J. P. Vary and A. M. Shirokov, *Phys. Rev. C.* **79** 014308 (2009); arXiv:0808.3420 [nucl-th] (2008).
- [16] G. Hagen, T. Papenbrock and D. J. Dean, *Phys. Rev. Lett.* **103**, 062503 (2009).
- [17] G. Hagen, T. Papenbrock, D. J. Dean and M. Hjorth-Jensen, *Phys. Rev. C* **82**, 034330 (2010); arXiv:1005.2627 [nucl-th] (2010) and references therein.
- [18] J. P. Vary, H. Honkanen, Jun Li, P. Maris, S. J. Brodsky, A. Harindranath, G. F. de Teramond, P. Sternberg, E. G. Ng and C. Yang, *Phys. Rev. C* **81**, 035205 (2010); arXiv:0905.1411 [nucl-th] (2009).
- [19] S. C. Pieper, V. R. Pandharipande, R. B. Wiringa and J. Carlson, *Phys. Rev. C* **64**, 014001 (2001).
- [20] S. C. Pieper, R. B. Wiringa and J. Carlson, *Phys. Rev. C* **70**, 054325 (2004).
- [21] M. Pervin, S. C. Pieper and R. B. Wiringa, *Phys. Rev. C* **76**, 064319 (2007).
- [22] L. E. Marcucci, M. Pervin, S. C. Pieper, R. Schiavilla and R. B. Wiringa, *Phys. Rev. C* **78**, 065501 (2008).
- [23] E. Epelbaum, H. Krebs, D. Lee and U.-G. Meissner, *Phys. Rev. Lett.* **106**, 192501 (2011); arXiv:1101.2547 [nucl-th] (2011).
- [24] R. Roth, *Phys. Rev. C* **79**, 064324 (2009); arXiv:0903.4605 [nucl-th] (2009).
- [25] T. Dytrych, K. D. Sviratcheva, J. P. Draayer, C. Bahri and J. P. Vary, *J. Phys. G* **35**, 123101 (2008); see also T. Dytrych, J. P. Draayer, K. D. Launey and D. Langr, in *Proc. Int. Workshop Nucl. Theor. Supercomputing Era (NTSE-2012), Khabarovsk, Russia, June 18–22, 2012*, edited by A. M. Shirokov and A. I. Mazur. Pacific National University, Khabarovsk, 2013 (*see this book*), p. 50.
- [26] T. Abe, P. Maris, T. Otsuka, N. Shimizu, Y. Utsuno and J. P. Vary, *Phys. Rev. C* **86**, 054301 (2012), arXiv:1204.1755 [nucl-th] (2012); see also Y. Utsuno, in *Proc. Int. Workshop Nucl. Theor. Supercomputing Era (NTSE-2012), Khabarovsk, Russia, June 18–22, 2012*, edited by A. M. Shirokov and A. I. Mazur. Pacific National University, Khabarovsk, 2013 (*see this book*), p. 26; T. Abe, P. Maris, T. Otsuka, N. Shimizu, Y. Utsuno and J. P. Vary, *ibid.*, p. 33.
- [27] A. F. Lisetskiy, B. R. Barrett, M. K. G. Kruse, P. Navrátil, I. Stetcu and J. P. Vary, *Phys. Rev. C* **78**, 044302 (2008); arXiv:0808.2187 [nucl-th] (2008).
- [28] P. Navrátil, M. Thoresen and B. R. Barrett, *Phys. Rev. C* **55**, 573 (1997); arXiv:nucl-th/9612015 (1997).

- [29] B. R. Barrett, P. Navrátil and J. P. Vary, *Progr. Part. Nucl. Phys.* **69**, 131 (2013).
- [30] D. H. Gloekner and D. R. Lawson, *Phys. Lett. B* **53**, 313 (1974).
- [31] P. Navrátil, V. G. Gueorguiev, J. P. Vary, W. E. Ormand and A. Nogga, *Phys. Rev. Lett.* **99**, 042501 (2007); arXiv:nucl-th/0701038 (2007).
- [32] A. M. Shirokov, J. P. Vary, A. I. Mazur and T. A. Weber, *Phys. Lett. B* **644**, 33 (2007).
- [33] P. Maris, M. Sosonkina, J. P. Vary, E. G. Ng and C. Yang, *Procedia CS* **1**, 97 (2010).
- [34] P. Maris, J. P. Vary, P. Navrátil, W. E. Ormand, H. Nam and D. J. Dean, *Phys. Rev. Lett.* **106**, 202502 (2011); arXiv:1101.5124 [nucl-th] (2011).
- [35] P. Maris, J. P. Vary and P. Navrátil, arXiv:1205.5686 [nucl-th] (2012).
- [36] S. K. Bogner, R. J. Furnstahl, P. Maris, R. J. Perry, A. Schwenk and J. P. Vary, *Nucl. Phys. A* **801**, 21 (2008); nucl-th/0708.3754 (2007).
- [37] P. Maris, A. M. Shirokov and J. P. Vary, *Phys. Rev. C* **81**, 021301(R) (2010).
- [38] C. Cockrell, J. P. Vary and P. Maris, *Phys. Rev. C* **86**, 034325 (2012); arXiv:1201.0724 [nucl-th] (2012).
- [39] Gianina Alina Negoita, *Ab initio Nuclear Structure Theory*. Doctoral dissertation, Iowa State University, 2010. ProQuest.com UMI 11359.
- [40] M. Caprio, P. Maris and J. P. Vary, *Phys. Rev. C* **86**, 034312 (2012); arXiv:1208.4156 [nucl-th] (2012).
- [41] S. A. Coon, M. I. Avetian, M. K. G. Kruse, B. van Kolck, P. Maris and J. P. Vary, *Phys. Rev. C* **86**, 054002 (2012); arXiv:1205.3230 [nucl-th] (2012). See also S. A. Coon, in *Proc. Int. Workshop Nucl. Theor. Supercomputing Era (NTSE-2012), Khabarovsk, Russia, June 18–22, 2012*, edited by A. M. Shirokov and A. I. Mazur. Pacific National University, Khabarovsk, 2013 (*see this book*), p. 171.
- [42] R. J. Furnstahl, G. Hagen and T. Papenbrock, *Phys. Rev. C* **86**, 031301 (2012); arXiv:1207.6100 [nucl-th] (2012).
- [43] D. C. Zheng, J. P. Vary and B. R. Barrett, *Phys. Rev. C* **50**, 2841 (1994); arXiv:nucl-th/9405018 (1994).
- [44] D. C. Zheng, B. R. Barrett, J. P. Vary and H. Muther, *Phys. Rev. C* **51**, 2471 (1995); arXiv:nucl-th/9410048 (1994).
- [45] S. Okubo, *Prog. Theor. Phys.* **12**, 603 (1954).
- [46] K. Suzuki and S. Y. Lee, *Prog. Theor. Phys.* **64**, 2091 (1980).
- [47] J. P. Vary, R. H. Behlrad and B. J. Dalton, *Nucl. Phys. A* **328**, 526 (1979).
- [48] J. P. Vary, in *Theory and Applications of Moment Methods in Many-Fermion Systems*, edited by B. J. Dalton, S. M. Grimes, J. P. Vary and S. A. Williams. Plenum Press, New York, 1980, p. 423.
- [49] F. J. Margetan and J. P. Vary, *Phys. Rev. C* **28**, 907 (1983).
- [50] H. Kümmel, K. H. Lürhmann and J. G. Zabolitsky, *Phys. Rep.* **36**, 1 (1978) and references therein.

-
- [51] A. M. Shirokov, J. P. Vary, A. I. Mazur, S. A. Zaytsev and T. A. Weber, *Phys. Lett. B* **621**, 96 (2005).
- [52] A. M. Shirokov, A. I. Mazur, S. A. Zaytsev, J. P. Vary and T. A. Weber, *Phys. Rev. C* **70**, 044005 (2004).
- [53] V. Z. Goldberg, B. T. Roeder, G. V. Rogachev, G. G. Chubarian, E. D. Johnson, C. Fu, A. A. Alharbi, M. L. Avila, A. Banu, M. McCleskey, J. P. Mitchell, E. Simmons, G. Tabacaru, L. Trache and R. E. Tribble, *Phys. Lett. B* **692**, 307 (2010).
- [54] S. K. Bogner, R. J. Furnstahl and R. J. Perry, *Phys. Rev. C* **75**, 061001 (2007); arXiv:[nucl-th/0611045 (2006) and references therein.
- [55] F. J. Wegner, *Phys. Rep.* **348**, 77 (2001).
- [56] S. Kehrein, *Springer Tracts Mod. Phys.* **217**, 137 (2006).
- [57] E. D. Jurgenson, S. K. Bogner, R. J. Furnstahl and R. J. Perry, *Phys. Rev. C* **78**, 014003 (2008).
- [58] S. D. Glazek and R. J. Perry, *Phys. Rev. D* **78**, 045011 (2008).
- [59] E. Anderson, S. K. Bogner, R. J. Furnstahl, E. D. Jurgenson, R. J. Perry and A. Schwenk, *Phys. Rev. C* **77**, 037001 (2008).
- [60] J. Da Providencia and C. M. Shakin, *Ann. Phys. (NY)* **30**, 95 (1964).
- [61] K. Suzuki, *Prog. Theor. Phys.* **68**, 1999 (1982); K. Suzuki and R. Okamoto, *Prog. Theor. Phys.* **92**, 1045 (1994).
- [62] C. P. Viazminsky and J. P. Vary, *J. Math. Phys.* **42**, 2055 (2001).
- [63] H. Kamada, A. Nogga, W. Glöckle, E. Hiyama, M. Kamimura, K. Varga, Y. Suzuki, M. Viviani, A. Kievsky, S. Rosati, J. Carlson, S. C. Pieper, R. B. Wiringa, P. Navrátil, B. R. Barrett, N. Barnea, W. Leidemann and G. Orlandini, *Phys. Rev. C* **64**, 044001 (2001).
- [64] S. D. Glazek and K. G. Wilson, *Phys. Rev. D* **48**, 5863 (1993).
- [65] S. K. Bogner, R. J. Furnstahl, R. J. Perry and A. Schwenk, *Phys. Lett. B* **649**, 488 (2007); arXiv:nucl-th/0701013 (2007).
- [66] F. Wegner, *Ann. Phys. (Leipzig)* **506**, 77 (1994).
- [67] R. Roth, T. Neff and H. Feldmeier, *Prog. Part. Nucl. Phys.* **65**, 50 (2010); arXiv:1003.3624 [nucl-th] (2010).
- [68] E. D. Jurgenson and R. J. Furnstahl, *Nucl. Phys. A* **818**, 152 (2009); arXiv:0809.4199 [nucl-th] (2008).
- [69] P. Navrátil and W. E. Ormand, *Phys. Rev. C* **68**, 034305 (2003); arXiv:nucl-th/0305090 (2003).
- [70] A. Nogga, P. Navrátil, B. R. Barrett and J. P. Vary, *Phys. Rev. C* **73**, 064002 (2006); arXiv:nucl-th/0511082 (2005).
- [71] R. Roth, J. Langhammer, A. Calci, S. Binder and P. Navratil, *Phys. Rev. Lett.* **107**, 072501 (2011); arXiv:1105.3173 [nucl-th] (2011).

- [72] L. D. Blokhintsev, in *Proc. Int. Workshop Nucl. Theor. Supercomputing Era (NTSE-2012), Khabarovsk, Russia, June 18–22, 2012*, edited by A. M. Shirokov and A. I. Mazur. Pacific National University, Khabarovsk, 2013 (*see this book*), p. 58; A. M. Shirokov, *ibid.*, p. 113; S. A. Zaytsev and G. Gasaneo, *ibid.*, p. 135; A. I. Mazur, A. M. Shirokov, J. P. Vary, P. Maris and I. A. Mazur, *ibid.*, p. 146.

Monte Carlo Shell Model and its Applications to Exotic Nuclei

Yutaka Utsuno

Advanced Science Research Center, Japan Atomic Energy Agency, 2-4 Shirakata-shirane, Tokai, Ibaraki 319-1195, Japan

Abstract

We give an overview of the development of the Monte Carlo shell model (MCSM). MCSM was originally based on the auxiliary-field Monte Carlo technique, but it is more like a stochastic variational method within multiple Slater determinants incorporating symmetry restoration. It is shown that complicated shell-model wave functions can be satisfactorily approximated with the MCSM calculation. MCSM has been applied to several cases, one of which is the neutron-rich region around $N = 20$, often called the island of inversion. A unified picture of the island of inversion is obtained with the MCSM calculations. The study of the island of inversion leads to a general concept of the shell evolution.

Keywords: *Shell model; Monte Carlo shell model; magic numbers; shell structure*

1 Introduction

Large-scale computing has been an indispensable tool in various fields of science. For instance, Japan has recently completed a new 10-PFlops supercomputer called K computer [1] in order to solve urgent problems in science and technology. Among various applications of the K computer, basic science including nuclear physics, has been regarded as one of the most important. In nuclear physics, large-scale computing enables one to describe nuclei from a more fundamental viewpoint. According to the forecast of Ref. [2], *ab initio* calculations in which a nucleus is built from nucleons interacting one with another via a bare nucleon-nucleon force only, will be extended to the *sd*-shell region in a near future. As for medium-heavy nuclei, the nuclear shell model, or the configuration interaction (CI) approach in terms of quantum chemistry, will be applicable up to the region around ^{132}Sn . Both methods need capability to deal with a huge number of many-body states. While exact calculation of the innumerable states such as the Lanczos diagonalization is developing accordingly, approximate methods should also be developed for surpassing the current limitation. The Monte Carlo shell model (MCSM) [3] is one of such methods, being developed to give a precise description of the CI problems with huge dimensionality. Its applicability is not limited to the conventional shell model which assumes an inert core and a relatively small number of valence orbits, but also includes *ab initio* calculations due to recent methodological and computational progress [4].

In this paper, we show some basics of MCSM and its early successful applications to the structure of exotic nuclei in the region near $N = 20$ which is often called “island of inversion” [5]. It is noted that a recent development of MCSM and a benchmark test for the *ab initio* calculation are presented in another paper [6]. We also show how the large-scale MCSM calculation plays an essential role in deeper understanding of exotic nuclei as exemplified by the so-called “shell evolution” that has been strongly motivated by the success of MCSM in the island of inversion.

2 Brief overview of the Monte Carlo shell model

The methodology of MCSM was proposed by Honma, Mizusaki and Otsuka in 1995 [7]. It is aimed at overcoming the limitation of CI due to huge dimensionality. It is noted that the first application was not the shell model but was the Interacting Boson Model (IBM). The computational method employed by MCSM is named the Quantum Monte Carlo Diagonalization (QMCD). QMCD was hinted by the shell model Monte Carlo (SMMC) method [8]. Thus, we first introduce basic ideas of SMMC in Sect. 2.1, and then present the QMCD method in Sect. 2.2.

2.1 SMMC: an auxiliary-field Monte Carlo method for the shell model

In general, the ground state of a quantum many-body system with the Hamiltonian H can be obtained, in principle, as

$$\exp(-\beta H)|\Phi\rangle \quad (1)$$

with $\beta \rightarrow \infty$ for any state $|\Phi\rangle$ that is not orthogonal to the ground state. However, in practice, a direct operation of $\exp(-\beta H)$ is almost impossible for a general Hamiltonian including two-body terms or higher. On the other hand, according to Thouless theorem [9], the operation of $\exp(-\beta h)$ on a Slater determinant leads to another Slater determinant for a one-body operator h . This is the starting point of SMMC.

Let us then take a simple two-body operator $H = O^2$ with O being a one-body operator. In this case, $\exp(-\beta H)$ is analytically expressed as

$$\exp(-\beta H) = \int_{-\infty}^{\infty} d\sigma \sqrt{\beta/\pi} \exp(-\beta\sigma^2 - 2\beta\sigma O). \quad (2)$$

Since any two-body operator disappears in Eq. (2), Eq. (1) can be computed for a Slater determinant $|\Phi\rangle$. For an arbitrary two-body operator H , a similar expression is obtained but is associated with more integration variables, which prevent one from directly performing the integration in practice. On the other hand, the integration can be practically carried out by using the Monte Carlo sampling. This is the essence of the so-called auxiliary-field Monte Carlo method where the integral variable σ is called the auxiliary field. The SMMC method [8] is based on this technique.

Although SMMC is suitable for studying properties of ground states and of systems at finite temperature, it is not so for properties of discrete excited levels. In addition, SMMC suffers from the sign problem for general two-body operators. These shortcomings are the motivation to develop another method called QMCD.

2.2 MCSM: application of the Quantum Monte Carlo Diagonalization method to the shell model

In the SMMC method, observables are obtained by using the Monte Carlo integration. In the QMCD method instead, a many-body wave function is obtained by using the diagonalization of the Hamiltonian in which basis states are generated by following the Monte Carlo sampling. This is the original idea of QMCD, and its efficiency has been demonstrated with an IBM Hamiltonian [7].

Once the many-body wave function is calculated with a finite number of basis states, it follows the variational principle. Namely, the energy of this wave function must be higher than the exact energy of the lowest state. In addition, the exact wave function must have good quantum numbers due to the symmetry of the Hamiltonian. Thus, keeping a stochastic procedure, the QMCD method has been developed to

directly utilize those properties. QMCD has adopted the projection technique in Ref. [10], and has been applied to the shell model in Ref. [11].

In the late 1990s, MCSM, the application of the QMCD method to the shell model, has been rather close to the present form and has been applied to systems beyond the limit of the exact diagonalization at that time [12]. Here, the formulation of MCSM is presented briefly. The many-body wave function of MCSM having total angular momentum J and its z component M is expressed as

$$|\Psi_{JM}\rangle = \sum_{k=1}^{N_{\text{MCSM}}} f^{(k)} P^\pi \sum_{K=-J}^J g_K^{(k)} P_{MK}^J |\Phi(D^{(k)})\rangle, \quad (3)$$

where P^π and P_{MK}^J are the parity and angular-momentum projectors. $g_K^{(k)}$ denotes the mixing amplitude of the state having the intrinsic K and the basis index k . $f^{(k)}$ is the mixing amplitude for the k -th basis state (Slater determinant¹) $|\Phi(D^{(k)})\rangle$ defined as

$$|\Phi(D^{(k)})\rangle = \prod_l \left(\sum_i D_{il}^{(k)} c_i^\dagger \right) |-\rangle. \quad (4)$$

In this expression, $g_K^{(k)}$, $f^{(k)}$ and $D_{il}^{(k)}$ are the parameters to be determined. Once all the $D_{il}^{(k)}$ are fixed, $g_K^{(k)}$ and $f^{(k)}$ that follows the variational principle are easily calculated by the diagonalization of the Hamiltonian. On the other hand, it is not straightforward to obtain the optimum form of each basis state, $D_{il}^{(k)}$.

In the MCSM calculation, $D_{il}^{(k)}$ are determined as follows. The number of the basis states, N_{MCSM} , increases step by step: only $D_{il}^{(k)}$ of the last basis with $k = N_{\text{MCSM}}$ can be varied at a time. The other $D_{il}^{(k)}$ with $k \leq N_{\text{MCSM}}$ are kept unchanged. As for determining $D_{il}^{(k=N_{\text{MCSM}})}$, at first, initial candidates are generated according to the Monte Carlo sampling using the auxiliary field σ (see Eq. (2)), and the $\sigma \mapsto D_{il}$ that gives the lowest energy is selected. The total energy labeled by σ is denoted as $E(\sigma)$. Next, around this σ , a small variation $\delta\sigma$ is applied. If $E(\sigma + \delta\sigma) < E(\sigma)$ is satisfied, $\sigma + \delta\sigma$ is adopted as the new σ . Otherwise, this $\sigma + \delta\sigma$ is discarded. This process is repeated until $E(\sigma)$ is saturated.

When the number of the basis states N_{MCSM} increases, the energy is lowered. The lowering of the energy at each increment becomes very small as the wave function is close to the eigenstate. Hence, the number of basis states N_{MCSM} increases until the energy is well converged. N_{MCSM} is typically several tens to hundred even though the dimension of the shell-model Hamiltonian is very large. In fact, it has been demonstrated that the ground-state energy of ^{56}Ni in the full pf -shell calculation with 1 billion M -scheme dimension is very well approximated by about 100 basis states in MCSM [12, 14].

3 MCSM description of the island of inversion

After the feasibility of MCSM was confirmed with some benchmark studies for the pf -shell calculation as shown in the last section, MCSM has been applied to cases where the exact diagonalization was impossible at that time. The neutron-rich region around $N = 20$, often referred to as the ‘‘island of inversion’’ [5], is one of the most successful applications of MCSM. The island of inversion is known as a region, including ^{32}Mg , where a strong deformation occurs in spite of the neutron magic number $N = 20$. The nuclei in the island are considered to be dominated by the $2p$ - $2h$ excitation across the $N = 20$ shell gap. The dominance of the $2p$ - $2h$ state is caused by energy gain due to

¹For different form of the basis state, the pair-condensed basis has been used for a description of medium-heavy nuclei [13].

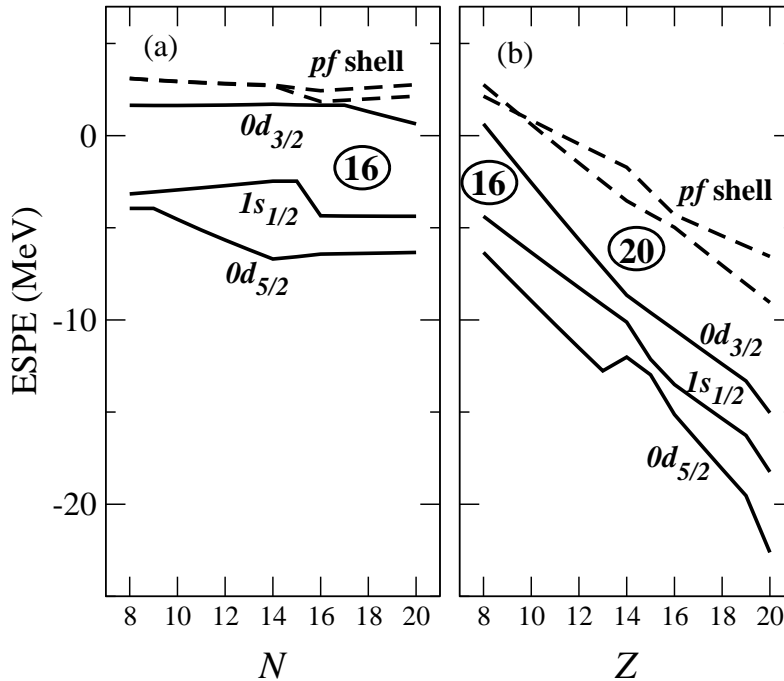


Figure 1: The neutron effective single-particle energies for (a) oxygen isotopes from $N = 8$ to 20 and (b) $N = 20$ isotones from $Z = 8$ to 20. See Ref. [3] for details. For the definition of the effective single-particle energy, see Ref. [15].

correlation or deformation that is larger than the energy loss of the spherical single-particle energy. Thus, accurate calculation of the correlation energy is needed for the description of the island of inversion.

Although the shell model is suitable for calculating the correlation energy, its application to the island of inversion was a difficult task due to the numerical limit of exact diagonalization. In order to describe excitation of nucleons from the sd to pf shell, the full sd shell and part of the pf shell should be included as the valence shell. Even if the pf shell is truncated up to $0f_{7/2}$ and $1p_{3/2}$, the number of single-particle states (including the degeneracy of j_z) reaches 24, which is larger than that of the full pf shell. For instance, the $M = 0$ dimension of ^{32}Mg in the $sd + f_{7/2} + p_{3/2}$ valence shell is larger than 10^9 , which is beyond the computational limit in the early 2000s.

Thus, MCSM was best fitted for the shell-model calculation of the island of inversion. Taking the advantage of MCSM that is applicable to any nucleus on the same footing, we have succeeded in obtaining a unified picture for the $N = 20$ region ranging from stable to unstable nuclei [15]. As mentioned above, the shell gap is one of the most important ingredients for the theoretical framework. We have proposed a neutron shell structure which strongly changes from a smaller to a larger Z as presented in Fig. 1. Whereas the $N = 20$ shell gap is large for stable nuclei around ^{40}Ca , it is sharply reduced for lower Z . Instead of the disappearance of the normal $N = 20$ magicity, a new $N = 16$ magic structure appears near oxygen isotopes. This strong change of the shell structure was phenomenologically introduced in the shell-model Hamiltonian named SDPF-M [15] so that the drip line of oxygen isotopes, $N = 16$, can be reproduced with the shell-model calculation. In Ref. [15], a systematic calculation of yrast states of even-even nuclei has been carried out, demonstrating good agreement with the experimental energy levels and the $B(E2)$ values.

According to the varying shell gap shown in Fig. 1, the $N = 20$ shell gap is rather reduced for nuclei in the island of inversion with $Z = 10$ –12. This helps those nuclei

to be dominated by the $2p$ - $2h$ configurations. When the shell gap is reduced, it is expected that the extent of the island of inversion is enlarged. Thus, investigating the boundary of the island is of a great interest for probing the quenching of the shell gap proposed in Ref. [15]. This has been conducted with a systematic calculation of neutron-rich sodium isotopes ($Z = 11$) in Ref. [16]. In sodium isotopes, although electromagnetic moments of the ground states were known, their dominant configurations were not clear due to the lack of precise nuclear-structure calculations such as the shell model. The MCSM calculation has clarified that the $2p$ - $2h$ dominance takes place at $N = 19$ from comparison between theoretical and experimental moments [16], enlarging the extent of the island of inversion from the original map [5]. It has been also demonstrated that this early onset of the $2p$ - $2h$ dominance occurs only with a Hamiltonian having a reduced $N = 20$ shell gap. Thus, exotic properties of neutron-rich nuclei around $N = 20$ are successfully accounted for by the sharp change of the shell structure from stable to unstable nuclei.

4 Shell evolution

In Sec. 3, guided by large-scale shell-model calculations with MCSM, a strongly varying shell structure was phenomenologically introduced. Its origin and universality were not clear. After the MCSM study of the island of inversion, the understanding of the evolution of the shell structure, often called shell evolution, has been advanced. Thus, the shell evolution is one of good examples that a large-scale nuclear structure calculation leads to a deeper understanding of the nuclear structure from the fundamental point of view. In the following, a brief overview about the shell evolution is presented on the basis of our works.

As for the single-particle structure shown in Fig. 1, what causes the shift of magicity is the strong lowering of the neutron $0d_{3/2}$ orbit as protons occupy the $0d_{5/2}$ orbit. This is a consequence of a strong attraction between a proton in $0d_{5/2}$ and a neutron in $0d_{3/2}$. Since those two orbits are opposite in spin direction, the nuclear force dependent on spin seems to be essential. In Ref. [17], we have pointed out that the spin dependent central force can explain this strong attraction, generalizing a strong $T = 0$ attraction between the $j_>$ orbit and the $j_<$ orbit, where $j_>$ and $j_<$ stand for the orbits whose j 's are $l + 1/2$ and $l - 1/2$, respectively. Indeed, realistic p -shell and pf -shell interactions have a strong attraction between $0p_{1/2}$ and $0p_{3/2}$ and between $0f_{5/2}$ and $0f_{7/2}$, respectively. As a result of this property, a new $N = 34$ magic number has been predicted in the neutron-rich calcium region.

Further study has clarified that the origin of this spin dependence is the tensor force [18], while the spin dependence of the central force plays a minor role. The tensor force gives the strong attraction between $j_>$ and $j'_<$ orbits even with different orbital angular momenta l and l' . The tensor force thus works to change the spin-orbit splitting. The *effective* tensor force turns out to be very close to the bare $\pi + \rho$ exchange force. This finding is based on comparison with experiment [18] and also on the analysis of the microscopic effective interaction [19, 20] using the spin-tensor decomposition [21]. It has also been found recently that the monopole part of the interaction, which is responsible for the shell evolution, after subtracting the tensor part is well simulated by a simple Gaussian force [19]. The tensor-subtracted effective interaction includes various effects such as a renormalization of the model space and the effect of the three-body force. Nonetheless, its monopole part can be well described by a simple interaction in terms of phenomenology. The reason for the validity of the Gaussian central force is yet to be clarified. The interaction consisting of the $\pi + \rho$ tensor force and the Gaussian central force seems to describe the shell evolution in a wide range of the nuclear chart, being named the monopole-based universal interaction (V_{MU}) [19]. It has been shown that the phenomenological shell evolution of Fig. 1 is followed by the V_{MU} interaction.

Quite recently, V_{MU} has been applied to the effective interaction of the shell-model calculation in the neutron-rich region around $N = 28$ [22]. Using the shell-model calculation, we are able to discuss the shell evolution beyond the framework of the single-particle state. It is shown that the distribution of the spectroscopic factors for one-proton removal from ^{48}Ca is excellently reproduced by a Hamiltonian based on V_{MU} . This result indicates that the proton spin-orbit splitting is strongly reduced from $N = 20$ to 28 by the tensor force, and that the reduction is quantitatively reproduced with V_{MU} including the $\pi + \rho$ tensor force. It is also shown that a very neutron-rich nucleus ^{42}Si is strongly oblate deformed because of quenching of proton sub-shell gaps induced by the tensor force. This deformation accounts for the low 2_1^+ state in ^{42}Si measured recently [23].

5 Summary

In summary, this paper reports a brief overview of the development of the Monte Carlo shell model (MCSM) and its earliest successful application to the neutron-rich region around $N = 20$. The shell evolution due to the effective interaction, an idea following the success of the MCSM calculation, is also presented. In the present paper, we stress that the development of large-scale nuclear-structure calculation leads not only to a quantitative description of various nuclei from a fundamental point of view but also to the construction of a new paradigm of nuclear physics.

Acknowledgment

The author is indebted to T. Otsuka, T. Mizusaki, M. Honma, N. Shimizu and T. Abe for a long term collaboration which constitutes the basis of this paper. He also acknowledges a collaboration with B. A. Brown for the shell-model study around $N = 28$. The study of this paper is in part supported by MEXT/JSPS KAKENHI Grant Numbers (13002001), (14740176), (17740165), and (21740204), and supported also by HPCI Strategic Program Field 5.

References

- [1] K computer, <http://www.aics.riken.jp/en/>.
- [2] SciDAC Review, Issue 6, p. 42 (2007).
- [3] T. Otsuka, M. Honma, T. Mizusaki, N. Shimizu and Y. Utsuno, *Prog. Part. Nucl. Phys.* **47**, 319 (2001).
- [4] N. Shimizu, T. Abe, Y. Tsunoda, Y. Utsuno, T. Yoshida, T. Mizusaki, M. Honma and T. Otsuka, *Prog. Theor. Exp. Phys.* **2012**, 01A205 (2012).
- [5] E. K. Warburton, J. A. Becker and B. A. Brown, *Phys. Rev. C* **41**, 1147 (1990).
- [6] T. Abe, P. Maris, T. Otsuka, N. Shimizu, Y. Utsuno and J. P. Vary, in *Proc. Int. Workshop Nucl. Theor. Supercomputing Era (NTSE-2012), Khabarovsk, Russia, June 18–22, 2012*, edited by A. M. Shirokov and A. I. Mazur. Pacific National University, Khabarovsk, 2013 (*see this book*), p. 33.
- [7] M. Honma, T. Mizusaki and T. Otsuka, *Phys. Rev. Lett.* **75**, 1284 (1995).
- [8] S. E. Koonin, D. J. Dean and K. Langanke, *Phys. Rep.* **278**, 1 (1997).
- [9] D. J. Thouless, *Nucl. Phys.* **21**, 225 (1960).

-
- [10] T. Mizusaki, M. Honma and T. Otsuka, Phys. Rev. C **53**, 2786 (1996).
 - [11] M. Honma, T. Mizusaki and T. Otsuka, Phys. Rev. Lett. **77**, 3315 (1996).
 - [12] T. Otsuka, M. Honma and T. Mizusaki, Phys. Rev. Lett. **81**, 1588 (1998).
 - [13] N. Shimizu, T. Otsuka, T. Mizusaki and M. Honma, Phys. Rev. Lett. **86**, 1171 (2001).
 - [14] K. W. Schmid, Prog. Part. Nucl. Phys. **52**, 565 (2004).
 - [15] Y. Utsuno, T. Otsuka, T. Mizusaki and M. Honma, Phys. Rev. C **60**, 054315 (1999).
 - [16] Y. Utsuno, T. Otsuka, T. Glasmacher, T. Mizusaki and M. Honma, Phys. Rev. C **70**, 044307 (2004).
 - [17] T. Otsuka, R. Fujimoto, Y. Utsuno, B. A. Brown, M. Honma and T. Mizusaki, Phys. Rev. Lett. **87**, 082502 (2001).
 - [18] T. Otsuka, T. Suzuki, R. Fujimoto, H. Grawe and Y. Akaishi, Phys. Rev. Lett. **95**, 232502 (2005).
 - [19] T. Otsuka, T. Suzuki, M. Honma, Y. Utsuno, N. Tsunoda, K. Tsukiyama and M. Hjorth-Jensen, Phys. Rev. Lett. **104**,
 - [20] N. Tsunoda, T. Otsuka, K. Tsukiyama and M. Hjorth-Jensen, Phys. Rev. C **84**, 044322 (2011).
 - [21] M. K. Kirson, Phys. Lett. **47B**, 110 (1973).
 - [22] Y. Utsuno, T. Otsuka, B. A. Brown, M. Honma, T. Mizusaki and N. Shimizu, arXiv:1210.5469 [nucl-th] (2012); to be published in Phys. Rev. C.
 - [23] B. Bastin *et al.*, Phys. Rev. Lett. **99**, 022503 (2007).

Application of the Monte Carlo Shell Model to *Ab Initio* No-Core Calculations

T. Abe^a, P. Maris^b, T. Otsuka^{a,c,d}, N. Shimizu^c, Y. Utsuno^e
and J. P. Vary^b

^a*Department of Physics, the University of Tokyo, Hongo, Tokyo 113-0033, Japan*

^b*Department of Physics and Astronomy, Iowa State University, Ames, Iowa 50011, USA*

^c*Center for Nuclear Study, the University of Tokyo, Hongo, Tokyo 113-0033, Japan*

^d*National Superconducting Cyclotron Laboratory, Michigan State University, East Lansing, Michigan 48824, USA*

^e*Advanced Science Research Center, Japan Atomic Energy Agency, Tokai, Ibaraki 319-1195, Japan*

Abstract

We report recent developments of the Monte Carlo Shell Model (MCSM) and its application to the no-core calculations. It is shown that recent developments enable us to apply the MCSM to the shell-model calculations without a core. Benchmarks between the MCSM and Full-Configuration Interaction (FCI) methods demonstrate consistent results with each other within estimated uncertainties. No-Core Full Configuration (NCFC) results are also presented as full *ab initio* solutions extrapolated to the infinite basis limit.

Keywords: *Shell model; Monte Carlo shell model; ab initio approaches*

1 Introduction

One of the major challenges in nuclear physics is to understand nuclear structure and reactions from *ab initio* calculations. Such calculations have recently become feasible for nuclear many-body systems beyond $A = 4$ due to the rapid evolution of computational technologies. Together with the Green's Function Monte Carlo [1] and Coupled Cluster theory [2], the No-Core Shell Model (NCSM) is one of the relevant *ab initio* methods and has been emerging for about a decade. It is now available for the study of nuclear structure and reactions in the p -shell nuclei [3].

As the NCSM treats all the nucleons democratically, computational demands for the calculations explode exponentially as the number of nucleons increases. Current computational resources limit the direct diagonalization of the Hamiltonian matrix using the Lanczos algorithm to basis spaces with a dimension of around 10^{10} . In order to access heavier nuclei beyond the p -shell region with larger basis dimensions, many efforts have been devoted to the NCSM calculations. One of these approaches is the Importance-Truncated NCSM [4] where the model spaces are extended by using an importance measure evaluated using perturbation theory. Another approach is the Symmetry-Adapted NCSM [5] where the model spaces are truncated by the selected symmetry groups. Similar to these attempts, the no-core Monte Carlo Shell Model (MCSM) [6, 7, 8] is one of the promising candidates to go beyond the Full Configuration Interaction (FCI) method which is a different truncation of the basis states that commonly used in the NCSM.

In these proceedings, we focus on the latest application of the MCSM toward the *ab initio* no-core calculations, which has become viable recently with the aid of major developments in the MCSM algorithm [8, 9, 10] and also a remarkable growth in the computational power of state-of-the-art supercomputers. The overview of the benchmarks in the no-core MCSM is based on the results mostly presented in Refs. [7, 8].

2 MCSM

The MCSM has been developed mainly for conventional shell-model calculations with an assumed inert core [11]. Recently the algorithm and code itself have been heavily revised and rewritten so as to accommodate massively parallel computing environments [8, 9, 10]. In this section, we briefly overview the MCSM and introduce some of recent developments.

2.1 Brief overview

The MCSM approach [11] proceeds through a sequence of diagonalization steps within the Hilbert subspace spanned by the deformed Slater determinants in the HO single-particle basis as the selected importance-truncated bases. A many-body basis state $|\Psi^{JM}\rangle$ is a linear combination of non-orthogonal angular-momentum (J) and parity (π) projected deformed Slater determinants with good total angular momentum projection (M) as a stochastically selected basis,

$$|\Psi^{JM}\rangle = \sum_{n=1}^{N_b} f_n \sum_{K=-J}^J g_{nK} P_{MK}^J P^\pi |\phi_n\rangle, \quad (1)$$

where the deformed Slater determinant is $|\phi\rangle = \prod_{i=1}^A a_i^\dagger |-\rangle$ with the vacuum $|-\rangle$ and the creation operator $a_i^\dagger = \sum_{\alpha=1}^{N_{\text{sp}}} c_\alpha^\dagger D_{\alpha i}$. N_{sp} is specified by the cutoff of the single particle orbits, N_{shell} . One then stochastically samples the coefficient $D_{\alpha i}$ in all possible many-body basis states around the mean field solutions through the auxiliary fields and diagonalizes the Hamiltonian matrix within the subspace spanned by these bases N_b . Stochastically sampled bases are accepted so as to minimize the energy variationally. Therefore the MCSM can evade the so-called negative sign problem, which is the fundamental issue that cannot be avoided in quantum Monte Carlo methods. With increasing MCSM basis dimension, N_b , the ground state energy of a MCSM calculation converges from above to the exact value. The energy, therefore, always gives the variational upper bound in this framework.

An exploratory no-core MCSM investigation demonstrating a proof-of-the principle has been done for the low-lying states of the Beryllium isotopes by applying the existing MCSM algorithm with a core to a no-core problem [6]. Recent improvements on the MCSM algorithm have enabled significantly larger calculations [8, 9, 10]. We adopt these improvements in the present work [7, 8].

2.2 Recent developments

Among the recently achieved developments of our MCSM algorithm [8, 9, 10], in this subsection, we focus on two improvements: (1) the efficient computation of the two-body matrix elements (TBMEs) for the most time-consuming part in our calculations [8, 9] and (2) the energy-variance extrapolation for our MCSM (approximated) results to the FCI (exact) ones [8, 10]. There are other improvements such as the conjugate gradient method in the process of the basis search and the re-ordering technique in the energy variance extrapolations. Because of space limitations, we refer for the details of these improvements to Refs. [8, 10].

2.2.1 Efficient computation of the TBMEs

One of the main issues in the shell-model calculations is to evaluate TBMEs efficiently. As the matrix for the TBMEs is sparse in general, the indirect-index (list-vector) method is usually adopted in the shell-model calculations by keeping the value of the non-zero matrix elements and their indices. However, it tends to give slow performance due to the irregular memory access patterns.

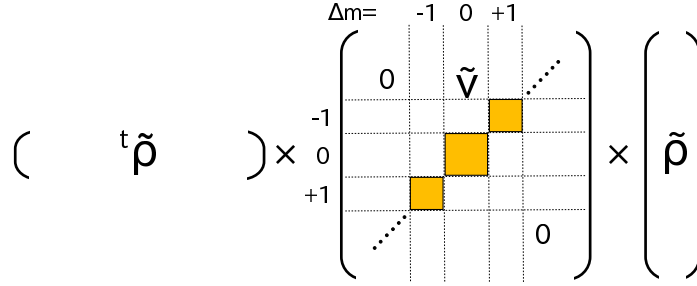


Figure 1: Schematic illustration of the $(\text{vector})^t \times (\text{matrix}) \times (\text{vector})$ operation.

Alternatively, in our recent MCSM code, we transform the sparse matrix to a block matrix with dense blocks by utilizing the symmetries of the two-body interaction [9]. The one-body density-matrix elements $\rho_{ll'}$ are grouped as $\tilde{\rho}(\Delta m)$ according to $\Delta m \equiv j_z(l') - j_z(l)$ where l and l' are the labels for the state. The TBMEs are also similarly categorized. Then, the two-body part of the Hamiltonian overlap can be expressed as schematically indicated in Fig. 1. Furthermore, most of the computational time is devoted to the $(\text{matrix}) \times (\text{vector})$ operation. It is usually repeated a number of times for different $\tilde{\rho}$'s. By binding N_{vec} $\tilde{\rho}$ -vectors into a matrix, repeated $(\text{matrix}) \times (\text{vector})$ operations are replaced by a $(\text{matrix}) \times (\text{matrix})$ operation at once. As shown in Fig. 2, we can achieve 70–80 % of the peak performance with $N_{\text{vec}} \sim 30$ –100 in the test case of the $(\text{matrix}) \times (\text{matrix})$ operation [9].

2.2.2 Energy-variance extrapolation to the FCI results

With increasing Monte Carlo basis dimension N_b , the MCSM results converge to the FCI results from above. In order to estimate the exact FCI answer, we extrapolate the energy and other observables evaluated by MCSM wave functions using the energy

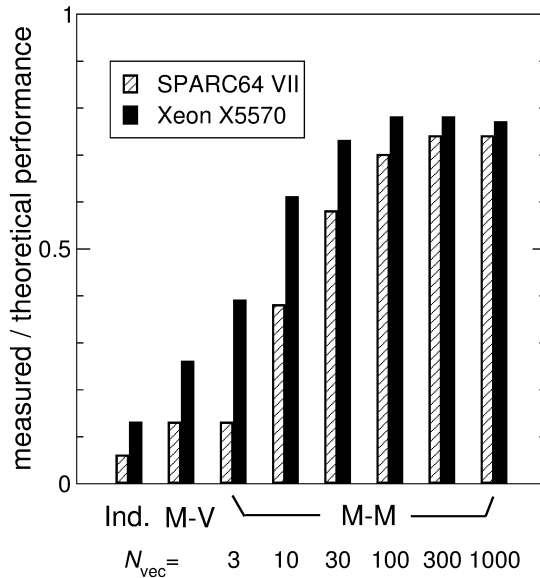


Figure 2: Comparison of the computational performance among the indirect-index method (Ind.), matrix-vector method (M-V) and matrix-matrix method (M-M) with different N_{vec} measured on the SPARC64 VII and Xeon X5570 systems. The values are normalized by their theoretical peak performance. See Ref. [9] for the details.

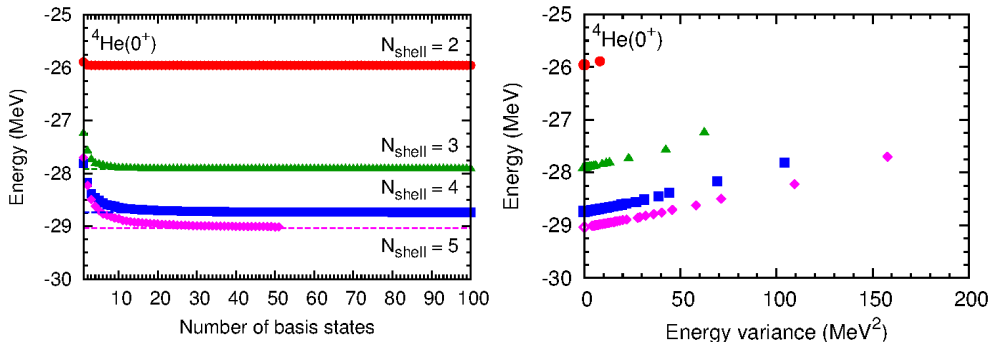


Figure 3: ${}^4\text{He}$ ground-state energies as functions of number of basis states (left) and energy variance (right). From the above to the bottom, the symbols (horizontal dashed lines in the left figure and open symbols at the zero energy variance in the right figure) are the MCSM (FCI) results in $N_{shell} = 2, 3, 4$ and 5 , respectively. See Ref. [7] for the details.

variance [8, 10]. That is, the MCSM results are plotted as a function of the evaluated energy variance, $\Delta E_2 = \langle \Psi | H^2 | \Psi \rangle - (\langle \Psi | H | \Psi \rangle)^2$, and then extrapolated to zero variance.

As a typical example, the behavior of the ground-state energies of ${}^4\text{He}$ (0^+) with respect to the number of basis states and to the energy variance are shown in Fig. 3. From Fig. 3, one can see that the MCSM results can be extrapolated to the FCI ones by using the quadratic fit function of $E(\Delta E_2) = E(\Delta E_2 = 0) + c_1 \Delta E_2 + c_2 (\Delta E_2)^2$ with the fitting parameters $E(\Delta E_2 = 0)$, c_1 , and c_2 .

3 Benchmarks

Augmented by the recent development of the MCSM algorithm [8, 9, 10], we have performed benchmarks of the no-core MCSM calculations [7, 8]. The main outcome of the initial benchmark project is summarized in Table 1. In Table 1, we illustrate the comparisons of the energies for each state and model space between the MCSM and FCI methods. The FCI gives the exact energies in the given model space while the MCSM gives approximate energies. Thus the comparisons between them show how well the MCSM works in no-core calculations. Furthermore, we also put the No-Core Full Configuration (NCFC) [12] results for the states of $4 \leq A \leq 10$ as the fully converged energies in the infinite model space.

For this benchmark comparison, the JISP16 two-nucleon interaction [13] is adopted and the Coulomb force is turned off. Isospin symmetry is assumed. The energies are evaluated for the optimal harmonic oscillator frequencies where the calculated energies are minimized for each state and model space. Here the contributions from the spurious center-of-mass motion are ignored for simplicity.

The comparisons are made for the states; ${}^4\text{He}$ (0^+), ${}^6\text{He}$ (0^+), ${}^6\text{Li}$ (1^+), ${}^7\text{Li}$ ($1/2^-$, $3/2^-$), ${}^8\text{Be}$ (0^+), ${}^{10}\text{B}$ (1^+ , 3^+) and ${}^{12}\text{C}$ (0^+). The model space ranges from $N_{shell} = 2$ to 5 for $A \leq 6$ (4 for $A \geq 7$). Note that the energies of ${}^{10}\text{B}$ (1^+ , 3^+) and ${}^{12}\text{C}$ (0^+) in $N_{shell} = 4$ are available only from the MCSM results. The M -scheme dimensions for these states are already close to or above the current limitation in the FCI approach. The numbers of basis states are taken up to 100 in $N_{shell} = 2-4$ and 50 in $N_{shell} = 5$.

As seen in Table 1, the energies are consistent with each other where the FCI results are available to within ~ 100 keV (~ 500 keV) at most of the MCSM results with(out) the energy-variance extrapolation of the MCSM results. The other

Table 1: Energies in MeV calculated for seven ground states and two excited states within the MCSM and FCI methods using the JISP16 *NN* interaction. The entries of the MCSM indicate the MCSM results before the energy variance extrapolation, while those of the “extrp” line denote the MCSM results after the extrapolations. Uncertainties in extrapolated results are quoted in parenthesis. See Ref. [7] for the details.

Nuclei	Method	E (MeV)				
		$N_{\text{shell}} = 2$	3	4	5	NCFC
${}^4\text{He}$ (0^+)	MCSM	-25.956	-27.914	-28.737	-29.011	-29.164(2)
	extrp			-28.738(1)	-29.037(1)	
	FCI	-25.956	-27.914	-28.738	-29.036	
${}^6\text{He}$ (0^+)	MCSM	-13.343	-19.186	-23.480	-25.080	-29.51(5)
	extrp		-19.196(1)	-23.687(4)	-26.086(76)	
	FCI	-13.343	-19.196	-23.684	-26.079	
${}^6\text{Li}$ (1^+)	MCSM	-14.218	-21.549	-26.757	-28.410	-33.22(4)
	extrp		-21.581(1)	-27.166(16)	-29.873(83)	
	FCI	-14.218	-21.581	-27.168	-29.893	
${}^7\text{Li}$ ($1/2^-$)	MCSM	-14.459	-24.073	-30.904		-39.8(1)
	extrp		-24.167(2)	-31.780(51)		
	FCI	-14.458	-24.165	-31.748		
${}^7\text{Li}$ ($3/2^-$)	MCSM	-17.232	-25.978	-32.494		-40.4(1)
	extrp		-26.061(4)	-33.272(89)		
	FCI	-17.232	-26.063	-33.202		
${}^8\text{Be}$ (0^+)	MCSM	-28.435	-41.242	-50.222		-59.1(1)
	extrp		-41.293(1)	-50.753(32)		
	FCI	-28.435	-41.291	-50.756		
${}^{10}\text{B}$ (1^+)	MCSM	-29.755	-41.965	-52.239		-68.5(1.5)
	extrp		-42.357(46)	-54.89(16)		
	FCI	-29.755	-42.338			
${}^{10}\text{B}$ (3^+)	MCSM	-34.221	-46.263	-56.346		-69.8(2)
	extrp		-46.618(22)	-58.41(13)		
	FCI	-34.221	-46.602			
${}^{12}\text{C}$ (0^+)	MCSM	-62.329	-76.413	-90.158		
	extrp		-76.621(4)	-91.957(43)		
	FCI	-62.329	-76.621			

observables besides the energies; the point-particle root-mean-square matter radii and electromagnetic moments also give reasonable agreements between the MCSM and FCI results. The detailed comparisons among the MCSM, FCI, and NCFC methods are discussed in Ref. [7].

4 Summary

By exploiting the recent development in the efficient computation of the Hamiltonian matrix elements between non-orthogonal Slater determinants and the technique of energy-variance extrapolation, the observables give good agreement between the MCSM and FCI results in the *p*-shell nuclei. From the benchmark comparison, the no-core MCSM is now verified in the application to the *ab initio* no-core calculations for light nuclei. The application to heavier nuclei is expected in the near future.

Acknowledgments

This work was supported in part by the SPIRE Field 5 from MEXT, Japan. We also acknowledge Grants-in-Aid for Young Scientists (Nos. 20740127 and 21740204), for Scientific Research (Nos. 20244022 and 23244049), and for Scientific Research on Innovative Areas (No. 20105003) from JSPS, and the CNS-RIKEN joint project for large-scale nuclear structure calculations. This work was also supported in part by the US DOE Grants No. DE-FC02-07ER41457, DE-FC02-09ER41582 (UNEDF SciDAC Collaboration), and DE-FG02-87ER40371, by US NSF grant 0904782, and through JUSTIPEN under grant no. DE-FG02-06ER41407. A part of the MCSM calculations was performed on the T2K Open Supercomputer at the University of Tokyo and University of Tsukuba, and the BX900 Supercomputer at JAEA. Computational resources for the FCI and NCFC calculations were provided by the National Energy Research Supercomputer Center (NERSC), which is supported by the Office of Science of the U.S. Department of Energy under Contract No. DE-AC02-05CH11231, and by the Oak Ridge Leadership Computing Facility at the Oak Ridge National Laboratory, which is supported by the Office of Science of the U.S. Department of Energy under Contract No. DE-AC05-00OR22725.

References

- [1] S. C. Pieper, R. B. Wiringa and J. Carlson, *Phys. Rev. C* **70**, 054325 (2004); K. M. Nollett, S. C. Pieper, R. B. Wiringa, J. Carlson and G. M. Hale, *Phys. Rev. Lett.* **99**, 022502 (2007).
- [2] G. Hagen, M. Hjorth-Jensen, G. R. Jansen, R. Machleidt and T. Papenbrock, *Phys. Rev. Lett.* **108**, 242501 (2012); **109**, 032502 (2012) and references therein.
- [3] P. Navrátil, J. P. Vary and B. R. Barrett, *Phys. Rev. Lett.* **84**, 5728 (2000); *Phys. Rev. C* **62**, 054311 (2000); S. Quaglioni and P. Navrátil, *Phys. Rev. Lett.* **101**, 092501 (2008); *Phys. Rev. C* **79**, 044606 (2009).
- [4] R. Roth, *Phys. Rev. C* **79**, 064324 (2009); R. Roth, S. Binder, K. Vobig, A. Calci, J. Langhammer and P. Navrátil, *Phys. Rev. Lett.* **109**, 052501 (2012).
- [5] T. Dytrych, K. D. Sviratcheva, C. Bahri, J. P. Draayer and J. P. Vary, *Phys. Rev. Lett.* **98**, 162503 (2007); *J. Phys. G.* **35**, 095101 (2008); T. Dytrych, K. D. Sviratcheva, J. P. Draayer, C. Bahri and J. P. Vary, *ibid.* **35**, 123101 (2008).
- [6] L. Liu, T. Otsuka, N. Shimizu, Y. Utsuno and R. Roth, *Phys. Rev. C* **86**, 014304 (2012).
- [7] T. Abe, P. Maris, T. Otsuka, N. Shimizu, Y. Utsuno and J. P. Vary, *AIP Conf. Proc.* **1355**, 173 (2011); *Phys. Rev. C* **86**, 054301 (2012).
- [8] N. Shimizu, T. Abe, Y. Tsunoda, Y. Utsuno, T. Yoshida, T. Mizusaki, M. Honma and T. Otsuka, *Prog. Theor. Exp. Phys.* 01A205 (2012).
- [9] Y. Utsuno, N. Shimizu, T. Otsuka and T. Abe, *Comput. Phys. Comm.* **184**, 102 (2013).
- [10] N. Shimizu, Y. Utsuno, T. Mizusaki, T. Otsuka, T. Abe and M. Honma, *Phys. Rev. C* **82**, 061305(R) (2010); N. Shimizu, Y. Utsuno, T. Mizusaki, M. Honma, Y. Tsunoda and T. Otsuka, *ibid.* **85**, 054301 (2012).
- [11] T. Otsuka, M. Honma, T. Mizusaki, N. Shimizu and Y. Utsuno, *Prog. Part. Nucl. Phys.* **47**, 319 (2001); Y. Utsuno, in *Proc. Int. Workshop*

Nucl. Theor. Supercomputing Era (NTSE-2012), Khabarovsk, Russia, June 18–22, 2012, edited by A. M. Shirokov and A. I. Mazur. Pacific National University, Khabarovsk, 2013 (*see this book*) p. 26.

- [12] P. Maris, J. P. Vary and A. M. Shirokov, *Phys. Rev. C* **79**, 14308 (2009); P. Maris, A. M. Shirokov and J. P. Vary, *ibid.* **81**, 021301 (2010); C. Cockrell, P. Maris and J. P. Vary, *ibid.* **86**, 034325 (2010).
- [13] A. M. Shirokov, J. P. Vary, A. I. Mazur and T. A. Weber, *Phys. Lett. B* **644**, 33 (2007); A. M. Shirokov, J. P. Vary, A. I. Mazur, S. A. Zaytsev and T. A. Weber, *ibid.* **621**, 96 (2005).

Deuteron-Equivalent Phase-Equivalent Transformation and Its Manifestation in Many-Body Systems

V. A. Kulikov^{a,b,c}, A. M. Shirokov^{a,b,c}, A. I. Mazur^b, J. P. Vary^c
and P. Maris^c

^a*Skobeltsyn Institute of Nuclear Physics, Moscow State University, Moscow 119991, Russia*

^b*Pacific National University, Tikhookeanskaya 136, Khabarovsk 680035, Russia*

^c*Department of Physics and Astronomy, Iowa State University, Ames, IA 50011-3160, USA*

Abstract

We propose a phase-equivalent transformation of NN interaction of a new type, the DET-PET transformation, which does not affect the wave function of the bound system (deuteron). The DET-PET properties and its manifestation in many-body systems are studied. In particular, we investigate the correlation of the ${}^3\text{H}$ and ${}^4\text{He}$ binding energies (Tjon line) in calculations with NN potentials obtained by means of DET-PET from the JISP16 NN interaction.

Keywords: *Phase-equivalent transformation; NN interaction.*

1 Introduction

One of the best *ab initio* approaches in the theory of light atomic nuclei is the No-core Full Configuration (NCFC) approach [1] based on extrapolation of results obtained in the No-core Shell Model (NCSM) calculations [2]. This approach does not imply any model assumption, a nucleon-nucleon interaction is the only input information utilized by NCFC. The NCFC approach was designed for calculations with the J -matrix Inverse Scattering Potentials (JISP) [3–5], the NN interactions obtained in the J -matrix inverse scattering approach, and was carefully tested in calculations with these NN interactions (see, e. g., Ref. [6–9]). Various versions of JISP interactions are related by phase-equivalent transformations (PETs) which do not affect the NN potential on-shell and hence preserve description of scattering phase shifts and deuteron binding energy, however modify the potential off-shell and therefore the description of few-body systems. A remarkable feature of JISP-type potentials is that they are able to reproduce nuclear properties without three-body nuclear forces reducing significantly the computer resources required for calculations. Up to now, nuclear studies were mostly performed [6–9] with the JISP16 interaction version [5, 10]; a more accurate interaction version JISP16₂₀₁₀ providing a better description of the binding energies of $A \geq 10$ nuclei, was introduced [11–13].

Recently we proposed a new type of PETs, a deuteron-equivalent transformation (DET-PET) [14], which properties we discuss here. Contrary to conventional PETs resulting in the modification of potential and bound state wave functions [3, 15–17], DET-PET guarantees that the transformed interaction generates not only the same scattering phase shifts but also the same bound state (deuteron) wave function as the initial untransformed interaction. To the best of our knowledge, such PETs have not been ever discussed in literature. Obviously, DET-PET preserves the description of deuteron observables. DET-PET, as well as any other PET, modifies a two-body interaction off-shell, and hence can be used for fitting potentials to many-body systems without violation of high-quality description of two-body data.

After introducing DET-PET, we discuss the DET-PET modification of the JISP16 NN interaction providing an accurate description of light nuclei [1, 2, 6–9]. A DET-PET manifestation in many-body systems is illustrated by the study ${}^3\text{H}$ and ${}^4\text{He}$ binding energies and their correlation (the so-called Tjon line [18]) in particular.

2 Theory

Two types of PETs are known in scattering theory: local PETs [15] that transform a local potential into another local potential and nonlocal PETs [16] which generate nonlocal potential terms. We focus the discussion here on nonlocal PETs.

The Schrödinger equation

$$H\Psi(E, r) = E\Psi(r) \quad (1)$$

describes a relative motion in two-body quantum system. The wave function $\Psi(r)$ can be expanded in infinite series of \mathcal{L}^2 functions which are supposed to form a complete orthonormalized basis. We denote these functions by $|a_n\rangle$, their orthonormalization condition is

$$\langle a_i | a_j \rangle = \delta_{ij}, \quad (2)$$

and the wave function expansion is

$$\Psi(E, r) = \sum_{n=0}^{\infty} c_n(E) |a_n\rangle. \quad (3)$$

Using this expansion we obtain an infinite set of algebraic equations defining the expansion coefficients $c_n(E)$,

$$\sum_{n'=0}^{\infty} (H_{nn'} - \delta_{nn'} E) c_{n'}(E) = 0, \quad (4)$$

where $H_{nn'} = \langle a_n | H | a_{n'} \rangle$ are the Hamiltonian matrix elements..

A phase-equivalent transformation of Hamiltonian H can be defined by means of a unitary transformation,

$$[\tilde{H}] = [U][H][U^\dagger], \quad (5)$$

where $[H]$ is the Hamiltonian H matrix in basis $\{|a_n\rangle\}$. The infinite unitary matrix $[U]$ is supposed to be of the form

$$[U] = [U^0] \oplus [I] = \begin{bmatrix} [U^0] & 0 \\ 0 & [I] \end{bmatrix}, \quad (6)$$

where $[I]$ is an infinite unit matrix and $[U^0]$ is a finite matrix mixing only a few low-lying states in a given basis. The Hamiltonian \tilde{H} is defined through its matrix $[\tilde{H}]$ in the initial basis $\{|a_n\rangle\}$.

Obviously, the Hamiltonians \tilde{H} and H have identical eigenvalue spectra and their eigenfunctions $\tilde{\Psi}(E, r)$ and $\Psi(E, r)$ differ by a linear combination of a finite number of functions $\{|a_n\rangle\}$. Any superposition of a finite number of \mathcal{L}^2 functions does not affect asymptotics of scattering wave functions, hence the Hamiltonian \tilde{H} is phase-equivalent to the initial Hamiltonian H .

The unitary operator U^0 can be written as

$$U^0 = \sum_{i,j \leq N'} |a_i\rangle \tilde{U}_{ij}^0 \langle a_j|. \quad (7)$$

$|a_i\rangle$ in Eq. (7) can be any \mathcal{L}^2 function, e. g., any oscillator function φ_l or any linear combination of oscillator functions φ_l . We shall use DET-PETs with the functions $|a_i\rangle$ defined as

$$|a_i\rangle = \sum_{l \leq N''} \alpha_i^l \varphi_l, \quad (8)$$

supposing that they fit the orthonormalization condition (2).

The transformation (5) becomes a DET-PET, i. e. it does not affect the deuteron wave function $|d\rangle$, when each of the functions $|a_i\rangle$ in Eq. (7) is orthogonal to $|d\rangle$:

$$\langle a_i | d \rangle = 0. \quad (9)$$

At this stage, we assert that we have obtained our DET-PET defined through the unitary transformation (5) with additional constraints (2), (7)–(9). The simplest DET-PET is obtained with arbitrary unitary matrix $[U^0]$ of the rank 2. In this case, $[U^0]$ is associated either with a rotation by the angle β , when $\det U^0 = +1$ (we will use the index $+$ to denote these transformations) or with a rotation by the angle β combined with reflection when $\det U^0 = -1$ (these type of transformations will be denoted by the index $-$).

We need to specify not only the unitary matrix but also the vectors $|a_1\rangle$ and $|a_2\rangle$ to define completely the simplest DET-PET. We use the deuteron wave function $|d\rangle$ to construct these vectors.

The function $|d\rangle$ can be expanded in infinite series of oscillator functions φ_i ,

$$|d\rangle = \sum_{i=0}^{\infty} d_i \varphi_i, \quad (10)$$

where, generally, all the coefficients d_i are non-zero,

$$d_i \neq 0. \quad (11)$$

Since the vectors $|a_1\rangle$ and $|a_2\rangle$ should fit Eq. (9), none of them can be one of the basis functions φ_i due to Eq. (10)–(11). The simplest way to construct the vectors $|a_1\rangle$ and $|a_2\rangle$ is to define each of them as a linear combination of two different oscillator functions φ_1 and φ_2 ,

$$|a_1\rangle = a_1^n \varphi_n + a_1^m \varphi_m, \quad (12)$$

$$|a_2\rangle = a_2^k \varphi_k + a_2^l \varphi_l, \quad (13)$$

The normalization of these vectors requires

$$(a_1^n)^2 + (a_1^m)^2 = 1, \quad (14)$$

$$(a_2^k)^2 + (a_2^l)^2 = 1. \quad (15)$$

Using Eqs. (9) and (10), we obtain

$$a_1^n d_n + a_1^m d_m = 0, \quad (16)$$

$$a_2^k d_k + a_2^l d_l = 0. \quad (17)$$

The solution of Eqs. (14) and (16) can be written as

$$a_1^n = + \frac{d_m}{\sqrt{d_n^2 + d_m^2}}, \quad (18a)$$

$$a_1^m = - \frac{d_n}{\sqrt{d_n^2 + d_m^2}}; \quad (18b)$$

the same type solution of Eqs. (15) and (17) for the vector $|a_2\rangle$ is

$$a_2^k = + \frac{d_l}{\sqrt{d_k^2 + d_l^2}}, \quad (19a)$$

$$a_2^l = - \frac{d_k}{\sqrt{d_k^2 + d_l^2}}. \quad (19b)$$

We need to find all coefficients $a_1^n, a_1^m, a_2^k, a_2^l$ fitting the orthogonality condition

$$\langle a_2 | a_1 \rangle = 0. \quad (20)$$

It means that all indexes k, l, m, n should be different, i. e., vectors $|a_1\rangle$ and $|a_2\rangle$ should be superpositions of different oscillator functions.

To define completely the simplest DET-PET, we need to fix the rotation angle β , the index \pm related to the sign of $\det U^0$, and the set of four oscillator functions used to build the vectors $|a_1\rangle$ and $|a_2\rangle$. To distinguish various DET-PET types we use notations like $0s2s1s2d^\pm$. In this example, the vector $|a_1\rangle$ is a linear combination of the oscillator states $0s$ and $2s$, the vector $|a_2\rangle$ is a linear combination of the oscillator states $1s$ and $2d$ and $\det U^0 = \pm 1$ respectively.

3 Results

We study modifications of JISP16 NN interaction induced by DET-PET. Vectors $|a_1\rangle$ and $|a_2\rangle$ [see Eqs. (12), (13)] are constructed as various superpositions of two low-lying oscillator functions $0s, 1s, 2s, 3s, 0d$ and $1d$. It is interesting to explore DET-PETs acting in the s channel only and compare them with DET-PETs mixing s and d channels in different ways. It is interesting also to investigate the transformations associated with both pure rotation and a rotation-reflection combination in case of each DET-PET type.

Plots of the np scattering wave functions in the sd coupled partial waves at laboratory energy $E_{lab} = 10$ MeV are presented in Figs. 1–3 in the K -matrix formalism. We use here the nomenclature and terminology adopted in Ref. [3]. The DET-PET $0s2s1s3s^\pm$ modifies significantly the large s wave component as is seen in Fig. 1. The modification of the small s wave component is much less pronounced. The d wave components, as expected, are nearly unaffected by $0s2s1s3s^\pm$. We observe modifications of both waves by DET-PETs $0s1s0d1d^\pm$ and $1s0d0s1d^\pm$ in Figs. 2 and 3, however, unlike the previous case, they are more pronounced in the small components of the scattering wave function since the DET-PETs mix s and d waves in these cases. We see that DET-PETs are able to generate essential modifications of scattering wave functions.

The NCSM calculations involve two basic parameters: the oscillator spacing $\hbar\Omega$ and model space dimension associated with the maximal excitation quanta N_{max} . It has been proposed [1] to use the $\hbar\Omega$ and N_{max} dependences to improve the results of calculations (the NCFC approach). Based on these dependences, we extrapolate the NCSM results to the infinite basis space limit and estimate the accuracy of the extrapolation. NCFC suggests two extrapolation methods: extrapolation A and extrapolation B [1]. The extrapolations A and B usually provide consistent results. We present here only the extrapolation A results based on the NCSM calculations with model spaces up through $N_{max} = 16$; we checked the consistency of our results with the ones obtained by extrapolation B in a number of cases. The evaluated uncertainties of results for binding energies presented here are less than 10 keV in most cases; in a few cases, we performed the NCSM calculations up to $N_{max} = 18$ to obtain the binding energies with uncertainty of about 10 keV.

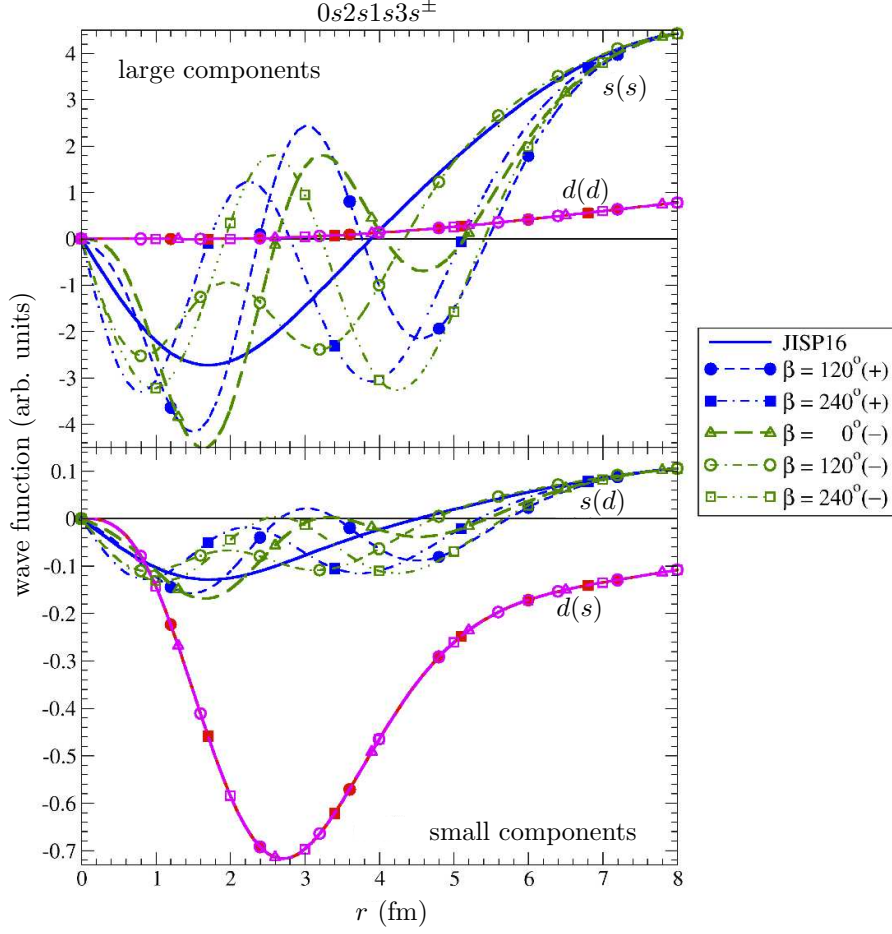


Figure 1: Large and small components of the np scattering wave function at the laboratory energy $E_{\text{lab}} = 10$ MeV in the sd coupled partial wave in the K -matrix formalism (see Ref. [3] for details and nomenclature) generated by JISP16 and NN interactions obtained from JISP16 by means of DET-PET $0s2s1s3s^{\pm}$. The sign of $\det U^0$ is given in the legends in parenthesis after the value of rotation angle β .

The binding energies of ${}^3\text{H}$ and ${}^4\text{He}$ nuclei were calculated with JISP16 NN interaction modified by DET-PETs $0s2s1s3s^{\pm}$, $0s1s0d1d^{\pm}$ and $1s0d0s1d^{\pm}$. The ranges of ${}^3\text{H}$ and ${}^4\text{He}$ binding energy variations for each DET-PET type are shown in Table 1. We see that the ${}^4\text{He}$ binding energy E_{α} can be varied by DET-PETs on the interval from 21.25 through 30.41 MeV, i. e., DET-PET can change E_{α} by more than 7 MeV

Table 1: Ranges of ${}^3\text{H}$ and ${}^4\text{He}$ binding energy variations (in MeV) caused by various types of DET-PET in comparison with the binding energies obtained with JISP16 and their experimental values.

${}^3\text{H}$	${}^4\text{He}$	${}^3\text{H}$	${}^4\text{He}$	${}^3\text{H}$	${}^4\text{He}$
	$0s2s1s3s^{+}$		$0s1s0d1d^{+}$		$1s0d0s1d^{+}$
7.2–8.37	21.25–28.49	7.67–8.41	23.50–28.83	7.98–8.64	25.79–30.36
	$0s2s1s3s^{-}$		$0s1s0d1d^{-}$		$1s0d0s1d^{-}$
7.25–8.35	21.46–28.59	7.68–8.39	23.46–28.91	8.05–8.67	26.18–30.41
JISP16			Experiment		
8.369(1)	28.299(1)			8.482	28.296

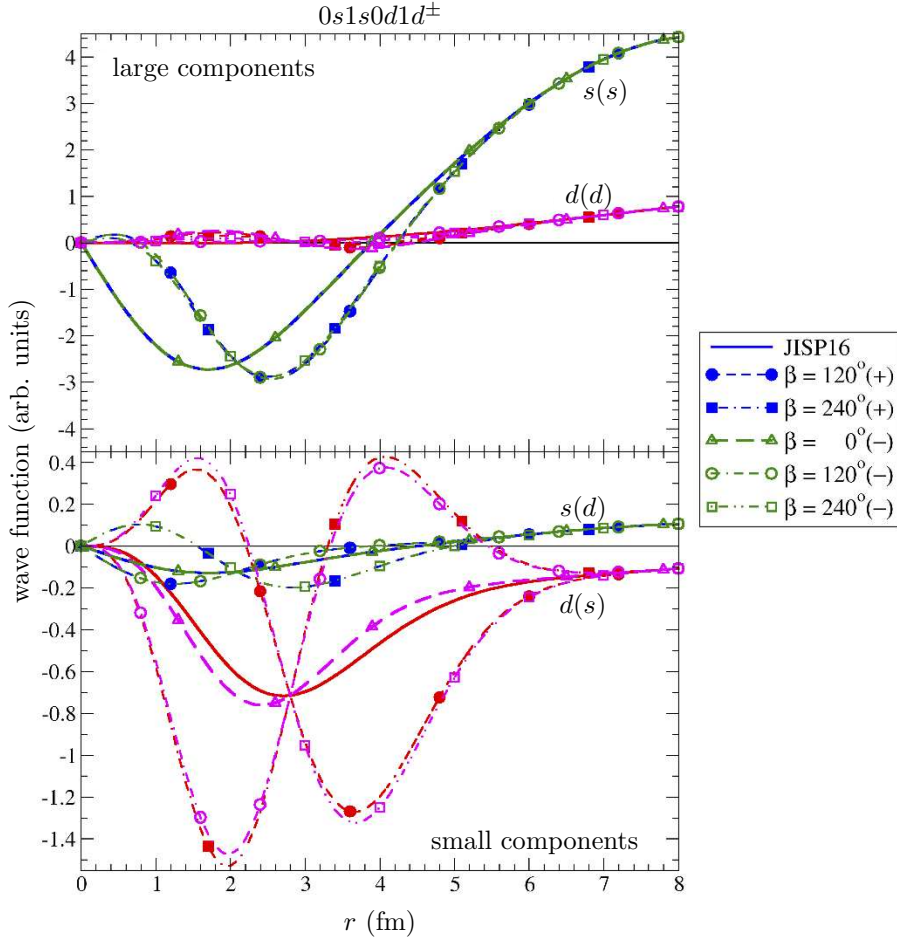
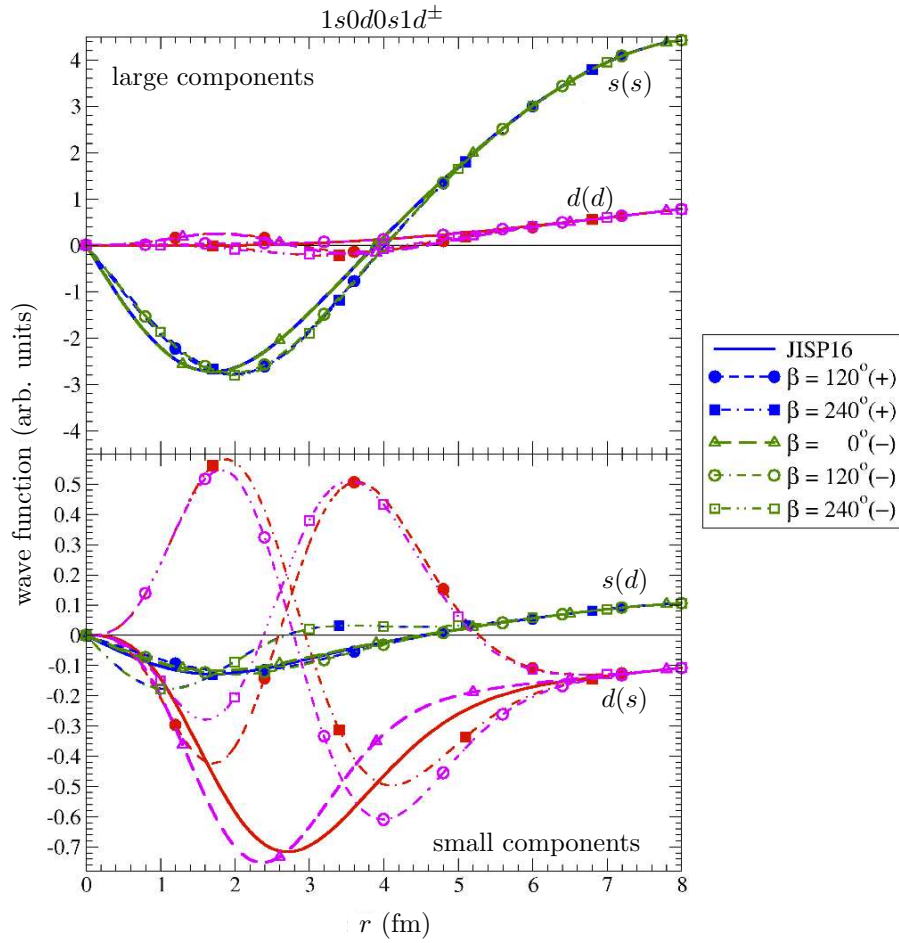
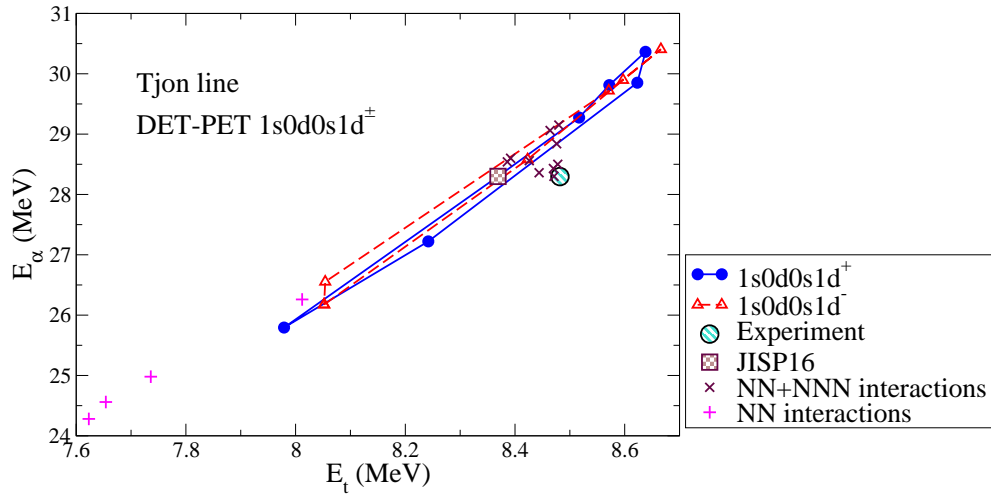


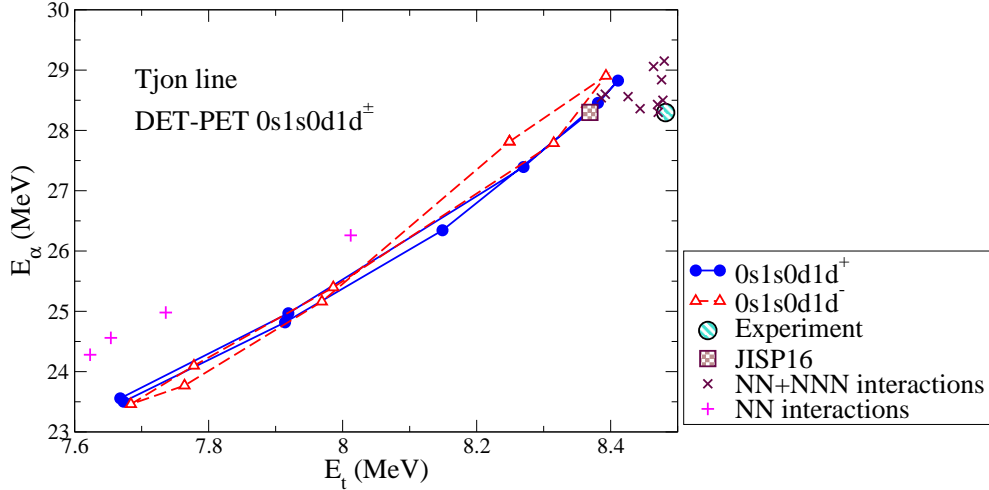
Figure 2: Same as Fig.1 but for DET-PET $0s1s0d1d^\pm$.

from its original value provided by the original JISP16 interaction. In the case of ${}^3\text{H}$ the range of the DET-PET binding energy variation is $7.21 \leq E_t \leq 8.67$, i. e., the ${}^3\text{H}$ binding energy E_t can be shifted by DET-PET by 1 MeV from its original JISP16 value.

The Tjon line [18] is a correlation of the ${}^3\text{H}$ and ${}^4\text{He}$ binding energies which was usually studied using results obtained with various NN interaction models allowing for two-nucleon forces only or various combinations of NN and NNN interactions (see, e. g., Ref. [19]). Here we study the Tjon line using families of NN potentials generated by DET-PET with continuous parameter which generate the same deuteron wave function. Two types of Tjon lines are shown in the each of Figs. 4-6. For each of DET-PETs mixing a particular combination of partial wave components, one of the Tjon line types corresponds to the case of pure rotation while the other corresponds to the rotation-reflection transformation. The symbols at the curves present the results obtained with different values of the angle β in the range from 0° through 360° . We use the step 60° for smooth regions of the curves and 30° in some cases around extremums of the ${}^3\text{H}$ and ${}^4\text{He}$ binding energies which are found usually around 180° and 360° . In addition to our results, we present in the figure also the experimental value and results of Refs. [19, 20, 21], obtained with other potential models which involve either two-nucleon forces only or combinations of two-nucleon and three-nucleon interactions.

We begin the discussion of the Tjon lines from the results obtained with the $1s0d0s1d^\pm$. It is seen from the Fig. 4 that our results are concentrated close to the Tjon line connecting the points extracted from other interactions. We recall here

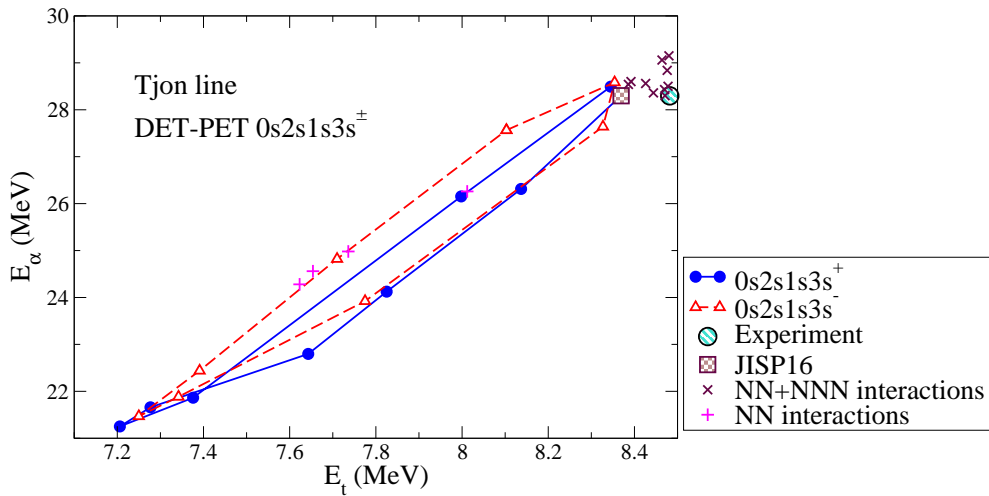
Figure 3: Same as Fig.1 but for DET-PET $1s0d0s1d^\pm$.Figure 4: Tjon line obtained with DET-PET $1s0d0s1d^\pm$ in comparison with results obtained with various NN and $NN+NNN$ interaction models from Refs. [19, 20, 21].

Figure 5: Same as Fig. 4 but for DET-PET $0s1s0d1d^\pm$.

that this DET-PET leave the large wave function components nearly unchanged while modifies essentially the small components as is seen from Fig. 3; such transformations correspond to strong modification of the tensor component of NN interaction.

Now we turn the discussion to the DET-PET $0s1s0d1d^\pm$. In this case, the DET-PET results in a very different range of binding energies variations (see the Table 1 and Fig. 5). The binding energies in this case are also correlated along a nearly straight line, however this line has a very different slope. As a result, our binding energy correlations around the maximal ${}^3\text{H}$ and ${}^4\text{He}$ binding energies accessible by this DET-PET are consistent with the correlations derived from other interaction models; however our correlations deviate from those obtained with other interactions as the binding energies decrease and the difference between our correlations and derived from other potential models become essential around the minimal binding energies. We have also a strong modification of the tensor component of the NN force in this case as seen in Fig. 2.

Let us discuss now the DET-PET $0s2s1s3s^\pm$. It results in the ${}^3\text{H}$ and ${}^4\text{He}$ binding energy correlation shown in Fig. 6. We see that in this case the Tjon lines transform

Figure 6: Same as Fig. 4 but for DET-PET $0s2s1s3s^\pm$.

into closed-loop curves surrounding large enough areas. In the case of the DET-PET $0s2s1s3s^-$ our Tjon curve surrounds the line derived from other NN interactions. The DET-PET $0s2s1s3s^+$ generates the Tjon curve shifted down from the Tjon line suggested by other interactions. This DET-PET $0s2s1s3s^\pm$ mixes only s -waves and does not affect the tensor component of the NN forces (see Fig. 1.)

4 Conclusions

We have introduced [14] a new type of phase-equivalent transformations, DET-PET, preserving the deuteron wave function and investigated transformations of the JISP16 NN interaction induced by few DET-PET versions mixing oscillator components in various combinations. We demonstrated that DET-PETs are able to modify significantly the np scattering wave functions. We studied DET-PET manifestations in the binding energies of ^3H and ^4He nuclei and found out that these bindings can be significantly changed by DET-PETs. We investigated also the correlation of these binding energies and found out that DET-PETs with some values of their parameters can significantly modify this correlation; more, in some cases, this correlation is washed out by DET-PET as compared with the conclusions based on the results obtained with other potential models. We speculate that DET-PET can be helpful in the further development of JISP-like NN interactions. It would be interesting to study DET-PET manifestations in binding energies and other observables of heavier nuclei.

Acknowledgements

This work was supported in part by the Ministry of Education and Science of the Russian Federation through the Contract 14.V37.21.1297 and by the Dynasty Foundation and Russian Foundation for Basic Research. This work was also supported in part by the US DOE Grants DESC0008485 (SciDAC-3/NUCLEI) and DE-FG02-87ER40371. AMS is also supported by the American Physical Society through the International Travel Grant Award Program. Calculations were performed on the supercomputers Hopper (NERSC) and Lomonosov (Moscow State University).

References

- [1] P. Maris, J. P. Vary and A. M. Shirokov, Phys. Rev. C **79**, 014308 (2009).
- [2] P. Navrátil, J. P. Vary and B. R. Barrett, Phys. Rev. Lett. **84**, 5728 (2000); Phys. Rev. C **62**, 054311 (2000).
- [3] A. M. Shirokov, A. I. Mazur, S. A. Zaytsev, J. P. Vary and T. A. Weber, Phys. Rev. C **70**, 044005 (2004).
- [4] A. M. Shirokov, J. P. Vary, A. I. Mazur, S. A. Zaytsev and T. A. Weber, Phys. Lett. B **621**, 96 (2005); J. Phys. G **31**, S1283 (2005).
- [5] A. M. Shirokov, J. P. Vary, A. I. Mazur and T. A. Weber, Phys. Lett. B **644**, 33 (2007).
- [6] A. M. Shirokov, J. P. Vary and P. Maris, in *Proc. 27th Int. Workshop Nucl. Theory, Rila Mountains, Bulgaria, 23–28 June, 2008*, edited by S. Dimitrova. Bulgarian Academy of Science, 2008, p. 205; arXiv:0810.1014 [nucl-th] (2008).
- [7] J. P. Vary, P. Maris and A. Shirokov, Int. J. Mod. Phys. E **17**, Suppl. 1, 109 (2008).

- [8] P. Maris, A. M. Shirokov and J. P. Vary, Phys. Rev. C **81**, 021301 (2010).
- [9] J. P. Vary, H. Honkanen, J. Li, P. Maris, A. M. Shirokov, S. J. Brodsky, A. Harindranath, G. F. de Teramond, E. G. Ng, C. Yang and M. Sosonkina, Pramana J. Phys. **75**, 39 (2010).
- [10] A Fortran code generating the JISP16 interaction matrix elements is available at <http://nuclear.physics.iastate.edu>.
- [11] A. M. Shirokov, J. P. Vary, V. A. Kulikov, P. Maris, A. I. Mazur and E. A. Mazur, Bull. Russ. Acad. Sci. Phys. **75**, 463 (2011).
- [12] A. M. Shirokov, V. A. Kulikov, P. Maris, A. I. Mazur, E. A. Mazur and J. P. Vary, EPJ Web Conf. **3**, 05015 (2010).
- [13] A. M. Shirokov, V. A. Kulikov, P. Maris, A. I. Mazur, E. A. Mazur and J. P. Vary, in *Proc. 3rd Int. Conf. Current Problems Nucl. Phys. At. Energy (NPAE—Kyiv2010). June 7–12, 2010, Kyiv, Ukraine*. Kyiv, 2011, Part I, p. 321; arXiv:1009.2993 [nucl-th] (2010).
- [14] A. M. Shirokov, V. A. Kulikov, A. I. Mazur, J. P. Vary and P. Maris, Phys. Rev. C **85**, 034004 (2012); Bul. Rus. Acad. Sci. Phys. **76**, 496 (2012).
- [15] R. G. Newton, *Scattering theory of waves and particles, 2nd. ed.* Springer-Verlag, New York, 1982.
- [16] F. Coester, S. Cohen, B. Day and C. M. Vincent, Phys. Rev. C **1**, 769 (1970).
- [17] A. M. Shirokov and V. N. Sidorenko, Phys. At. Nucl. **63**, 1993 (2000).
- [18] J. A. Tjon, Phys. Lett. B **56**, 217 (1975).
- [19] A. Nogga, H. Kamada and W. Glöckle, Phys. Rev. Lett. **85**, 944 (2000).
- [20] A. Nogga, P. Navrátil, B. R. Barrett and J. P. Vary, Phys. Rev. C **73**, 064002 (2006).
- [21] I. Brida, S. C. Pieper and R. B. Wiringa, Phys. Rev. C **84**, 024319 (2011).

Symmetry-Guided *Ab Initio* Approach to Light and Medium-Mass Nuclei

T. Dytrych^a, J. P. Draayer^a, K. D. Launey^a and D. Langr^b

^a*Department of Physics and Astronomy, Louisiana State University, Baton Rouge, LA 70803, USA*

^b*Department of Computer Systems, Czech Technical University, Prague, Czech Republic*

Abstract

We use algorithms of computational group theory to perform *ab initio* no-core shell model calculations in a $SU(3)$ -based coupling scheme for p -shell nuclei. Details given for ${}^6\text{Li}$ are reflective of similar results found for ${}^8\text{B}$, ${}^8\text{Be}$, ${}^{12}\text{C}$, and ${}^{16}\text{O}$, all of which exhibit a strong preference for large quadrupole deformations and a narrow set of intrinsic spin quantum numbers. Our results suggest that a small subspace of symmetry-adapted configurations can very closely approximate the exact solutions while allowing for exact factorization of the center-of-mass degrees of freedom. This, in turns, promises to allow us to extend the reach of the *ab initio* framework for structure and reaction studies towards sd -shell nuclei and beyond.

Keywords: *No-core shell model; $SU(3)$ coupling scheme; p -shell nuclei*

1 Introduction

Theoretical advances achieved in recent years in the development of realistic nuclear potential models [1, 2, 3, 4] along with progress in high performance computing have placed *ab initio* many-particle approaches [5, 6, 7] at the frontier of nuclear structure explorations. The *ab initio* methods are built on fundamental principles and therefore hold promise to provide predictive capabilities essential for a description of the structure and reactions of unstable and exotic nuclei, many of which are of high interest, e. g., in nucleosynthesis, but remain inaccessible even to experiment.

The no-core shell model (NCSM) [5] is a prominent *ab initio* method that has achieved a good description of low-lying states and associated spectroscopic properties up through p -shell nuclei [8, 9, 10]. The NCSM typically employs the Lanczos algorithm to solve the eigenvalue problem for a realistic Hamiltonian. Matrix elements of the Hamiltonian are calculated in a many-particle basis of m -scheme states, which are constructed as an antisymmetrized product of the harmonic oscillator single-particle wave functions, and carry the z -component of the total angular momentum along with the total parity as good quantum numbers. The main limitation of this approach, and the predictive power thereof, is inherently coupled with the combinatorial growth in the size of the many-particle model space with increasing nucleon numbers and expansion in the number of single-particle levels in the model space.

We developed an innovative *ab initio* model, the symmetry-adapted no-core shell model (SA-NCSM), which utilizes a many-particle basis that exploits the physically relevant $SU(3) \supset SO(3)$ group-subgroup chain. The significance of the $SU(3)$ group for a microscopic description of the nuclear collective dynamics can be readily seen from the fact that it is the symmetry group of the Elliott model [11], and a subgroup of the $Sp(3, \mathbb{R})$ symplectic model of nuclear collective motion [12, 13]. The concept of symmetry-adapted many-particle basis represents a powerful tool that allows one to winnow a model space to correlations indispensable for modeling important modes of nuclear collective dynamics, specifically nuclear deformation and cluster substructures, thereby overcoming the scale explosion bottleneck of *ab initio* nuclear structure

computations. Hence, the SA-NCSM framework holds promise to expand dramatically the reach of current *ab initio* approaches toward describing heavier mass nuclei with unprecedented accuracy.

2 *Ab initio* calculations in SU(3)-scheme basis

The basis states of the SA-NCSM are constructed in the proton-neutron formalism and are labeled by the physical $SU(3) \supset SO(3)$ subgroup chain quantum numbers $(\lambda \mu) \kappa L$, and by proton, neutron, and total intrinsic spins S_p , S_n , and S . The orbital angular momentum L is coupled with S to the total angular momentum J and its projection M_J . Each basis state is thus labeled in the SU(3)-scheme as

$$|\vec{\alpha} N(\lambda \mu) \kappa L; S_p S_n S; J M_J\rangle, \quad (1)$$

where N signifies the number of harmonic oscillator quanta with respect to the minimal number for a given nucleus. The deformation-related $(\lambda \mu)$ set of quantum numbers labels SU(3) irreducible representations (irreps) and bring forward important information about nuclear shapes and deformation. For example, (00) , $(\lambda 0)$ and (0μ) describe spherical, prolate and oblate shapes, respectively. The label κ distinguishes multiple occurrences of the same L value in the parent irrep $(\lambda \mu)$. The symbol $\vec{\alpha}$ schematically denotes the additional quantum numbers needed to unambiguously distinguish between irreps carrying the same $N(\lambda \mu) S_p S_n S$ quantum numbers. These irreps compose a well-defined subspace with a unique feature that allows for the complete separation of intrinsic and center-of-mass degrees of freedom [14].

The SA-NCSM implements a set of powerful algorithms [15, 16] which facilitate calculations of matrix elements of arbitrary (currently up to two-body, but expandable to higher-rank) operators in the SU(3)-scheme basis. This allows for both the evaluation of the Hamiltonian matrix elements, and the use of the resulting eigenvectors to evaluate other experimental observables. The underlying principle behind the SA-NCSM computational kernel is the SU(3) Wigner-Eckhart theorem, which allows the problem to be factorized into SU(3) reduced matrix elements (RMEs) and SU(3) coupling/recoupling coefficients. The former are calculated from a set of single-shell RMEs by the repetitive application of the SU(3) reduction formula for RMEs of operators acting on two independent proton and neutron subsystems, while the latter are computed using a publicly available library [17].

3 Structure of nuclear wave functions

Here we use the SA-NCSM with the bare JISP16 NN interaction [1] to calculate binding energies and determine low-lying eigenstates of ${}^6\text{Li}$, ${}^8\text{Be}$, ${}^{12}\text{C}$, and ${}^{16}\text{O}$ nuclei. The resulting wave functions are used to determine values or physical observables such as point-particle root-mean-square (rms) matter radii, electric quadrupole moments, magnetic dipole moments, reduced electromagnetic $B(E2)$ and $B(M1)$ transition strengths.

The expansion of calculated wave functions in a physically relevant SU(3)-scheme basis is illuminating salient features that emerge from the complex dynamics of strongly interacting many-particle systems. To explore the nature of the most important correlations, the probability distribution of intrinsic spins ($S_p S_n S$) and deformation-related $(\lambda \mu)$ quantum numbers of SU(3) for the lowest-lying $T = 0$ states of ${}^6\text{Li}$ were analyzed. Figure 1a shows the probability distribution of intrinsic spins across their Pauli-allowed deformations in the ground state of ${}^6\text{Li}$. This figure illustrates a facet common to low-energy solutions considered: a highly structured and coherent mix of intrinsic spins and SU(3) spatial quantum numbers that has heretofore gone unrecognized in other *ab initio* studies. These results clearly corroborate

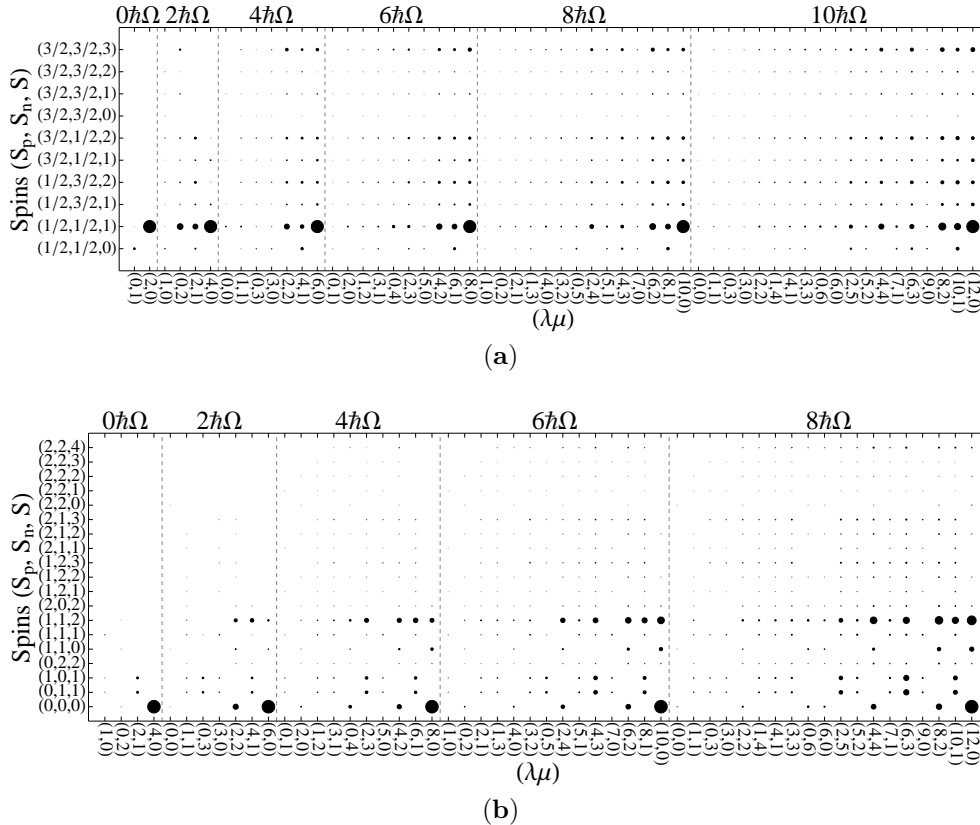


Figure 1: Probability distribution of proton, neutron, and total intrinsic spins ($S_p S_n S$) across their Pauli-allowed ($\lambda\mu$) deformations (horizontal axis) in the ground 1^+ state of ${}^6\text{Li}$ (a) and the ground 0^+ state of ${}^8\text{Be}$ (b) obtained with JISP16 bare interaction for $\hbar\Omega = 20$ MeV in $N_{\text{max}} = 10$ (a) and $N_{\text{max}} = 8$ (b) full model spaces. The area of each circle is proportional to the total probability of $N(\lambda\mu) S_p S_n S$ states normalized with respect to the total probability of $N(2+N0) \frac{1}{2} \frac{1}{2} 1$ and $N(4+N0) 0 0 0$ stretched states, respectively.

the much earlier phenomenological work carried out within the context of the Elliott SU(3) model [11].

Specifically, we found that over 99% of the SA-NCSM eigenstates are accounted for by a small fraction of intrinsic spin combinations. For instance, the lowest-lying eigenstates in ${}^6\text{Li}$ are almost entirely realized in terms of configurations characterized by the following intrinsic spin ($S_p S_n S$) quantum numbers: $(\frac{3}{2} \frac{3}{2} 3)$, $(\frac{1}{2} \frac{3}{2} 2)$, $(\frac{3}{2} \frac{1}{2} 2)$, and $(\frac{1}{2} \frac{1}{2} 1)$, with the last one carrying over 90% of each eigenstate. Likewise, the same spin components as in the case of ${}^6\text{Li}$ are found to dominate the ground state and the lowest 1^+ , 3^+ , and 0^+ excited states of ${}^8\text{B}$ (Table 1). Similarly, the ground state band of ${}^8\text{Be}$ and ${}^{12}\text{C}$ along with the ground state of ${}^{16}\text{O}$ are found to be dominated by many-particle configurations carrying total intrinsic spin of the protons and neutrons equal to zero and one, with the largest contribution due to $(S_p S_n S) = (0 0 0)$ configurations. This is illustrated in Figure 1b for the ground state of ${}^8\text{Be}$.

The mixing of ($\lambda\mu$) spatial quantum numbers induced by the SU(3) symmetry breaking terms of realistic interactions, exhibits a remarkably simple coherent pattern. One of its key features is the preponderance of a single $0\hbar\Omega$ SU(3) irrep, the so-called leading irrep, that is, the one characterized by the largest value of the second order SU(3) Casimir invariant, \hat{C}_2 , and hence corresponding to a large intrinsic

Table 1: Probability amplitude of the dominant ($S_p S_n S$) spin configuration and the dominant nuclear shapes according to Eq. (2) for the ground state of p -shell nuclei.

Nucleus	$(S_p S_n S)$	Prob. [%]	$(\lambda_0 \mu_0)$	Prob. [%]
${}^6\text{Li}$	$(\frac{1}{2} \frac{1}{2} 1)$	93.26	(2 0)	98.13
${}^8\text{B}$	$(\frac{1}{2} \frac{1}{2} 1)$	85.17	(2 1)	87.94
${}^8\text{Be}$	(0 0 0)	85.25	(4 0)	90.03
${}^{12}\text{C}$	(0 0 0)	55.19	(0 4)	48.44
${}^{16}\text{O}$	(0 0 0)	83.60	(0 0)	89.51

quadrupole deformation [18]. For instance, the low-lying $T = 0$ states of ${}^6\text{Li}$ project at 40%-70% level onto the prolate-like $0\hbar\Omega$ SU(3) irrep (2 0). For the considered states of ${}^8\text{B}$, ${}^8\text{Be}$, ${}^{12}\text{C}$, and ${}^{16}\text{O}$, qualitatively similar dominance of the leading $0\hbar\Omega$ SU(3) irreps is observed – (2 1), (4 0), (0 4), and (0 0) irreps, associated with triaxial, prolate, oblate, and spherical shapes, respectively. Such a clear dominance of the largest $0\hbar\Omega$ deformation within the low-lying states of p -shell nuclei points to the fact that the effective quadrupole-quadrupole interaction of the Elliott SU(3) model of nuclear rotations [11] is realized naturally within the framework of modern realistic interactions.

The analysis reveals that the dominant SU(3)-scheme states at each $N\hbar\Omega$ subspace are typically those with $(\lambda \mu)$ quantum numbers such that

$$\lambda + 2\mu = \lambda_0 + 2\mu_0 + N, \quad N = 0, 2, \dots, \quad (2)$$

where λ_0 and μ_0 denote labels of a leading SU(3) irrep at the $0\hbar\Omega$ ($N = 0$) subspace (Table 1). We conjecture that this coherent pattern of SU(3) quantum numbers reflects the presence of an underlying symplectic $\text{Sp}(3, \mathbb{R})$ symmetry of microscopic nuclear collective motion [12] that governs the low-energy structure of both even-even and odd-odd p -shell nuclei. This can be seen from the fact that configurations with a $(\lambda \mu)$ shape that satisfies condition (2) can be determined from the leading SU(3) irrep $(\lambda_0 \mu_0)$ through a successive application of a specific subset of the $\text{Sp}(3, \mathbb{R})$ symplectic $2\hbar\Omega$ raising operators. This subset is composed of the three operators, \hat{A}_{zz} , \hat{A}_{zx} , and \hat{A}_{xx} , that distribute two oscillator quanta in z and x directions, but none in y direction, thereby inducing SU(3)-scheme configurations with ever-increasing values of the Casimir invariant \hat{C}_2 . These three operators are the generators of the $\text{Sp}(2, \mathbb{R}) \subset \text{Sp}(3, \mathbb{R})$ subgroup [19], and give rise to a hierarchy of deformed shapes that are energetically favored by an attractive quadrupole-quadrupole interaction [13]. Furthermore, there is an apparent hierarchy among states that fulfill condition (2). In particular, the $N\hbar\Omega$ configurations with $(\lambda_0 + N \mu_0)$, the so-called stretched states, carry a noticeably higher intensity than the others. For instance, the $(2 + N 0)$ stretched states contribute at the 85% level to the ground state of ${}^6\text{Li}$. The sequence of the stretched-states, that is, the states with the highest possible deformations, can be formed from many-nucleon correlations of a leading SU(3) irrep by application of the \hat{A}_{zz} operator, which is the generator of $\text{Sp}(1, \mathbb{R}) \subset \text{Sp}(2, \mathbb{R}) \subset \text{Sp}(3, \mathbb{R})$ subgroup.

The revealed pattern of intrinsic spin and deformation mixing supports a symmetry guided truncation of the N_{max} model space. Clearly, one can take advantage of the physical relevance of the SU(3)-scheme basis to winnow the full space down to the most relevant configurations that support the strongest many-nucleon correlations of the system using the underlying $\text{Sp}(1, \mathbb{R}) \subset \text{Sp}(2, \mathbb{R}) \subset \text{Sp}(3, \mathbb{R})$ symmetry considerations. As noted previously, this truncation, while significantly reducing the size of the model space, also preserves the ability to factor out exactly the spurious center-of-mass degrees of freedom.

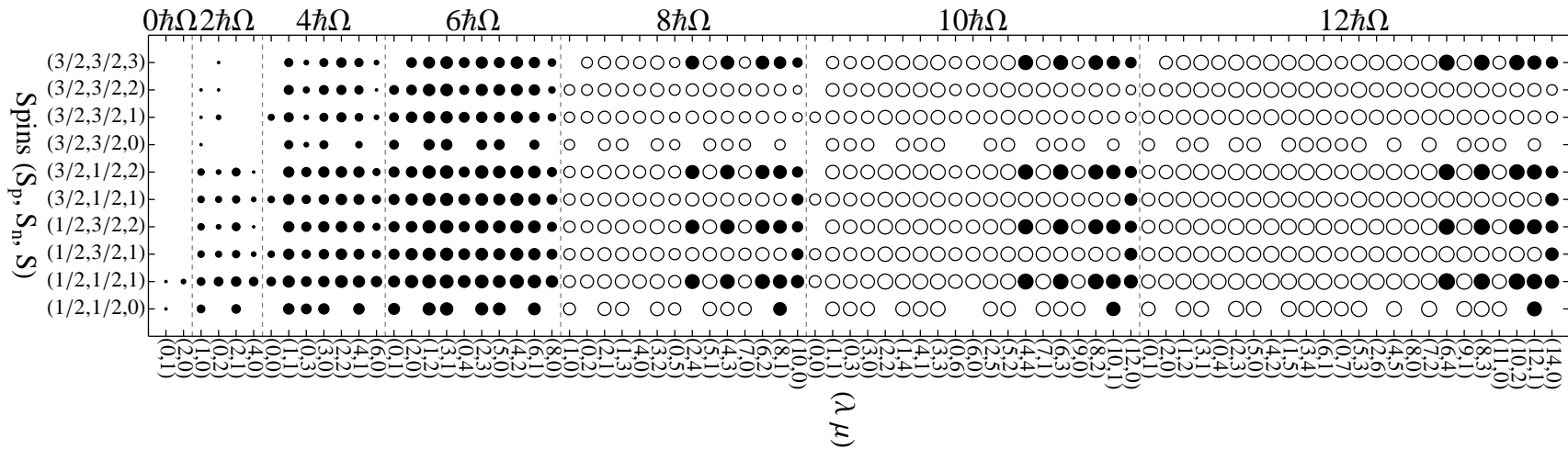


Figure 2: Pauli-allowed $(\lambda\mu)$ deformations and their proton, neutron, and total intrinsic spins $(S_p S_n S)$ for the positive-parity $J = 1$ states of ${}^6\text{Li}$ spanning the full $N_{\text{max}} = 12$ model space. Each circle represents basis states carrying the same $N(\lambda\mu) S_p S_n S$ quantum numbers, with the radius being proportional to \log_{10} of the number of such states. Configurations symbolized by the filled circles constitute the symmetry-truncated model space 12[6].

4 Efficacy of the SU(3) basis

To probe the adequacy of the symmetry-adapted approach for the *ab initio* modelling of nuclear structure, we used the calculated eigenstates to determine spectroscopic properties of low-lying $T = 0$ states of ${}^6\text{Li}$ using a model space winnowed through symmetry considerations, and compared the outcomes with the corresponding results obtained in the full $N_{\text{max}} = 12$ space. In the study, Coulomb and bare JISP16 NN interactions were used for $\hbar\Omega$ oscillator strengths ranging from 17.5 up to 25 MeV. The selected model space, depicted in Fig. 2 and denoted by 12[6], incorporates all configurations carrying excitations up to 6 oscillator quanta (labeled by [6]) and only a subset of the shapes and a few intrinsic spin components to realize the leading modes of nuclear collective motion for the higher $8\hbar\Omega$, $10\hbar\Omega$ and $12\hbar\Omega$ configurations. The model space 12[6] constitutes a small percentage of the full space. For example, the full $N_{\text{max}} = 12$ model space dimension is 4.9×10^7 whereas the dimensions of the 12[6] subspaces with total angular momenta $J = 1$, $J = 2$, and $J = 3$, are 4.3×10^5 (0.87%), 6.5×10^5 (1.32%), and 8.3×10^5 (1.70%), respectively.

The ground state binding energies calculated in 12[6] for oscillator energy $\hbar\Omega$ ranging from 17.5 to 25 MeV represent from 98% up to 98.7% of the full-space binding energy. Furthermore, the excitation energies of 3_1^+ , 2_1^+ , and 1_2^+ states calculated in 12[6] model space differ only by 20 keV to a few hundreds of keV from the corresponding full-space results, see Fig. 3.

As illustrated in Table 2 for $\hbar\Omega = 17.5$ MeV, the magnetic dipole moments agree to within less than about 0.3%, or 5% for the $\mu(2_1^+0)$. As the dipole moment is a short-range operator, the results suggest that it may suffice to include all low-lying $\hbar\Omega$ states up to a fixed limit, e. g. $N_{\text{max}} = 6$ for ${}^6\text{Li}$, to account for the most important short-range correlations.

To explore how closely one comes to reproducing the important long-range correlations of the full $N_{\text{max}} = 12$ space in terms of nuclear collective excitations within the more restricted 12[6] space, we compared observables that are sensitive to the tails of the wave functions; specifically, the point-particle rms matter radii, the electric quadrupole moments and the reduced electromagnetic $B(E2)$ transition strengths. The results for the rms matter radii, listed in Table 2 for $\hbar\Omega = 17.5$ MeV, agree to within 1%. Similarly, the 12[6] eigensolutions yield results for these quantities that track very closely with their full [12] space counterparts for all values of $\hbar\Omega$, as can be

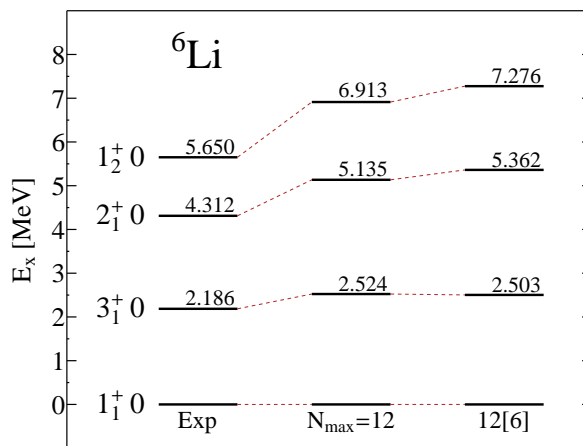


Figure 3: Experimental and theoretical excitation energies of $T = 0$ states of ${}^6\text{Li}$. Theoretical estimates were obtained at $\hbar\Omega = 22.5$ MeV in the full $N_{\text{max}} = 12$ (middle) and the symmetry-truncated 12[6] (right) model spaces.

Table 2: Magnetic dipole moments μ [μ_N] and point-particle rms matter radii [fm] of $T = 0$ states of ${}^6\text{Li}$ calculated in the full $N_{\text{max}} = 12$ and 12[6] model spaces for $\hbar\Omega = 17.5$ MeV. The experimental value for the 1^+ ground state is known to be $\mu = +0.822 \mu_N$.

	1_1^+0	3_1^+0	2_1^+0	1_2^+0
	μ			
Full $N_{\text{max}} = 12$	0.838	1.866	0.960	0.336
12[6] SU(3)	0.840	1.866	1.015	0.337
	rms			
Full $N_{\text{max}} = 12$	2.146	2.092	2.257	2.373
12[6] SU(3)	2.139	2.079	2.236	2.355

seen in Fig. 4. Also, as the $B(E2)$ strengths almost doubles upon increasing the basis space from $N_{\text{max}} = 6$ to $N_{\text{max}} = 12$ — a result that suggests that further expansion of the basis space may be needed to reach the experimental value of $21.8(4.8) e^2\text{fm}^4$, the close correlation between the $N_{\text{max}} = 12$ and 12[6] results is even more impressive.

5 Conclusion

We have developed a novel approach that capitalizes on advances being made in *ab initio* methods while exploiting exact and partial symmetries of nuclear many-body system. Using this approach we have demonstrated that the low-lying eigenstates of ${}^6\text{Li}$, ${}^8\text{Be}$, ${}^{12}\text{C}$, and ${}^{16}\text{O}$, which were obtained using the JISP16 NN interaction, exhibit a strong dominance of few intrinsic spin components and carry an intriguingly simple pattern of dominant deformations. The results very clearly underscore the significance of the SU(3) scheme, LS -coupling, and underlying symplectic symmetry in enabling an extension, through symmetry-guided model space reductions, of *ab initio* methods to heavier nuclei beyond ${}^{16}\text{O}$.

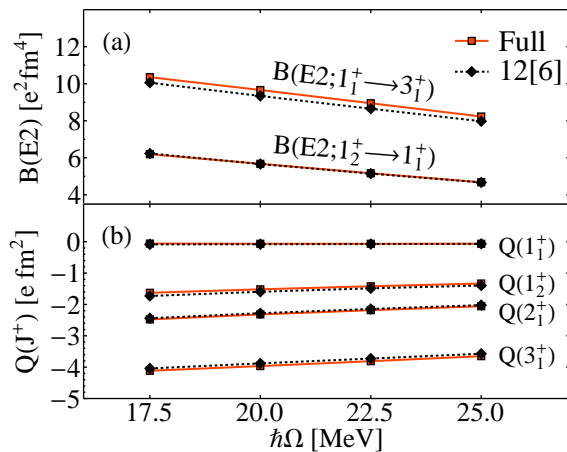


Figure 4: Electric quadrupole transition probabilities (a) and quadrupole moments (b) as a function of $\hbar\Omega$ for $T=0$ states of ${}^6\text{Li}$ calculated in the full $N_{\text{max}} = 12$ (solid red line) and symmetry-truncated 12[6] (dashed black line) model spaces.

Acknowledgments

This work was supported by the National Science Foundation under Grants No. PHY-0500291 and OCI-0904874, the US Department of Energy under Grants No. DEFG02-95ER-40934 and DE-SC0005248, the Southeastern Universities Research Association, and by the Research Corporation for Science Advancement under a Cottrell Scholar Award. This research used computing resources of the Louisiana Optical Network Initiative, LSU's Center for Computation & Technology, and the National Energy Research Scientific Computing Center, which is supported by the Office of Science of the U.S. Department of Energy under Contract No. DE-AC02-05CH11231.

References

- [1] A. M. Shirokov, J. P. Vary, A. I. Mazur and T. A. Weber, *Phys. Lett. B* **644**, 33 (2007).
- [2] R. B. Wiringa, V. G. J. Stoks and R. Schiavilla, *Phys. Rev. C* **51**, 38 (1995).
- [3] D. R. Entem and R. Machleidt, *Phys. Rev. C* **68**, 041001 (2003).
- [4] E. Epelbaum, *Prog. Part. Nucl. Phys* **57**, 654 (2006).
- [5] P. Navrátil, J. P. Vary and B. R. Barrett, *Phys. Lett.* **84**, 5728 (2000).
- [6] S. C. Pieper, K. Varga and R. B. Wiringa, *Phys. Rev. C* **66**, 044310 (2002).
- [7] M. Wloch, D. J. Dean, J. R. Gour, M. Hjorth-Jensen, K. Kowalski, T. Papenbrock and P. Piecuch, *Phys. Rev. Lett.* **94**, 212501 (2005).
- [8] P. Navrátil, S. Quaglioni, I. Stetcu and B. R. Barrett, *J. Phys. G* **36**, 083101 (2009).
- [9] R. Roth and P. Navrátil, *Phys. Rev. Lett.* **99**, 092501 (2007).
- [10] P. Navratil, V. G. Gueorguiev, J. P. Vary, W. E. Ormand and A. Nogga, *Phys. Rev. Lett.* **99**, 042501 (2007); arXiv: nucl-th/0701038 (2007).
- [11] J. P. Elliott, *Proc. Roy. Soc. A* **245**, 128 (1958).
- [12] G. Rosensteel and D. J. Rowe, *Phys. Rev. Lett.* **38**, 10 (1977).
- [13] D. J. Rowe, *Rep. Prog. Phys.* **48**, 1419 (1985).
- [14] F. Q. Luo, M. A. Caprio and T. Dytrych, *Nucl. Phys. A*, *in press* (2012), <http://dx.doi.org/10.1016/j.nuclphysa.2012.11.003>; arXiv:1211.3187 [nucl-th] (2012).
- [15] J. P. Draayer, Y. Leschber, S. C. Park and R. Lopez, *Comput. Phys. Comm.* **56**, 279 (1989).
- [16] C. Bahri and J. P. Draayer, *Comput. Phys. Comm.* **83**, 59 (1994).
- [17] Y. Akiyama and J. P. Draayer, *Comput. Phys. Comm.* **5**, 405 (1973).
- [18] O. Castanos, J. P. Draayer and Y. Leschber, *Z. Phys. A* **329**, 33 (1988).
- [19] D. R. Peteron and K. T. Hecht, *Nucl. Phys. A* **344**, 361 (1980).

Analytic Continuation Methods in Nuclear Reaction Theory and Indirect Approaches in Nuclear Astrophysics

L. D. Blokhintsev

Skobeltsyn Institute of Nuclear Physics, Lomonosov Moscow State University, Moscow 119991, Russia

Abstract

General properties of nuclear vertex constants and asymptotic normalization coefficients as well as the methods of their determination are discussed. Selected problems of nuclear astrophysics are outlined. A relation between asymptotic normalization coefficients (ANCs) and astrophysical nuclear reactions is elucidated. An analytic continuation of the effective range expansion is applied to the $\alpha + d$ system which is of interest for nuclear astrophysics.

Keywords: *Analytic continuation; vertex constants; lithium; nuclear astrophysics*

1 Introduction

Asymptotic normalization coefficients (ANCs) determine the asymptotics of nuclear wave functions in binary channels. ANCs are proportional to nuclear vertex constants (NVC) which determine the virtual processes $a \rightarrow b + c$ and are related directly to the residue in energy of the elastic bc scattering amplitude at the pole corresponding to the bound state a [1]. NVCs and ANCs are fundamental nuclear characteristics. They are used actively in analyses of nuclear reactions within various approaches. NVCs and ANCs extracted from one process can be used for the prediction of characteristics of other processes. Comparing empirical values of NVCs and ANCs with theoretical ones enables one to evaluate the quality of a model.

The ANC for the channel $a \rightarrow b + c$ determines a probability of the configuration $b + c$ in nucleus a at distances greater than the radius of nuclear interaction. Thus ANCs arise naturally in the expressions for cross sections of nuclear reactions between charged particles at low energies, in particular, of astrophysical nuclear reactions. Nuclear reactions in stars and stellar explosions are responsible for the synthesis of chemical elements. Note that due to the Coulomb barrier cross sections at astrophysical energies are so small that their direct measurement in laboratories is very difficult, or even impossible. Hence knowing ANCs allows one to obtain additional and important information on astrophysical nuclear reactions.

ANC values could be determined from microscopic calculations, however such calculations are rather tedious. The theoretical results should be matched to the empirical ones obtained from data on scattering and reactions. One of the promising methods to extract ANCs is the analytic continuation of bc -scattering data to a pole of a scattering amplitude corresponding to a bound state a lying in the unphysical region of negative energies. The most effective way of realization of that procedure is the analytic continuation of the effective range function.

The present paper deals with various problems related to the methods of analytic continuation of scattering data and to utilization of these methods for obtaining an information on astrophysical nuclear reactions. The plan of the paper is as follows. We discuss the general properties of NVCs and ANCs and methods of their determination

in Section 2. Section 3 is dedicated to selected problems of nuclear astrophysics including indirect methods of obtaining information on astrophysical nuclear reactions. The analytic continuation of the effective range expansion is applied in Section 4 to the $\alpha + d$ system which is of interest for nuclear astrophysics.

The system of units with $\hbar = c = 1$ is used throughout the paper.

2 ANCs and NVCs

2.1 Definition and properties of ANCs and NVCs

ANC $C_{abc}(LS)$ for the $a \rightarrow b + c$ channel is defined as a coefficient in the asymptotics of the radial overlap integral of the wave functions of a , b , and c nuclei [1]

$$I_{abc}(LS; r)|_{r \rightarrow \infty} \rightarrow C_{abc}(LS)W_{-\eta_b, L+1/2}(2\kappa r)/r. \quad (1)$$

Here r is the distance between b and c , L and S are the channel orbital angular momentum and the channel spin, $\kappa^2 = 2\mu\epsilon$, $\epsilon = m_b + m_c - m_a$, m_i is the mass of particle i , $\mu = m_b m_c / m_a$, $\eta_b = Z_b Z_c e^2 \mu / \kappa$ is the Sommerfeld parameter for the bound state and $W_{m,n}(z)$ is the Whittaker function.

Note that the asymptotical form (1) has been rigorously proved only for the simplest case when the composite system a consists of two elementary constituents. In that case the form (1) follows directly from the Schrödinger equation. For three- and more particle systems the asymptotics of overlap integrals may differ from (1) ('anomalous asymptotics') [2, 3].

NVC $G_{abc}(LS)$ is the on-shell matrix element of the virtual $a \rightarrow b + c$ process in the given partial-wave state LS . It is related to the amplitude of elastic bc scattering

$$\text{res} \langle LS | M^{J_a} | LS \rangle = (-1)^L G_{abc}^2(LS). \quad (2)$$

G_{abc} and C_{abc} are interrelated:

$$G_{abc}(LS) = -(\pi N_{bc} / \mu^2)^{1/2} L! / \Gamma(L + 1 + \eta_b) C_{abc}(LS). \quad (3)$$

N_{bc} arises due to the identity of nucleons. Its value depends on the way of antisymmetrization of wave functions: $1 \leq N_{bc} \leq (A_b + A_c)! / (A_b! A_c!)$, A_i being the mass number of the nucleus i . N_{bc} is often included into C_{abc} .

2.2 Methods of determination of ANCs and NVCs

1) Microscopic calculations of ANCs and NVCs are very tedious. Working in the configuration representation, one should make calculations in the asymptotical region where wave functions decrease exponentially entailing a low accuracy of the results. Using the momentum representation needs analytic continuation to imaginary values of momenta that is non-trivial. To author's knowledge, there are only two *ab initio* calculations of ANCs for nuclei with $A > 3$ [4, 5].

2) Theoretical results should be matched to the empirical ones obtained from analyses of scattering and reactions. There are various methods of extracting ANCs and NVCs from experimental data.

2a) Analysis of data on transfer reactions. If the pole diagram corresponding to the transfer of particle c contributes to the amplitude of the $a(x, y)b$ reaction, the differential cross section $\sigma(z)$ of this reaction possesses the 2nd order pole at $z = z_0$ ($z = \cos \theta$, θ is the c.m. scattering angle, $|z_0| > 1$) (Fig. 1). If one extrapolates the experimental values of $(z - z_0)^2 \sigma(z)$ to the pole position, one immediately obtains the value of $|G_{abc} G_{yxc}|^2$.²

²Account of the Coulomb interaction in the vertices of the pole diagram turns a pole to a branch point.

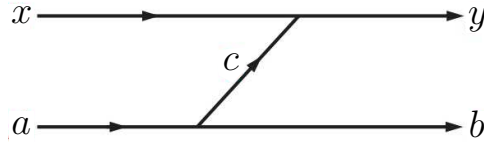


Figure 1: A pole diagram for a transfer reaction.

2b) Extrapolation in energy E of the partial-wave amplitude of elastic bc scattering (obtained by the phase-shift analysis) to the pole corresponding to the bound state a .

Note that the problem of using continuum-state data to obtain information on bound-state characteristics is non-trivial. It is written in the well-known monograph [6]: “It is impossible to obtain information on bound states from characteristics of scattering processes, as a matter of principle”.

This assertion is based on the inverse scattering theory which states that to restore a local potential one needs to know: i) phase shifts $\delta_L(E)$ for some arbitrary L in the whole region $0 \leq E < \infty$ and ii) $2N_L$ parameters characterizing N_L bound states for a given L [7]. One can use N_L binding energies and N_L ANCs as those parameters. Thus, if the system possesses bound states, knowing $\delta_L(E)$ is not sufficient to restore unambiguously a potential describing the system. Instead one gets an infinite set of so-called phase equivalent potentials (PEP) which lead to identical scattering phase shifts $\delta_L(E)$ but to different properties of the bound states for a given L .

There are various methods of constructing PEPs, e. g., Bargmann potentials [6] or the supersymmetric transformation [8]. In particular, the supersymmetric transformation can be used to construct a PEP which differs from the initial potential by any modification of the bound spectrum. A bound state can be added or suppressed; its binding energy and/or the ANC can be modified.

Hence within the formal potential approach with arbitrary potentials and without any additional conditions, it is impossible to determine unambiguously characteristics of bound states knowing only $\delta_L(E)$. A way to resolve this ambiguity problem is to use a natural requirement that amplitudes of processes are analytic functions of their kinematic variables. The analyticity property follows from a fundamental microcausality principle.

Using the analyticity and knowing the partial wave bc scattering amplitude $f_L(E)$ on some segment of the real positive semiaxis, one can continue analytically $f_L(E)$ to the unphysical region $E < 0$ and obtain both the position of the pole $E = -\epsilon < 0$ and the residue of $f_L(E)$ at that pole, that is, the NVC and ANC. (Note that we discuss here a principal side of the problem and not a practical realization of analytic continuation.)

Thus, in the case of potential scattering, knowing ϵ , ANC C_{abc} , and $f_L(E)$ at $0 \leq E < \infty$, one can construct unambiguously a local potential $V(r)$ using methods of the inverse scattering theory [7]. As a result, a unique ‘analytic’ potential would be selected out of the set of PEPs, which leads to the needed analytic properties of the scattering amplitude. This potential describes all bound and continuum states of the given system.

Now let us discuss why the characteristics of a bound state obtained by the direct analytic continuation of $f_L(E)$ from $E \geq 0$ to $E < 0$ may differ from the characteristics found by solving the bound state problem with the potential which describes correctly $f_L(E)$ at $E \geq 0$. To be specific, we will consider the case $L = 0$ (the index 0 will be omitted). According to [6, Chapter 12], one can continue analytically the amplitude $f(k)$ to the band $|\text{Im } k| < \alpha$ in the k plane if the potential $V(r)$ satisfies the condition

$$\int_0^\infty |V(r)|e^{2\alpha r} r dr < \infty, \quad \alpha > 0. \quad (4)$$

In the potential scattering theory the procedure of analytic continuation is based on the expression for the partial-wave amplitude in the form

$$f_L(k) = -\frac{\mu}{2\pi} \int_0^\infty \varphi_L(kr)V(r)\psi_L(kr)dr, \quad (5)$$

where φ_L and ψ_L are the plane wave and the exact wave function for given L , respectively. Upon the continuation of k from the positive semiaxis to the complex plane, the integrand in the r.h.s. of (5) develops terms proportional to $e^{2|\text{Im } k|V(r)}$ causing a divergence of the integral in (5) at the upper limit if $V(r)$ decreases insufficiently fast for $r \rightarrow \infty$. In this case, the condition (4) ceases to hold and the analytic continuation of the amplitude with the aid of expression (5) becomes impossible. However, there is a possibility to perform an analytic continuation by a different method. This can be done, for example, if an expression for $f_L(E)$ in the region $E \geq 0$ is known or if $f_L(E)$ for $E \geq 0$ can be approximated quite accurately by some analytic expression.

Consider a trivial example

$$f(z) = \int_0^\infty e^{(a-z)t} dt. \quad (6)$$

$f(z)$ is defined initially only for $\text{Re } z > \text{Re } a$ since the integral diverges if this inequality is violated. On the other hand, the integration can be performed explicitly: $f(z) = 1/(z - a)$. This expression defines a function analytic on the entire complex z plane with a pole at $z = a$.

Let us consider an instructive example of the Bargmann-type potential specified in [6, Chapter 14] as

$$V_d(r) = -\frac{\kappa}{\mu} \frac{d}{dr} \left[\sinh(br) \frac{g_d(\kappa, r)}{g_d(\kappa + b, r) - g_d(\kappa - b, r)} \right], \quad (7)$$

where $g_d(x, r) = x^{-1}[e^{-\kappa r} + d \sinh(xr)]$.

In the S wave, this potential has one bound state, its binding energy $\epsilon = \kappa^2/2\mu$. The respective normalized radial wave function has the form:

$$\varphi_d = 2\sqrt{\frac{\kappa d}{b^2 - \kappa^2}} \frac{\sinh(br)}{g_d(\kappa + b, r) - g_d(\kappa - b, r)}, \quad b > \kappa. \quad (8)$$

For the potential (7), the effective-range approximation coincides with the exact solution. In this case, the S wave phase shift is determined by the equation

$$k \cot \delta = -\kappa b/(b + \kappa) + k^2/(b + \kappa). \quad (9)$$

The S wave scattering amplitude has the form:

$$f(k) = \frac{e^{2i\delta} - 1}{2ik} = \frac{1}{k \cot \delta - ik} = \frac{b + \kappa}{-b\kappa + k^2 - i(b + \kappa)k}. \quad (10)$$

As follows from (10), $f(k)$ is independent of the parameter d ; that is, expression (7) determines a family of phase-equivalent potentials differing by the value of d . The amplitude $f(k)$ in (10) can be analytically continued to the region of imaginary k where it has a pole at $k = i\kappa$. Expressing the vertex constant G and the asymptotic normalization coefficient C in terms of the residue of $f(k)$ at this pole, one obtains:

$$G = \left[\frac{2\pi\kappa(b + \kappa)}{\mu^2(b - \kappa)} \right]^{1/2}, \quad C = \left[\frac{2\kappa(b + \kappa)}{b - \kappa} \right]^{1/2}. \quad (11)$$

On the other hand, a d -dependent expression for the asymptotic normalization coefficient can be obtained directly from (8). Specifically, one has:

$$C_d = \left[\frac{4\kappa(b + \kappa)}{d(b - \kappa)} \right]^{1/2}. \quad (12)$$

One can see that only at $d = 2$ does C_d given by (12) coincide with C given by (11). The fact that the value of $d = 2$ stands out becomes understandable upon examining the asymptotic behavior of the potential $V_d(r)$ for $r \rightarrow \infty$. It can be shown that this asymptotic behavior is given by

$$V_d(r) = \begin{cases} -V_1 e^{-2\kappa r}, & d \neq 2 \\ -V_2 e^{-2br}, & d = 2. \end{cases} \quad (13)$$

Since $b > \kappa$, the analyticity condition (4) for $V_d(r)$ is satisfied at $d = 2$ but is violated for all $d \neq 2$. Thus, an analytic continuation of the amplitude $f(k)$ to the region of imaginary values of k makes it possible to select among the set of phase-equivalent potentials $V_d(r)$, the only ‘analytic’ potential which corresponds to $d = 2$, and to find the relevant correct values of the ANC C . As for phase-equivalent potentials that are obtained by means of supersymmetry transformations, they develop at the origin a singularity of the $1/r^2$ type (see [8]) and, hence, do not satisfy the analyticity condition (4) just in the same way as the potential (7) does not satisfy it for $d \neq 2$.

So far, we have addressed a problem of a pure potential scattering of structureless particles. For practical purposes, including applications in astrophysics, the case of composite particles, first of all, nuclei, is of greater importance. Complex nuclei are the subject of many-body theory. An attempt at describing elastic nucleon-nucleus or nucleus-nucleus scattering within a two-body potential problem would lead to a complex-valued optical potential that is in general nonlocal and energy and angular-momentum dependent. Nevertheless, both the bound-state energy (which is usually known from experimental data) and the respective NVC and ANC can in principle be found as before by performing an analytic continuation of the partial-wave amplitude $f_L(E)$ to the region of negative values of E (imaginary values of k). This continuation may be realized in various ways. For example, $G_{6\text{Li}\alpha d}$ and $C_{6\text{Li}\alpha d}$ for the S wave state of the $\alpha + d$ system were found by two methods in Ref. [9]. Within the first method, an analytic Padé approximation of the scattering function $k \cot \delta$ obtained for $E > 0$ from the experimental phase shifts for the $d^4\text{He}$ scattering was analytically continued to the region $E < 0$, the parameters of the respective Padé approximants being determined by means of the χ^2 minimization. Within the second method, an effective two-body $d\alpha$ potential $V_{d\alpha}(r)$ describing the same $d^4\text{He}$ phase shifts was constructed using the harmonic oscillator basis and the χ^2 minimization. The next step of this method involved deriving the two-body $(d + \alpha)$ wave function for the ${}^6\text{Li}$ bound state in the potential $V_{d\alpha}(r)$ and determining the respective ANC $C_{6\text{Li}\alpha d}$. The two methods yielded rather close values of $C_{6\text{Li}\alpha d}$. Since the potential $V_{d\alpha}(r)$ was a finite sum of harmonic-oscillator wave functions, it obviously satisfied the necessary analyticity condition (4).

It should be noted that, in a general case, when b or c (or both) are composite systems, the ANC C_{abc} refers to the overlap integral $I_{abc}(r)$ which is normalized to the spectroscopic factor S_{abc} rather than to unity. If, however, the ANC is found by solving the bound-state problem for nucleus A on the basis of two-body potential V_{bc} fitted to the bc phase shifts, the respective two-body wave function should be normalized to unity. It would be incorrect to normalize this function to the independently determined spectroscopic factor as was done, for example, in Ref. [10] for the ${}^3\text{He} + \alpha$ system.

2.3 Inference

- Using the fundamental analyticity property of scattering amplitudes and analytic continuation methods allows one to obtain information on characteristics of nuclear bound states (including ANCs) from the phase shift data. Thus the ambiguity related to the existence of phase-equivalent potentials is removed.

2. The most efficient method of analytic continuation is the analytic approximation of the experimental values of $k \cot \delta$.
3. If the continuation is performed by fitting a two-body potential, one should use a potential which decreases rapidly enough at $r \rightarrow \infty$. One should set the spectroscopic factor equal to 1.

3 Selected problems of nuclear astrophysics

3.1 Introduction

Nuclear reactions in stars and stellar explosions are responsible for ongoing synthesis of chemical elements. Nuclear physics plays an important role as it determines the signatures of isotopic and elemental abundances found in spectra of stars, novae, supernovae, and X -ray bursts.

The rapid neutron capture process (r -process) is responsible for existence of about a half of stable nuclei heavier than iron. Capture cross sections for most of nuclei involved are hard if just impossible to measure in the laboratory and indirect experimental approaches have to be employed to gather the relevant nuclear structure information. The same concerns (p, γ) and (p, α) reactions.

Quantities used in nucleosynthesis calculations are reaction rates. A thermonuclear reaction rate is a function of density of interacting nuclei, their relative velocity and the reaction cross section. Extrapolation procedures are often needed to derive cross sections in the energy or temperature region of astrophysical relevance. While non-resonant cross sections can be extrapolated rather well to the low-energy region, the presence of continuum or sub-threshold resonances can complicate these extrapolations.

As an example of an important astrophysical reaction one may mention ${}^7\text{Be}(p, \gamma){}^8\text{B}$ which plays a major role for the production of high energy neutrinos from the β -decay of ${}^8\text{B}$. These neutrinos come directly from the center of the Sun and are ideal probes of the Sun structure. The reaction ${}^{12}\text{C}(\alpha, \gamma){}^{16}\text{O}$ is extremely relevant for the fate of massive stars. It determines if the remnant of a supernova explosion becomes a black hole or a neutron star. These two reactions are two examples only of a large number of reactions not known yet with an accuracy needed for astrophysics.

3.2 Thermonuclear cross sections and reaction rates

The number r of reactions between a target j and a projectile k per unit volume and time can be expressed as $r = \sigma v n_j n_k$ or, more generally, as

$$r_{jk} = \int \sigma v d^3 n_j d^3 n_k. \quad (14)$$

Here σ is the cross section, v is the relative velocity, n_j and n_k are number densities. For nuclei j and k in an astrophysical plasma obeying a Maxwell–Boltzmann distribution,

$$d^3 n_j = n_j \left(\frac{m_j}{2\pi kT} \right)^{3/2} \exp \left(-\frac{m_j v_j^2}{2kT} \right) d^3 v_j, \quad (15)$$

k is the Boltzmann constant and T is the absolute temperature. Using (15), one can rewrite (14) as

$$r_{jk} = \langle \sigma v \rangle_{jk}, \quad \langle \sigma v \rangle_{jk} = \left(\frac{8}{\pi \mu_{jk}} \right)^{1/2} (kT)^{-3/2} \int_0^\infty E \sigma(E) \exp \left(-\frac{E}{kT} \right) dE, \quad (16)$$

where $\langle \sigma v \rangle_{jk}$ is an average over the temperature distribution.

3.3 Charged particles

Experimentally, it is more convenient to work with an astrophysical S factor:

$$S(E) = E\sigma(E)e^{2\pi\eta}, \quad \eta = Z_j Z_k e^2/v. \quad (17)$$

Eq. (16) can be written as

$$\langle\sigma v\rangle_{jk} = \left(\frac{8}{\pi\mu_{jk}}\right)^{1/2} (kT)^{-3/2} \int_0^\infty S(E) \exp\left(-\frac{E}{kT} - \frac{b}{E^{1/2}}\right) dE, \quad b = 2\pi\eta E^{1/2}. \quad (18)$$

If one assumes that $S(E)$ is a constant, the integrand in (18) is maximal at the Gamow energy $E_0 = (bkT/2)^{2/3}$.

Measurements of cross sections at low energies are difficult and their extrapolation from higher energies can be complicated by presence of unknown resonances.

3.4 Nuclear reactions at the Sun

The Sun belongs to the main-sequence stars which energy is governed by the pp - and CNO-cycles (Figs. 2, 3).

According to the Standard Sun model, 99% of the Sun energy is generated by the pp -cycle (see Fig. 4), an ultimate result of this cycle is the transmutation of 4 protons into helium



The explosive nuclear burning in astrophysical environments produces short-lived exotic nuclei which in turn can play a role of targets in subsequent reactions. In addition, it involves a very large number of stable nuclei still not fully explored in experiments. Thus, it is necessary to be able to predict reaction cross sections and thermonuclear rates with the aid of theoretical models, moreover, a direct cross section measurement is often not possible with existing experimental techniques. For getting a reliable result obtained by extrapolation down to the stellar energies of the cross sections measured at the lowest possible energies in the laboratory, such extrapolations should have as strong theoretical foundation as possible. The theory is even more mandatory when excited or unstable nuclei are involved in the entrance channel.

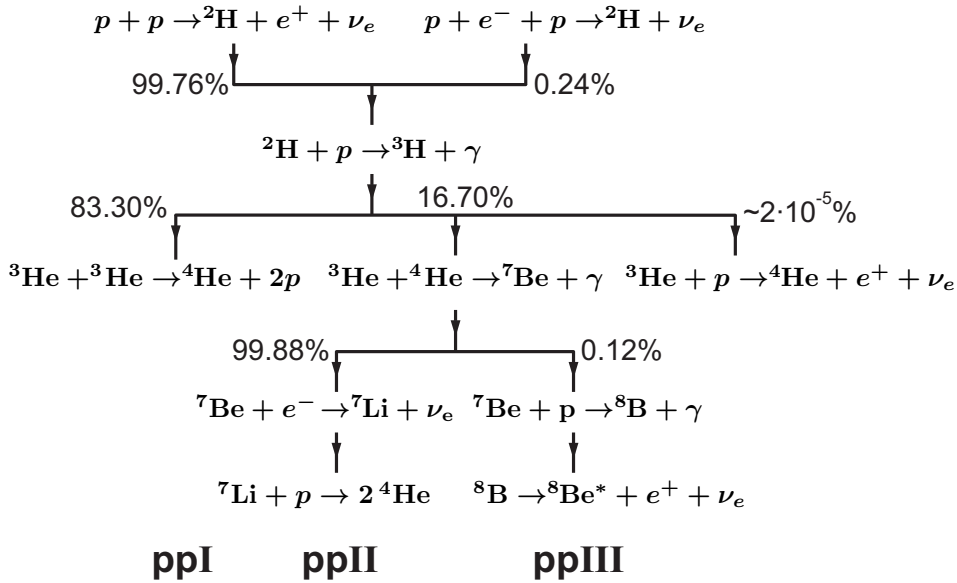


Figure 2: The pp -cycle.

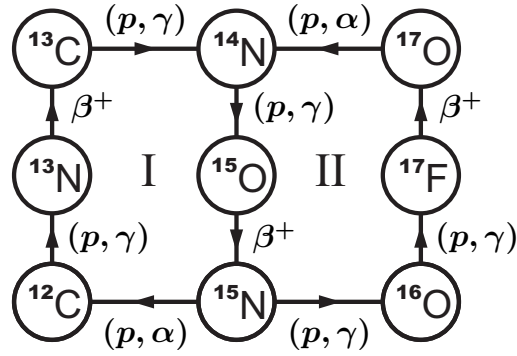


Figure 3: The CNO-cycle.

3.5 Nuclear reaction models

1. Potential models assume that physically important degrees of freedom are the relative motions between structureless nuclei in the entrance and exit channels. Interaction between them is described by an optical potential (usually of the Woods–Saxon form). DWBA is used practically for all astrophysical nuclear reactions. The only microscopic information is introduced in terms of spectroscopic factors and parameters of the optical potential. A deficiency of these models is that the optical parameters cannot be determined unambiguously.

2. In microscopic models, nucleons are grouped into clusters and completely antisymmetrized relative wave functions between various clusters are determined by solving the Schrödinger equation for a many-body Hamiltonian with an effective nucleon–nucleon interaction. Typical cluster models are based on the Resonating Group Method (RGM) or the Generator Coordinate Method (GCM). They result in a complicate set of coupled integro-differential equations. Modern nuclear shell-model calculations, such as the Monte Carlo shell model, or the no-core shell model, are able to provide the wave functions for light nuclei. However so far they cannot describe scattering wave functions with a sufficient accuracy.

Theoretical results for the astrophysical S -factor for the $^7\text{Be}(p, \gamma)^8\text{B}$ reaction are shown in Fig. 5. The dashed line corresponds to the no-core shell model and the dotted line to RGM. Experimental data are taken from 8 different papers. It is evident that

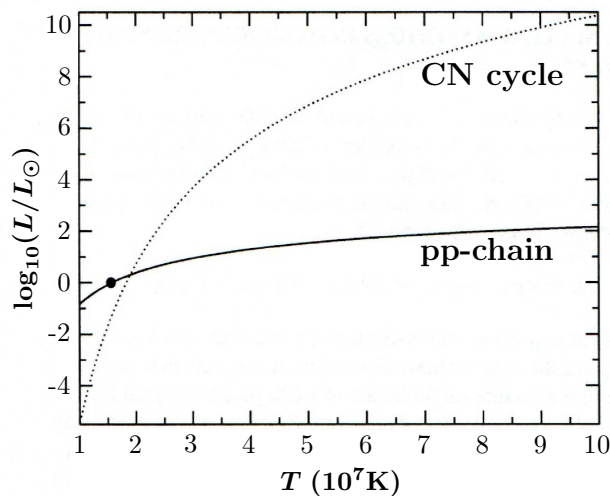


Figure 4: Relative energy release in stars as a function of temperature. The dotted line corresponds to the Sun.

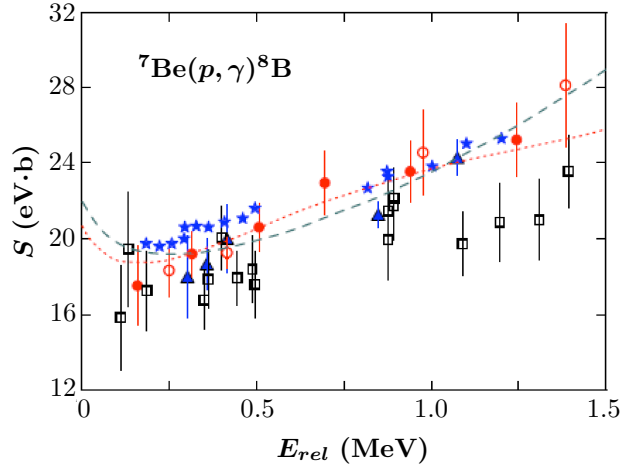


Figure 5: Comparison of theoretical and experimental results for the ${}^7\text{Be}(p, \gamma){}^8\text{B}$ reaction. Dashed line — no-core shell model, dotted line — RGM. See Ref. [11] for details.

both theory and experiment need improvement for this important reaction.

3. Field theories adopt a completely independent approach to nuclear physics calculations which does not use the concept of nuclear potentials. The basic method of field theories is to start with a Lagrangian for the fields which is used to construct Feynman diagrams that are utilized for practical calculations. Effective field theory (EFT) bypasses complications of quantum chromodynamics (QCD) using an expansion over a small parameter determined as a ratio of short-range and long-range (or ‘light’ and ‘heavy’) scales. Practically, for the NN interaction, this parameter is conventionally defined as

$$p = \frac{(1/a, B, k)}{\Lambda}, \quad (20)$$

where for the ‘light’ scale one uses either $1/a$ (a is the NN scattering length), or a typical binding energy B , or a typical nucleon momentum k . The ‘heavy’ scale is determined by the pion mass: $\Lambda \sim m_\pi \sim 140$ MeV.

The reaction rates dominated by the contributions from a few resonant or bound states, are often extrapolated to energies of astrophysical interest in terms of R -matrix fits. The appeal of these methods rests on the fact that analytical expressions can be derived from underlying formal reaction theories allowing for a rather simple parameterization of the data. However, the relation between the parameters of the R -matrix model and the experimental data is quite indirect.

A large fraction of the reactions of interest proceed through compound systems that exhibit high enough level densities to provide a reliable description of the reaction mechanism by means of statistical methods. A theoretical treatment of nuclear reactions leading to formation and decay of compound nuclei was developed by Ewing and Weisskopf based on two ideas: (a) the compound nucleus formation independence hypothesis as proposed by Niels Bohr, and (b) the reciprocity theorem, or time-reversal properties of the underlying Hamiltonian. This allows one to relate capture and decay cross sections.

3.6 Effects of electron screening

The form of the astrophysical S factor given in Eq. (17) assumes that the electric charges of nuclei are ‘bare’ charges. However, this is the case neither at very low laboratory energies, nor in stellar environments. In stars, the bare Coulomb interaction between nuclei is screened by the electrons in the plasma surrounding them. If one

measures reaction rates in the laboratory using atomic targets (always), the atomic electrons provide screening as well.

1. Stellar electron screening

Coulomb interaction between two charges in a neutral plasma can be written as

$$V(r) = \frac{Z_1 Z_2 e^2}{r} \exp\left(-\frac{r}{R_D}\right), \quad (21)$$

where R_D is the Debye radius, i. e., the scale over which mobile charge carriers in the neutral medium screen out electric fields. In the weak screening approximation

$$V(r) \approx \frac{Z_1 Z_2 e^2}{r} \left(1 - \frac{r}{R_D}\right) = V_b(r) + U_0, \quad U_0 = -\frac{Z_1 Z_2 e^2}{R_D}. \quad (22)$$

As a result, the reaction velocity increases:

$$\langle \sigma v \rangle_{\text{screened}} = f \langle \sigma v \rangle_{\text{bare}}, \quad f = \exp(|U_0|/kT). \quad (23)$$

2. Atomic electron screening

The laboratory screening can be evaluated in the adiabatic approximation assuming that the electron velocities in the target are much larger than the velocity of the relative motion between the projectile and the target nucleus. In this case, the electronic cloud at each instant time t adjusts to the ground state of a ‘molecule’ consisting of two nuclei separated by a time-dependent distance $R(t)$. Since the closest approach distance between the nuclei is much smaller than typical atomic cloud sizes, the binding energy of the electrons will be given by the ground-state energy B of the $Z_p + Z_t$ atom. Energy conservation implies that the relative energy between the nuclei increases by

$$U_e = B(Z_p + Z_t) - B(Z_t). \quad (24)$$

U_e is the screening potential. This energy increment enhances the fusion (tunneling) probability. Supposing that U_e/E is small and using (17) one gets

$$\sigma(E + U_e) = \exp\left[\pi\eta(E)\frac{U_e}{E}\right] \sigma(E). \quad (25)$$

The values of U_e needed to reproduce the experimental data are systematically larger than the theoretical ones by a factor of 2 (see Fig. 6).

3.7 Indirect methods of obtaining information on astrophysical nuclear reactions

1. Trojan horse method

The Trojan horse (TH) method [12, 13] is an efficient indirect method of determining cross sections of astrophysical binary reactions by measuring cross sections of reactions with three particles in the final state. Suppose we are interested in the $A + x \rightarrow B + y$ reaction at low (astrophysical) energies, and direct measurements are not possible due to the Coulomb barrier. Consider the reaction $1 + A \rightarrow 3 + B + y$ where $1 = 3 + x$. The particle 1 is the Trojan horse which includes the particle x .

Consider the quasifree mechanism (Fig. 7). At low momentum transferred from 1 to 3, this mechanism may provide a dominant contribution (or at least determine angular and energy dependencies). The respective differential cross section is of the form:

$$\sigma_{3\text{diff}}(A + 1 \rightarrow B + y + 3) = \text{KF} \psi^2(1 \rightarrow 3 + x) \bar{\sigma}_{2\text{diff}}(A + x \rightarrow B + y). \quad (26)$$

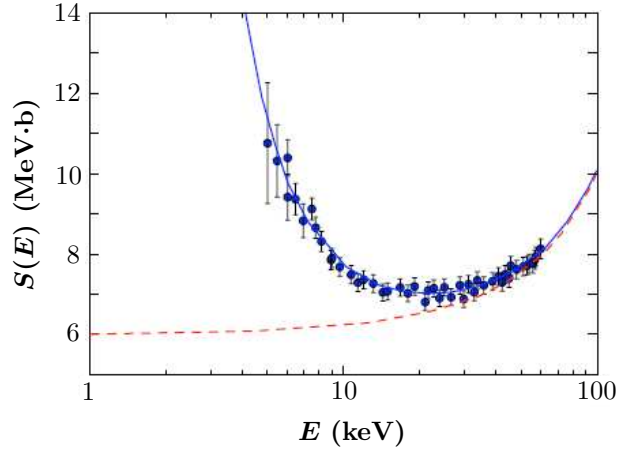


Figure 6: S factor of the ${}^3\text{He}(d,p){}^4\text{He}$ reaction. Dashed curve — bare nuclei, solid curve — screened nuclei with $U_e = 219$ eV (theory gives $U_e = 119$ eV). See Ref. [11] for details.

Here KF is a known kinematical factor, ψ is the wave function of particle 1 in the $3 + x$ channel, and $\tilde{\sigma}_{2\text{diff}}$ is a modified differential cross section of the binary reaction of interest. If KF and ψ are known, $\tilde{\sigma}_{2\text{diff}}$ can be extracted from $\sigma_{3\text{diff}}$.

As a typical example, one sets $1 = d$, $x = p$, and $3 = n$.

$\tilde{\sigma}_2$ differs from the free cross section σ_2 by particle x being virtual (off-shell), that is $\tilde{\sigma}_2$ describes the $A + x \rightarrow B + y$ process half-off-shell.

Using the energy and momentum conservation laws at the vertices of the diagram of Fig. 7, one can show that the relative momentum k of particles A and x in the initial state of the reaction $A + x \rightarrow B + y$ remains non-zero as the relative kinetic energy $E_{Ax} \rightarrow 0$. Hence the Coulomb barrier factor $e^{-2\pi\eta_i}$ does not appear in the expression for $\tilde{\sigma}_2$, and it remains finite at $E_{Ax} \rightarrow 0$. A qualitative explanation is that at the moment of interaction with particle A , the particle x has already penetrated through the Coulomb barrier in the initial state as a part of particle 1.

Note that the initial energy E_{A1} should be chosen large enough so that the reaction can be measured. A proper choice of E_{By} and the use of Eq. (26) and energy conservation in the $A + x \rightarrow B + y$ vertex makes it possible to find $\tilde{\sigma}_2$ at $E_{Ax} \approx 0$ and to obtain finally the desired $\sigma_2(E)$ and $S(E)$ at $E_{Ax} \approx 0$ by multiplying $\tilde{\sigma}_2$ by the Coulomb penetration factor. Practically, the absolute value of $S(E)$ is found by the normalization to direct measurements at higher energies when the penetration factor $e^{-2\pi\eta_i} \approx 1$.

By comparing the cross section thus obtained with the laboratory one at lower energies one can obtain an information on the electron screening effects. These effects which are essential at very low energies, are accounted by multiplication of the reaction cross section on the ‘bare’ nucleus by a factor $\exp(\pi\eta U_e/E)$ that results in the increase of the cross section. The TH cross section is free from the screening effects, and its

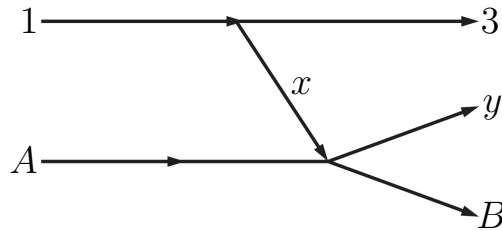


Figure 7: Quasifree mechanism of the $A + 1 \rightarrow B + y + 3$ reaction.

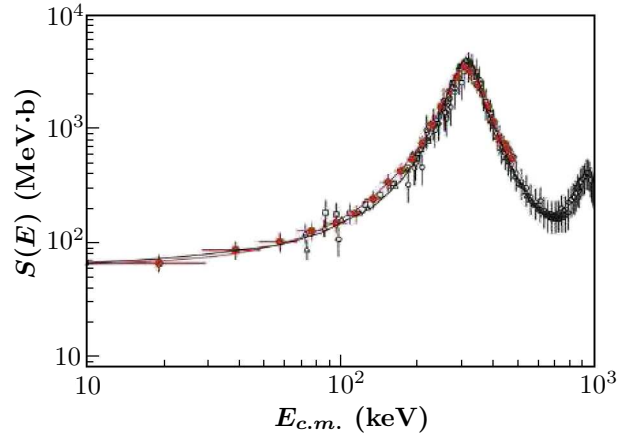


Figure 8: S factor for the $^{15}\text{N}(p, \alpha)^{12}\text{C}$ reaction obtained by the TH method using the $^{15}\text{N}(d, n\alpha)^{12}\text{C}$ reaction at $E_d = 60$ MeV (filled dots). Open dots are the direct data. The line corresponds to the Breit–Wigner fit. See Ref. [11] for details.

comparison with the directly measured cross section allows one to obtain information on U_e .

An example of using the TH method is shown in Fig. 8. Other examples of astrophysical reactions for which $S(0)$ has been found by the TH method (C.Spitaleri, A.M.Mukhamedzhanov *et al.*, INFN-LNS, Catania, Italy) are

- $^7\text{Li} + p \rightarrow \alpha + \alpha$ (from $d + ^7\text{Li} \rightarrow \alpha + \alpha + n$) ($x = p, 1 = d$).
- $^6\text{Li} + d \rightarrow \alpha + \alpha$ (from $^6\text{Li} + ^6\text{Li} \rightarrow \alpha + \alpha + \alpha$) ($x = d, 1 = ^6\text{Li}$).
- $^6\text{Li} + p \rightarrow \alpha + ^3\text{He}$ (from $d + ^6\text{Li} \rightarrow \alpha + ^3\text{He} + n$) ($x = p, 1 = d$).
- $^{11}\text{B} + p \rightarrow ^8\text{Be} + \alpha$ (from $d + ^{11}\text{B} \rightarrow ^8\text{Be} + \alpha + n$) ($x = p, 1 = d$).

2. Coulomb dissociation method

In this method, the use is made of experimental data on a dissociation of a fast nucleus a in the Coulomb field of a heavy nucleus A (e. g. lead): $a + A \rightarrow b + c + A$. The cross section of this process induced by a high energy virtual photon could be related to the photoeffect cross section ($\gamma + a \rightarrow b + c$), which by the time reversal is related to the sought-for cross section of the inverse process of the radiative capture $b + c \rightarrow \gamma + a$. The strong interaction effects could be reduced if one performs the measurements at low scattering angles when the electromagnetic interaction dominates over the nuclear one.

3. Method of asymptotical normalization coefficients (ANC)

The ANC method [14] allows one to determine $S(E \approx 0)$ for radiative capture reactions using their peripheral character due to the Coulomb (or centrifugal) barrier. The cross section for a non-resonant radiative-capture reaction $b(c, \gamma)a$ at zero relative energy depends only on the long-distance behavior of the $b + c$ wave function (and on the overlap of that extended wave function with that of a). The detailed short-range behavior of the scattering state $b + c$ or the bound state a is not relevant to the reaction mechanism. At large distances the overlap integral of the wave functions of b, c , and a is determined by the corresponding ANC (see (1)).

The ANC needed for the $b(c, \gamma)a$ reaction may be found from another nuclear reaction which mechanism includes the $b + c \rightarrow a$ vertex. Usually ANCs are determined from peripheral transfer reactions using the DWBA. The particle energies in the initial and final states can be large enough.

The test of the method has been performed by comparing the experimental data for the $^{16}\text{O}(^3\text{He}, d)^{17}\text{F}$ and $^{16}\text{O}(p, \gamma)^{17}\text{F}$ reactions. The ANC method was used for many radiative capture reactions. In particular, the $^{10}\text{B}(^7\text{Be}, ^8\text{B})^9\text{Be}$ and $^{14}\text{N}(^7\text{Be}, ^8\text{B})^{13}\text{C}$

Table 1: Summary of updates to S values and derivatives for CNO reactions. The table is taken from review [15].

Reaction	Cycle	$S(0)$ keV b	$S'(0)$ b	$S''(0)$ keV ⁻¹ b
$^{12}\text{C}(p, \gamma)^{13}\text{N}$	I	1.34 ± 0.21	2.6×10^{-3}	8.3×10^{-5}
$^{13}\text{C}(p, \gamma)^{14}\text{N}$	I	7.6 ± 1.0	-7.83×10^{-3}	7.29×10^{-4}
		7.0 ± 1.5		
$^{14}\text{N}(p, \gamma)^{15}\text{O}$	I	1.66 ± 0.12	-3.3×10^{-3}	4.4×10^{-5}
$^{15}\text{N}(p, \alpha)^{12}\text{C}$	I	$(7.3 \pm 0.5) \times 10^4$	351	11
$^{15}\text{N}(p, \gamma)^{16}\text{O}$	II	36 ± 6		
		64 ± 6		
		29.8 ± 5.4		
$^{16}\text{O}(p, \gamma)^{17}\text{F}$	II	10.6 ± 0.8	-0.054	
$^{17}\text{O}(p, \alpha)^{14}\text{N}$	II		Resonances	
$^{17}\text{O}(p, \gamma)^{18}\text{F}$	III	6.2 ± 3.1	1.6×10^{-3}	-3.4×10^{-7}
$^{18}\text{O}(p, \alpha)^{15}\text{N}$	III		Resonances	
$^{18}\text{O}(p, \gamma)^{19}\text{F}$	IV	15.7 ± 2.1	3.4×10^{-4}	-2.4×10^{-6}

reactions were used to obtain the S factor $S(0)$ for an important process $^7\text{Be}(p, \gamma)^8\text{B}$. Other examples of using the ANC method to calculate the $S(E = 0)$ for radiative capture processes are

$$^4\text{He}(d, \gamma)^6\text{Li}, \quad ^4\text{He}(^3\text{He}, \gamma)^7\text{Be}, \quad ^7,^9\text{Be}(p, \gamma)^{8,10}\text{B}, \quad ^8\text{B}(p, \gamma)^9\text{C}, \quad ^{11,13}\text{C}(p, \gamma)^{12,14}\text{N}, \\ ^{12-14}\text{N}(p, \gamma)^{13-15}\text{O}, \quad ^{17}\text{F}(p, \gamma)^{18}\text{Ne}, \quad ^{20}\text{Ne}(p, \gamma)^{21}\text{Na}.$$

The sensitivity of the extracted cross section to the parameters of the optical potential used in the DWBA, has been also tested.

Nowadays astrophysical factors $S(E \approx 0)$ for numerous astrophysical reactions and their derivatives with respect to energy are determined by various methods (see Table 1). However such data are not available for many important processes, and the accuracy of available data should be improved.

3.8 Nuclear experiments using beams of rare (unstable) isotopes

Unstable nuclei take part in many astrophysical nuclear processes (r -process, rp -process). Experiments using beams of such nuclei are performed actively nowadays. Two main mechanisms of formation and separation of exotic nuclei are:

1. Beams of short-lived nuclei are formed in a thin target and are separated in-flight;
2. Exotic nuclei are formed and stopped in a thick target and then are extracted and accelerated anew (on-line).

Several examples of important astrophysical processes with unstable nuclei measured recently are ($T_{1/2}$ is shown in brackets):

$$^7\text{Be}(53 \text{ d})(p, \gamma)^8\text{B}; \quad ^{13}\text{N}(10 \text{ m})(p, \gamma)^{14}\text{O}; \quad ^{19}\text{Ne}(17 \text{ s})(p, \gamma)^{20}\text{Na}; \quad ^{15}\text{O}(122 \text{ s})(\alpha, \gamma)^{19}\text{Ne}; \\ ^{18}\text{F}(110 \text{ m})(p, \alpha)^{15}\text{O}; \quad ^{14}\text{O}(71 \text{ s})(\alpha, p)^{17}\text{F}.$$

Along with cross section measurements, measuring of unstable nucleus masses is an important goal when dealing with radioactive beams. There are two main methods of mass determination: by energy release in reaction and by deflection of ions in electromagnetic fields.

Recently a considerable progress has been achieved in experimental nuclear astrophysics and in developing theoretical methods of describing astrophysical processes. The further progress in this field is related both with creation of the next generation of installations (GSI/FAIR in Germany and FRIB in the USA) and with modernization of existing installations (GANIL in France and TRIUMF in Canada).

4 Analytic continuation of effective range expansion for $\alpha + d$ system

One of the most widespread methods of obtaining information on bound states from scattering data is an analytic continuation in energy of data on the partial wave amplitude of elastic bc scattering to the pole corresponding to the bound state a . The most efficient way of realization of this procedure is the analytic continuation of the effective range (ER) function $K_L(k^2)$. This method was used successfully in several works (see Refs. [9,16–19]). In these works, NVCs and ANCs were determined for the processes ${}^6\text{Li} \rightarrow \alpha + d$ [9], ${}^2\text{He} \rightarrow p + p$, ${}^3\text{He} \rightarrow p + d$, ${}^8\text{Be} \rightarrow \alpha + \alpha$ [16], ${}^5\text{He}({}^5\text{Li}) \rightarrow n(p) + \alpha$ [17], ${}^{17}\text{O}({}^{17}\text{F}) \rightarrow n(p) + {}^{16}\text{O}$, ${}^{16}\text{O} \rightarrow {}^{12}\text{C} + \alpha$ [18] and ${}^7\text{Li}({}^7\text{Be}) \rightarrow \alpha + t({}^3\text{He})$ [19].

All cited works treated a one-channel elastic scattering. However, a description of scattering of particles with nonzero spins usually demands accounting for the channel coupling even in the absence of inelastic channels. The most typical situation induced by tensor forces is the case of two coupled channels, 1 and 2, with the same J^π but different L (L_1 and $L_2 = L_1 + 2$). A generalization of the ER expansion to the case of two coupled channels and its utilization for determination of ANCs and NVCs was considered in Refs. [20, 21] using the np scattering as an example. The formalism developed in Refs. [20, 21] can be applied to any two-channel nuclear system for which the results of the phase-shift analysis are known. One of similar important systems is ${}^6\text{Li}$ in the $\alpha + d$ channel. The ANC values for this system determine the cross section of the radiative capture ${}^4\text{He}(d, \gamma){}^6\text{Li}$ which is the main source of ${}^6\text{Li}$ formation in the Big Bang model. Direct measurement of this process at astrophysical energies is impossible due to the smallness of the cross section. Available data on the values of NVCs and ANCs for the ${}^6\text{Li} \rightarrow \alpha + d$ channel ($L = 0; 2$) are characterized by a large spread, especially by the spread of the D state constants G_2 and C_2 .

In the work [22], the NVCs and ANCs for ${}^6\text{Li} \rightarrow \alpha + d$ are obtained by analytic continuation of the two-channel ER expansion. Several sets of $d\alpha$ scattering phase shifts are used as an input.

1. The energy-dependent phase-shift analysis of Ref. [23] neglecting the coupling of $L = 0$ and $L = 2$ channels (set 1).
2. The energy-independent phase-shift analysis of Ref. [24] accounting for the channel coupling (set 2).
3. Faddeev calculations neglecting the Coulomb interaction [9] (set 3).

Combining sets 1 and 2 results in $C_0 = 2.3\text{--}2.4 \text{ fm}^{-1/2}$. Set 3 gives $C_0 = 2.0 \text{ fm}^{-1/2}$. A low accuracy of phase-shift analysis at low energies and simplicity of Faddeev equations used make it impossible to obtain an accurate value of the ANC for $L = 2$: $C_2 = 0.02\text{--}0.07 \text{ fm}^{-1/2}$. The sign of C_2 (relative to C_0) appears to be positive.

The method developed in Refs. [20, 21] and utilized in Ref. [22] considers elastic channels only. On the other hand, low-lying inelastic thresholds may modify the ER expansion. The simplest way to allow for an inelastic channel at $E = E_0$, is to include in the ER expansion an additional term which is complex at $E > E_0$. The form of this term should provide the correct analytic behavior of scattering amplitudes at the threshold $E = E_0$. According to the general theory of singularities of Feynman diagrams, a singular part of a scattering amplitude near a threshold

behaves as $(E - E_0)^{(3n-5)/2}$ for even n and as $(E - E_0)^{(3n-5)/2} \ln(E - E_0)$ for odd n , where $n = 2, 3, 4, \dots$ is a number of intermediate particles at the threshold.

The work on accounting for inelastic channels in the ER expansion for ad scattering is in progress.

References

- [1] L. D. Blokhintsev, I. Borbeli and E. I. Dolinskii, Part. Nucl. **8**, 485 (1977).
- [2] L. D. Blokhintsev, Yad. Fiz. **34**, 944 (1981).
- [3] L. D. Blokhintsev, Izv. RAN, Ser. Fiz., **65** 74 (2001).
- [4] M. Viviani, A. Kievsky and M. Rosati, Phys. Rev. C **71**, 024006 (2005).
- [5] K. M. Nolett and R. B. Wiringa, Phys. Rev. C **83**, 041001 (2011).
- [6] R. G. Newton, *Scattering theory of waves and particles, 2nd. ed.* Springer-Verlag, New York, 1982.
- [7] K. Chadan and P. C. Sabatier, *Inverse problems of quantum scattering theory.* Springer-Verlag, New York, 1977.
- [8] E. Witten, Nucl. Phys. B **188**, 513 (1981).
- [9] L. D. Blokhintsev, V. I. Kukulín, A. A. Sakharuk and D. A. Savin, Phys. Rev. C **48**, 2390 (1993).
- [10] K. M. Nolett, Phys. Rev. C **63**, 054002 (2001).
- [11] C. A. Bertulani and A. Gade, Phys. Rep. **485**, 195 (2010).
- [12] G. Baur, Phys. Lett. B **178**, 35 (1986).
- [13] C. Spitaleri, in *Problems of fundamental modern physics, Vol. II*, edited by R. Cherubini, P. Dalpiaz and B. Minetti. World Sci., 1990, p. 21.
- [14] A. M. Mukhamedzhanov and R. E. Tribble, Phys. Rev. C **52**, 3418 (1999).
- [15] E. G. Adelberger *et al.*, Rev. Mod. Phys. **83**, 195 (2011).
- [16] V. O. Yeremenko, L. I. Nikitina and Yu. V. Orlov, Izv. RAN, Ser. Fiz. **71**, 819 (2007).
- [17] Yu. V. Orlov, B. F. Irgaziev and L. I. Nikitina, Phys. At. Nucl. **73**, 757 (2010).
- [18] J.-M. Sparenberg, P. Capel and D. Baye, Phys. Rev. C **81**, 011601 2010.
- [19] R. Yarmukhamedov and D. Baye, Phys. Rev. C **84**, 024603 (2011).
- [20] L. D. Blokhintsev, Phys. At. Nucl. **74**, 1008 (2011).
- [21] L. D. Blokhintsev, Izv. RAN, Ser. Fiz., **76** 481 (2012).
- [22] L. D. Blokhintsev and D. A. Savin, Few Body Syst. (in press).
- [23] V. M. Krasnopol'sky, V. I. Kukulín, E. V. Kuznetsova, J. Horáček and N. M. Queen, Phys. Rev. C **43**, 822 (1991).
- [24] B. Jenny, W. Grüebler, V. König, P. A. Schmelzbach and C. Schweizer, Nucl. Phys. A **397**, 61 (1983).

On Nature of Bound and Resonance States in ^{12}C

V. S. Vasilevsky^a, F. Arickx^b, W. Vanroose^b
and J. Broeckhove^b

^a*Bogolyubov Institute for Theoretical Physics, Kiev, Ukraine*

^b*Departement Wiskunde-Informatica, Universiteit Antwerpen, Antwerpen, Belgium*

Abstract

We investigate both bound and resonance states in ^{12}C embedded in a three- α -cluster continuum using a three-cluster microscopic model. The model relies on the Hyperspherical Harmonic basis to enumerate channels describing the three-cluster discrete and continuous spectrum states. It yields the most probable distribution of three α -clusters in space, and the dominant decay modes of the three-cluster resonances.

Keywords: *Cluster model; resonance state; Hoyle state; hyperspherical harmonics*

1 Introduction

The ^{12}C nucleus is an interesting example of the so-called Borromean nuclei as it has no bound states in any two-cluster subsystem of its three-cluster configuration. The lowest dissociation threshold (7.276 MeV above the ground state) is that of a three α particles disintegration. This three-cluster configuration is thus responsible to a great extent for the formation of a few bound and many resonance states. The next threshold is of a two-cluster nature: $^{11}\text{B} + p$ [1]. It opens when the excitation energy of ^{12}C exceeds 15.96 MeV. One therefore expects only a negligible influence of the latter channel on bound and resonance states of ^{12}C in the vicinity of the $\alpha + \alpha + \alpha$ threshold.

The ^{12}C nucleus is unique because of its excited “Hoyle state”. This state is important in the context of nucleosynthesis of carbon in helium-burning red giant stars. It is a 0^+ state with an energy of 7.65 MeV above the ground state, or 0.4 MeV above the three-cluster $\alpha + \alpha + \alpha$ threshold. Its width is only 8.5 eV indicating a long lifetime. One immediately relates this to the 0^+ state in ^8Be described by two α particles with an energy of 0.092 MeV above the $\alpha + \alpha$ threshold and a width of 5.57 eV.

Many efforts have been made to reproduce the experimentally observed structure of ^{12}C and to explore and understand the nature of the ground, excited and resonance states. This was, for example, done within so-called semi-microscopic models (considering structureless α -particles) [2–8] and within fully microscopic models [9–24].

A somewhat general feature of the calculations is that, with potentials which adequately reproduce the α - α interaction (this includes the phase shifts for 0^+ , 2^+ and 4^+ states and the position of the corresponding resonance states), one obtains a noticeably overbound ground state for ^{12}C .

To determine the energies and widths of resonance states created by a three-cluster continuum, only a few methods can be used. A popular method for obtaining the resonance properties in many-cluster, many channel systems is the Complex Scaling Method (see reviews [25, 26] and references therein). Other methods start from a calculated form of the S -matrix in a wide energy range and determine the resonance states as the pole(s) of the S -matrix. The advantage of these methods is that they provide the scattering quantities (such as phase-shifts, cross-sections, etc.) and the resonance properties (energies and widths), as well as the wave functions of scattering

and resonance states. The latter then allow one to obtain more information about the nature of the resonance states.

^{12}C is known from theory and experiment (see, e. g., [27] and [28]) to have very narrow resonances above the three α threshold. One may wonder why a system with several open channels does not decay instantly but manifests these narrow resonance states. There are two possible answers to this question. First, a resonance state appears in one single channel of the multi-channel system. Such particular channel is usually weakly coupled to a number, or all, of the other open channels. It is well-known that this weak coupling of channels predetermines the existence of long-lived resonance states. Second, a resonance can be more or less uniformly distributed over all open channels, and the compound system needs (some) time for the resonance to be accumulated by one or a few open channels to decay into. Such a distribution over many open channels leads to very narrow resonances, as was predicted by A. Baz' [29]. It is referred to as diffusion-like processes in scattering. This type of resonance is attributed to the effect that “the system spends most of its time wandering from one channel to another” [29].

In this paper we wish to calculate and analyze the bound and continuum structure of ^{12}C , and gain some insight in the nature of these states. Indeed, in some publications (e. g., [30–33]) the suggestion for a dominant linear, chain-like, three-cluster structure appears for some of the ^{12}C resonances. We will look for a confirmation of this structure. To this end, we determine the most probable configuration of three α particles both in coordinate and momentum space. We also qualify the channels through which the resonance states of ^{12}C preferentially decay.

The main results of this paper are obtained by applying the “Algebraic Model in a Hyperspherical Harmonic Basis” (AMHHB) [34, 35, 36] to a configuration of three α particles. In this model, the three clusters are treated equally and their relative motion is described by Hyperspherical Harmonics. The latter enumerate the channels of the three-cluster continuum and allow one to implement the correct boundary conditions for the three-cluster exit channels. The AMHHB has been applied successfully to a study of resonances in nuclei with a large excess of protons or neutrons such as ^6He , ^6Be , ^5H . The method provides energies and widths of resonances and their total and partial widths, as well as the corresponding wave functions. The latter allow one to analyze the nature of the resonance states. The results of this model are compared to those obtained in other, more or less comparable, microscopic descriptions from the literature and to experiment.

In the next section we elaborate the method used to calculate the spectrum of ^{12}C . Section three focuses on the results obtained using this method. We also present correlation functions and density functions to characterize more precisely the spatial configuration of the three α particles for specific resonance states. We also compare the results to those of other microscopic calculations as well as to experiment.

2 Microscopic cluster model

In this section we describe the microscopic model used to determine the structure of ^{12}C in the present paper. As it has been already introduced and used in several publications, we will limit ourselves to the most important notations and aspects of importance to the current calculations.

2.1 Three-cluster AMHHB model

The three-cluster “Algebraic Model in a Hyperspherical Harmonic Basis” (AMHHB) [34–36] will be applied to a single $^{12}\text{C} = \alpha + \alpha + \alpha$ three-cluster configuration.

This model takes a Hyperspherical Harmonic basis (HH) to characterize and enumerate different three-cluster channels. In each of these channels, an oscillator basis

describes the radial behavior and is used to expand the many-particle wave function. A matrix version of the Schrödinger equation is obtained after substitution of this wave function. It is solved by the Algebraic Method (also called the Modified J -Matrix method [36]) for both bound and scattering states using the correct asymptotics.

A similar approach utilizing the Hyperspherical Harmonics, was proposed in [38, 39] in the coordinate representation using the generator coordinate technique to solve the corresponding Schrödinger equation.

The AMHHB wave function for ^{12}C is written as

$$\begin{aligned}\Psi &= \widehat{\mathcal{A}}\{\Phi(\alpha_1)\Phi(\alpha_2)\Phi(\alpha_3)f(\mathbf{x},\mathbf{y})\} \\ &= \widehat{\mathcal{A}}\{\Phi(\alpha_1)\Phi(\alpha_2)\Phi(\alpha_3)f(\rho,\theta;\widehat{\mathbf{x}},\widehat{\mathbf{y}})\} \\ &= \sum_{n_\rho,K,l_1,l_2} C_{n_\rho,K,l_1,l_2} |n_\rho,K,l_1,l_2;LM;(\rho,\theta;\widehat{\mathbf{x}},\widehat{\mathbf{y}})\rangle,\end{aligned}\quad (1)$$

where $|n_\rho,K,l_1,l_2;LM\rangle$ is a cluster oscillator function [34]:

$$|n_\rho,K,l_1,l_2;LM\rangle = \widehat{\mathcal{A}}\{\Phi(\alpha_1)\Phi(\alpha_2)\Phi(\alpha_3)R_{n_\rho,K}(\rho)\chi_{K,l_1,l_2}(\theta)\{Y_{l_1}(\widehat{\mathbf{y}})Y_{l_2}(\widehat{\mathbf{x}})\}_{LM}\}.\quad (2)$$

These functions are labelled by the number of hyperradial excitations n_ρ , hyperspherical momentum K and two partial orbital momenta l_1, l_2 . The vectors \mathbf{x} and \mathbf{y} form a set of Jacobi coordinates, and ρ and θ are hyperspherical coordinates related to the Jacobi vectors by:

$$\rho = \sqrt{\mathbf{x}^2 + \mathbf{y}^2}, \quad |\mathbf{x}| = \rho \cos \theta, \quad |\mathbf{y}| = \rho \sin \theta.\quad (3)$$

The notation $\widehat{\mathbf{x}}$ and $\widehat{\mathbf{y}}$ refers to the unit length vectors. The vector \mathbf{x} corresponds to the distance between two selected α particles with the associated partial orbital angular momentum l_2 . The vector \mathbf{y} is the displacement of the third α particle with respect to the center of mass of two others with the associated angular momentum l_1 . The three quantum numbers $c = \{K, l_1, l_2\}$ determine channels of the three-cluster system in the AMHHB.

The fact that all three clusters are identical leads to some specific issues. The wave function (1) for ^{12}C is antisymmetric with respect to the permutation of any pair of nucleons. Because the three clusters are identical, this function should be symmetric with respect to the permutation of any pair of alpha particles. This imposes constraints on the allowed quantum numbers of the wave function. Because of this symmetry, for instance, the partial orbital momentum l_2 of a two-cluster subsystem can only have even values. As the parity of ^{12}C states is defined as $\pi = (-1)^{l_1+l_2}$, it is fully determined by the partial orbital angular momentum l_1 of the relative motion of the remaining cluster with respect to the two-cluster subsystem.

It was suggested in Refs. [40] and [12] to use a symmetrization operator to construct the proper basis states. For a discussion on the symmetry of a system with three identical clusters we refer to [41].

The symmetrical Hyperspherical Harmonic basis for a three-particle system was realized many years ago (see, e. g., [42, 43]). An explicit form of a few basis functions for small values of the total orbital momentum ($L = 0, 1$ and 2) can be derived. However it is extremely intricate to use for explicit calculation of matrix elements.

An alternative approach to obtain such matrix elements without an explicit realization of the basis functions consists in using the generating function technique. One can indeed construct a generating function for the overlap and Hamiltonian kernels of ^{12}C using the procedure explained in [34] that satisfies all required symmetry conditions including the cluster symmetric permutation behavior. Explicit matrix elements of the operators can then be obtained by using recurrence relations. The standard

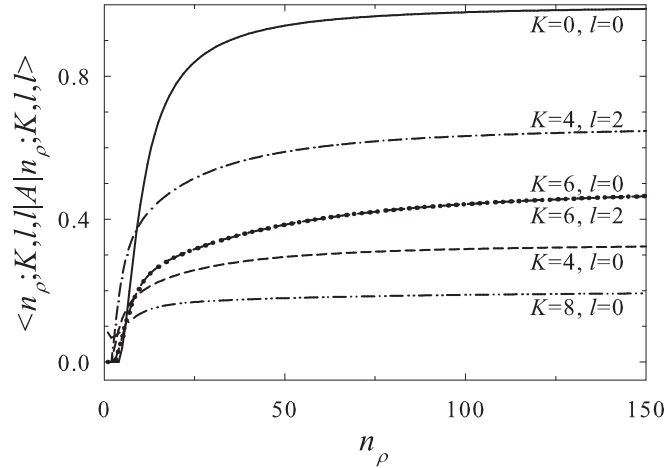


Figure 1: Matrix elements of the antisymmetrization operator in the nonsymmetrized hyperspherical basis ($K = 6, l = 0$ and $K = 6, l = 2$ coincide).

approach in the AMHHB is to extract matrix elements characterized by explicit l_1, l_2 quantum numbers. These, however, do not yet correspond to the desired symmetrical Harmonics. Indeed, the states $|n_\rho, K, l_1, l_2; LM\rangle$ for fixed n_ρ and K do not belong to the desired symmetrical irreducible representation of $S(3)$, the permutation group of the three α clusters, with the Young tableau [3]. They are, in fact, linear combinations of the Young tableau [3] and the non-symmetrical Young tableaux [2,1] and [111].

The antisymmetrization operator in the standard AMHHB basis has non-zero matrix elements

$$\langle n_\rho, K, l_1, l_2; LM | \hat{A} | \tilde{n}_\rho, \tilde{K}, \tilde{l}_1, \tilde{l}_2; LM \rangle \quad (4)$$

for fixed oscillator shells with $N_{sh} = 2n_\rho + K = 2\tilde{n}_\rho + \tilde{K}$. By selecting only matrix elements with hyperradial quantum number $n_\rho = \tilde{n}_\rho$ and hypermomentum $K = \tilde{K}$, one obtains relatively small matrices whose eigenfunctions $|n_\rho, K, \nu; LM\rangle$ with non-zero eigenvalues are of the correct symmetrical hyperspherical type due to the symmetry properties of the generating function. Index $\nu = 1, 2, \dots$ enumerates the symmetrical Hyperspherical Harmonics for a given value of the hypermomentum K . This procedure is similar to the procedure of obtaining Pauli allowed states in three-cluster systems (see Ref. [44] for details).

This is demonstrated in Fig. 1 where the diagonal matrix elements of the antisymmetrization operator between the original Hyperspherical Harmonics are displayed for total orbital momentum $L = 0$ for all channels up to $K = 8$. One notices that matrix elements

$$\langle n_\rho, K, l_1 = l_2; L = 0 | \hat{A} | n_\rho, K, l_1 = l_2; L = 0 \rangle \quad (5)$$

do not tend to unity, as one could expect, but to some fixed values. Analysis shows that these asymptotic values of (5) correspond to the weights of the symmetrized Hyperspherical Harmonics with Young tableau [3], within the original Harmonic.

The eigenvalues obtained after diagonalization which are matrix elements of symmetrized Harmonics, however, do display the correct asymptotic behavior, i. e. they all tend to unity as can be seen in Fig. 2.

In Table 1, we display both the total number of (original) nonsymmetrized and of symmetrized channels for different values of the total orbital momentum. The symmetrization significantly reduces the number of channels compatible with the maximal value of hypermomentum K_{\max} . Only even values of the partial orbital momentum l_2 are considered because of the symmetry rules for two-cluster subsystems.

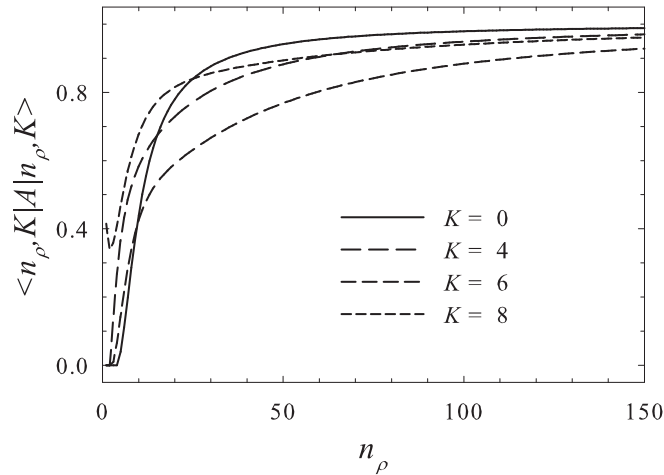


Figure 2: Matrix elements of the antisymmetrizer in the symmetrized hyperspherical basis.

Table 1: Number of channels for nonsymmetrized and symmetrized Hyperspherical Harmonics (enumerated by ν for given K).

J^{π}	0^+	2^+	4^+	1^-	3^-
K_{\max}	14	14	14	13	13
$N_{ch}(\{K, l_1, l_2\})$	20	44	54	28	42
$N_{ch}(\{K, \nu\})$	8	16	19	9	14

Effective charges $Z_{c,\tilde{c}}$ were defined in Refs. [34] and [35] in the context of the AMHHB and their importance and meaning were explicitly discussed for the ^6Be nucleus in the three-cluster configuration $^4\text{He} + p + p$. The effective charge determines the asymptotic form of the three-cluster potential originating from the Coulomb interaction, which has the form

$$V_{c,\tilde{c}}^{(C)} = \frac{Z_{c,\tilde{c}}}{\rho}. \quad (6)$$

It was shown that it is of a crucial importance for implementing the correct boundary conditions for the three-cluster continuum states.

The symmetrization influences the behavior of the effective charges. In Table 2, we display the effective charges for the 0^+ state of ^{12}C calculated in the original

Table 2: Effective charges for the $J^{\pi} = 0^+$ state of ^{12}C .

(K, l_1, l_2)	(0,0,0)	(4,0,0)	(4,2,2)	(6,0,0)	(6,2,2)	(8,0,0)	(8,2,2)	(8,4,4)
(0,0,0)	28.81	2.47	3.49	2.74	-2.74	0.87	0.00	1.04
(4,0,0)	2.47	32.157	-1.13	3.95	-0.31	4.67	0.00	1.95
(4,2,2)	3.49	-1.13	31.35	1.72	-4.30	0.00	0.66	0.00
(6,0,0)	2.74	3.95	1.72	33.48	-2.51	4.63	0.00	0.45
(6,2,2)	-2.74	-0.31	-4.30	-2.51	34.29	0.00	0.62	0.00
(8,0,0)	0.87	4.67	0.00	4.63	0.00	34.29	0.00	-2.38
(8,2,2)	0.00	0.00	0.66	0.00	0.62	0.00	33.08	0.00
(8,4,4)	1.04	1.95	0.00	0.45	0.00	-2.38	0.00	32.41

Table 3: Effective charges for the $J^\pi = 0^+$ state of ^{12}C for symmetrized channels.

(K, ν)	(0,1)	(4,1)	(6,1)	(8,1)
(0,1)	28.810	4.277	3.880	1.139
(4,1)	4.277	30.556	5.217	2.301
(6,1)	3.880	5.217	35.990	1.457
(8,1)	1.139	2.301	1.457	31.450

nonsymmetrized basis of the Hyperspherical Harmonics for $K_{max} = 8$. One easily verifies that they coincide with those calculated in [23].

We display the effective charges in the symmetrized basis in Table 3. Only four channels remain after symmetrization. In particular, no $K = 2$ channel remains, so, we omitted these also in Table 2 even though they have a non-zero contribution.

It goes without saying that the asymptotic form of the effective three-cluster potential which originates from the nucleon-nucleon interaction [34],

$$V_{c,\tilde{c}}^{(NN)} = \frac{V_{c,\tilde{c}}}{\rho^3}, \quad (7)$$

is also influenced by the symmetrization. This asymptotic component is very important for obtaining the correct values of the S -matrix. We do not dwell on its explicit form here but apply a procedure similar to that for the effective charges.

2.2 Phases, eigenphases and resonances

After solving the system of linear equation of the AMHHB model, we obtain the wave functions of continuous spectrum states and the scattering S -matrix. We consider two different representations of the S -matrix.

In the first representation, the elements of the S -matrix are described through the phase shifts δ_{ij} and inelastic parameters η_{ij} ,

$$S_{ij} = \eta_{ij} \exp(2i\delta_{ij}), \quad (8)$$

of which one usually analyzes only the diagonal matrix elements by displaying the δ_{ii} and η_{ii} quantities. In the second representation, the S -matrix is reduced to the diagonal form leading to the so-called eigenphases which now represent the elastic scattering of the many-channel system in terms of independent (uncoupled) eigenchannels:

$$\|S\| = \|U\|^{-1} \|D\| \|U\|. \quad (9)$$

Here $\|U\|$ is an orthogonal matrix relating both representations, and $\|D\|$ is a diagonal matrix with nonzero elements

$$D_{\alpha\alpha} = \exp(2i\delta_\alpha) \quad (10)$$

defining the eigenphases δ_α .

The phases shifts δ_{ii} , inelastic parameters η_{ii} and eigenphases δ_α provide a sufficiently detailed information about the channels that are involved in production of resonance states. The eigenphases are used to extract resonance positions and total widths in a traditional way:

$$\left. \frac{d^2\delta_\alpha}{dE^2} \right|_{E=E_r} = 0, \quad \Gamma = 2 \left(\left. \frac{d\delta_\alpha}{dE} \right|_{E_r} \right)^{-1}; \quad (11)$$

whereas the orthogonal matrix $\|U\|$ leads to the partial decay widths of the resonance (see, e. g., Ref. [36] for details).

2.3 Correlation functions and density distributions.

As we have pointed out, the AMHHB model allows one not only to calculate the scattering observables but also to obtain the wave function at any energy, in particular, at the resonance. The latter is of the utmost importance for the analysis of the nature of the system at these energies.

Within the AMHHB model, the solution is fully expressed by the expansion coefficients $\{C_{n_\rho,c}\}$ and the S -matrix. The expansion coefficients $\{C_{n_\rho,c}\}$ determine both the total three-cluster wave function of a compound system Ψ as well as the wave function of the relative motion of three clusters $f(\mathbf{x}, \mathbf{y})$ (see eq. (1)).

The latter contains all information on the dynamic behavior of the three-cluster system in bound states and continuum as well. It is interesting to note that these coefficients are identical in representations of the wave function both in coordinate and momentum space because of the Fourier transform properties of the oscillator states. The wave function $f(\mathbf{k}, \mathbf{q})$ in momentum space has arguments that are directly related to the coordinate representation: \mathbf{k} is the momentum of relative motion of two clusters, whereas \mathbf{q} is the momentum of the third cluster with respect to the center of mass of the two-cluster subsystem.

We obtain the density distribution in the coordinate space as

$$D(x, y) = D(\rho, \theta) = \int |f(\mathbf{x}, \mathbf{y})|^2 d\hat{\mathbf{x}} d\hat{\mathbf{y}}, \quad (12)$$

and the corresponding correlation function as

$$C(x, y) = C(\rho, \theta) = x^2 y^2 \int |f(\mathbf{x}, \mathbf{y})|^2 d\hat{\mathbf{x}} d\hat{\mathbf{y}} \quad (13)$$

directly from the wave function of relative motion $f(\mathbf{x}, \mathbf{y})$. Both the density distribution and correlation function in the momentum space are obtained in the same way using the wave function of relative motion in momentum space $f(\mathbf{k}, \mathbf{q})$.

In a calculation with N_{ch} open channels, one obtains N_{ch} independent wave functions describing elastic and inelastic processes in the many-channel system. It is quite impossible to analyze all of these wave functions when many channels are open. Some principles have to be set up on how to select the most important wave functions. We have formulated some criteria for selecting the dominant wave function of a resonance in Ref. [36]. We will use the same criteria in this paper to select the ‘‘resonance wave functions’’.

3 Calculations and results

In the present calculations for ^{12}C , we consider the Minnesota potential [45] for the nucleon-nucleon interaction. The oscillator basis is characterized by the oscillator length $b = 1.2846$ fm to minimize the ground state energy of the α particle using the above potential.

The parameter u of the Minnesota potential is taken to be $u = 0.94$ to reproduce the phase shifts of $\alpha + \alpha$ scattering and the 0^+ , 2^+ and 4^+ resonances in ^8Be . The same parameters were used by Arai [17].

The $^8\text{Be} = \alpha + \alpha$ two-cluster substructure is of a key importance in the description of ^{12}C . We present $\alpha + \alpha$ resonance properties in Table 4. The AMOB model (Algebraic Model using an Oscillator Basis) takes a set of oscillator functions to describe the intercluster behavior and the Algebraic Model to obtain the phase shifts for $\alpha + \alpha$ scattering (see, e. g., Ref. [46]). We include a comparison to the results of Arai from his paper on ^{12}C [17] where he uses the ‘‘analytical continuation of the S -matrix to the complex plane’’ method to obtain the resonance characteristics.

Table 4: Resonance properties of ${}^8\text{Be}$ obtained with different methods.

J^π	AMOB		Arai [17]	
	E , MeV	Γ , keV	E , MeV	Γ , MeV
0^+	0.022	$6.30 \cdot 10^{-10}$	0.03	$<10^{-6}$
2^+	2.93	1.51	2.9	1.4
4^+	12.55	5.01	12.5	4.8

These results form a first test of the consistency of the different expansion methods applied to the two-cluster subsystem. Although quite similar, one still notices that the resonance properties of the two-cluster α - α system have a slight dependence on the method.

3.1 Potential and Coulomb interaction in AMHHB

Diagonal matrix elements of the nucleon-nucleon and Coulomb interactions within the AMHHB model are displayed in Figs. 3 and 4 for the channels up to $K = 8$. One observes that the nucleon-nucleon interaction creates a deep potential well with a long tail in the hyperspherical coordinate. This tail reflects the asymptotic form of the potential indicated in Eq. (7). The matrix elements of the Coulomb interaction indicate the magnitude of the Coulomb barrier which is the main factor for generating resonance states in ${}^{12}\text{C}$.

3.2 Phase shifts and eigenphases

We show in Fig. 5 the results of the AMHHB calculations for the 2^+ state in terms of the symmetrical Hyperspherical Harmonic channels through the (diagonal) phase shifts δ_{ii} and inelastic parameters η_{ii} .

The scattering parameters are obtained from a calculation with maximal hypermomentum $K_{\max} = 14$. One observes from Fig. 5 that for small energies the channels are completely uncoupled ($\eta_{ii} \approx 1$). The first 2^+ resonance appears at $E = 2.731$ MeV and is mainly produced in the first channel with the hypermomentum $K = 2$, whereas the second resonance at energy $E = 3.113$ MeV is dominated by the hypermomentum $K = 4$. The inelastic parameters for the first two channels have pronounced

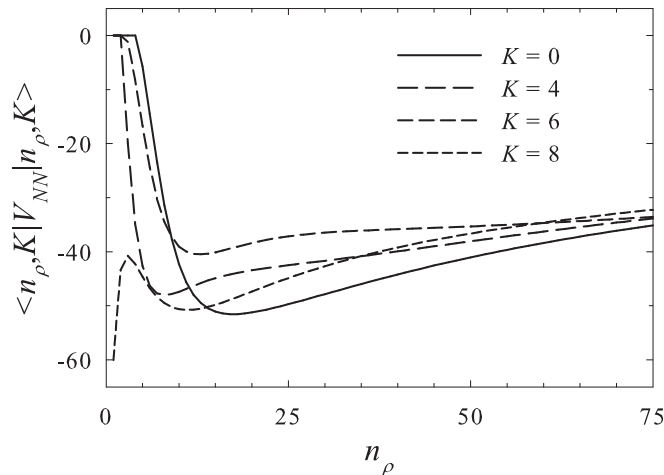


Figure 3: Diagonal matrix elements of \widehat{V}_{NN} between symmetrized Hyperspherical Harmonics for the $J^\pi = 0^+$ state.

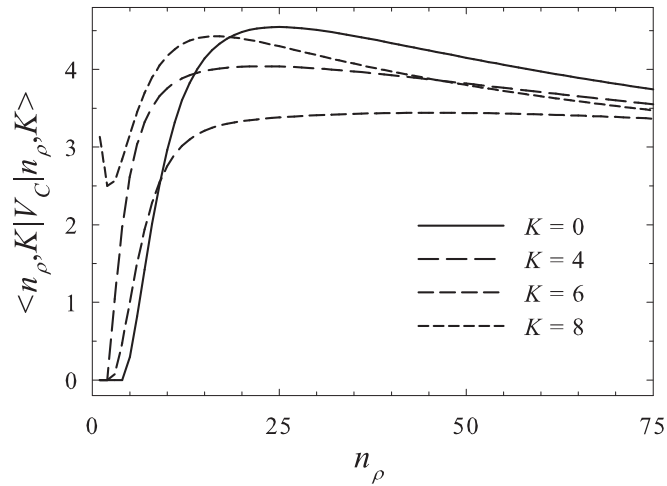


Figure 4: Diagonal matrix elements of \widehat{V}_C between symmetrized Hyperspherical Harmonics for the $J^\pi = 0^+$ state.

minima at the energy of the first resonance and shallow minima at the second resonance energy. Besides, the first resonance displays a “shadow resonance” behavior in the second channel. This is typical for resonances in a many-channel system (see, for instance, a detailed analysis of two-channel resonances in ^5He in Ref. [47]). The minima of inelastic parameters indicate that the compound system is being reconstructed at this energy and transits from one channel to the other.

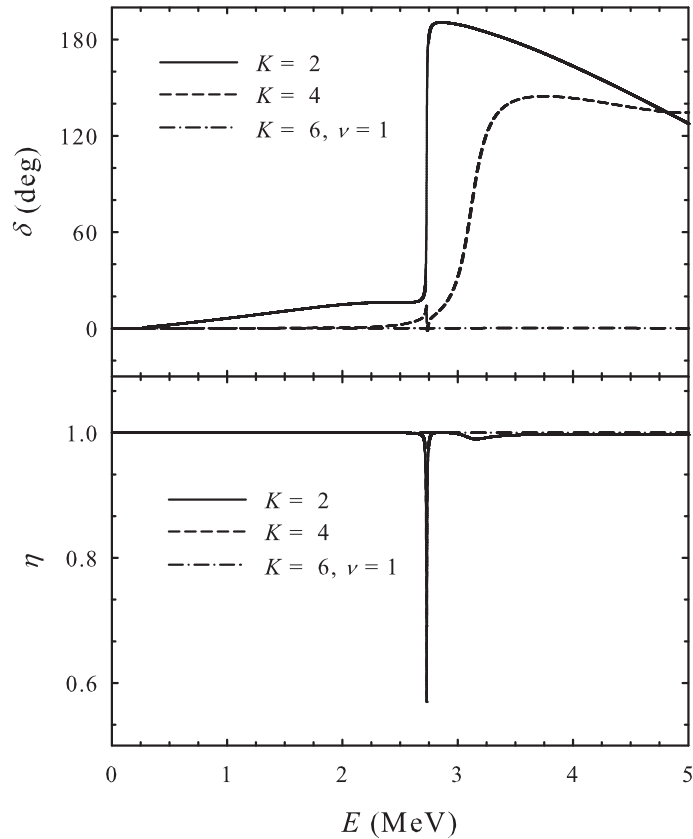


Figure 5: Diagonal phase shifts and inelastic parameters for the $J^\pi = 2^+$ state.

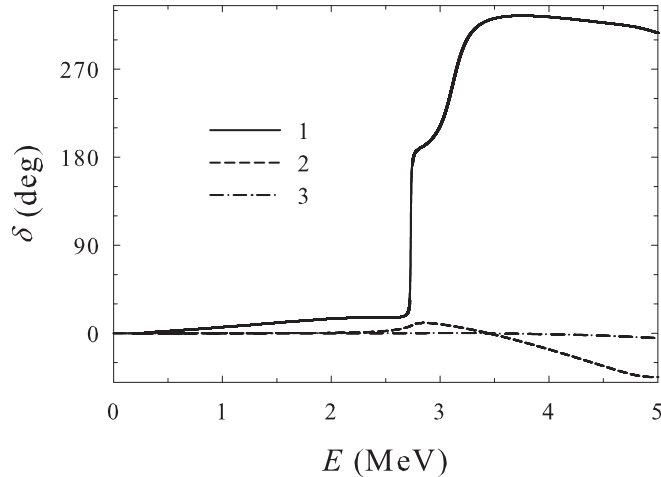


Figure 6: Eigenphase shifts for $J^\pi = 2^+$ for the first three eigenchannels.

We display in Fig. 6 the respective eigenphase shifts δ_α for the first three eigenchannels. One observes now that both resonance states are mainly associated with the first eigenchannel while the second eigenchannel contributes only marginally.

3.3 Convergence properties

A convergence study of energies (and widths) of bound and resonance states should indicate whether the Hilbert space is sufficiently large for obtaining stable and reliable results. The AMHHB model space is characterized by two parameters: the maximal value of the hypermomentum K_{\max} and the maximal value of the hyper-radial excitation $n_{\rho_{\max}}$. Usually the choice of parameters is a compromise between the convergence of the results and the computational burden. A set of Hyperspherical Harmonics with $K_{\max} = 14$ for even parity states and $K_{\max} = 13$ for odd parity states, seems sufficient and remains computationally feasible. This choice accounts for a large number of three-cluster configurations or, in other words, for a sufficient number of inherent (triangular) shapes for three clusters. We refer to Ref. [48] for examples of the most probable triangular shapes associated with the Hyperspherical Harmonics with hypermomentum ranging from $K = 0$ to $K = 10$.

The first convergence test considers the energies of 0^+ , 2^+ and 4^+ bound states of ^{12}C shown in Fig. 7 as functions of K_{\max} . One observes that the deeply bound states ($J^\pi = 0^+$, 2^+) require significantly less Hyperspherical Harmonics for a converged energy than the shallow, or weakly bound, state with $J^\pi = 4^+$. At least all Hyperspherical Harmonics with $K_{\max} \geq 6$ are required to bind the latter state, whereas the $J^\pi = 0^+$ one already obtains binding with a single Hyperspherical Harmonic with $K = 0$. Figure 7 demonstrates also that the above choice of K_{\max} is amply sufficient for bound states.

We turn to the energies and widths of the 0^+ and 2^+ resonances obtained with increasing number of Hyperspherical Harmonics in Table 5. One observes that a sufficient convergence of the resonances occurs at $K_{\max} = 12$. It is furthermore interesting to note that these resonances already appear with reasonable energy and width values when only the lowest channel ($K = 0$ for the 0^+ and $K = 2$ for the 2^+ state) is considered. This is a remarkable result for ^{12}C as, e. g., for ^6Be it was impossible to generate a 0^+ resonance with a single $K = 0$ channel (see Ref. [35]).

In all calculations we considered states with hyperradial excitation up to $n_{\rho_{\max}}=70$ which cover a wide range of intercluster distances and go far enough into the asymptotic region.

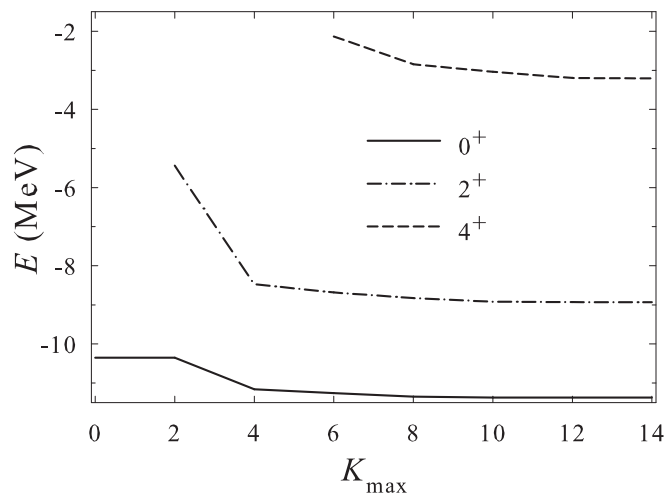


Figure 7: Convergence of bound states in AMHHB.

Table 5: Energy (MeV) and width (keV) of the low-lying resonances obtained with various K_{\max} truncations.

J^π	K_{\max}	0	4	6	8	10	12	14
0^+	E	0.40	0.75	0.74	0.72	0.70	0.68	0.68
	Γ	205.08	13.40	11.79	7.10	4.35	2.71	2.78
0^+	E	1.15	7.34	6.09	5.55	5.54	5.16	5.14
	Γ	510.16	897.64	422.50	539.21	586.08	534.33	523.46
2^+	E	—	3.28	2.89	2.83	2.78	2.74	2.73
	Γ	—	30.19	13.07	11.85	9.95	8.84	8.75
2^+	E	—	3.50	3.27	3.22	3.17	3.14	3.11
	Γ	—	274.51	351.57	308.29	280.23	263.80	246.78

3.4 Partial widths

We display the energy E , total width Γ and partial widths Γ_i , $i = 1, 2, \dots$ in the corresponding decay channels of the even parity resonances in Table 6 and of the odd parity resonances in Table 7.

One observes that in most cases only one or two channels are responsible for the decay of resonance states. The remaining channels contribute negligibly, and the corresponding partial widths do not exceed 10^{-5} keV. A significant distribution over multiple channels is apparent only in the case of the 4^+ resonance.

One should note that although the resonances are created by only a few channels, the role of other very weakly coupled channels is still important. This can be seen from

Table 6: Partial widths of even parity resonances in ^{12}C . Energy is in MeV, widths are in keV.

J^π		0^+	2^+	2^+	4^+
E		0.68	2.78	3.17	5.60
Γ		2.78	9.95	280.24	0.55
Γ_1	$K = 0$	2.78	$K = 2$ 6.11	$K = 2$ 13.46	$K = 4$ 0.23
Γ_2	$K = 4$	0	$K = 4$ 3.84	$K = 4$ 278.89	$K = 6$ 0.15
Γ_3	$K = 6$	0	$K = 6$ $<10^{-5}$	$K = 6$ $<10^{-5}$	$K = 8$ 0.16

Table 7: Partial widths of odd parity resonances in ^{12}C . Energy is in MeV, widths are in keV.

J^π	1^-		3^-	
E		3.52		0.67
Γ		0.21		8.34
Γ_1	$K = 3$	0.206	$K = 3$	8.34
Γ_2	$K = 5$	0.002	$K = 5$	0
Γ_3	$K = 7$	$<10^{-5}$	$K = 7$	0

Table 5 for the first 0^+ resonance: it is indeed generated mainly by the channel with the minimal hypermomentum $K = 0$ but is modified substantially with increasing number of hypermomenta. The same applies to other resonance states.

3.5 Correlation functions and density distributions.

We show the correlation function for the ^{12}C ground state in Fig. 8 and observe that this state displays a compact spatial configuration, as it is expected for such a deeply bound state. The most probable shape of the three α -cluster system is an almost equilateral triangle with a distance between any two α -particles of approximately 3 fm.

The correlation function for the first 0^+ resonance state shown in Fig. 9, on the other hand, shows a more deformed system with two α -particles relatively close to each other (about 3.5 fm) and the third alpha-particle located further away (approximately at a distance of 5 fm). So, ^{12}C features a prolate triangle as a dominant configuration in this state.

One also observes in Fig. 9 a small maximum of the correlation function corresponding to an almost linear configuration of three α -particles, two of them being approximately 4 fm apart, and the third one is located 0.2 fm away from their center of mass. However, the weight of this linear configuration is approximately 6 times less

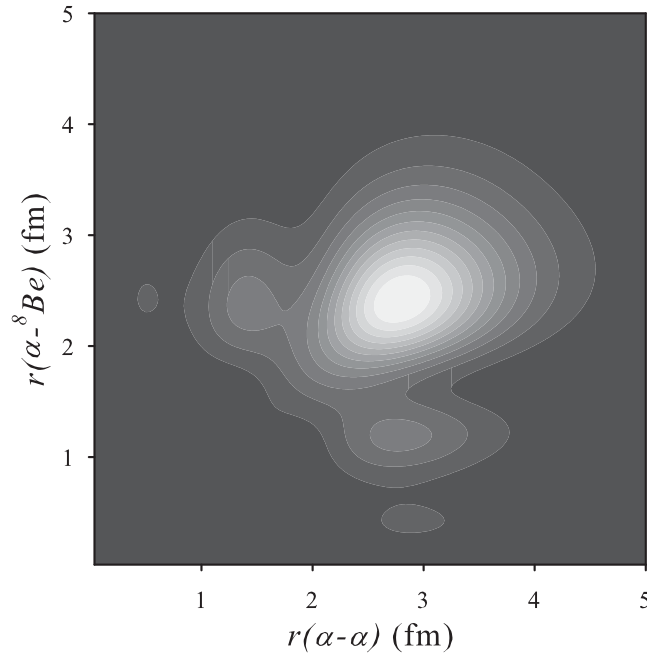


Figure 8: Correlation function for the ^{12}C ground state in the coordinate space.

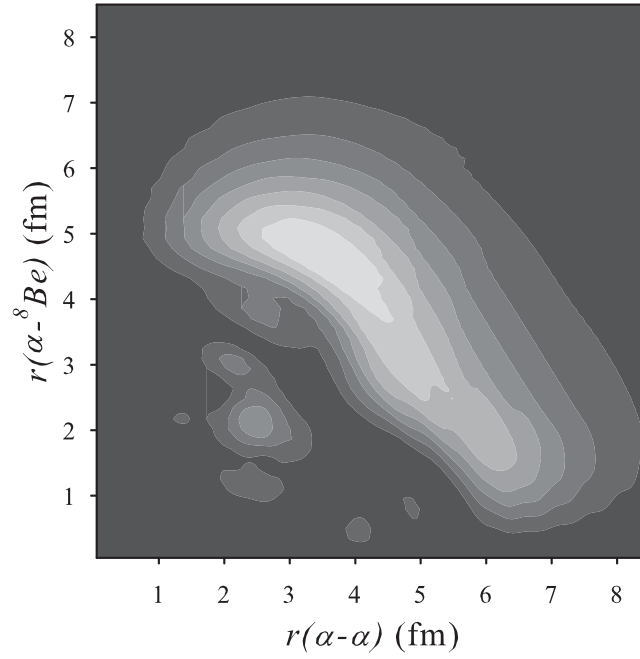


Figure 9: Correlation function for the first 0^+ resonance state of ^{12}C in the coordinate space.

than the weight of the prolate triangular configuration. Our calculations therefore do not agree with other authors advancing a dominant linear structure [30–33].

We display in Fig. 10 the correlation function of the first resonance state in the momentum space. One observes a huge maximum corresponding to relatively slowly moving α -particles. A small maximum corresponding to faster moving alpha-particles is also present.

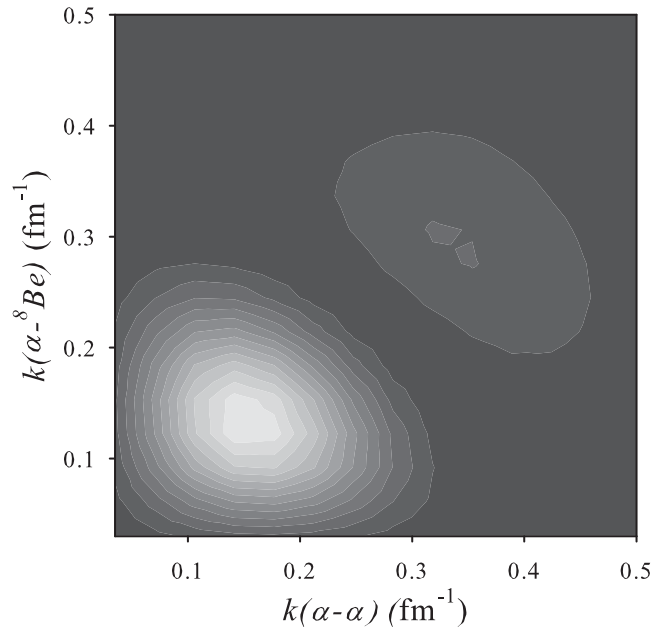


Figure 10: Correlation function for the first 0^+ resonance state of ^{12}C in the momentum space.

Table 8: Bound and resonance states in ^{12}C obtained with the AMHHB model, compared to CSM results from the literature.

Method Reference J^π	AMHHB		CSM		CSM	
	Present paper		Arai [17]		Pichler <i>et al.</i> [9]	
	E , MeV	Γ , keV	E , MeV	Γ , keV	E , MeV	Γ , keV
0^+	-11.372		-11.37		-10.43	
	0.684	2.78	0.4	< 1	0.64	14
	5.156	534.00	4.7	1000	5.43	920
2^+	-8.931		-8.93		-7.63	
	2.775	9.95	2.1	800	6.39	1100
	3.170	280.24	4.9	900		
4^+	-3.208		-3.21			
	5.603	0.55	5.1	2000		
1^-	3.516	0.21	3.4	200	3.71	360
3^-	0.672	8.34	0.6	< 50	1.16	25
	4.348	2.89	7.1	5400	11.91	1690
	5.433	334.90	9.6	400		

3.6 Comparison to the literature

We now compare the AMHHB results to the existing literature. We display in Table 8 the AMHHB results together with those of Arai [17] and Pichler *et al.* [9], both obtained by the Complex Scaling Method (CSM). The authors of Ref. [9] use a somewhat different value for the parameter u of the Minnesota potential and a different oscillator length b ; because of this, different results are obtained for the bound states.

Comparison with the results of Arai [17] indicates that the AMHHB model leads to resonance states with higher energies and smaller widths than those obtained with the CSM. This can be attributed to the difference of methods and to the different Hilbert spaces. Formally, the Hilbert space of basis functions used by Arai [17] is quite close to the one considered in the AMHHB. Actually, in the present calculations the partial orbital momenta l_1 and l_2 are restricted by the condition

$$L \leq l_1 + l_2 \leq K_{\max}$$

so that, for instance, for the total orbital momentum $L = 0$, they run from $l_1 = l_2 = 0$ to $l_1 = l_2 = 6$ with $K_{\max} = 14$. Arai, on the other hand, restricted himself with $l_1, l_2 \leq 4$. In [35, 36, 37] we observed the tendency that the more Hyperspherical Harmonics (thus the more channels) are involved in the calculation, the smaller becomes the resonance energy and width. This tendency is again confirmed by the present AMHHB calculations. Thus some reduction of the width of the resonances observed in our calculations with respect to Arai [17], can be attributed to a larger number of channels in our model.

Comparing the AMHHB results with the Complex Scaling Model calculations of Pichler *et al.* [9], one observes that both yield close results for the first and the second 0^+ resonance states.

On the whole one can conclude that there is consistency in the results for resonance properties in all three microscopic models.

3.7 Comparison to experiment

We compare the theoretical AMHHB results for ^{12}C with available experimental data in Table 9.

Table 9: Bound and resonance states in ^{12}C obtained with the AMHHB model, compared to experiment.

Method Reference J^π	AMHHB Present paper		Experiment [1]	
	E , MeV	Γ , keV	E , MeV	Γ , keV
0^+	-11.372		-7.2746	
	0.684	2.78	0.3796 ± 0.0002	$(8.5 \pm 1.0) \times 10^{-3}$
	5.156	534.00	3.0 ± 0.3	3000 ± 700
2^+	-8.931		-2.8357 ± 0.0003	
	2.775	9.95	3.89 ± 0.05	430 ± 80
	3.170	280.24	8.17 ± 0.04	1500 ± 200
4^+	-3.208			
	5.603	0.55	6.808 ± 0.015	258 ± 15
1^-	3.516	0.21	3.569 ± 0.016	315 ± 25
	0.672	8.34	2.366 ± 0.005	34 ± 5
3^-	4.348	2.89		
	5.433	334.90		

One notices that the first 0^+ resonance state (the Hoyle state) appears in the current calculations as a narrow resonance with the energy of 0.684 MeV and the width of 2.7 keV, which is considerably wider than the experimental Hoyle state (about $8.5 \cdot 10^{-3}$ keV). This contrasts with a generally observed feature of the AMHHB calculations that the calculated widths are significantly less than the respective experimental widths of ^{12}C resonances. The discrepancies between the theoretical and experimental data have essentially two origins. The first one relates to the choice of the nucleon-nucleon interaction: it was tuned to reproduce the phase shifts and resonance properties for alpha-alpha scattering. As a result, it leads to the overbound 0^+ and 2^+ states in ^{12}C and binds the 4^+ state. The second one relates to the specific choice of the three-cluster model and corresponding model space, as well as to the method by which energies and widths of resonance states are obtained.

3.8 Optimizing the nucleon-nucleon potential

In this paper, we used a Minnesota nucleon-nucleon potential tuned to reproduce phase shifts of α - α scattering as well as ^8Be resonances. This however leads to overbound 0^+ and 2^+ states and a bound 4^+ state in ^{12}C . Moreover, the obtained resonance structure of the ^{12}C three-cluster continuum deviates from the experimentally observed one which can be also attributed to the specific choice of the semi-realistic nucleon-nucleon potential.

We therefore wish to discuss the dependence of the results on the choice of parameter u of the potential. To do so, we use different criteria to optimize this parameter. First, we determine a value reproducing the ground state energy of ^{12}C , followed by an attempt to reproduce the energy and width of the 0^+ Hoyle state.

We display in Fig. 11 the ground state energy as a function of the parameter u , compared to the experiment (dashed line). One observes that the ground state is reproduced with $u = 0.910$. One observes a monotonously decreasing linear dependence of the ground state energy on u within the selected range. For the Hoyle state position and width, the dependency is less trivial as is shown in Fig. 12. One however observes that the value $u = 0.948$ reproduces the position of the Hoyle state and leads to a close match for its width too.

The correlation functions for the ground state and the Hoyle state obtained with their respective optimal values are very close to those obtained with the value $u = 0.94$ displayed in Figs. 8 and 9; so, our conclusions remain unaltered.

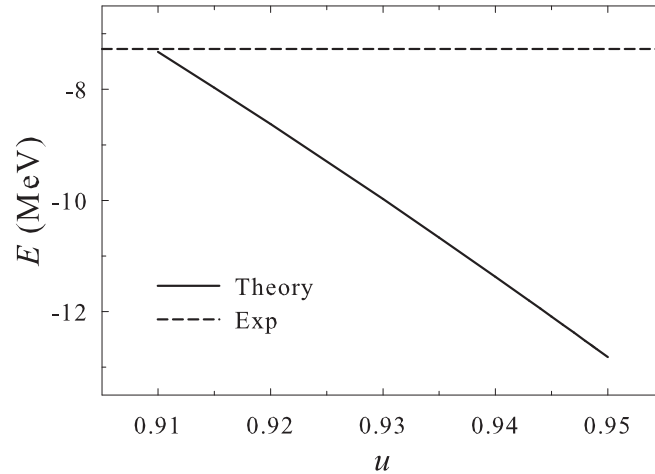


Figure 11: Energy of the ground state as a function of parameter u of the Minnesota potential.

4 Conclusions

In this paper we described the ^{12}C nucleus with a three-cluster microscopic model.

The model correctly handles the three-cluster continuum, i. e., correctly implements the suitable boundary conditions by using the Hyperspherical Harmonic basis. It leads to the scattering matrix S in many-channel space, and energies, total and partial widths of resonance states and their corresponding wave functions can be obtained.

It was shown that the obtained resonances of ^{12}C agree well with those obtained by other methods, and that the lowest resonances are generated by only a few weakly coupled channels leading to narrow resonance states. Partial widths determine the

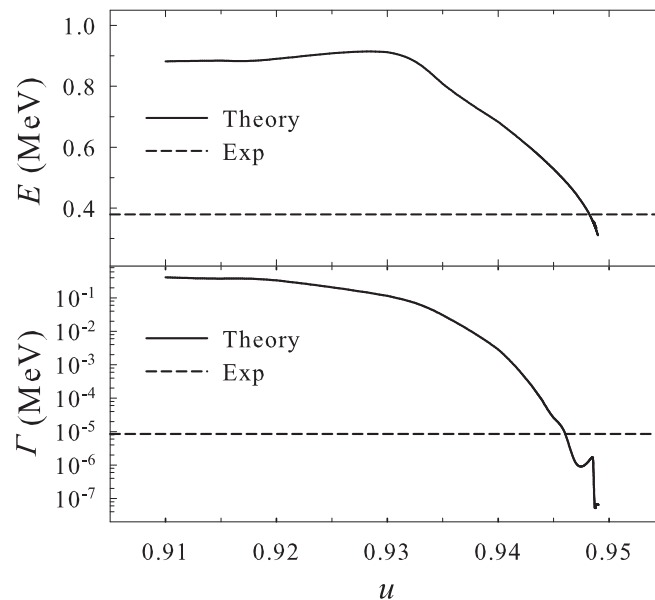


Figure 12: Position and total width of the first 0^+ resonance state as a function of parameter u .

most probable channels for resonance decay. Correlation functions and density distributions reveal the dominant shape of the three-cluster triangle configuration for the lowest bound and resonance states of ^{12}C . There is no indication of a prominent linear three-cluster structure for resonance states.

It was also shown that it is impossible to fix a unique value for the u parameter of the Minnesota nucleon-nucleon potential to fit all desired physical properties of ^{12}C and of the disintegrating α -particles. However, the qualitative conclusions remained unaltered under a slight adaptation of u .

As a final conclusion, we can state that the model is consistent with other microscopic models using the Complex Scaling methodology to determine energies and total widths of three-cluster resonance states.

5 Acknowledgments

Support from the Fonds voor Wetenschappelijk Onderzoek Vlaanderen (FWO), G0120-08N is gratefully acknowledged. V. S. Vasilevsky is grateful to the Department of Mathematics and Computer Science of the University of Antwerp for hospitality. This work was supported in part by the Program of Fundamental Research of the Physics and Astronomy Department of the National Academy of Sciences of Ukraine.

References

- [1] F. Ajzenberg-Selove, Nucl. Phys. A **506**, 1 (1990).
- [2] S. I. Fedotov, O. I. Kartavtsev, V. I. Kochkin and A. V. Malykh, Phys. Rev. C **70**, 014006 (2004).
- [3] I. Filikhin, V. M. Suslov and B. Vlahovic, J. Phys. G **31**, 1207 (2005).
- [4] R. Álvarez-Rodríguez, E. Garrido, A. S. Jensen, D. V. Fedorov and H. O. U. Fynbo, Eur. Phys. J. A **31**, 303 (2007).
- [5] R. Álvarez-Rodríguez, A. S. Jensen, D. V. Fedorov, H. O. U. Fynbo and E. Garrido, J. Phys. Conf. Ser. **111**, 012017 (2008).
- [6] R. Álvarez-Rodríguez, A. S. Jensen, E. Garrido, D. V. Fedorov and H. O. U. Fynbo, Phys. Rev. C **77**, 064305 (2008).
- [7] M. Chernykh, H. Feldmeier, T. Neff, P. von Neumann-Cosel and A. Richter, Phys. Rev. Lett. **105**, 022501 (2010).
- [8] R. de Diego, E. Garrido, D. V. Fedorov and A. S. Jensen, Phys. Lett. B **695**, 324 (2011).
- [9] R. Pichler, H. Oberhummer, A. Csótó and S. A. Moszkowski, Nucl. Phys. A **618**, 55 (1997).
- [10] C. Kurokawa and K. Katō, Nucl. Phys. A **738**, 455 (2004).
- [11] Y. Fujiwara, K. Miyagawa, M. Kohno, Y. Suzuki, D. Baye and J.-M. Sparenberg, Nucl. Phys. A **738**, 495 (2004).
- [12] Y. Fujiwara, Y. Suzuki and M. Kohno, Phys. Rev. C **69**, 037002 (2004).
- [13] Y. Fujiwara, M. Kohno and Y. Suzuki, Few-Body Syst. **34**, 237 (2004).
- [14] Y. Fujiwara and H. Nemura, Prog. Theor. Phys. **107**, 745 (2002).

- [15] Y. Fujiwara, K. Miyagawa, M. Kohno, Y. Suzuki, D. Baye and J.-M. Sparenberg, *Phys. Rev. C* **70**, 024002 (2004).
- [16] C. Kurokawa and K. Katō, *Phys. Rev. C* **71**, 021301 (2005).
- [17] K. Arai, *Phys. Rev. C* **74**, 064311 (2006).
- [18] M. Theeten, H. Matsumura, M. Orabi, D. Baye, P. Descouvemont, Y. Fujiwara and Y. Suzuki, *Phys. Rev. C* **76**, 054003 (2007).
- [19] C. Kurokawa and K. Katō, *Nucl. Phys. A* **792**, 87 (2007).
- [20] P. Descouvemont and D. Baye, *Phys. Rev. C* **36**, 54 (1987).
- [21] M. Orabi, Y. Suzuki, H. Matsumura, Y. Fujiwara, D. Baye, P. Descouvemont and M. Theeten, *J. Phys. Conf. Ser.* **111**, 012045 (2008).
- [22] Y. Suzuki, H. Matsumura, M. Orabi, Y. Fujiwara, P. Descouvemont, M. Theeten and D. Baye, *Phys. Lett. B* **659**, 160 (2008).
- [23] P. Descouvemont, *J. Phys. G* **37**, 064010 (2010).
- [24] T. Yoshida, N. Itagaki and K. Katō, *Phys. Rev. C* **83**, 024301 (2011).
- [25] N. Moiseyev, *Phys. Rep.* **302**, 212 (1998).
- [26] Y. K. Ho, *Phys. Rep.* **99**, 1 (1983).
- [27] T. Muñoz-Britton, M. Freer, N. I. Ashwood, T. A. D. Brown, W. N. Catford, N. Curtis, S. P. Fox, B. R. Fulton, C. W. Harlin, A. M. Laird, P. Mumby-Croft, A. S. J. Murphy, P. Papka, D. L. Price, K. Vaughan, D. L. Watson and D. C. Weissner, *J. Phys. G* **37**, 105104 (2010).
- [28] M. Freer, H. Fujita, Z. Buthlezi, J. Carter, R. W. Fearick, S. V. Förtsch, R. Neveling, S. M. Perez, P. Papka, F. D. Smit, J. A. Swartz and I. Usman, *Phys. Rev. C* **80**, 041303 (2009).
- [29] A. I. Baz', *Sov. Phys. JETP* **43**, 205 (1976).
- [30] G. S. Anagnostatos, *Phys. Rev. C* **51**, 152 (1995).
- [31] A. C. Merchant and W. D. M. Rae, *Nucl. Phys. A* **549**, 431 (1992).
- [32] Y. Kanada-En'yo, *Progr. Theor. Phys.* **117**, 655 (2007).
- [33] T. Neff and H. Feldmeier, *Nucl. Phys. A* **738**, 357 (2004).
- [34] V. Vasilevsky, A. V. Nesterov, F. Arickx and J. Broeckhove, *Phys. Rev. C* **63**, 034606 (2001).
- [35] V. Vasilevsky, A. V. Nesterov, F. Arickx and J. Broeckhove, *Phys. Rev. C* **63**, 034607 (2001).
- [36] J. Broeckhove, F. Arickx, P. Hellinckx, V. S. Vasilevsky and A. V. Nesterov, *J. Phys. G* **34**, 1955 (2007).
- [37] V. S. Vasilevsky, F. Arickx, J. Broeckhove and V. N. Romanov, *Ukr. J. Phys.* **49**, 1053 (2004).
- [38] S. Korenov and P. Descouvemont, *Nucl. Phys. A* **740**, 249 (2004).
- [39] A. Damman and P. Descouvemont, *Phys. Rev. C* **80**, 044310 (2009).

-
- [40] Y. Fujiwara, Y. Suzuki, K. Miyagawa and Michio, *Prog. Theor. Phys.* **107**, 993 (2002).
- [41] Yu. A. Lashko and G. F. Filippov, *Nucl. Phys. A* **826**, 24 (2009).
- [42] W. Zickendraht, *Ann. Phys. (NY)* **35**, 18 (1965).
- [43] J. Nyiri and Ya. A. Smorodinsky, *Yad. Fiz.* **29**, 833 (1979).
- [44] A. V. Nesterov, F. Arickx, J. Broeckhove and V. S. Vasilevsky, *Phys. Part. Nucl.* **41**, 716 (2010).
- [45] D. R. Thompson, M. LeMere and Y. C. Tang, *Nucl. Phys. A.* **286**, 53 (1977).
- [46] A. Sytcheva, F. Arickx, J. Broeckhove and V. S. Vasilevsky, *Phys. Rev. C* **71**, 044322 (2005).
- [47] K. Wildermuth and Y. Tang, *A unified theory of the nucleus*. Vieweg Verlag, Braunschweig, 1977.
- [48] V. Vasilevsky, A. V. Nesterov, F. Arickx and J. Broeckhove, *Phys. Rev. C* **63**, 064604 (2001).

Composite-Particle Interaction

S. Yu. Igashov^a and Yu. M. Tchuvil'sky^b

^a*All-Russia Research Institute of Automatics, Moscow 127055, Russia*

^b*Skobeltsyn Institute of Nuclear Physics, Lomonosov Moscow State University, Moscow 119991, Russia*

Abstract

A theoretical technique for description of composite nuclear particle interaction, in particular, the resonating group model and the orthogonality conditions model, is demonstrated. The discussion is focused on an algebraic version of the orthogonality conditions model proposed by the authors. In the framework of the developed formalism, it is possible to take into account among others the exchange terms of the kinetic energy operator precisely. Thus an approximation which is close to the original resonating group model, is built. Both a direct algebraic approach and a method based on the solution of integro-differential Schrödinger equation containing nonlocal terms related to forbidden and semi-forbidden states, are proposed as computational schemes. This equation turns out to be preferable in studies of narrow resonances. It is demonstrated that a decay width of a system to two-heavy-fragment channel is strongly affected by the nonlocal terms.

Keywords: *Clustering; Pauli principle; nucleus-nucleus interaction; resonance states*

1 Introduction

Properties of interaction of composite nuclear particles, i. e. the particles consisting of some identical fermion constituents, contrast dramatically with the properties of interaction of structureless ones. The principal origin of this contrast is the Pauli exclusion principle. As a consequence of the identity of the fermions composing two (or more) fragments in a realistic approach to the interaction of composite particles, it is necessary to take into account an antisymmetry of the wave function of the system as a whole and thus to consider internal multi-nucleon structures of the fragments. As a result, some eigenfunctions of the Hamiltonian describing the composite-particle interaction may vanish after the action of the antisymmetrization operator (forbidden states) or be renormalized by this operator (antisymmetrizer).

If the internal states of the interacting composite particles are fixed, the resonating group model (RGM) proposed in Refs. [1, 2] allows one to reduce the problem of description of their interaction to a two-body one (we do not consider systems of three or more fragments below). However the resulting two-body equation turns out to be not a Schrödinger-type one because it contains exchange integral kernels in all its terms. Methods of reduction of the RGM equation to the Schrödinger-type equation with a Hermitian Hamiltonian, are known (see, for example, Ref. [3]). However, even after these rearrangements, the RGM is an overcomplicated approach which looks still far from a habituated scheme of description of two-body interactions. Any pair of the composite particles should be described individually. In fact, the RGM remains a many-nucleon but not a two-body technique. Another problem of RGM is its inflexibility. As a consequence of incompleteness of the space of solutions inherent for the model, experimental observables are not well-reproduced within the RGM sometimes.

A goal of a lot of papers published after the original ones is to construct a method which, on the one hand, allows one to account for the property of fermion identity in

a system of two composite particles (and thus for the Pauli exclusion principle and various exchange effects caused by this identity) and, on the other hand, is relatively simple and flexible. The basic step on this way was made in the paper [4]. An approximation of the RGM which makes it more or less similar to an ordinary two-body approach is proposed there. Various alternatives of this approach have been developed up to now. These alternatives differ by methods of manipulation with the exchange terms. They are known under a unified name of orthogonality conditions model (OCM).

An algebraic version (AV) of OCM was proposed in Ref. [5]. It was built by analogy with the AV RGM proposed in Refs. [6, 7, 8]. Due to a unique potentiality of the algebraic formalism, it was possible to express precisely the exchange terms originated by the kinetic energy operator through eigenvalues of the so-called “norm” kernel of RGM and thus to construct a simple approximation which is very close to the original RGM.

In the present paper we demonstrate the lines of development of the method presented in Ref. [5]. In particular, an integro-differential equation of the Schrödinger type with a Hermitian Hamiltonian containing nonlocal terms related to the forbidden by the Pauli principle and semi-forbidden states, is obtained. This “comeback” to the methods of continuous mathematics turns out to be convenient in description of widths of narrow resonances decaying through cluster-cluster channels.

A number of characteristic examples including an interaction of light clusters, a nucleon-nucleus interaction, and an interaction of heavy ions, are considered. It is demonstrated by means of AV OCM that the values of the decay widths are strongly affected by the exchange effects in case of heavy-ion interactions. A pair of heavy magic fragments $^{16}\text{O} + ^{16}\text{O}$ is considered as an example.

2 Composite-particle interaction in the framework of RGM and OCM. One-channel problem

2.1 RGM and OCM. Conventional formalism

Let us consider a traditional method of the description of composite particle interaction in the framework of RGM and its approximations used in OCM. Here we restrict this consideration to a one-channel problem for the sake of brevity.

The wave function of RGM [1, 2] is chosen in the form:

$$\Psi_{A_1+A_2} = \hat{A} \{ \Psi_{A_1} \Psi_{A_2} \Phi(\rho) \}, \quad (1)$$

$$\hat{A} = \left(\begin{array}{c} A \\ A_1 \end{array} \right)^{-1/2} \left(1 + \sum_p (-1)^p \hat{P} \right), \quad (2)$$

where the sum is over all permutations \hat{P} of A ($A = A_1 + A_2$) nucleons, p is the parity of the permutation and $\Phi(\rho)$ is a probe wave function. Inserting (1) into the A -fermion equation

$$\hat{H}_A \Psi_A = E \Psi_A, \quad (3)$$

$$\hat{H}_A = \hat{T} + \hat{V}, \quad \hat{T} = \sum_{i=1}^A \frac{\hat{\mathbf{p}}_i^2}{2m}, \quad (4)$$

$$\hat{V} = \sum_{i < j=1}^A V(\mathbf{r}_i - \mathbf{r}_j), \quad (5)$$

one can obtain a two-body equation:

$$\left(\hat{T}_\rho + \hat{V}_\rho - E' \hat{N}_\rho \right) \Phi(\rho) = 0, \quad (6)$$

where

$$E' = E - E_1 - E_2, \quad (7)$$

and the normalization condition

$$\left\langle \hat{N}_\rho^{1/2} \Phi(\rho) \left| \hat{N}_\rho^{1/2} \Phi(\rho) \right. \right\rangle = (1, \delta(E - E'), \delta(k - k'), \text{ etc.}) \quad (8)$$

for bound and continuous states respectively. For a fixed value of the angular momentum of the relative motion l , the integral operators can be presented as

$$\begin{pmatrix} \hat{N}_{\rho,l} \\ \hat{T}_{\rho,l} \\ \hat{V}_{\rho,l} \end{pmatrix} \varphi_l(\rho) \equiv \int \begin{pmatrix} N_l(\rho', \rho) \\ T_l(\rho', \rho) \\ V_l(\rho', \rho) \end{pmatrix} \varphi_l(\rho') \rho'^2 d\rho', \quad (9)$$

$$\begin{aligned} & \begin{pmatrix} N_l(\rho', \rho'') \\ T_l(\rho', \rho'') \\ V_l(\rho', \rho'') \end{pmatrix} \\ &= \left\langle \hat{A} \left\{ \Psi_{A_1} \Psi_{A_2} \frac{1}{\rho^2} \delta(\rho - \rho') Y_{lm}(\Omega_\rho) \right\} \left| \begin{pmatrix} \hat{1} \\ \hat{T} \\ \hat{V} \end{pmatrix} \right| \hat{A} \left\{ \Psi_{A_1} \Psi_{A_2} \frac{1}{\rho^2} \delta(\rho - \rho'') Y_{lm}(\Omega_\rho) \right\} \right\rangle. \end{aligned} \quad (10)$$

Thus the discussed two-body equation turns out to be an integro-differential equation of the form which differs from the Schrödinger one.

The equation (6) can be transformed to a Schrödinger-like form by action of the operator $\hat{N}_{\rho,l}^{-1}$:

$$\left(\hat{N}_{\rho,l}^{-1} \hat{T}_{\rho,l} + \hat{N}_{\rho,l}^{-1} \hat{V}_{\rho,l} - E' \right) \varphi_l(\rho) = 0, \quad (11)$$

but the resulting Hamiltonian turns out to be a non-Hermitian one. Introducing a new wave function

$$\phi_l(\rho) = \hat{N}_{\rho,l}^{1/2} \varphi_l(\rho), \quad (12)$$

one can obtain a Schrödinger-like equation with a Hermitian Hamiltonian

$$\left(\hat{N}_{\rho,l}^{-1/2} \hat{T}_\rho \hat{N}_{\rho,l}^{-1/2} + \hat{N}_{\rho,l}^{-1/2} \hat{V}_{\rho,l} \hat{N}_{\rho,l}^{-1/2} - E' \right) \phi_l(\rho) = 0 \quad (13)$$

and usual normalization conditions:

$$\langle \phi_{E,l}(\rho) | \phi_{E',l}(\rho) \rangle = 1 \quad (14)$$

for states of discrete spectrum, and

$$\langle \phi_{E,l}(\rho) | \phi_{E',l}(\rho) \rangle = \delta(E - E') \quad (15)$$

(or similar) for states in continuum.

The basic approximation of the original OCM [4] is

$$V(\rho', \rho'') = V(\rho') \delta(\rho' - \rho''). \quad (16)$$

If the forbidden components are extracted from the function sought, then the initial equation becomes

$$\left(\hat{T}_\rho + \hat{V}(\rho) - E' \right) \tilde{\Phi}(\rho) = 0, \quad (17)$$

where $\hat{V}(\rho)$ is a direct (double folding) potential. Usually the exchange terms are neglected in the kinetic energy operator. In this approximation,

$$\hat{T}_\rho = \frac{\hat{\mathbf{p}}_\rho^2}{2\mu}. \quad (18)$$

In some cases, a quality of description of data is not high enough in the initial version of OCM. Other versions of OCM (presented, e. g., in Refs. [9, 10]) utilize a phenomenological local potential in contrast to the direct one and explore two alternative ways to take into account the Pauli exclusion principle:

1. A two-body model with forbidden states which are eigenstates of the Hamiltonian. This version is rather simple because the redundant states are easily excluded due to their orthogonality to the others in this case.
2. A two-body model with forbidden states which are eigenstates of the norm kernel \hat{N}_ρ .

A possibility of adjusting the two-body local potential makes the approaches more flexible and improves the quality of the results. At the same time, the resulting OCM (notably with the forbidden eigenstates of the Hamiltonian) occurs to be an approximation of the RGM falling far from the original model. Therefore more accurate approximations are of interest for the theory of composite-particle interaction.

2.2 Algebraic version of RGM and the developed version of OCM.

Within RGM, the functions Ψ_{A_1} and Ψ_{A_2} are most often considered as the ground state (i. e. the lowest compatible with the Pauli exclusion principle) oscillator wave functions with the same parameter $\hbar\omega$. In the algebraic version of RGM, the relative motion function is sought in the form of expansion

$$\varphi_l(\rho) = \sum_n C_{nl} \phi_{nl}(\rho) \quad (19)$$

in oscillator basis functions $\phi_{nl}(\rho)$ (also characterized by the same parameter $\hbar\omega$). Under these conditions, the wave functions $\phi_{nl}(\rho)$ are eigenfunctions of the norm kernel:

$$\hat{N}_{\rho,l} \phi_{nl}(\rho) = \varepsilon_n \phi_{nl}(\rho). \quad (20)$$

The eigenvalues ε_n are equal to zero for the forbidden states and tend to unity as $n \rightarrow \infty$. Semi-forbidden states are defined as states with ε_n considerably lower than the unity. There are rare cases for which the eigenvalues are higher than the unity. A mathematical formalism described below also allows one to include these states in a similar way as semi-forbidden states, thus we do not discuss this case separately.

A fundamental advantage of AV OCM is a possibility to apply the following relation presented in Ref. [11]:

$$\left\langle \phi_{nl} \left| \hat{N}_{\rho,l}^{-1/2} \hat{T}_\rho \hat{N}_{\rho,l}^{-1/2} \right| \phi_{n'l} \right\rangle = \sqrt{\frac{\varepsilon_{n_<}}{\varepsilon_{n_>}}} T_{nn'}, \quad (21)$$

where $n_< = \min(n, n')$, $n_> = \max(n, n')$ and $T_{nn'}$ is the matrix element of the ordinary two-body kinetic energy operator between the oscillator functions. Due to this, the set of the AV RGM equations looks as follows:

$$\sum_{n'} \left[\sqrt{\frac{\varepsilon_{n_<}}{\varepsilon_{n_>}}} T_{nn'} + \left(\hat{N}_{\rho,l}^{-1/2} \hat{V}_{\rho,l} \hat{N}_{\rho,l}^{-1/2} \right)_{nn'} - E' \delta_{nn'} \right] C_{n'l} = 0; \quad n \geq n_{\min}. \quad (22)$$

So, the A -fermion exchange properties of the kinetic energy operator are precisely determined by the eigenvalues of the norm kernel.

The approach present here allows one, first, to take into consideration the exchange terms of the kinetic energy completely and, second, to use an alternative (well-grounded microscopically) way of exclusion of the forbidden states.

It should be noted that due to the equality (21), the potential energy term $\hat{V}_{\rho,l}$ contained in Eqs. (13) and (22) remains the only term of the Hamiltonian in AV RGM equations that includes the fermion exchange operators in the explicit form. It is just the term which is responsible for turning out RGM into a non-universal and overcomplicated model. The idea is to consider the term $\hat{N}_{\rho,l}^{-1/2}\hat{V}_{\rho,l}\hat{N}_{\rho,l}^{-1/2}$ phenomenologically, approximating it by a local potential $\hat{V}_{cl}(\rho)$. As a result, we obtain the equation

$$\left(\hat{T}_{\rho} + \hat{V}_{cl}(\rho) - E'\right)\tilde{\Phi}(\rho) = 0. \quad (23)$$

It should be noted that the choice of another scheme considering as a local potential the term $\hat{V}_{\rho,l}$ instead of $\hat{N}_{\rho,l}^{-1/2}\hat{V}_{\rho,l}\hat{N}_{\rho,l}^{-1/2}$, is also possible and does not present any additional problem. The latter choice looks less reasonable because the semi-forbidden states with small values of ε_n (if such values exist in a particular example) may cause an instability in the fitting procedure of the parameters of the local potential in this case.

The approach is called AV OCM independently of methods (which may be algebraic or that of ‘‘continuous’’ mathematics) applied to solve it.

In the algebraic versions of the canonic two-body problem, RGM as well as OCM presented here, the expansion coefficients C_{nl} of Eq. (19) satisfy an infinite set of linear equations

$$\sum_{n=0}^{\infty} \left(\langle \phi_{n'tm} | \hat{H} | \phi_{nlm} \rangle - E\delta_{n'n} \right) C_{nl} = 0, \quad n' = 0, 1, \dots, \quad (24)$$

which follows from the respective Schrödinger equation. For ordinary bound states, the eigenvalue problem,

$$\det \left\| \hat{H} - EI \right\| = 0, \quad (25)$$

is solved on the truncated basis with $n \leq n_{\max}$. Here truncation means the boundary condition $C_{nl} = 0$, $n > n_{\max}$ in the oscillator representation. For states of continuous spectrum (including rather broad near-barrier resonances), the convergence of the functional series (19) is not uniform; therefore the so-called J -matrix method [12] is applied. The expansion coefficients decrease rather slowly with n , and their asymptotic behavior should be introduced in the set of equations:

$$\sum_{n=0}^{N-1} \left(\langle \phi_{n'tm} | \hat{H} | \phi_{nlm} \rangle - E\delta_{n'n} \right) C_{nl} = - \sum_{n=N}^{\infty} \langle \phi_{n'tm} | \hat{H} | \phi_{nlm} \rangle C_{nl}^{(as)}, \quad n' = 0, 1, \dots \quad (26)$$

The papers [6, 7, 8] were the first works in which the discussed method was applied to solve the RGM equations.

A high-precision form of the asymptotic coefficients was obtained in Refs. [13, 14, 15]. In particular, for the wave function asymptotically behaving as an outgoing Coulomb wave, the expansion coefficient has the following form:

$$C_{nl}^{(as)} = \frac{1}{\sqrt{kr_0\varsigma_n}} \left\{ G_l(\eta, kr_0\varsigma_n) + iF_l(\eta, kr_0\varsigma_n) - \frac{k^3 r_0^3}{6\varsigma_n} [G'_l(\eta, kr_0\varsigma_n) + iF'_l(\eta, kr_0\varsigma_n)] \right\}, \quad n \rightarrow \infty, \quad (27)$$

where $r_0 = \sqrt{\hbar/\mu\omega}$ is the oscillator radius, $\varsigma_n = \sqrt{2n+3}$, the prime denotes the derivatives of the Coulomb wave functions with respect to the second argument. The first term in the figure brackets of Eq. (27) provides a rather good approximation in most cases.

A related approach may be also useful for calculations of near-threshold bound states.

The presence of the forbidden states in Eq. (20) restricts the set of equations (26) and the sums in the left-hand side of them by the conditions $n, n' \geq n_{\min}$. Semi-forbidden states are taken into account by means of renormalization of the kinetic energy matrix. The explicit form of the of the kinetic energy matrix elements (21) is applied for that. The matrix of the renormalized kinetic energy operator (21) retains a tridiagonal form in the oscillator basis as the initial one.

The method developed here is applicable to the calculations of phase shifts and cross-section of composite particle scattering including calculations in the framework of the optical model, near-threshold bound cluster-nucleus states, resonance states of various cluster-cluster pairs excluding too narrow resonances, amplitudes of entrance and exit channels of various reactions.

It should be noted that the one-channel formalism developed here is valid in the case when both clusters are SU(3)-scalars (it is true for magic and light clusters) and, in addition, one of them is an SU(4)-scalar. Otherwise a channel coupling appears due to the antisymmetrization. As a result, some modifications of the technique are required. The quality of the one-channel approximation in this multi-channel problem depends on the dynamics of the channel under investigation.

2.3 AV OCM. Equivalent integro-differential equation.

In some cases it is hard to explore the direct algebraic approach presented above because the asymptotic behavior of the expansion coefficients is achieved at too large distances, and a huge basis in Eq. (19) is required. It is the case of a narrow resonance in a system decaying through a two charged composite-particle channel. In this situation, it occurs more convenient to apply methods of “continuous” mathematics. To do this, a number of separable terms related to forbidden and semi-forbidden states are introduced into the Hamiltonian. The idea of this rearrangement is that the initial cluster Hamiltonian matrix elements $H_{nn';l}$ between the states at least one of which is forbidden, are cancelled by the corresponding matrix elements of separable terms. The kinetic energy matrix elements in the Hamiltonian are renormalized according to the formula (21) to account for the presence of semi-forbidden states. The additional potential term denoted as \hat{V}_l^{sep} , takes the form:

$$\begin{aligned} \hat{V}_l^{sep} = & - \sum_{n,n'=0}^{n_0} |nl\rangle H_{nn';l} \langle n'l| - \sum_{n=0}^{n_0} \sum_{n'=n_0+1}^{\infty} (|nl\rangle H_{nn';l} \langle n'l| + |n'l\rangle H_{n'n;l} \langle nl|) \\ & + \sum_{n=n_0+1}^{\infty} \left(\sqrt{\frac{\varepsilon_n}{\varepsilon_{n+1}}} - 1 \right) (|nl\rangle T_{n,n+1;l} \langle n+1, l| + |n+1, l\rangle T_{n+1,n;l} \langle nl|), \quad (28) \end{aligned}$$

where

$$\hat{H} = \hat{T}_\rho + \hat{V}_{cl}(\rho). \quad (29)$$

Usually $\varepsilon_n/\varepsilon_{n+1}$ tends to unity rather rapidly as n increases (for example, $\varepsilon_{n=80} = 0.999$ for the system $^{16}\text{O} + ^{16}\text{O}$), therefore the sum in Eq. (28) can be truncated by a relatively small value of n_0 .

Here we demonstrate an appropriate method to solve the Schrödinger equation

$$\left(\frac{d^2}{dr^2} + k^2 - 2V_{cl;l}(\rho) \right) \chi_l(\rho) = 2\hat{V}_l^{sep} \chi_l(\rho) \quad (30)$$

with the additional separable terms. The solution of this equation $\chi_l(\rho)$ must behave asymptotically as $G_l(\eta, k\rho) + iF_l(\eta, k\rho)$ at large distances. $G_l(\eta, k\rho)$ exceeds significantly $F_l(\eta, k\rho)$ in the under-barrier domain far enough from the external turning

point. Thus, according to Ref. [16], it is enough to satisfy the matching condition in this region with the function $G_l(\eta, k\rho)$ only. Consequently, the solution $\chi_l(\rho)$ should satisfy the following boundary conditions:

- (i) it is regular at the origin ($\rho = 0$);
- (ii) it behaves as $G_l(\eta, k\rho)$ under the barrier beyond the radius of the strong interaction.

To find the solution of Eq. (30), let us consider the equation

$$\left(\frac{d^2}{dr^2} + k^2 - 2V_{cl;l}(\rho) \right) \chi_l(\rho) = 0 \quad (31)$$

with a local potential $V_{cl;l}(\rho)$ including the centrifugal part, and introduce its solutions $\chi_{1;l}(\rho)$ which satisfies the condition (i) and $\chi_{2;l}(\rho)$ which satisfies (ii). The corresponding Green's function takes the form

$$G(\rho, \rho') = \frac{\chi_{1;l}(\rho_{<}) \chi_{2;l}(\rho_{>})}{W}, \quad (32)$$

where $\rho_{<} = \min(\rho, \rho')$, $\rho_{>} = \max(\rho, \rho')$, and the Wronskian W is written as follows:

$$W = \chi_{1;l}(\rho) \frac{d\chi_{2;l}(\rho)}{d\rho} - \frac{d\chi_{1;l}(\rho)}{d\rho} \chi_{2;l}(\rho). \quad (33)$$

This Green's function allows one to deduce the homogeneous integral equation

$$\chi_l(\rho) = -2 \int_0^\infty G(\rho, \rho') \left[\hat{V}_l^{sep} \chi_l \right](\rho') d\rho' \quad (34)$$

for the resonance solution $\chi_l(\rho)$. Here $\left[\hat{V}_l^{sep} \chi_l \right](\rho')$ means the function of ρ' which is the result of action of the operator \hat{V}_l^{sep} on the function $\chi_l(\rho)$. The homogeneous equation (34) has solutions only for unique resonance energy values. Substituting \hat{V}_l^{sep} in Eq. (34) by its explicit expression (28), we obtain:

$$\begin{aligned} \chi_l(\rho) = & 2 \sum_{n=0}^{n_0} \int_0^\infty G(\rho, \rho') \phi_{nl}(\rho') \langle \phi_{nl} | V_{cl;l} | \chi_l \rangle d\rho' \\ & + 2 \left[\int_0^\infty d\rho' G(\rho, \rho') \phi_{n_0 l}(\rho') T_{n_0, n_0+1;l} \right. \\ & \left. + \int_0^\infty d\rho' G(\rho, \rho') \phi_{n_0+2, l}(\rho') \left(1 - \sqrt{\frac{\varepsilon_{n_0+1}}{\varepsilon_{n_0+2}}} \right) T_{n_0+1, n_0+2;l} \right] \langle \phi_{n_0+1, l} | \chi_l \rangle \\ & + 2 \sum_{n=n_0+2}^{n_{\max}-1} \left[\int_0^\infty d\rho' G(\rho, \rho') \phi_{n-1, l}(\rho') \left(1 - \sqrt{\frac{\varepsilon_{n-1}}{\varepsilon_n}} \right) T_{n-1, n;l} \right. \\ & \left. + \int_0^\infty d\rho' G(\rho, \rho') \phi_{n+1, l}(\rho') \left(1 - \sqrt{\frac{\varepsilon_n}{\varepsilon_{n+1}}} \right) T_{n, n+1;l} \right] \langle \phi_{nl} | \chi_l \rangle \\ & + 2 \int_0^\infty d\rho' G(\rho, \rho') \phi_{n_{\max}-1, l}(\rho') \left(1 - \sqrt{\frac{\varepsilon_{n_{\max}-1}}{\varepsilon_{n_{\max}}}} \right) T_{n_{\max}-1, n_{\max};l} \langle \phi_{n_{\max}, l} | \chi_l \rangle, \quad (35) \end{aligned}$$

where n_{max} means the maximum value of the radial quantum number of the truncated oscillator basis. A simple form of the first term is caused by the completeness of the oscillator basis allowing one to calculate the infinite sum over n' in the expression (28) explicitly.

There is an opportunity to treat Eq. (35) in the following way. Multiplying it by $\langle \phi_{nl} |$ and $\langle \phi_{nl} | V_{cl;l}$ one can obtain a set of homogeneous algebraic equations for the unknown coefficients $\langle \phi_{nl} | \chi_l \rangle$ and $\langle \phi_{nl} | V_{cl;l} | \chi_l \rangle$. The condition of solvability (zero value of the determinant) determines the value of E_{res} , after that the coefficients $\langle \phi_{nl} | \chi_l \rangle$ and $\langle \phi_{nl} | V_{cl;l} | \chi_l \rangle$ can be calculated. This procedure determines the function $\chi_l(\rho)$ and thus the width of the resonance.

However such a method of numerical calculations of widths turns out to be unstable at least for narrow resonances in systems possessing a number of semi-forbidden states with eigenvalues of the norm kernel essentially different from the unity. In particular, a very high accuracy (ten significant digits for the 2 MeV resonance in the $^{16}\text{O} + ^{16}\text{O}$ system) of the E_{res} value is required to calculate the width reliably.

A way to overcome this difficulty looks as follows. Consider the above mentioned function obtained via the direct algebraic approach:

$$\tilde{\chi}_l(\rho) = \sum_{n=n_0+1}^{n_{max}} C_{nl} \phi_{nl}(\rho). \quad (36)$$

This function is a partial sum of the oscillator expansion of $\chi_l(\rho)$. It reproduces precisely the behavior of the wave function $\chi_l(\rho)$ in the interior domain. It is just what is needed to calculate the values of $\langle \phi_{nl} | \chi_l \rangle$ and $\langle \phi_{nl} | V_{cl;l} | \chi_l \rangle$ due to a rapid decrease of the functions $\phi_{nl}(\rho)$, $V_{cl;l}(\rho)$ and $\chi_l(\rho)$ with ρ . Thus, substituting $\chi_l(\rho)$ in the right-hand side of the basic equation (35) by $\tilde{\chi}_l(\rho)$, one can obtain the solution for all values of ρ including the asymptotic region. Numerical calculations by means of the proposed method occur to be significantly more stable.

The width of a narrow resonance can be obtained from the solution $\chi_l(\rho)$ by means of the approach presented in the monograph [16]. According to this approach, the following asymptotic relation

$$\chi_l(\rho) \simeq \sqrt{\frac{\Gamma k}{2E_{res}}} G_l(\eta, k\rho) \quad (37)$$

is valid in the case $G_l(\eta, k\rho) \gg F_l(\eta, k\rho)$ in the under-barrier region far enough from the external turning point. The normalization condition

$$\int_0^R \chi_l^2(\rho) d\rho = 1 \quad (38)$$

in the interior region is implied. The described above method of calculation of the resonance wave function with the aid of Eq. (35), allows one to apply directly the formula (37) to determining the decay width Γ .

3 AV OCM and exchange effects in decay processes

3.1 Alpha-decay of 91.84 keV 0^+ resonance in ^8Be

To analyze the interrelation between various approaches based on OCM and RGM models, a canonical object of the physics of clustering, the 91.84 keV 0^+ resonance in the ^8Be nucleus, was studied in Ref. [17].

The width of the ground state of ^8Be nucleus which is a low-laying resonance of the α - α system (the experimental value of the width $\Gamma = 6.8$ eV), was calculated

in various versions of two-body, OCM and RGM dynamics. The proper resonance energy $E = 91.84$ keV was achieved, if necessary, by fitting the depth of the potential well. The following results were obtained.

For an illustration of the results obtained in two-body models with forbidden eigenstates of the Hamiltonian, we consider the model with the Buck potential proposed in Ref. [18] which has the form

$$V(\rho) = V_0 \exp(-b\rho^2) + V_{Coul}, \quad (39)$$

where

$$V_{Coul}(\rho) = (Z_1 Z_2 e^2 / \rho) \operatorname{erf}(\rho/d), \quad (40)$$

and parameters $V_0 = 122.6$ MeV, $b = 0.22$ fm⁻² and $d = 1.33$ fm. The fitting is not required in this case. The value of the resonance energy $E = 91.10$ keV is reproduced in this dynamics. The value of the width coincides with the experimental one ($\Gamma = 6.8$ eV).

The same two-body model with forbidden states which are eigenstates of the kernel \hat{N}_ρ , is used for an illustration of this type of two-body models. The procedure of the resonance energy fit by variation of the potential well depth results in the value $V_0 = 116.9$ MeV. The values deduced for this version are: $E = 91.84$ keV, $\Gamma = 5.8$ eV. Thus the properties of the discussed channel obtained in these two versions of the dynamics, are close enough.

The straightforward RGM calculation using the Hasegawa–Nagata NN potential (see, for example, Ref. [19]) with no fitting results in the values $E = 91.84$ keV, $\Gamma = 4.9$ eV.

At last, the OCM version with the RGM-projected kinetic energy operator (21) and forbidden states which are eigenstates of the kernel \hat{N}_ρ , is analyzed. The Gaussian form of the phenomenological potential with the width equal to the width of the Buck potential ($b = 0.22$ fm⁻²), results in the values: $V_0 = 136.1$ MeV, $E = 91.84$ keV, $\Gamma = 4.7$ eV. Thus the direct inclusion of semi-forbidden states changes the local potential significantly and the results obtained in RGM are well-reproduced by AV OCM.

3.2 Asymptotic normalization coefficient for loosely bound state of the ¹⁷F nucleus

To analyze weakly bound states in the framework of AV OCM, the closed channel ¹⁶O + p , $J^\pi = 1/2^+$ at the energy $E_p = -104.94$ keV was studied in Ref. [20]. This sub-threshold resonance is actively analyzed for astrophysical purposes [21]. The asymptotic behavior of the radial wave function in the two-body model is expressed through the Whittaker function:

$$\phi_l(\rho) \rightarrow D_l W_{-\eta, l+1/2}(2k\rho)/\rho, \quad (41)$$

where

$$\eta = Z_1 Z_2 e^2 \mu / \hbar^2 k \quad (42)$$

is the Coulomb parameter.

The asymptotic normalization coefficient D_l is the factor determining the amplitude of the wave function as $\rho \rightarrow \infty$. In the algebraic version of OCM, the coefficients C_{nl} obtained as the solution of the set of equations (26) are compared with the asymptotic ones which, by analogy with the first approximation of the formula (27), take the form:

$$C_n^{(as)} = \sqrt{r_0} [4/(2n+3)]^{1/4} W_{-\eta, l+1/2}(2k\rho_n) D_l, \quad (43)$$

where $\rho_n = r_0 \zeta_n$ is the turning point of the oscillator wave function $\phi_{nl}(\rho)$. The matching condition $C_n = C_n^{(as)}$ determines the coefficient D_l .

Table 1: The eigenvalues of the overlap kernel for $^{16}\text{O} + N$.

n	0	2	4	6
ε_n	0	1.128906	1.001022	1.000006

Table 2: Depth of the nucleon-nucleus potential V_0 and asymptotic normalization coefficient D_l for the $^{16}\text{O} + p$ system within TBM and AV OCM.

Alternative	V_0 , MeV	D_l , $\text{fm}^{-1/2}$
TBM	49.24	83.33
OCM	47.61	94.18

The nucleon-nucleus potential is chosen in the form:

$$V(\rho) = -V_0 \{1 + \exp[(\rho - R_0)/a]\}^{-1} + V_c(\rho), \quad (44)$$

$$V_c(\rho) = \begin{cases} (4\alpha_e \hbar c / R_c)(3 - \rho^2 / R_c^2), & \rho < R_c, \\ 8\alpha_e \hbar c / \rho, & \rho > R_c, \end{cases} \quad (45)$$

where $\alpha_e = e^2/\hbar c$, and parameters $R_0 = 3.29$ fm, $a = 0.65$ fm, $R_c = 3.48$ fm are used in the model calculations. A numerical solution of the two-body Schrödinger equation is used to test the accuracy of both two-body and the AV OCM variational calculations.

For the discussed channel, the eigenvalues of the norm kernel which are involved in the expression of the renormalized kinetic energy, can be calculated using the formula:

$$\varepsilon_n = 1 + (-1)^n (17n - 1) / 16^n. \quad (46)$$

They are presented in Table 1. As is seen, only $\varepsilon_{n=2}$ differs significantly from the unity.

The values of the D_l coefficient are calculated both in the ordinary two-body model (TBM) and in AV OCM with the RGM-projected kinetic energy operator and forbidden states which are eigenstates of the kernel \hat{N}_ρ . The depth of the local nuclear potential (44) is varied to fit the proton binding energy of 104.94 keV just in the same manner as in the examples of the previous subsection. The results of these calculations are presented in Table 2.

As is seen from Table 2, the inclusion of the exchange terms increases the value of the asymptotic normalization coefficient by 10% in comparison with the two-body one. Microscopic calculations of the asymptotic normalization coefficient in the framework of RGM using NN potentials from Refs. [22] and [23] result in the values of $91.15 \text{ fm}^{-1/2}$ and $86.20 \text{ fm}^{-1/2}$ respectively. The value of $85.65 \text{ fm}^{-1/2}$ was obtained in our RGM calculations with the Hasegawa–Nagata NN potential [19].

3.3 Width of the lowest $^{16}\text{O} + ^{16}\text{O}$ resonance state

To demonstrate the effect of forbidden and the semi-forbidden states on the decay widths of nuclear states in the case of emission of heavy clusters, let us consider the pair $^{16}\text{O} + ^{16}\text{O}$ as an example. Three alternatives are studied:

- (I) OCM with forbidden states considered as eigenstates of the two-body Hamiltonian,
- (II) OCM with forbidden states considered as eigenstates of the norm kernel,

Table 3: Width of the lowest $^{16}\text{O} + ^{16}\text{O}$ resonance state for three versions of the interaction (see the text).

Alternative	(I)	(II)	(III)
V_0 , MeV	399.2	225.6	422.8
E_{res} , MeV	2.103	2.103	2.102
Γ , MeV	$0.59 \cdot 10^{-27}$	$0.53 \cdot 10^{-28}$	$0.64 \cdot 10^{-35}$

(III) OCM with forbidden states of the latter type and semi-forbidden states.

The local cluster-cluster potential from Ref. [24]

$$V_{cl}(\rho) = V_{Coul}(\rho) + \frac{V_0}{(1 + \exp[(\rho - R)/a])^2} \quad (47)$$

is considered. The Coulomb part is chosen in the form of interaction potential of two uniformly charged spherical volumes. According to one of the versions of the model used in Ref. [24], there are 12 forbidden states (eigenstates of the Hamiltonian with the interaction (47)) and a narrow resonance state at the energy of $E = 2.103$ MeV in the partial wave with $l = 0$. This result is reproduced in our calculations realizing the alternative (I). For the alternatives (II) and (III), the depth V_0 of the local potential $V_{cl}(\rho)$ is varied to restore the resonance energy of the alternative (I). The values of the decay width for three versions of OCM are presented in Table 3. The resonance energy is presented to demonstrate the accuracy of its reproduction.

It is clear from the Table that the forbidden and notably the semi-forbidden states change drastically the decay width. If the forbidden states are considered as eigenstates of the norm kernel, the value of the width Γ becomes one order of magnitude smaller than the one obtained assuming these states to be the eigenstates of the two-body Hamiltonian. If, in addition, the semi-forbidden states are also considered, the value of the width Γ turns out to be eight orders of magnitude smaller. Thus a very pronounced exchange effect manifests itself in the properties of a resonance decaying through a channel with a long list of semi-forbidden states which differ significantly from the unity.

It should be noted that parameters of the $^{16}\text{O} + ^{16}\text{O}$ channel (the penetrability of the barrier, the eigenvalues of the norm kernel for the semi-forbidden states, the Γ values) are more or less close to the ones typical for alpha-decays of heavy nuclei. Therefore one may expect similar exchange effects in the latter process.

4 Summary

In the present paper, results of the study of a new version of the orthogonality conditions model are demonstrated in details. The model allows one to take into account exchange effects originating from the norm and kinetic energy overlap kernels. Both continuous and pure algebraic formalisms of the model are developed. The former one is used for the calculation of decay widths of very narrow resonances. The pairs of particles $\alpha + \alpha$, $^{16}\text{O} + p$ and $^{16}\text{O} + ^{16}\text{O}$ are given as examples. The results of the study demonstrate that:

1. Properties of interaction of composite particles are essentially different from the ones of structureless particles.
2. The basic cause of the differences is the exchange effects manifesting themselves via forbidden and semi-forbidden states.

3. Algebraic approaches are convenient tools for considering these effects.
4. The methods developed here for description of composite particle interaction are applicable to the calculations of:
 - a) phase shifts and cross-sections of composite particle scattering including calculations in the framework of the optical model,
 - b) near-threshold bound cluster-nucleus states,
 - c) resonance states of various cluster-cluster pairs including very narrow resonances,
 - d) amplitudes of entrance and exit channels of various reactions.
5. The formalism developed is valid in the case of both clusters being SU(3)-scalars and additionally one of them being an SU(4)-scalar.
6. The effect of semi-forbidden states is drastic in calculations of widths of narrow resonances in interaction of a heavy nucleus with alpha-particle or in interaction of two heavy clusters.

References

- [1] J. A. Wheeler, Phys. Rev. **52**, 1083 (1937).
- [2] J. A. Wheeler, Phys. Rev. **52**, 1107 (1937).
- [3] T. Fließbasch and H.-J. Mang, Nucl. Phys. A **263**, 75 (1976).
- [4] S. Saito, Progr. Theor. Phys. **41**, 705 (1969).
- [5] S. Yu. Igashov, Yu. F. Smirnov and Yu. M. Tchuvil'sky, Bul. Rus. Acad. Sci. Phys. **73**, 756 (2009).
- [6] G. F. Filippov and I. P. Okhrimenko, Phys. At. Nucl. **33**, 932 (1980).
- [7] G. F. Filippov and I. P. Okhrimenko, Phys. At. Nucl. **32**, 928 (1980).
- [8] I. P. Okhrimenko, Nucl. Phys. A **424**, 121 (1984).
- [9] V. G. Neudatchin, V. I. Kukul'in, A. N. Boyarkina and V. P. Korennoy, Lett. Nuovo Cimento **5**, 834 (1971).
- [10] V. G. Neudatchin, V. I. Kukul'in, V. L. Korotkikh and V. P. Korennoy, Phys. Lett. B **34**, 581 (1971).
- [11] H. Horiuchi, Prog. Theor. Phys. Suppl. **62**, 90 (1977).
- [12] H. A. Yamani and L. Fishman, J. Math. Phys. **16**, 410 (1975).
- [13] S. Yu. Igashov, in *The J-Matrix Method. Developments and Applications*, edited by A. D. Alhaidari, E. J. Heller, H. A. Yamani and M. S. Abdelmonem. Springer, 2008, p. 49.
- [14] S. Yu. Igashov, Comp. Math. Math. Phys. **43**, 78 (2003).
- [15] S. Yu. Igashov, Bul. Rus. Acad. Sci. Phys. **65**, 104 (2001).
- [16] S. G. Kadmsky and V. I. Furman, *Alpha-decay and related nuclear reactions*. Energoatomizdat, Moscow, 1985 (in Russian).

- [17] S. Yu. Igashov, A. V. Sinyakov and Yu. M. Tchuvil'sky, *Bul. Rus. Acad. Sci. Phys.* **74**, 1608 (2010).
- [18] B. Buck, H. Fridrich and C. Wheatny, *Nucl. Phys. A* **275**, 246 (1977).
- [19] H. Kanada, T. Kaneko, S. Nagata and M. Nomoto, *Prog. Theor. Phys.* **61**, 1327 (1979).
- [20] S. Yu. Igashov, A. V. Sinyakov and Yu. M. Tchuvil'sky, *Bul. Rus. Acad. Sci. Phys.* **74**, 1612 (2010).
- [21] D. Baye, P. Descouvemont and M. Hesse, *Phys. Rev. C* **58**, 545 (1998).
- [22] A. B. Volkov, *Nucl. Phys.*, **A74**, 33 (1965).
- [23] D. R. Tompson, M. LeMere and Y. C. Tang, *Nucl. Phys. A* **286**, 53 (1977).
- [24] Y. Kondö, in *Proc. Int. Conf. Microscopic Cluster Models of Light Nuclei and Related Topics*. Yukawa Inst. Theor. Phys., 1992, p. 191.

Extreme Neutron Rich Sector of the Nuclear Chart: New Horizons!

K. A. Gridnev^a, V. N. Tarasov^b, D. K. Gridnev^{a,c},
D. V. Tarasov^b, X. Viñas^d and Walter Greiner^c

^a*Department of Physics, St. Petersburg State University, 1 Ulyanovskaya st., St. Petersburg 198504, Russia*

^b*NSC, Kharkov Institute of Physics and Technology, 1 Akademicheskaya st., 61108 Kharkov, Ukraine*

^c*FIAS, Frankfurt University, 1 Ruth-Moufang-Str., Frankfurt am Main 60438, Germany*

^d*Facultat de Física, Universitat de Barcelona, 1 Martí i Franquès, Barcelona E-08028, Spain*

Abstract

Using Hartree-Fock + BCS approach we analyze the behavior of the neutron drip line and predict the appearance of stability peninsulas. The conditions and mechanism for appearance of such peninsulas are analyzed and the properties of newly predicted stable isotopes are investigated.

Keywords: *Hartree-Fock method; BCS; stability; neutron drip line*

One of the fundamental questions in nuclear physics is what combinations of neutrons and protons can build up a stable nucleus. The nuclear landscape called nuclear chart is shown in Figs. 1, 2, 3. A large number of stable isotopes are still nuclear “terra incognita”. Moving away from stable nuclei by adding either protons or neutrons, one finally reaches the particle drip lines where the nuclear binding ends. Nuclei beyond the drip lines are unbound with respect to nucleon emission; that is, for those systems the strong interaction is unable to bind up the constituent nucleons as one nucleus.

The main objective of my talk is to discuss some interesting new qualitative features of the neutron drip line that were predicted in [1, 2, 3, 4], namely, the formation of stability peninsulas. A relatively recent experiment [5] revealed new squares on the nuclear chart, which correspond to stable isotopes ⁴⁰Mg and ⁴²Al. Fig. 1 shows also comparison with existing theoretical predictions. Interestingly, the Nature chooses the most optimistic theoretical scenario regarding stability of isotopes at the drip line. So far the experiment is not capable to detect the entire neutron drip line and, as can be seen in Fig. 2, it is, probably, very far from that. It is, of course, important to foresee the experimental setup that would be able to confirm or invalidate present theoretical predictions.

In our discussion we shall focus on even-even nuclei. A reliable microscopic description of nuclei is obtained with the so-called effective forces between nucleons called Skyrme forces. Their use has become popular since the seminal papers of Vautherin and Brink [6], where these forces were successfully used for systematic description of spherical and deformed nuclei. These forces generally predict very well deformations, sizes, nuclear densities, nucleon separation energies, etc. Their advantage is a relatively small number of parameters and delta-functions in the interaction terms, which facilitate the calculation of integrals considerably.

Let us write out an explicit expression of the Skyrme interaction:

$$V_{ij} = t_0(1 + x_0 P_\sigma)\delta(\mathbf{r}) + \frac{1}{2}t_1(1 + x_1 P_\sigma)[\mathbf{k}'^2\delta(\mathbf{r}) + \delta(\mathbf{r})\mathbf{k}^2] + t_2(1 + x_2 P_\sigma)\mathbf{k}'\delta(\mathbf{r})\mathbf{k} + \frac{1}{6}t_3(1 + x_3 P_\sigma)\rho^\alpha(\mathbf{R})\delta(\mathbf{r}) + iW_0[\mathbf{k}' \times \delta(\mathbf{r})\mathbf{k}](\sigma_i + \sigma_j), \quad (1)$$

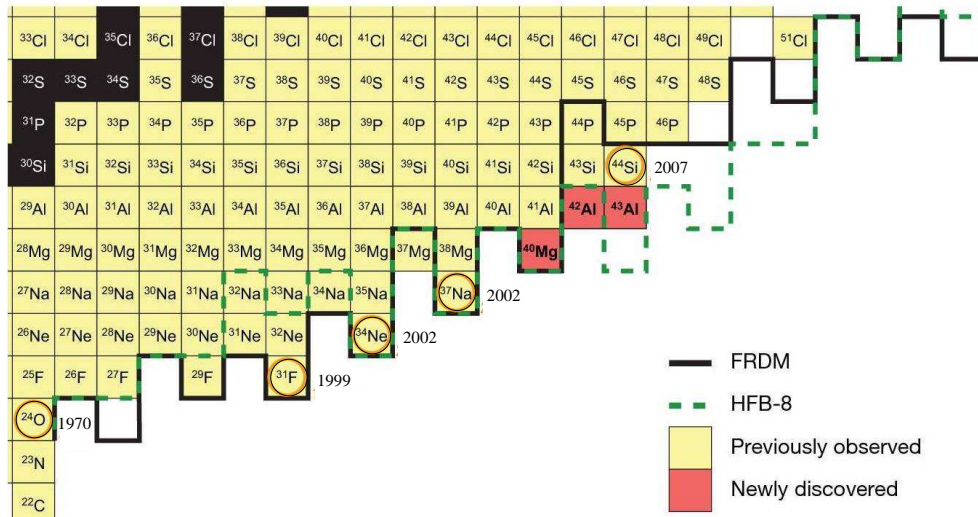


Figure 1: Fragment of the nuclear chart. The proton number increases vertically and the neutron number horizontally. Light squares denote previously observed nuclei. The neutron drip lines predicted by the FRDM and HFB-8 models are shown by the solid and dashed lines, respectively. Recently observed drip-line nuclei are indicated by circles with their year of discovery. The latest discovery also includes ^{40}Mg , ^{42}Al and ^{43}Al which are highlighted with dark fill, see [5].

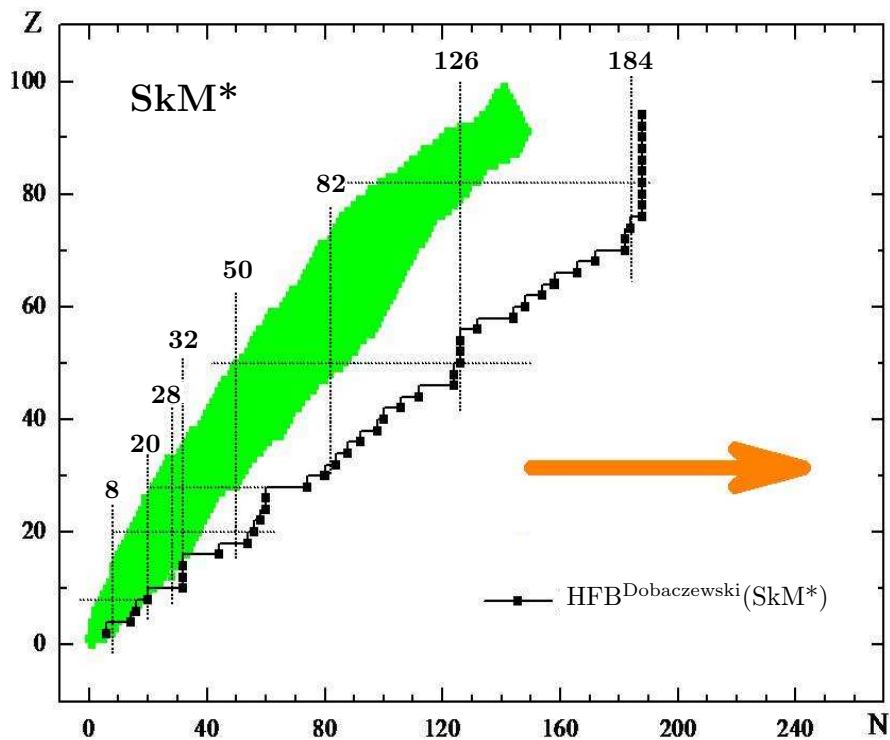


Figure 2: Nuclear chart. Filled area shows experimentally observed nuclei. Black squares correspond to the neutron drip line calculated with the Hartree-Fock-Bogoliubov method [7-8]. The arrow indicates typical direction of the calculations, when one tries to detect the drip line, namely, one increases the neutron number until the saturation point is reached.

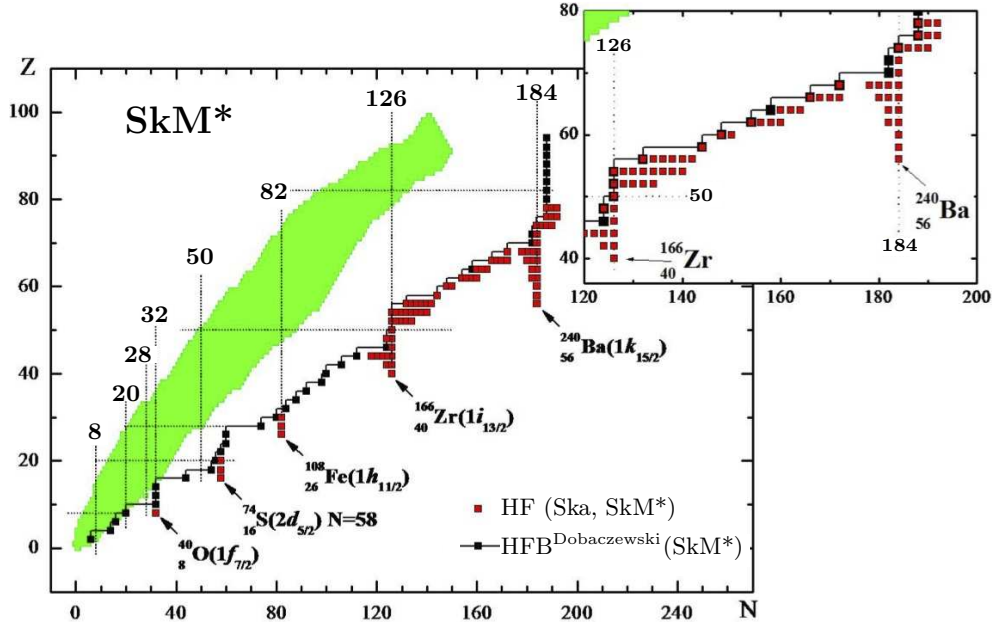


Figure 3: Formation of peninsulas at the neutron drip line. Black squares indicate the drip line obtained within HFB approach using SkM* forces. Filled area shows experimentally known nuclei. Grey squares are nuclei that are predicted stable against one neutron emission in our calculations using Ska and SkM* forces. One can see formation of peninsulas at “magic” numbers and “quenched magic” numbers (see text for details).

where $\mathbf{r} = \mathbf{r}_i - \mathbf{r}_j$, $\mathbf{R} = (\mathbf{r}_i + \mathbf{r}_j)/2$, $\mathbf{k} = -i(\vec{\nabla}_i - \vec{\nabla}_j)/2$, $\mathbf{k}' = -i(\vec{\nabla}_i + \vec{\nabla}_j)/2$, $P_\sigma = (1 + \sigma_i \sigma_j)/2$.

One can see that the force is density dependent. The parameters entering the expression are usually fixed so as to reproduce various bulk nuclear properties as well as selected properties of certain doubly magic nuclei. Some Skyrme forces are presented in Table 1. There is no unique set of parameters and this leads to various versions of the Skyrme force, each of which has its advantages and disadvantages.

After fixing the parameters, the Skyrme forces are used as ingredient in Hartree–Fock calculations, where the ground state wave function is written in the form of a Slater determinant. One also has to introduce a pairing force, which in our case is

Table 1: Parameters of Skyrme forces.

Force	t_0	t_1	t_2	t_3	W_0
	MeV fm ³	MeV fm ⁵	MeV fm ⁵	MeV fm ^{3+3α}	MeV fm ⁵
Sly4	-2488.91	486.82	-546.39	13777.0	123.0
Ska	-1602.78	570.88	-67.70	8000.0	125.0
SkM*	-2645.00	410.00	-135.00	15595.0	130.0

Force	x_0	x_1	x_2	x_3	α
Sly4	0.834	-0.344	-1.0	1.354	1/6
Ska	-0.020	0.0	0.0	-0.286	1/3
SkM*	0.090	0.0	0.0	0.0	1/6

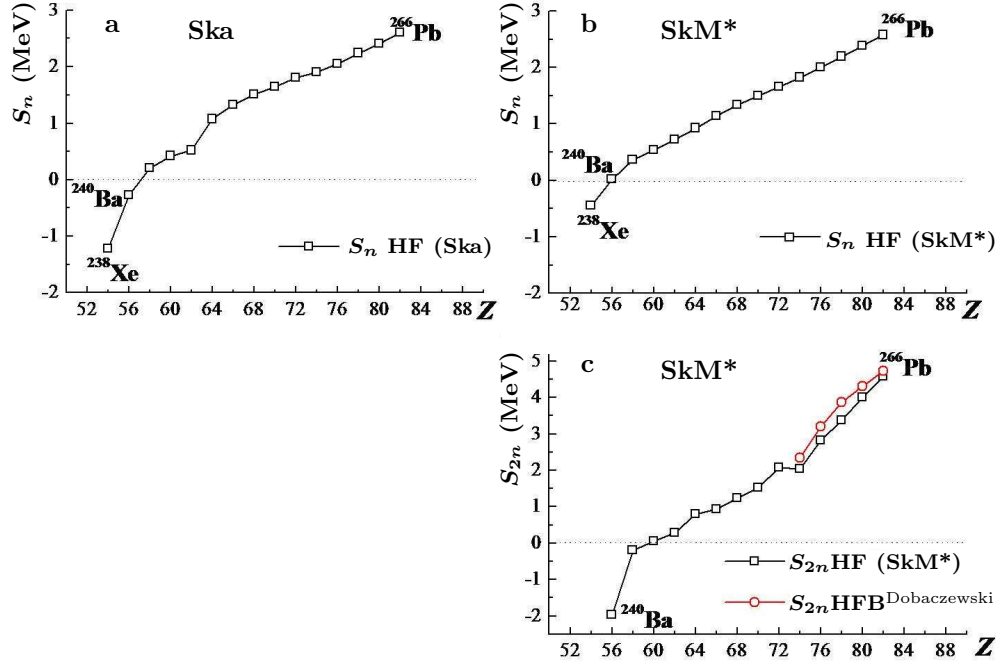


Figure 4: One and two neutron separation energies for the isotones with $N=184$ calculated with Ska, SkM* forces. Circles correspond to HFB calculations [7, 8]. The last element, which is stable against one and two neutrons emission, is ^{244}Nd .

treated in the BCS framework with a pairing constant. We use two procedures to solve Hartree–Fock equations. In the DHF method, which is always used in the case of deformed nuclei, the Hartree–Fock equations are solved using basis functions of the deformed harmonic oscillator. Since we focus our attention on the neutron drip line, one encounters wave functions which correspond to small neutron separation energies, and therefore are very spatially extended. Clearly, one needs basis functions that match such exotic behavior. This is done by adjusting the parameters of the harmonic oscillator on each iteration step. The parameters of the oscillator are chosen in order to minimize the resulting total energy. This helpful procedure of readjusting basis functions reduces substantially the required basis dimension as well as the required number of iterations. In the case of nuclei with spherical symmetry we also employ the SPH procedure, where the equations after reductions due to symmetry are solved on a grid.

In the BCS pairing scheme of DHF calculations, we include only bound one particle states. In spite of ignoring the continuum states this method still provides a good agreement with the HFB (Hartree–Fock–Bogoliubov) calculations [7, 8], see Fig. 4 for comparison. In the BCS scheme of the spherical code, we implement the inclusion of quasibound continuum states which are confined under the centrifugal barrier. To spot such states one introduces a fictitious “wall” forcing the wave functions to vanish beyond it. States remaining localized when the wall is being moved at a large distance, are regarded quasistable and taken into account in the pairing scheme.

The standard theoretical approach in locating the neutron drip line is to take a stable nucleus with a fixed proton charge Z and increase the number of neutrons N until the resulting nucleus would be “overloaded” in the sense that it gets rid of extra neutrons through decay, see Fig. 2. This method, however, implies a simple structure of the drip line, namely, that every line corresponding to a fixed number of protons on the nuclear chart crosses the neutron drip line only once. Yet, it might happen that the drip line has a more complicated structure [1, 2, 3, 4]. In the vicinity of “magic”

numbers or “quenched magic” numbers the following scenario can take place. At some point being filled with neutrons the nucleus loses its stability but then after adding more neutrons the stability is restored. This leads to formation of stability peninsulas on the nuclear chart, see Fig. 3.

The analysis of the phenomenon of stability restoration through adding neutrons has been undertaken in [1, 2, 3, 4]. We have considered long isotope rows of the elements Pb, Zr, Ar, Kr, Rn, Gd, Ba, S, as well as many other elements. Thereby, the phenomenon of stability restoration through adding neutrons was in focus. Having found such new isotopes we also investigated their properties like masses, deformation, root mean square radii, etc.

An important point is also that nuclei forming stability peninsulas are spectrally bound in the sense that there exists a well-defined ground state wave function which minimizes the energy functional for such nuclei. At this point they become well-defined objects and the question about their lifetime is correctly formulated. Even though for some nuclei it may be energetically favorable to get rid of two or more neutrons, a large centrifugal barrier of the last filled levels may serve as an indication that this lifetime would be large. For some nuclei the energetically favorable decay would be into four or more neutrons that enhances the lifetime considerably (such decays were not experimentally observed so far).

In searching for extensions of the neutron drip line limits we proceeded in the standard way adding as many neutrons to the nucleus as possible. Having found an unstable nucleus we did not stop and added more neutrons to see whether the stability can be restored. Gradually, the general picture became clear. One can see in Fig. 3 that stability peninsulas are formed at neutron “magic” numbers or “quenched magic” numbers like in the case of ^{40}O ($N = 32$) or ^{74}S ($N = 58$), which correspond to the filled subshells $1f_{7/2}$ and $2d_{5/2}$ respectively. The stability peninsulas extend vertically along the Z axis in the direction of diminishing Z . Fig. 4 shows how the stability peninsula corresponding to $N = 184$ (a closed shell) extends in Z . This can be seen from one and two neutron separation energies of the isotones. Let us also remark that recent calculations confirm the existence of stability peninsula at $N = 258$, see [9].

In our approach we try different versions of the Skyrme force. Let us stress that just by definition for nuclei at the neutron drip line one expects small one and two neutron separation energies. So it would be rather naive to expect that the drip line calculated with effective forces would exactly match the real one. Even for different forces the difference between separation energies is of order of 0.1 MeV. This is why it is important to check the results with various versions of the Skyrme force. It turns out that the neutron numbers where the stability peninsulas appear, are the same for all forces, only the edges of these peninsulas and the degree to which they are extended depend on the specific version of the force. In view of this striking invariance with respect to the choice of the Skyrme force, we claim that such peninsulas constitute a general qualitative feature of the neutron drip line! Again, let us stress that the nucleon distributions are spherical for nuclei lying on stability peninsulas. This results from the fact that the shells are completely filled at magic numbers. Fig. 5 (top) shows the first isotope ^{40}O that was predicted to form a stability peninsula [1]. It also has a spherically symmetric distribution of nucleons.

The mechanism working behind the formation of stability peninsulas, is usually the same in all cases. When one adds neutrons to an unstable nucleus the totally filled subshell immerses from the continuum to the states with negative energy. For example, in Fig. 5 (bottom) we show how this happens in the case of Radon isotopes. The shell effects are the key to the understanding of these phenomena. Below we list some of the isotopes from the stability peninsulas and the subshells responsible for the stability enhancement:

- $1f_{7/2}$ ^{40}O ;

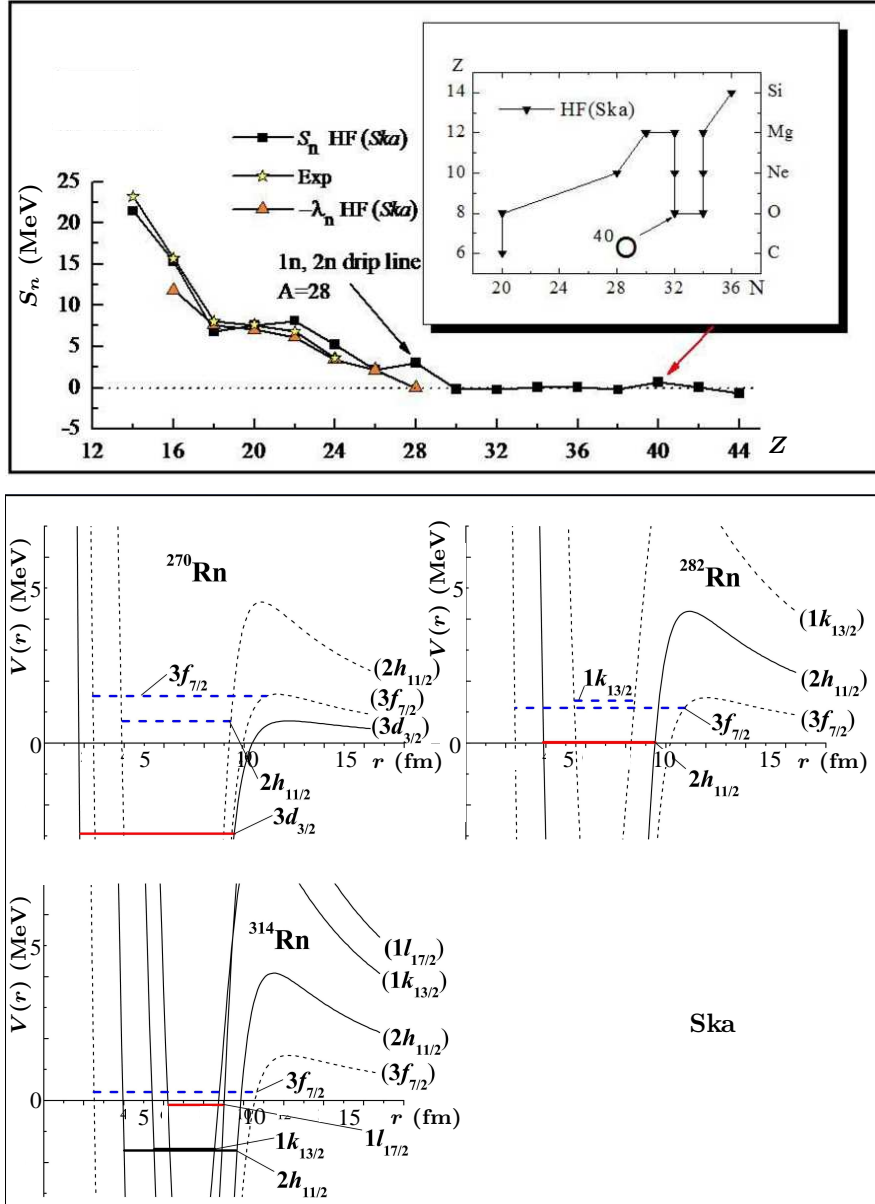


Figure 5: Top: One neutron separation energies of Oxygen isotopes and a fragment of the neutron drip line near ^{40}O . The exotic isotope ^{40}O is stable against one neutron emission and forms a peninsula at the drip line. It has a spherical density distribution. Bottom: the mechanism of stability restoration. In the case of Rn isotopes adding neutrons affects the effective HF potential in such a way that one particle states with high angular momentum are immersed from continuum into the bound spectrum. In the case of magic numbers this leads to stability enhancement. Dashed line show unfilled levels in HF+BCS calculations with Ska forces.

- $2d_{5/2}$ ^{76}Ar , ^{74}S ;
- $1h_{11/2}$ ^{110}Ni , ^{108}Fe ;
- $1i_{13/2}$ ^{174}Cd , ^{172}Pd , ^{170}Ru , ^{168}Mo , ^{166}Zr ;
- $1k_{15/2}$ ^{256}Hf , ^{254}Yb , ^{252}Er , ^{250}Dy , ^{248}Gd , ^{246}Sm , ^{244}Nd , ^{242}Ce , ^{240}Ba .

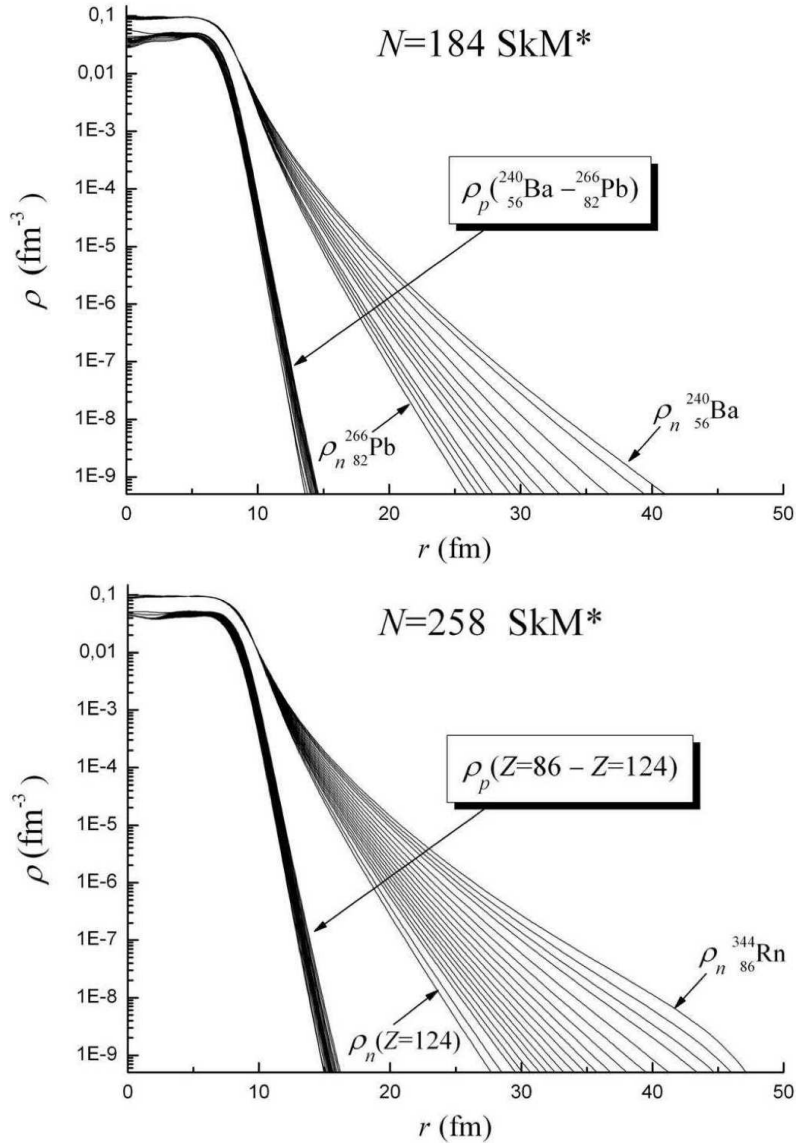


Figure 6: Proton and neutron density distributions for the isotones with $N = 184$ (top) and $N = 258$ (bottom). The calculations are performed with SkM* forces. These are closed shells and the distributions possess spherical symmetry. One can see the enormous spatial extension (halo formation) for a large number of neutrons.

Let us also mention that the wave functions near the drip line produce very spatially extended neutron densities, see Fig. 6. Here one can speak of a large halo formation. To illustrate this we shall compare proton and neutron root mean square radii, which we denote R_p and R_n respectively. For nuclei in the stability valley one has normally $R_n - R_p \simeq 0.1-0.2$ fm. For ^{40}O we obtain $R_n - R_p \simeq 1.29$ fm and $R_n/R_p \simeq 1.44$. For ^{248}Gd we get $R_n - R_p \simeq 0.77$ fm and $R_n/R_p \simeq 1.14$. For ^{240}Ba we obtain $R_n - R_p \simeq 0.94$ fm and $R_n/R_p \simeq 1.17$.

References

- [1] K. A. Gridnev, D. K. Gridnev, V. G. Kartavenko, V. E. Mitroshin, V. N. Tarasov, D. V. Tarasov and W. Greiner, *Eur. Phys. J. A* **25**, 353 (2005).
- [2] K. A. Gridnev, D. K. Gridnev, V. G. Kartavenko, V. E. Mitroshin, V. N. Tarasov, D. V. Tarasov and W. Greiner, *Phys. Atom. Nucl.* **69**, 3 (2006).
- [3] K. A. Gridnev, V. N. Tarasov, D. V. Tarasov, D. K. Gridnev, V. V. Pilipenko and W. Greiner, *Int. J. Mod. Phys. E* **15**, 673 (2006).
- [4] V. N. Tarasov, D. V. Tarasov, K. A. Gridnev, D. K. Gridnev, V. G. Kartavenko and W. Greiner, *Int. J. Mod. Phys. E* **17**, 1273 (2008).
- [5] T. Baumann *et al.*, *Nature* **449**, 1022 (2007).
- [6] D. Vautherin and D. M. Brink, *Phys. Rev. C* **5**, 626 (1972); *Phys. Rev. C* **7**, 296 (1973).
- [7] M. V. Stoitsov, J. Dobaczewski, P. Ring, and S. Pittel, *Phys. Rev. C* **61**, 034311 (2000); <http://www.fuw.edu.pl/~dobaczew/thodri/thodri.html>.
- [8] M. V. Stoitsov, J. Dobaczewski, W. Nazarewicz, S. Pittel, and D. J. Dean, *Phys. Rev. C* **68**, 054312 (2003).
- [9] V. N. Tarasov, K. A. Gridnev, W. Greiner, S. Schramm, D. K. Gridnev, D. V. Tarasov and X. Viñas, *Bull. Russ. Acad. Sci. Phys.* **76**, 876 (2012).

Scattering and Nuclear Structure with Oscillator Basis

A. M. Shirokov

Skobeltsyn Institute of Nuclear Physics, Moscow State University, Moscow 119991, Russia
Department of Physics and Astronomy, Iowa State University, Ames, IA 50011-3160, USA
Pacific National University, Tikhookeanskaya 136, Khabarovsk 680035, Russia

Abstract

We demonstrate that the harmonic oscillator basis can be generated by the Lanczos algorithm. We use this remarkable feature to formulate a formalism in quantum scattering theory utilizing an expansion of scattering wave functions in infinite series of oscillator functions. The continuum spectrum solutions of the Schrödinger equation are found by means of Lanczos iterations. This formalism provides a possibility to extend a nuclear shell model, in particular, an *ab initio* no-core shell model, on a scattering domain.

Keywords: *Non-relativistic quantum scattering theory; nuclear structure; oscillator basis*

An impressive progress in *ab initio* description of nuclear structure has been achieved during the last decade. In addition, research projects aimed at an *ab initio* description of nuclear reactions have advanced. First should be mentioned a combined no-core shell model/resonating group method (NCSM/RGM) approach developed by Navrátil, Quaglioni *et al.* [1]. Various reactions with light nuclei were successfully calculated by means of the NCSM/RGM method. Unfortunately, the RGM approach involves some model assumptions regarding the reaction mechanism which limit the predictive power usually associated with *ab initio* methods. The first attempt to calculate nucleon-nucleus scattering based on quantum Monte Carlo calculations was performed in Ref. [2]. The Gamow shell model [3] provides a possibility to calculate widths of nuclear resonant states. A Lorentz Integral Transform method [4] makes it possible to calculate observables in photonuclear and electroweak reactions within various *ab initio* approaches. This method was successfully used in calculations of cross sections of various photodisintegration, electrodisintegration and electroweak reactions on light nuclei within the hyperspherical harmonics approach [5]. A generalized Lanczos technique was suggested in Ref. [6] for calculations of nuclear response for any multipole operator and general electroweak response functions and electromagnetic responses in particular within theoretical approaches utilizing Slater determinants built on harmonic oscillator basis functions.

A harmonic oscillator provides a natural basis for many-body nuclear structure studies. It is widely used in various shell model applications, in particular, in *ab initio* NCSM [7, 8]. A diagonalization of the shell model Hamiltonian matrix in the many-body oscillator basis is conventionally performed using the Lanczos algorithm.

We demonstrate below that the complete infinite harmonic oscillator basis can be generated by the Lanczos algorithm. The Lanczos technique of generating the oscillator basis can be naturally reformulated as a formalism of non-relativistic quantum scattering theory where scattering wave functions are expanded in infinite series of oscillator functions. We note that this scattering theory formalism is formally equivalent to the J -matrix formalism with oscillator basis [9–12]. An advantage of our formalism is that it utilizes the Lanczos iterations and oscillator basis, the basic tools of various conventional approaches to nuclear structure. Therefore this scattering formalism can be naturally integrated into modern *ab initio* methods for nuclear structure studies

generalizing them to the scattering domain. As a result, one can hope to obtain a unified *ab initio* theory of nuclear structure and reactions.

We start the discussion of the proposed formalism from the case of a two-body scattering problem. Within the quantum scattering theory, one compares the asymptotics of the wave functions Ψ_E fitting the Schrödinger equation with the Hamiltonian H describing the relative motion in the system of interest,

$$H\Psi_E = E\Psi_E, \quad (1)$$

with the asymptotics of the wave function Ψ_E^0 of the reference Hamiltonian H^0 ,

$$H^0\Psi_E^0 = E\Psi_E^0. \quad (2)$$

We discuss here the case of H^0 being a free Hamiltonian, i. e., it includes the operator of kinetic energy of relative motion of colliding particles T only,

$$H^0 = T. \quad (3)$$

We are studying the states of a given angular momentum J and denote by ϕ_i the oscillator state with i excitation quanta, i. e. the state with i oscillator excitations as compared with the lowest oscillator state with the particular value of J . The kinetic energy operator is known to have a tridiagonal matrix in the basis of states ϕ_i , i. e., matrix elements $T_{ij} = \langle \phi_i | T | \phi_j \rangle$ differ from zero only if $i = j$ or $i = j \pm 2$. Therefore applying the operator T to the state ϕ_i , we obtain

$$T\phi_i = T_{i,i-2}\phi_{i-2} + T_{ii}\phi_i + T_{i,i+2}\phi_{i+2}. \quad (4)$$

We note that the Lanczos algorithm with kinetic energy operator T generates the oscillator basis of states with any given angular momentum. ϕ_0 is the lowest oscillator state with the angular momentum J . Let us use ϕ_0 as a pivot vector in the Lanczos procedure. By applying T to ϕ_0 , we get

$$T\phi_0 = T_{00}\phi_0 + T_{02}\phi_2. \quad (5)$$

Orthogonalizing $T\phi_0$ to ϕ_0 and normalizing the resulting function, we obtain ϕ_2 as the first Lanczos vector. The second Lanczos vector is obtained by applying T to ϕ_2 ,

$$T\phi_2 = T_{20}\phi_0 + T_{22}\phi_2 + T_{24}\phi_4, \quad (6)$$

by orthogonalizing the result to ϕ_0 and ϕ_2 and normalization. Clearly, ϕ_4 appears to be the second Lanczos vector. In the same manner we obtain ϕ_6 as the third Lanczos vector, etc. Thus the oscillator basis appears to be a Lanczos basis generated by the kinetic energy operator with ϕ_0 as a pivot vector.

We can construct the oscillator basis by Lanczos procedure not only from below, i. e. starting from the lowest oscillator state, but also from above starting from oscillator states with arbitrary large oscillator quanta. Suppose we have oscillator functions ϕ_N and ϕ_{N+2} . Applying T to ϕ_N , orthogonalizing the result to ϕ_N and ϕ_{N+2} and normalizing, we obtain ϕ_{N-2} as the next Lanczos basis state. At the next step we obtain ϕ_{N-4} , etc.

Expanding the wave function Ψ_E in series of oscillator functions,

$$\Psi_E = \sum_{n=0}^{\infty} a_{2n}(E) \phi_{2n}, \quad (7)$$

we reduce the free Schrödinger equation (2) to an infinite set of three-term recurrent relations (TRR)

$$T_{N,N-2} a_{N-2}(E) + (T_{NN} - E) a_N(E) + T_{N,N+2} a_{N+2}(E) = 0. \quad (8)$$

For positive energies E , these TRR have two linearly-independent solutions, $S_N(E)$ and $C_N(E)$, which analytical expressions are well-known [9, 11, 12]. Only $S_N(E)$ fits the physical TRR boundary condition,

$$T_{00} S_0(E) + (T_{02} - E) S_2(E) = 0, \quad (9)$$

while $C_N(E)$ does not,

$$T_{00} C_0(E) + (T_{02} - E) C_2(E) \neq 0. \quad (10)$$

The solution $S_N(E) \equiv S_{2n}(E)$ is related to the physical solution Ψ_E^0 of the free Schrödinger equation (2) with sine-like asymptotics:

$$\sum_{n=0}^{\infty} S_{2n}(E) \phi_{2n} = \Psi_E^0 = \sqrt{\frac{2}{\pi}} kr j_l(kr) \xrightarrow{r \rightarrow \infty} \sqrt{\frac{2}{\pi}} \sin\left(kr - \frac{\pi l}{2}\right), \quad (11)$$

where $k = \sqrt{2mE}/\hbar$ is the momentum, m is the reduced mass, and l is the orbital angular momentum. The solution $C_N(E) \equiv C_{2n}(E)$ defines the function

$$\Psi_E^C = \sum_{n=0}^{\infty} C_{2n}(E) \phi_{2n} \quad (12)$$

which is regular at the origin and asymptotically coincides with the irregular solution

$$\Psi_E^{0irreg} = -\sqrt{\frac{2}{\pi}} kr n_l(kr) \quad (13)$$

of the free Schrödinger equation (2):

$$\Psi_E^C \xrightarrow{r \rightarrow \infty} \Psi_E^{0irreg} \xrightarrow{r \rightarrow \infty} \sqrt{\frac{2}{\pi}} \cos\left(kr - \frac{\pi l}{2}\right). \quad (14)$$

An arbitrary solution of the TRR (8) is a linear combination of the solutions $S_N(E)$ and $C_N(E)$. Properly normalized solutions can be expressed as

$$a_N(E) = \cos \delta S_N(E) + \sin \delta C_N(E), \quad N = 0, 2, 4, \dots \quad (15)$$

The respective wave function defined through Eq. (7) behaves asymptotically as

$$\Psi_E \xrightarrow{r \rightarrow \infty} \sqrt{\frac{2}{\pi}} \sin\left(kr - \frac{\pi l}{2} + \delta\right), \quad (16)$$

where δ is a scattering phase shift.

Instead of the TRR solutions $S_N(E)$ and $C_N(E)$, one can use another pair of linearly independent solutions, $C_N^+(E)$ and $C_N^-(E)$:

$$C_N^{\pm}(E) = C_N(E) \pm i S_N(E). \quad (17)$$

With the help of $C_N^+(E)$ and $C_N^-(E)$ we can define wave functions Ψ_E^+ and Ψ_E^- ,

$$\Psi_E^{\pm} = \sum_{N=0}^{\infty} C_N^{\pm}(E) \phi_N, \quad (18)$$

with asymptotic behavior

$$\Psi_E^{\pm} \xrightarrow{r \rightarrow \infty} \sqrt{\frac{2}{\pi}} (\mp i)^l e^{\pm ikr}. \quad (19)$$

The functions Ψ_E^\pm are of a particular importance in the case of negative energies E when $k = i\sqrt{2m|E|}/\hbar$ since they decrease asymptotically as bound state wave functions.

We suppose that the Hamiltonian H can be accurately enough approximated by

$$H = T + V^{N_{\max}}, \quad (20)$$

where T is a kinetic energy operator and $V^{N_{\max}}$ is a potential energy in the P space spanned by oscillator states with excitation quanta $N \leq N_{\max}$, i. e. an infinite potential energy matrix in the oscillator basis is well-approximated by a truncated finite matrix which involves only oscillator states with excitation quanta $N \leq N_{\max}$:

$$V^{N_{\max}} = \sum_{n,m=0}^{N_{\max}/2} |\phi_{2n}\rangle \langle \phi_{2n}| V |\phi_{2m}\rangle \langle \phi_{2m}|. \quad (21)$$

The kinetic energy operator T is not truncated in Eq. (20). We note that in conventional shell model applications not only the potential energy V but the kinetic energy operator T is also truncated to the P space. Therefore the suggested approach can be used to extend the nuclear shell model Hamiltonian which is expected to improve the results obtained in conventional nuclear structure calculations. Note also that the potential energy matrix elements $\langle \phi_N | V | \phi_M \rangle$ decrease with N and M when excitation quanta N and M are large enough. On the other hand, the diagonal T_{NN} and off-diagonal $T_{N,N\pm 2}$ kinetic energy matrix elements increase linearly with N for large excitation quanta N . This different behavior of T and V matrix elements with excitation quanta justifies the approximation (20).

We use H to produce the Lanczos basis from above. When applied to the oscillator states ϕ_N and ϕ_{N+2} with large enough quanta N and $N+2$, $N > N_{\max}$, H has the same effect as the pure kinetic energy operator T . Therefore we reproduce with H the oscillator basis states ϕ_{N-2} , ϕ_{N-4} , ..., $\phi_{N_{\max}+2}$ in the Q space and the highest oscillator state in the P space $\phi_{N_{\max}}$. The matrix elements of H in our Lanczos basis in the Q space and the only off-diagonal matrix element $H_{N_{\max}, N_{\max}+2}$ relating the P and Q spaces are equivalent to the kinetic energy matrix elements in the oscillator basis:

$$H_{NN} = T_{NN}, \quad (22)$$

$$H_{N,N-2} = H_{N-2,N} = T_{N,N-2}, \quad (23)$$

$$H_{N,N-m} = H_{N-m,N} = 0, \quad (24)$$

where $N > N_{\max}$ and $m > 2$.

Starting from $\phi_{N_{\max}}$, the potential energy enters the Lanczos procedure. The Lanczos procedure mixes the oscillator states in the P space. The obtained matrix elements in the Lanczos basis H_{NN} and $H_{N,N-2} = H_{N-2,N}$ with $N \leq N_{\max}$ differ from T_{NN} and $T_{N,N+2}$ respectively, all matrix elements $H_{N,N-m} = H_{N-m,N}$ with any N and $m > 2$ vanish. As a result, for the set of coefficients $a_N(E)$ of the expansion (7) of the wave function Ψ_E in the Lanczos basis, we obtain a TRR

$$H_{N,N-2} a_{N-2}(E) + (H_{NN} - E) a_N(E) + H_{N,N+2} a_{N+2}(E) = 0. \quad (25)$$

This TRR should be supplemented by the boundary condition at $N = 0$:

$$H_{00} a_0(E) + (H_{02} - E) a_2(E) = 0. \quad (26)$$

The TRR (25) is infinite, i. e. N can take any even positive value.

To find the solutions of TRR (25), we assign any non-zero value to $a_0(E)$ and obtain $a_2(E)$ using the boundary condition (26), with known $a_0(E)$ and $a_2(E)$ we calculate $a_4(E)$ using TRR (25), next we calculate $a_6(E)$ by means of TRR (25), etc.

In the case of scattering states ($E > 0$), the expansion coefficients $a_N(E)$ with $N \geq N_{\max}$ should be proportional to the r.h.s. of Eq. (15). Knowing the values of two expansion coefficients in the Q space, say, $a_N(E)$ and $a_M(E)$ with $M \neq N$, $M \geq N_{\max}$, $N \geq N_{\max}$, we obtain the scattering phase shift as

$$\tan \delta = -\frac{a_M(E) S_N(E) - a_N(E) S_M(E)}{a_M(E) C_N(E) - a_N(E) C_M(E)}. \quad (27)$$

Expression (27) can be easily derived from Eq. (15).

In the case of bound states ($E < 0$), the coefficients $a_N(E)$ in the Q space are linear combinations of $C_N^+(E)$ and $C_N^-(E)$. The solution $C_N^-(E)$ exponentially increases with N while $C_N^+(E)$ exponentially decreases with N in the limit of $N \rightarrow \infty$. We need to find numerically a negative energy E which provides the decreasing behavior of $a_N(E)$ with N . This is the bound state energy associated with the S -matrix pole which improves the pure variational calculation in the finite oscillator basis.

We use the neutron-nucleus elastic scattering as an example to demonstrate how this Lanczos formalism can be used for a description of nuclear reactions. In this case, we construct a conventional shell model Hamiltonian H^{A+1} of the $(A+1)$ -body system which includes all oscillator states with excitation quanta $N \leq N_{\max}^{A+1}$. The Hamiltonian H^{A+1} acts in the P space and describes the relative kinetic energy of all $A+1$ particles and interactions between them.

We need to define also a channel Hamiltonian

$$h^{ch} = T^{n-A} + H^A \quad (28)$$

describing scattering of the neutron on the A -body nucleus. The Hamiltonian h^{ch} includes a kinetic energy operator of the relative $n-A$ motion T^{n-A} and a truncated Hamiltonian of the A -body subsystem

$$H^A = T^A + V^A. \quad (29)$$

The operator T^A describes the relative kinetic energy of A particles and interaction V^A between them. The operator H^A is defined in the A -body relative motion oscillator states with excitation quanta $N \leq N_{\max}^A$. The wave function Ψ^A describes the internal motion of the A -body subsystem in the ground state,

$$H^A \Psi^A = E^A \Psi^A. \quad (30)$$

The A -body nucleus is supposed to be bound, and hence $E^A < 0$.

We need the channel Hamiltonian to extend the action of the $(A+1)$ -body Hamiltonian H^{A+1} on the subspace of the $(A+1)$ -body Q space associated with the motion in our channel. We note that the channel Hamiltonian h^{ch} acts not only in the Q space but has also some terms acting in the P space already included in H^{A+1} . Therefore we cannot add h^{ch} to H^{A+1} , we should first project out P -space terms in h^{ch} to avoid double counting. However we should preserve the terms of h^{ch} providing a coupling between the P and Q spaces. Therefore we define the projected channel Hamiltonian as

$$H^{ch} = P h^{ch} Q + Q h^{ch} P + Q h^{ch} Q, \quad (31)$$

where P is a projector on the P space, Q is a projector on the Q space and

$$Q + P = 1. \quad (32)$$

Now we can define the Hamiltonian describing our system as

$$H = H^{A+1} + H^{ch}. \quad (33)$$

We construct the Lanczos basis from above starting from channel states $\phi_N \Psi^A$ and $\phi_{N+2} \Psi^A$. Here ϕ_N and ϕ_{N+2} are oscillator functions of relative $n-A$ motion

with N and $N + 2$ quanta respectively. It is supposed that $N > N_{\max}^{A+1}$ where $N_{\max}^{A+1} = N_{\max}^{A+1} + N_{\text{tot}}^{A+1} - N_{\text{tot}}^A$ and N_{tot}^A and N_{tot}^{A+1} are the *total* oscillator quanta in the lowest configuration of the A -body and $(A + 1)$ -body systems respectively. Clearly our states belong to the Q space, and applying the Hamiltonian H to them is equivalent to the application of the channel Hamiltonian H^{ch} to them. Applying H^{ch} to $\phi_N \Psi^A$ we obtain successively Lanczos states $\phi_{N-2} \Psi^A$, $\phi_{N-4} \Psi^A$, ..., $\phi_{N_{\max}^{A+1}} \Psi^A$. The respective TRR is

$$T_{N,N-2}^{n-A} a_{N-2}(E) + (T_{NN}^{n-A} - E^{A+1} + E^A) a_N(E) + T_{N,N+2}^{n-A} a_{N+2}(E) = 0, \quad N > N_{\max}^{A+1}. \quad (34)$$

Here E^{A+1} is the total energy of the $(A + 1)$ -body system, and

$$E^{n-A} = E^{A+1} - E^A \quad (35)$$

is a kinetic energy of the relative $n-A$ motion.

Up to this point all Lanczos states $\phi_{N-2} \Psi^A$, $\phi_{N-4} \Psi^A$, ..., $\phi_{N_{\max}^{A+1}} \Psi^A$ were obtained analytically. Starting from the Lanczos vector $\phi_{N_{\max}^{A+1}} \Psi^A$, the complete $(A + 1)$ -particle P -space Hamiltonian H^{A+1} is involved in the Lanczos procedure. All the remaining Lanczos iterations look like the conventional Lanczos procedure used in standard shell model codes with a specific pivot vector $\phi_{N_{\max}^{A+1}} \Psi^A$. Note however that the Hamiltonian (33) involves an additional term H^{ch} [see Eq. (31)] and the pivot vector $\phi_{N_{\max}^{A+1}} \Psi^A$ generally includes a few terms with excitation quanta $N > N_{\max}^{A+1}$ when the A -body wave function Ψ^A is a mixture of A -body components Ψ_M^A with excitation oscillator quanta $M = 0, 2, 4, \dots, N_{\max}^A$:

$$\Psi^A = \alpha_0 \Psi_0^A + \alpha_2 \Psi_2^A + \alpha_4 \Psi_4^A + \dots + \alpha_{N_{\max}^A} \Psi_{N_{\max}^A}^A. \quad (36)$$

By means of the Lanczos algorithm we obtain TRR

$$H_{N,N-2}^{A+1} a_{N-2}(E) + (H_{NN}^{A+1} - E^{A+1}) a_N(E) + H_{N,N+2}^{A+1} a_{N+2}(E) = 0, \quad N \leq N_{\max}^{A+1}, \quad (37)$$

where

$$H_{N_{\max}^{A+1}, N_{\max}^{A+1}+2}^{A+1} = T_{N_{\max}^{A+1}, N_{\max}^{A+1}+2}^{n-A}. \quad (38)$$

The Lanczos iterations will mix all many-body states in the $(A + 1)$ -body system. Generally the number of Lanczos iterations can be as large as the dimensionality of the $(A + 1)$ -body P space. N in the TRR (37) does not have a meaning of oscillator quanta, it is used only to distinguish various Lanczos basis states and can take negative values. After some reasonable number of Lanczos iterations we should stop and solve the combined set of TRR (34) and (37) for bound or scattering states by the methods discussed above.

The proposed approach can be extended to describe the scattering of charged particles. The Coulomb interaction between all protons should be, of course, included in H^{A+1} . The problem is how to account for the long-range Coulomb interaction between two colliding clusters $V^{Coulomb}$ in the channel Hamiltonian H^{ch} . This can be done by two different ways.

One of the respective techniques has been suggested in Ref. [13] and was widely used in various applications within Resonating Group Method by Kiev group (see, e. g., Ref. [14]). In this case, we explicitly include the Coulomb interaction between two colliding clusters $V^{Coulomb}$ in the channel Hamiltonian H^{ch} . At large excitation quanta, the operator $T^{n-A} + V^{Coulomb}$ can be accurately approximated by a tridiagonal matrix [13]. Therefore at large excitation quanta we can still use TRR (34) with

matrix elements T_{NN}^{n-A} corrected by the Coulomb interaction. However the Coulomb interaction starts mixing P and Q space states at larger values of excitation quanta than the strong nucleon-nucleon interaction. Therefore Lanczos iterations will involve the P space states at larger values of excitation quanta than in the case of neutron-nucleus scattering. This is equivalent to adding a few additional vectors from the Q space to a huge number of basis states in the P space in the conventional diagonalization of the shell model Hamiltonian by means of Lanczos iterations.

Another method for calculating of Coulomb-distorted scattering phase shifts was suggested in Ref. [12] and further verified in Ref. [15]. The idea of this method is that we can cut the Coulomb interaction at some distance r_b from the origin and to use the above technique to calculate the scattering phase shifts in this system which does not have a long-range interaction any more. The Coulomb-distorted scattering phase shifts should be recalculated from the obtained phase shifts by means of a simple analytical formula (see Refs. [12, 15] for details). If the cutoff distance r_b coincides with the classical turning point of the highest single-particle oscillator state involved in the P space, the matrix elements of the Hamiltonian H^{A+1} , the most complicated part of the total Hamiltonian (33), are unaffected (or only very slightly affected) by the Coulomb potential cutoff due to the fast decrease of oscillator functions beyond the classical turning point. The Coulomb interaction can be omitted in the Q -space part of the channel Hamiltonian H^{ch} ; however it may be needed to account for the Coulomb interaction in calculation of some of the H^{ch} matrix elements coupling the P and Q spaces.

We hope that the suggested Lanczos approach will be efficient in the *ab initio* description of various nuclear reactions with light nuclei and for improving results for bound state energies obtained in shell model calculations.

This work was supported in part by the US Department of Energy Grants Nos DE-FG02-ER40371 and DESC0008485 (SciDAC-3/NUCLEI), by the Ministry of Education and Science of the Russian Federation Grant 14.V37.21.1297, by the Russian Foundation of Basic Research and by the American Physical Society through the International Travel Grant Award Program.

References

- [1] P. Navrátil, S. Quaglioni, I. Stetcu and B. R. Barrett, *J. Phys. G* **36**, 083101 (2009); P. Navrátil, S. Quaglioni and R. Roth, *J. Phys. Conf. Ser.* **312**, 082002 (2011).
- [2] K. M. Nollett, S. C. Pieper, R. B. Wiringa, J. Carlson and G. M. Hale, *Phys. Rev. Lett.* **99**, 022502 (2007).
- [3] N. Michel, W. Nazarewicz, M. Płoszajczak and K. Bennaceur, *Phys. Rev. Lett.* **89**, 042502 (2002).
- [4] V. D. Efros, *Phys. At. Nucl.* **62**, 1833 (1999).
- [5] V. D. Efros, W. Leidemann, G. Orlandini and N. Barnea, *J. Phys. G* **34**, R459 (2007); W. Leidemann, *Nucl. Phys. A* **790**, 24 (2007); W. Leidemann, *Int. J. Mod. Phys. E* **18**, 1339 (2009).
- [6] W. Haxton, K. M. Nollett and K. M. Zurek, *Phys. Rev. C* **72**, 065501 (2005).
- [7] D. C. Zheng, J. P. Vary and B. R. Barrett, *Phys. Rev. C* **50**, 2841 (1994); D. C. Zheng, B. R. Barrett, J. P. Vary, W. C. Haxton and C. L. Song, *Phys. Rev. C* **52**, 2488 (1995).
- [8] P. Navrátil, J. P. Vary and B. R. Barrett, *Phys. Rev. Lett.* **84**, 5728 (2000); P. Navrátil, J. P. Vary and B. R. Barrett, *Phys. Rev. C* **62**, 054311 (2000).

- [9] H. A. Yamani and L. Fishman, *J. Math. Phys.* **16**, 410 (1975).
- [10] G. F. Filippov and I. P. Okhrimenko, *Sov. J. Nucl. Phys.* **32**, 480 (1980);
G. F. Filippov, *Sov. J. Nucl. Phys.* **33**, 488 (1981).
- [11] Yu. F. Smirnov and Yu. I. Nechaev, *Kinam* **4**, 445 (1982); Yu. I. Nechaev and
Yu. F. Smirnov, *Sov. J. Nucl. Phys.* **35**, 808 (1982).
- [12] J. M. Bang, A. I. Mazur, A. M. Shirokov, Yu. F. Smirnov and S. A. Zaytsev,
Ann. Phys. (NY) **280**, 299 (2000).
- [13] I. P. Okhrimenko, *Nucl. Phys. A* **424**, 121 (1984).
- [14] A. Sytcheva, F. Arickx, J. Broeckhove and V. S. Vasilevsky, *Phys. Rev. C* **71**,
044322 (2005).
- [15] A. M. Shirokov, A. I. Mazur, J. P. Vary and E. A. Mazur, *Phys. Rev. C* **79**,
014610 (2009).

Computing Binary Scattering and Breakup in Three-Body System

P. A. Belov, E. R. Nugumanov and S. L. Yakovlev

*Department of Computational Physics, St. Petersburg State University, 1 Ulyanovskaya st.,
Saint-Petersburg 198504, Russia*

Abstract

Two approaches for computing binary and breakup amplitudes for three-body scattering above the breakup threshold are presented. The asymptotic approach provides a way to take into account the orthogonality of the binary and breakup channels. It reduces the problem to a boundary value problem with known inhomogeneous boundary conditions. The scattering amplitudes are calculated without reconstruction of the solution over the entire configuration space. The complex-scaling method reduces the scattering problem to a boundary value problem with homogeneous zero boundary conditions. It allows calculating the amplitudes via an integral representations. Both methods are applied to neutron-deuteron scattering. The binary and breakup amplitudes are calculated using a developed parallel algorithm.

Keywords: *Three-body systems; Faddeev equations; binary amplitude; breakup amplitude; asymptotic approach; complex-scaling method; domain decomposition method*

1 Introduction

Study of three-body scattering problems includes developing reliable analytical approaches as well as effective computational techniques. One of the approaches for treating neutron-deuteron (nd) scattering above the breakup threshold is based on the three-body configuration space Faddeev formalism [1]. The differential Faddeev equations are reduced to a boundary value problem by implementing appropriate boundary conditions. The existing boundary conditions have been introduced by S. P. Merkuriev [2]. In this paper we continue developing the boundary value problem approach for Faddeev equations. We introduce a new representation for Merkuriev boundary conditions and apply the complex-scaling method for obtaining the zero boundary value problem for Faddeev equations.

In the first approach [3], the asymptotic boundary conditions are represented in the form of the hyperspherical adiabatic expansion. This expansion is constructed in such a way that the binary and breakup channels are orthogonal at any value of the hyper-radius. This property allows using the asymptotic value of the Faddeev component as the boundary value [4] for the Faddeev equation. This approach makes it possible to calculate scattering parameters at the asymptotic region through the solution of the boundary value problem with the inhomogeneous boundary conditions in the asymptotic region, i. e. without reconstruction of the solution in the entire configuration space.

The second approach is to take advantage of the exterior complex-scaling method [5] for the inhomogeneous Faddeev equations. The method allows us to reduce the asymptotic boundary conditions to the homogeneous zero conditions at large separation of particles by the rotation of the hyper-radius into the upper complex half-plane. This approach demands calculation of the integral representation [1, 6] for scattering amplitudes. Therefore, it needs the reconstruction of the full solution over the entire configurational space.

The numerical solution of the problem includes solving the linear systems of equations with block tridiagonal matrices of large orders. The matrix sweeping algorithm [7] is a traditional computational scheme for such problems. Despite the fact that the algorithm is well defined and robust for matrices with diagonal dominance its recursive nature leads to a negative effect for taking advantage of parallel computers for large matrices. For our first approach, we use a technically simple scheme of matrix sweeping algorithm for forward elimination step which produces the solution only at the asymptotic region. For the second approach which requires the complete solution, we have to take advantage of parallel algorithms and to perform calculations using supercomputing facilities. In this case, the sweeping algorithm is applicable only as a brute-force algorithm due to its hard parallelization. For this case we have developed a new domain decomposition method (DDM). Using DDM on the supercomputer cluster allows us to reduce the computation time by an order of magnitude comparing to the brute-force algorithm.

The developed algorithms include conventional linear algebra packages as LAPACK and principal implementations of parallel programming concepts. The scattering amplitudes obtained by both approaches have been compared against each other and with results in [8].

The plan of the paper is as follows. In the second section a brief formulation of the three-body scattering problem is presented. The third section describes methods of solving the stated problem. The equations and the corresponding boundary conditions for each of approaches are given here. The computational methods as well as its parallelization are discussed in the fourth section. The obtained results are summarised and compared in the last fifth section before the conclusion.

The authors are thankful to E. A. Yarevsky for valuable suggestions concerning the application of the complex-scaling method. All calculations presented in the paper have been performed using the supercomputing facilities of the Computational Resources Center of SPbSU.

2 Formulation of the problem

The nd system under consideration is described by differential Faddeev equation of the form [1]

$$(-\Delta + V(\mathbf{x}) - E)U(\mathbf{X}) = -V(\mathbf{x})(P^+ + P^-)U(\mathbf{X}) \quad (1)$$

for the Faddeev component U of the wave function Ψ . The center-of-mass frame of standard Jacobi coordinates $\{\mathbf{x}, \mathbf{y}\} = \mathbf{X}$ [1] is used throughout. The expansion of the wave function into components is written as

$$\Psi(\mathbf{X}) = (I + P^+ + P^-)U(\mathbf{X}),$$

where P^\pm is the cycling and anti-cycling permutation operators of three particles and I is the unit operator. The s -wave equations for the radial part of the Faddeev wave function component appear from the equation (1) after projection onto the states with zero orbital momentum in all pairs of the three-body system. These s -wave Faddeev equations are given by [9]

$$\left(-\frac{\partial^2}{\partial x^2} - \frac{\partial^2}{\partial y^2} + V^J(x) - E\right)U^J(x, y) = -V^J(x) \int_{-1}^1 d\mu \frac{xy}{x'y'} \mathbf{B}^J U^J(x', y'), \quad (2)$$

where

$$x' = \left(\frac{x^2}{4} - \frac{\sqrt{3}}{2}xy\mu + \frac{3y^2}{4}\right)^{1/2},$$

$$y' = \left(\frac{3x^2}{4} + \frac{\sqrt{3}}{2}xy\mu + \frac{y^2}{4} \right)^{1/2},$$

$$\mu = \cos(\hat{x}, \hat{y}).$$

The superscript J labels states with a given total momentum that coincides with the total spin of the system in our case. For $J = 1/2$ (doublet), $U^{1/2}$ is a three-component function $(U_1^{1/2}, U_2^{1/2}, U_3^{1/2})^T$, whereas $U^{3/2}$ is a scalar (quartet). The potentials are defined as follows: $V^{1/2} = \text{diag}\{V^t, V^s, V^s\}$, $V^{3/2} = V^t$, where V^t and V^s are triplet and singlet potentials of NN -interaction [8]. Numerical matrices \mathbf{B}^J are given as

$$\mathbf{B}^{1/2} = \begin{pmatrix} 1/4 & -3/4 & 0 \\ -3/4 & 1/4 & 0 \\ 0 & 0 & -1/2 \end{pmatrix}, \quad \mathbf{B}^{3/2} = -1/2.$$

The energy E in the center-of-mass system and the relative neutron momentum q are associated with the deuteron ground state energy $\varepsilon < 0$ by the equation $q^2 = E - \varepsilon$. The deuteron ground state wave function satisfies the equation

$$\left(-\frac{d^2}{dx^2} + V^{3/2}(x) \right) \varphi(x) = \varepsilon \varphi(x) \quad (3)$$

with the zero boundary conditions at zero and infinity.

The solution of the s -wave Faddeev equations (2) for nd scattering above the breakup threshold ($E > 0$) should satisfy the boundary conditions [2]

$$U_1^{1/2}(x, y) \sim \varphi(x) \left(\sin qy + a_0^{1/2}(q) \exp i qy \right) + A_1^{1/2}(\theta, E) \frac{\exp i\sqrt{E}\rho}{\sqrt{\rho}}, \quad (4)$$

$$U_i^{1/2}(x, y) \sim A_i^{1/2}(\theta, E) \frac{\exp i\sqrt{E}\rho}{\sqrt{\rho}}, \quad i = 2, 3, \quad (5)$$

$$U^{3/2}(x, y) \sim \varphi(x) \left(\sin qy + a_0^{3/2}(q) \exp i qy \right) + A^{3/2}(\theta, E) \frac{\exp i\sqrt{E}\rho}{\sqrt{\rho}}, \quad (6)$$

where $\rho = \sqrt{x^2 + y^2}$, $\tan \theta = y/x$, as $\rho \rightarrow \infty$, and the conditions $U(x, 0) = U(0, y) = 0$ guarantee the regularity of the solution at zero. The structure of the numerical matrix $\mathbf{B}^{1/2}$ makes it possible to reject the third uncoupled equation in (2) and thus to simplify the problem. The functions $a_0^J(q)$ and $A_i^J(\theta, E)$ are the binary amplitude and the Faddeev component of the breakup amplitude, respectively. The integral representations for these functions in the simplest case $J = 3/2$ are of the form [1]

$$a_0^{3/2}(q) = \frac{1}{q} \int_0^\infty dy \sin qy \int_0^\infty dx \varphi(x) \mathcal{K}(x, y) \quad (7)$$

and

$$A^{3/2}(\tilde{\theta}, E) = \sqrt{\frac{2}{\pi\sqrt{E}}} e^{i\pi/4} \int_0^\infty dy \sin qy \int_0^\infty dx \phi(\sqrt{E} \cos \tilde{\theta}, x) \mathcal{K}(x, y), \quad (8)$$

where $\phi(k, x)$ is the scattering two-body wave function

$$\phi(k, x) \xrightarrow{x \rightarrow \infty} e^{i\delta(k)} \sin(kx + \delta(k))$$

and

$$\mathcal{K}(x, y) = \frac{1}{2} V^{3/2}(x) \int_{-1}^1 d\mu \frac{xy}{x'y'} U^{3/2}(x', y').$$

Taking into account the change of the unknown function $\mathcal{U}^J(\rho, \theta) \equiv \sqrt{\rho} U^J(x, y)$, the transformation to the hyperspherical coordinates $\{\rho, \theta\}$ leads to the following equations:

$$\begin{aligned} \left(-\frac{\partial^2}{\partial \rho^2} - \frac{1}{4\rho^2} - \frac{1}{\rho^2} \frac{\partial^2}{\partial \theta^2} + V^{3/2}(\rho \cos \theta) - E \right) \mathcal{U}^{3/2}(\rho, \theta) \\ = \frac{2}{\sqrt{3}} V^{3/2}(\rho \cos \theta) \int_{\theta_-(\theta)}^{\theta_+(\theta)} \mathcal{U}(\rho, \theta') d\theta' \quad (9) \end{aligned}$$

for $J = 3/2$ and

$$\begin{aligned} \left(-\frac{\partial^2}{\partial \rho^2} - \frac{1}{4\rho^2} - \frac{1}{\rho^2} \frac{\partial^2}{\partial \theta^2} + V^t(\rho \cos \theta) - E \right) \mathcal{U}_1^{1/2}(\rho, \theta) \\ = -\frac{1}{\sqrt{3}} V^t(\rho \cos \theta) \int_{\theta_-(\theta)}^{\theta_+(\theta)} \left(\mathcal{U}_1^{1/2}(\rho, \theta') - 3\mathcal{U}_2^{1/2}(\rho, \theta') \right) d\theta', \quad (10a) \end{aligned}$$

$$\begin{aligned} \left(-\frac{\partial^2}{\partial \rho^2} - \frac{1}{4\rho^2} - \frac{1}{\rho^2} \frac{\partial^2}{\partial \theta^2} + V^s(\rho \cos \theta) - E \right) \mathcal{U}_2^{1/2}(\rho, \theta) \\ = -\frac{1}{\sqrt{3}} V^s(\rho \cos \theta) \int_{\theta_-(\theta)}^{\theta_+(\theta)} \left(-3\mathcal{U}_1^{1/2}(\rho, \theta') + \mathcal{U}_2^{1/2}(\rho, \theta') \right) d\theta' \quad (10b) \end{aligned}$$

for $J = 1/2$. The integration limits are defined, in turn, as $\theta_-(\theta) = |\pi/3 - \theta|$, $\theta_+(\theta) = \pi/2 - |\pi/6 - \theta|$ and the boundary conditions (4)–(6) should be multiplied by $\sqrt{\rho}$.

3 The solution methods

3.1 The asymptotic approach

The equations (9)–(10) are solved via expansion of the unknown function in basis functions associated with the eigenvalue problem for the operator $h(\rho)$:

$$h(\rho)\phi_k(\rho|\theta) = \left(-\frac{1}{\rho^2} \frac{\partial^2}{\partial \theta^2} + V^J(\rho \cos \theta) \right) \phi_k(\rho|\theta) = \lambda_k^J(\rho)\phi_k(\rho|\theta), \quad \theta \in [0, \pi/2]. \quad (11)$$

The spectral properties of this operator [3] allow us to orthogonalize the binary and breakup scattering channels and hence to reformulate [3] the problem in such a way that the boundary conditions (4)–(6) can be represented as the following equivalent ones:

$$\mathcal{U}^{3/2}(\rho, \theta) \sim \phi_0(\rho|\theta) \left(\mathcal{Y}_0(q\rho) + a_0^{3/2}(q) \mathcal{H}_0(q\rho) \right) + \sum_{k=1}^{N_\phi} \phi_k(\rho|\theta) a_k^{3/2}(E) \mathcal{H}_k(\sqrt{E}\rho) \quad (12)$$

for $J = 3/2$, and

$$\mathcal{U}_1^{1/2}(\rho, \theta) \sim \phi_0(\rho|\theta) \left(\mathcal{Y}_0(q\rho) + a_0^{1/2}(q) \mathcal{H}_0(q\rho) \right) + \sum_{k=1}^{N_\phi} a_{1,k}^{1/2}(E) \phi_k(\rho|\theta) \mathcal{H}_k(\sqrt{E}\rho), \quad (13a)$$

$$\mathcal{U}_2^{1/2}(\rho, \theta) \sim \sum_{k=1}^{N_\phi} a_{2,k}^{1/2}(E) \phi_k(\rho|\theta) \mathcal{H}_k(\sqrt{E}\rho) \quad (13b)$$

for $J = 1/2$. Here $\mathcal{Y}_0(t)$ and $\mathcal{H}_k(t)$ are expressed by

$$\mathcal{Y}_0(t) = \sqrt{\frac{\pi t}{2}} \frac{Y_0(t) + J_0(t)}{\sqrt{2}},$$

$$\mathcal{H}_k(t) = \sqrt{\frac{\pi t}{2}} H_{2k}^{(1)}(t) \exp i\left(\frac{\pi}{4} + \pi k\right)$$

through Bessel functions J_0 , Y_0 and Hankel functions of the first kind $H_k^{(1)}$ [10]. The Faddeev component of the breakup amplitude is expressed in this case as a linear combination

$$A_i^J(\theta, E) = \lim_{\rho \rightarrow \infty} A_i^J(\theta, E, \rho) = \lim_{\rho \rightarrow \infty} \sum_{k=1}^{N_\phi} a_{i,k}^J(E) \phi_k(\rho|\theta),$$

whereas the binary amplitude is given by $a_0^J(q)$.

The extraction of the coefficients $a_{i,k}^J$ of the presented linear combination, for example, in the case $J = 3/2$ is performed as follows. The boundary value problems with the boundary conditions given by separate terms of Eq. (12) and taken at some last knot $\rho_{max} + h$ are solved and the solutions $\mathcal{U}_k(\rho_{max})$ at the next-to-last knot are obtained. Parameter ρ_{max} is chosen to be large enough in order to use the asymptotic representation for the solutions in the asymptotic region. Constructing the complete solution as a linear combination

$$\mathcal{U} = \mathcal{U}_{\sin} + a_0^{3/2} \mathcal{U}_0 + \sum_{k=1}^{N_\phi} a_k^{3/2} \mathcal{U}_k, \quad (14)$$

we assume that in this asymptotic region $\rho = \rho_{max}$ the constructed solution (14) is equal to the asymptotics (12):

$$\mathcal{U}_{\sin} + a_0^{3/2} \mathcal{U}_0 + \sum_{k=1}^{N_\phi} a_k^{3/2} \mathcal{U}_k = \phi_0 \left(\mathcal{Y}_0 + a_0^{3/2} \mathcal{H}_0 \right) + \sum_{k=1}^{N_\phi} a_k^{3/2} \phi_k \mathcal{H}_k. \quad (15)$$

This provides the system of linear equations for calculation of $a_k^{3/2}$ in the asymptotic region, i. e. using the orthogonality of the basis and projecting Eqs. (15) on the basis functions ϕ_l , one can obtain the desired system of equations for $a_k^{3/2}$:

$$a_0^{3/2} [\langle \phi_l | \mathcal{U}_0 \rangle - \langle \phi_l | \phi_0 \mathcal{H}_0 \rangle] + \sum_{k=1}^{N_\phi} a_k^{3/2} [\langle \phi_l | \mathcal{U}_k \rangle - \langle \phi_l | \phi_k \mathcal{H}_k \rangle] = -\langle \phi_l | \mathcal{U}_{\sin} \rangle + \langle \phi_l | \phi_0 \mathcal{Y}_0 \rangle.$$

3.2 The exterior complex-scaling method

The exterior complex-scaling method [5] implies a substitution of the variable ρ in Eqs. (9)–(10) by a complex function $R(\rho)$ according to the formula

$$R(\rho) = \begin{cases} \rho & \rho < \rho_0 \\ \rho_0 + f(\rho, \rho_0, \omega, \{p_i\}) & \rho \geq \rho_0 \end{cases},$$

where the introduced complex function f defines the curve of $R(\rho)$ in the complex plane and can depend on some number of predefined parameters p_i . Then the partial second derivative in equations (9)–(10) is expressed as

$$\frac{\partial^2}{\partial R^2} = -\frac{R''_\rho}{(R'_\rho)^3} \frac{\partial}{\partial \rho} + \frac{1}{(R'_\rho)^2} \frac{\partial^2}{\partial \rho^2}. \quad (16)$$

The continuity properties of $R(\rho)$ define the validity of Eq. (16) and the smoothness of the scaling. The simplest case of the sharp exterior complex-scaling demands to have f in the form

$$f(\rho, \rho_0, \omega, \{p_i\}) = (\rho - \rho_0)e^{i\omega}, \quad (17)$$

which prescribes the rotation to the upper complex half-plane by the angle ω . The derivative R'_ρ in this case has the discontinuity at ρ_0 and this might affect the applicability of the formula (16). A smooth exterior complex-scaling can be given by a more complicated function f which provides a continuity of function $R(\rho)$ together with the first and second derivatives. Nevertheless, the limiting behavior of f as $\rho \rightarrow \infty$ should have a form (17). For example, the function f for the smooth scaling can be given by

$$f(\rho, \rho_0, \omega, p) = (\rho - \rho_0) e^{i\omega} (1 - \exp[-p(\rho - \rho_0)]).$$

In the present work for this type of scaling we use fifth order polynomial function with some chosen coefficients.

The impact of the complex rotation on the asymptotics results in an exponential decrease of the scattered waves. For simplicity, we will consider the quartet asymptotics $\mathcal{U}^{3/2}$ and the sharp complex-scaling. In the hyperspherical coordinates the asymptotics (4) is given by the formula

$$\mathcal{U}^{3/2}(R, \theta) \sim \sqrt{R} \varphi(R \cos \theta) \left(\sin qy + a_0^{3/2}(q) \exp i qy \right) + A^{3/2}(\theta, E) \exp i\sqrt{E}R.$$

The sharp complex rotation of the binary scattered wave $\exp(iqR \cos \theta)$ produces the term

$$\exp(iq[\rho_0 + (\rho - \rho_0) \cos \omega] \sin \theta) \exp(-q(\rho - \rho_0) \sin \omega \sin \theta),$$

which exponentially vanishes as $\rho \rightarrow \infty$ and the angle of the rotation determines the rate of vanishing. The breakup scattered wave shows a similar behaviour. In contrast, the incoming wave $\sin(qR \cos \theta)$ does not vanish after the complex rotation. This wave is subtracted from the asymptotics and consequently from the unknown solution. Hence, in the case of $J = 3/2$, the inhomogeneous equation

$$\begin{aligned} & \left(-\frac{\partial^2}{\partial R^2} - \frac{1}{4R^2} - \frac{1}{R^2} \frac{\partial^2}{\partial \theta^2} + V(R \cos \theta) - E \right) \tilde{\mathcal{U}}^{3/2}(R, \theta) \\ & - \frac{2}{\sqrt{3}} V(R \cos \theta) \int_{\theta_-(\theta)}^{\theta_+(\theta)} \tilde{\mathcal{U}}^{3/2}(R, \theta') d\theta' \\ & = \frac{2}{\sqrt{3}} V(R \cos \theta) \int_{\theta_-(\theta)}^{\theta_+(\theta)} \sqrt{R} \varphi(R \cos \theta') \sin(qR \sin \theta') d\theta'. \end{aligned}$$

for $\tilde{\mathcal{U}}^{3/2} = \mathcal{U}^{3/2} - \sqrt{R} \varphi(R \cos \theta') \sin(qR \sin \theta')$ with homogeneous zero boundary conditions

$$\tilde{\mathcal{U}}^{3/2}(R, \theta) \Big|_{\rho=0} = 0, \quad \tilde{\mathcal{U}}^{3/2}(R, \theta) \Big|_{\rho \rightarrow \infty} = 0$$

is obtained. The similar equations with vanishing zero boundary conditions can be obtained for the case $J = 1/2$.

Within a framework of this method, the binary and breakup amplitudes are calculated using the integral representations (7) and (8), respectively. The complete solution for all values of hyper-radius $\rho \in [0, \rho_{max}]$, where $\rho_{max} > \rho_0$, is reconstructed and a part of the solution at real values of $R(\rho)$ is then used for calculation.

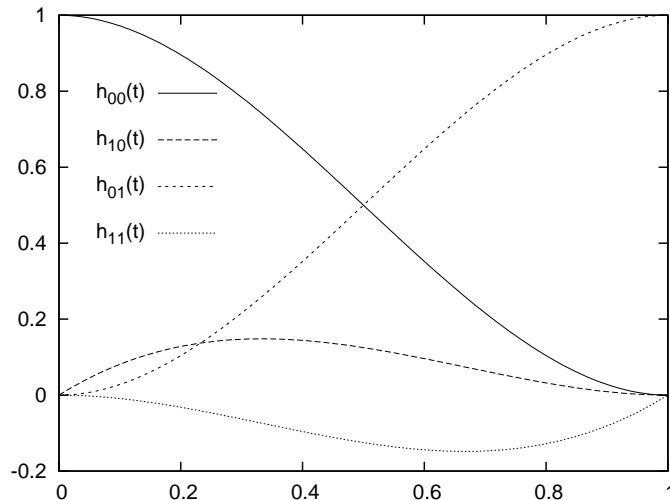


Figure 1: The cubic Hermite splines (18) at the unit interval.

4 The computational scheme

The two-dimensional boundary value problem is solved in the hyperspherical coordinates $\{\rho, \theta\}$ due to proper description of the boundary conditions and appropriate representation of the two-body operator (11). Therefore, the computational scheme meets the requirements of a good representation of this θ -dependent operator. As a result, the unknown solution as a function of the coordinate θ is expanded in the basis of cubic Hermit splines [11]. These four splines are defined at the unit interval by the formulae

$$\begin{aligned} h_{00}(t) &= 2t^3 - 3t^2 + 1, \\ h_{10}(t) &= t^3 - 2t^2 + t, \\ h_{01}(t) &= -2t^3 + 3t^2, \\ h_{11}(t) &= t^3 - t^2, \end{aligned} \quad (18)$$

and can be transferred by linear transformations to two consecutive intervals of θ -grid. The splines are shown in Fig. 1. In order to obtain the θ -grid, a specially chosen nonequidistant x -grid for operator (3) has been used and transformed by the relation

$$\theta_i(\rho) = \arccos \frac{x_i}{X(\rho)}, \quad \theta_i \in [0, \pi/2].$$

Here the parameter $X(\rho)$ defines the x -coordinate of the right zero boundary condition for some ρ . The quality of the x -grid and consequently of the θ -grid has been estimated by a precision of the ground state eigenvalue of the two-body Hamiltonian (3). For the MT I-III potential [8], the achieved value is $E_{2b} = -2.23069$ MeV. The obtained nonequidistant θ -grid has the highest density near $\pi/2$ and makes it possible to calculate the precise ground state eigenvalue with about 500 intervals. The spline-expansion of the solution demands using as many as twice of numbers of coefficients in the expansion. The orthogonal collocation method with two gauss knots within one interval is used for discretisation of differential equations. Therefore, the common size for a matrix of the two-body operator representation is about 1000. The second partial derivative of the equation (9) is approximated over the equidistant ρ -grid with the mesh parameter $h = \rho_m - \rho_{m-1}$ by the finite-difference formula

$$\frac{\partial}{\partial \rho^2} \mathcal{U}(\rho, \theta) \rightarrow \frac{\mathcal{U}(\rho_{m-1}, \theta) - 2\mathcal{U}(\rho_m, \theta) + \mathcal{U}(\rho_{m+1}, \theta)}{h^2}.$$

This approximation generates the block tridiagonal structure for the matrix of the linear system. The matrix sweeping and the domain decomposition algorithms are

applied for solving the obtained system.

The matrix sweeping algorithm for the block tridiagonal system

$$\mathbf{A}_i X_{i-1} + \mathbf{C}_i X_i + \mathbf{B}_i X_{i+1} = S_i, \quad \mathbf{A}_1 = \mathbf{B}_{N_\rho} = 0, \quad (19)$$

where $\mathbf{A}_i, \mathbf{B}_i, \mathbf{C}_i, i = 1, \dots, N_\rho$ are the blocks of the left hand side matrix and blocks S_i present the right hand side, includes two sweep procedures: the forward one and the backward one. The forward sweep consists of a sequential calculation of the auxiliary blocks

$$\begin{cases} \hat{\alpha}_1 &= \mathbf{C}_1^{-1} \mathbf{B}_1, \\ \hat{\alpha}_i &= (\mathbf{C}_i - \mathbf{A}_i \hat{\alpha}_{i-1})^{-1} \mathbf{B}_i, \quad i = 2, \dots, N_\rho - 1 \end{cases}$$

for the left hand side and similar ones for the right hand side. As a result, the matrix of the system is reduced using these blocks to the upper diagonal form with $\tilde{\mathbf{C}}_i$ blocks on the diagonal, unchanged \mathbf{B}_i on the upper diagonal and \tilde{S}_i in the right side. The backward sweep consists in the reconstruction of the solution of the linear system by formulae

$$\begin{cases} X_{N_\rho} &= \tilde{\mathbf{C}}_{N_\rho}^{-1} \tilde{S}_{N_\rho} \\ X_i &= \tilde{\mathbf{C}}_i^{-1} (\tilde{S}_i - \mathbf{B}_i X_{i+1}), \quad i = N_\rho - 1, \dots, 1 \end{cases}$$

The solution is also calculated sequentially starting from the last block at the matrix diagonal. This makes it possible to calculate the solution corresponding to the last block by performing the complete forward sweep and only the first step of the backward sweep. In spite of its sufficient simplicity and efficiency, the matrix sweeping algorithm is recursive and parallelized only at the level of matrix operations. This does not allow us to use the given method on contemporary supercomputing facilities.

Besides the matrix sweeping algorithm, we have developed a new solution method called the domain decomposition method (DDM). It was designed to perform fast parallel solving and obtain a complete solution of the linear system. The idea of the method is presented in Fig. 2. The initial tridiagonal system (19) is rearranged into an equivalent form which allows the parallel solving. The matrix is logically divided into independent subsystems and last components of the solution corresponding to each subsystem are moved to the end of the full solution. The subsystems are shown in Fig. 2 (middle) by thin squares. This procedure affects the transformation of the initial matrix and reduces it to the new block ‘‘arrow’’-form which is shown in Fig. 2 (bottom). The obtained system can be expressed as

$$\begin{pmatrix} \mathbf{M}_{11} & \mathbf{M}_{12} \\ \mathbf{M}_{21} & \mathbf{M}_v \end{pmatrix} \begin{pmatrix} u \\ v \end{pmatrix} = \begin{pmatrix} P_{11} \\ P_v \end{pmatrix}, \quad (20)$$

where the unknown solution v corresponds to the moved part of the full solution, the superblock \mathbf{M}_{11} consists of the new independent blocks at the diagonal, \mathbf{M}_v is the bottom right coupling superblock which is the ‘‘arrowhead’’, and other superblocks present additional blocks of the matrix. The solution of the system (20) is given by the relations

$$\begin{cases} u &= \mathbf{M}_{11}^{-1} P_{11} - \mathbf{M}_{11}^{-1} \mathbf{M}_{12} v, \\ v &= (\mathbf{M}_v - \mathbf{M}_{21} \mathbf{M}_{11}^{-1} \mathbf{M}_{12})^{-1} (P_v - \mathbf{M}_{21} \mathbf{M}_{11}^{-1} P_{11}). \end{cases}$$

Due to the structure of obtained superblocks, the inversion of \mathbf{M}_{11} is reduced to independent inversions of the diagonal blocks corresponding to each subsystem. Only two nonzero blocks for each subsystem of \mathbf{M}_{21} and \mathbf{M}_{12} drastically reduce the number of matrix operations and their sparse allocation allows us to perform multiplications $\mathbf{M}_{11}^{-1} \mathbf{M}_{12}$ independently for each subsystem. The calculated supermatrix $\mathbf{M}_v - \mathbf{M}_{21} \mathbf{M}_{11}^{-1} \mathbf{M}_{12}$ has a block tridiagonal form. Although its size equals to the

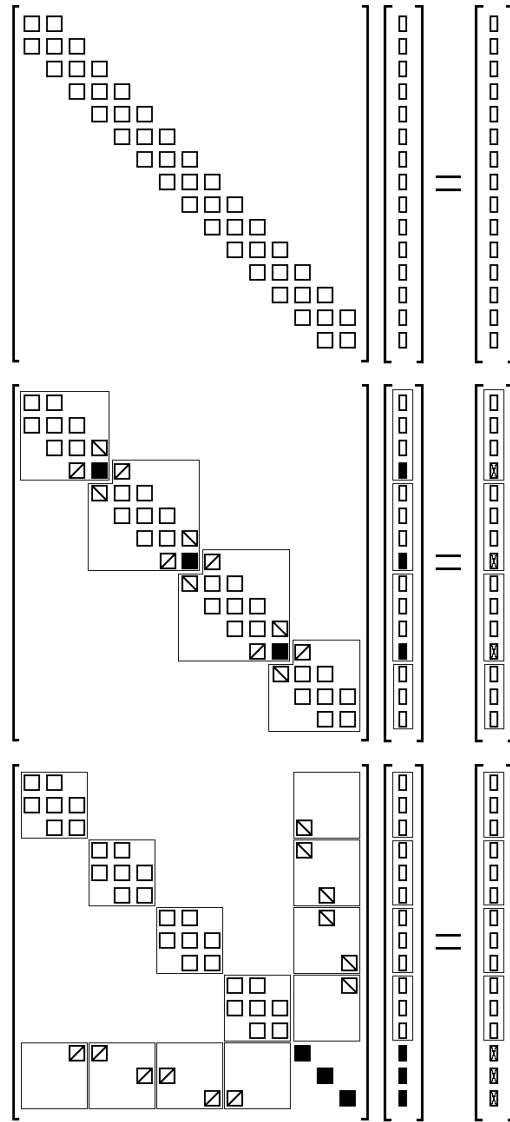


Figure 2: A simple graphical scheme of the domain decomposition method: (top) the initial block tridiagonal system; (middle) a rearrangement of the initial system to independent subsystems, the moved elements are highlighted by the diagonal lines and solid filling; (bottom) the obtained system in the “arrow”-form which can be solved using parallel calculations.

number of subsystems (multiplied by the size of one block) and can be chosen much smaller than the size of the initial system (19), the matrix sweeping algorithm is used for computation of the solution v . After obtaining v , the solution u is calculated in parts independently for each subsystem.

The DDM is successfully integrated in modern parallel programming models and it allows us to obtain a linear growth of performance with the increase of a number of computing units for not so large supercomputing systems. Fig. 3 shows obtained values of the computation acceleration with respect to the number of computing units. The linear dependence is clearly observed and the acceleration larger than 10 is easily reached. Nevertheless, further increase of computing hubs leads to violation of the linear dependence and stagnation of the performance increase because of the growth of hardly parallelized matrix sweeping part.

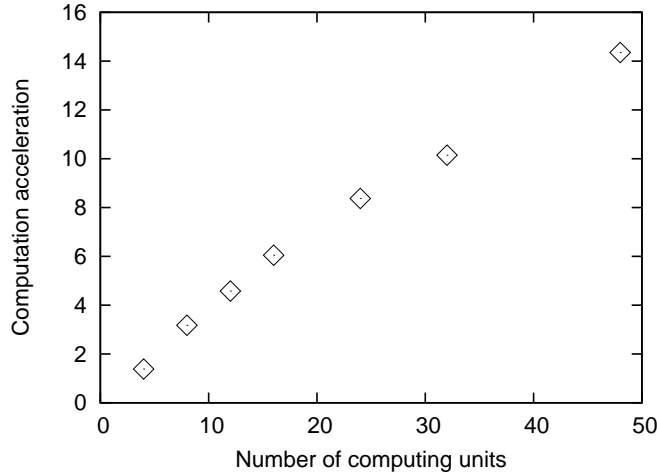


Figure 3: Computation acceleration for the domain decomposition method as a function of a number of computing units. The linear growth of the performance is observed.

5 Results of calculations

The calculations have been carried out for energies in the laboratory frame $E_{lab} = 14.1, 42.0$ MeV using the MT I-III potential [8] for the description of the two-body subsystem (3). A number of knots for the nonequidistant θ -grid was chosen to be about 1000 and the mesh step of the uniform ρ -grid was varied from 0.033 fm to 0.01 fm.

Within the asymptotic approach, the boundary value problems consisting of equations (9), (10) and boundary conditions (12), (13) taken at the hyper-radius $\rho = \rho_{max}$, have been solved. The expansion coefficients $a_{i,k}^J(E, \rho_{max})$ as functions of ρ_{max} have been calculated and used for reconstructing of the Faddeev component of the breakup amplitude

$$A_i^J(\theta, E, \rho_{max}) = \lim_{\rho \rightarrow \infty} A_i^J(\theta, E, \rho_{max}, \rho) = \lim_{\rho \rightarrow \infty} \sum_{k=1}^{N_\phi} a_{i,k}^J(E, \rho_{max}) \phi_k(\rho|\theta).$$

The prelimiting doublet breakup amplitudes $A_i^{1/2}(\theta, E, \rho_{max}, \rho)$ for $E_{lab} = 14.1$ MeV at some finite value of ρ_{max} are shown in Fig. 4. The breakup amplitudes $A_i^{1/2}(\theta, E, \rho_{max})$ as $\rho \rightarrow \infty$ for the same energy are presented in Fig. 5. A convergence to a limit is explicitly guaranteed by properties of the functions $\phi_k(\rho|\theta)$. The limiting forms of these functions as $\rho \rightarrow \infty$ are known and they are smooth for $\theta \in [0, \pi/2]$:

$$\phi_k(\rho|\theta) \underset{\rho \rightarrow \infty}{\sim} \frac{2}{\sqrt{\pi}} \sin 2k\theta.$$

Therefore, in contrast to the prelimiting case, a smooth behavior of the breakup amplitudes near 90 degrees is observed.

The convergence of the binary amplitude $a_0(q, \rho_{max})$ and breakup amplitude $A_i^{3/2}(\theta, E, \rho_{max})$ as $\rho_{max} \rightarrow \infty$ has been obtained. For example, the ρ_{max} -dependence of the inelasticity coefficient and the phase shift, defined as

$$a_0^J = \frac{\eta^J e^{2i\delta^J} - 1}{2i}, \quad (21)$$

for $J = 3/2$ are presented in Fig. 6. It is shown in the figure that the decrease of the mesh step h for the ρ -grid to 0.01 fm leads to obtaining of oscillating but significantly less biased values of the phase shift as ρ_{max} increases. The oscillations are vanishing as

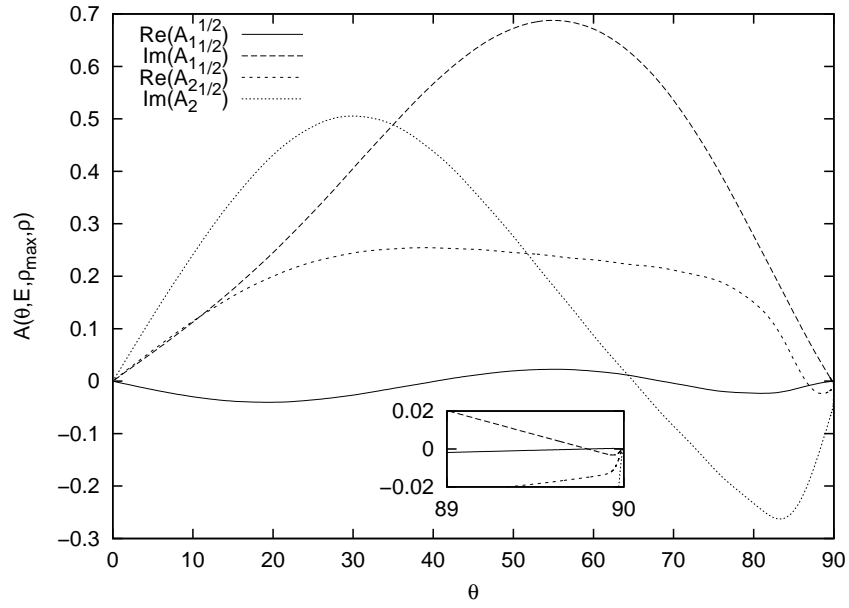


Figure 4: The prelimiting doublet breakup amplitudes $A_i^{1/2}(\theta, E, \rho_{max}, \rho)$ for $E_{lab} = 14.1$ MeV and $\rho = \rho_{max} = 1400$ fm. The amplitudes have been obtained using the asymptotic approach.

$\rho_{max} \rightarrow \infty$ and the limiting value of the amplitude can be obtained by extrapolation. Nevertheless, in order to reach relatively small oscillations it is necessary to achieve values of $\rho_{max} > 1000$ fm. The obtained values of the binary amplitude for different laboratory frame energies are summarized in Table 1. The calculated values are in a good agreement with the binary amplitudes of Ref. [8].

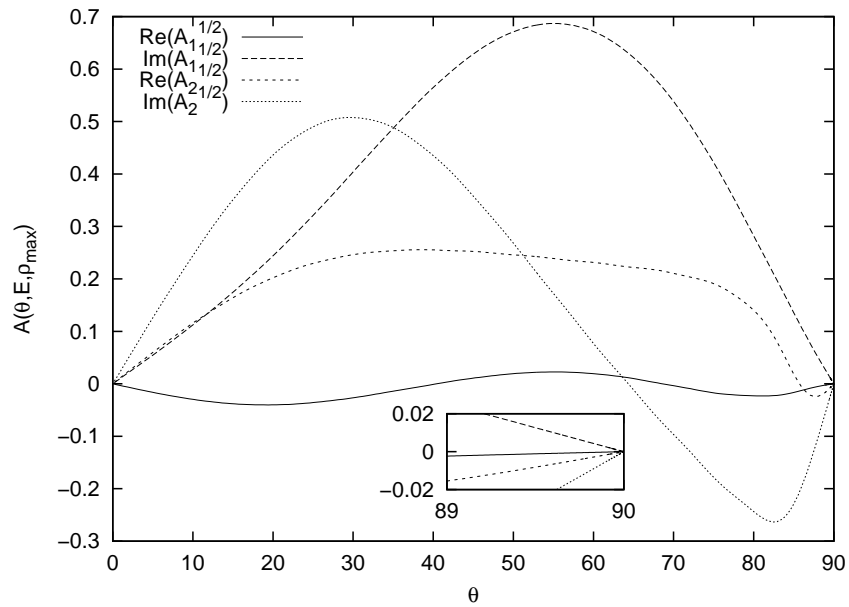


Figure 5: The breakup doublet amplitudes $A_i^{1/2}(\theta, E, \rho_{max})$ for $E_{lab} = 14.1$ MeV and $\rho_{max} = 1400$ fm. The amplitudes have been obtained using the asymptotic approach.

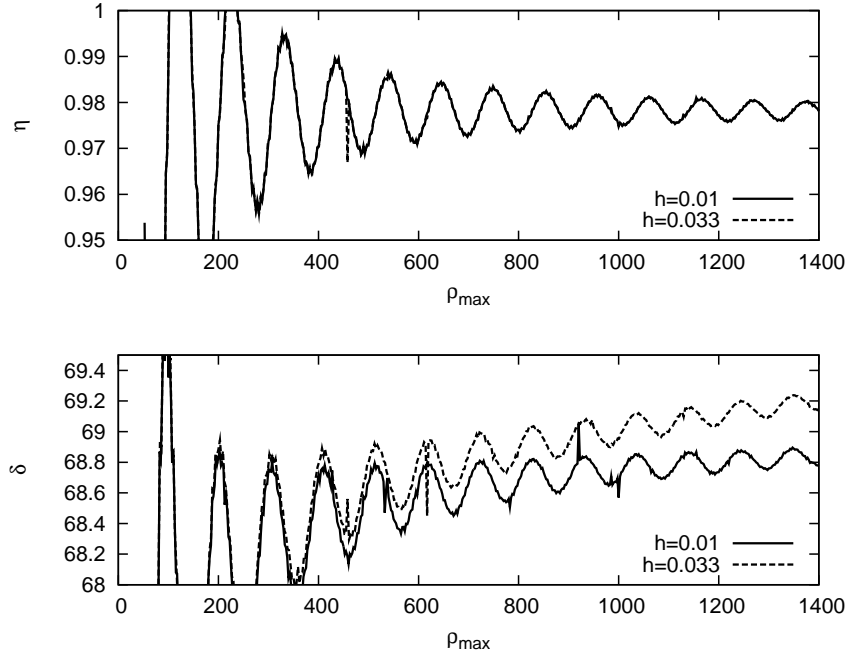


Figure 6: Calculated values of the quartet inelasticity coefficient η and phase shift δ [see Eq. (21)] for $E_{lab} = 14.1$ MeV as functions of ρ_{max} . The dashed line represents the values obtained using the ρ -grid with relatively large mesh $h = 0.033$ fm, whereas the solid line shows the values obtained using $h = 0.01$ fm. The values have been obtained using the asymptotic approach.

The complex-scaling approach calculations have been carried out using the smooth rotation by angle $\omega = 30^\circ$ and mesh step of the ρ -grid $h = 0.033$ fm. Due to rotation, the boundary condition values have vanished and become smaller than 10^{-6} . The full solution was reconstructed and the amplitudes were calculated by the integral representations (7), (8). The most consistent preliminary values of the binary and breakup amplitudes have been obtained for the starting rotation at $\rho_{max} \sim 900$ fm and using the solution for $\rho_{max} < 900$ fm in formulae (7), (8). The achieved value of binary amplitude is expressed by the inelasticity coefficient $\eta = 0.9789$ and phase shift $\delta = 68.79^\circ$. The obtained quartet breakup amplitudes $A^{3/2}(\theta, E, \rho_{max})$ were compared with the results of Ref. [8]. This comparison for $E_{lab} = 14.1$ MeV is presented in Fig. 7. The results are in good agreement for values of $\theta < 80^\circ$, whereas differences are observed for $\theta \sim 90^\circ$.

Table 1: The values of the inelasticity coefficient η and phase shift δ obtained using the asymptotic approach for different laboratory frame energies.

E_{lab} , MeV	14.1	42.0
$J = 3/2$, quartet		
$\eta^{3/2}$	0.9781	0.9031
$\delta^{3/2}$	68.78	37.66
$J = 1/2$, doublet		
$\eta^{1/2}$	0.4648	0.5021
$\delta^{1/2}$	105.40	41.21

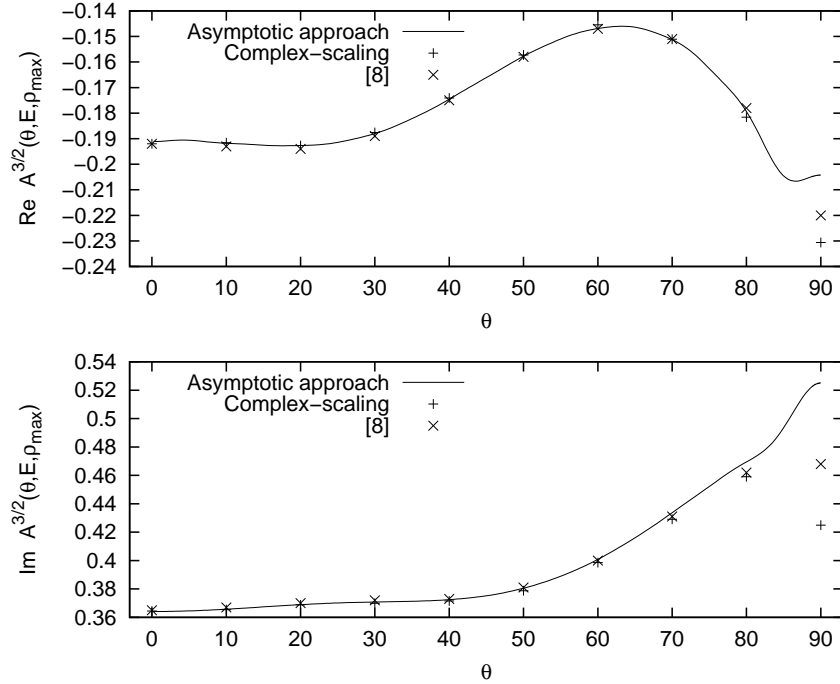


Figure 7: Real and imaginary parts of the breakup quartet amplitude $A^{3/2}(\theta, E, \rho_{max})$ for $E_{lab} = 14.1$ MeV. The values have been obtained using the asymptotic approach and the complex-scaling method. The results of Ref. [8] are also shown for comparison.

6 Conclusion

In the paper we have presented two methods for solving the three-body scattering problem above the breakup threshold. In the method 1, an orthonormal basis related to the two-body subsystem Hamiltonian is constructed. The asymptotic boundary condition is modified in terms of this basis. The breakup amplitude is represented by a linear combination of basis functions which allows an extrapolation of this amplitude to infinity exclusively by the properties of the basis functions. The coefficients of the linear combination together with the binary amplitude are numerically obtained from the comparison with the asymptotic form of the wave function. In the method 2, the exterior complex scaling is used for reducing the asymptotic boundary conditions to zero. The binary and breakup amplitudes are obtained from their integral representations. Both methods include solving the system of linear algebraic equations. The domain decomposition method which allows a parallelization of the solution process has been developed and successfully applied reducing the overall time of calculation up to 10 times.

References

- [1] L. D. Faddeev and S. P. Merkuriev, *Quantum scattering theory for several particle systems*. Kluwer, Dordrecht, 1993.
- [2] S. P. Merkuriev, C. Gignoux and A. Laverne, *Ann. Phys. (NY)* **99**, 30 (1976).
- [3] P. A. Belov and S. L. Yakovlev, *Bull. Russ. Acad. Sci. Phys.* **76**, 913 (2012).
- [4] P. A. Belov and S. L. Yakovlev, *Vestnik St. Petersburg Univ., Ser. 4*, 95 (2010).

- [5] M. V. Volkov, N. Elander, E. A. Yarevsky and S. L. Yakovlev, *Europhys. Lett.* **85**, 30001 (2009).
- [6] G. L. Payne, W. Glöckle and J. L. Friar, *Phys. Rev. C* **61**, 024005 (2000).
- [7] A. A. Samarskiy and E. S. Nikolaev, *Methods for solving finite-difference equations*. Nauka, Moscow, 1978 (*in Russian*).
- [8] J. L. Friar, G. L. Payne, W. Glöckle, D. Hüber and H. Witała, *Phys. Rev. C* **51**, 2356 (1995).
- [9] S. L. Yakovlev and I. N. Filikhin, *Phys. Atom. Nucl.* **56**, 1676 (1993).
- [10] M. Abramowitz and I. A. Stegun, *Handbook of Mathematical Functions with Formulas, Graphs, and Mathematical Tables*. Dover, New York, 1972.
- [11] G. L. Payne in *Proc. 8th Autumn School Models and Methods Few-Body Phys., Lisboa, 1986*, edited by L. S. Ferreira *et al.* Springer-Verlag, Berlin, 1987, p. 64.

Quasi-Sturmian Approach to the Three-Body Continuum Coulomb Problem

S. A. Zaytsev^a and G. Gasaneo^b

^a*Pacific National University, Khabarovsk, 680035, Russia.*

^b*Departamento de Física, Universidad Nacional del Sur, 8000 Bahía Blanca, Buenos Aires, Argentina.*

Abstract

The three-body continuum Coulomb problem is treated in terms of generalized parabolic coordinates. Specifically, the original problem is reduced to a driven equation where the ‘perturbation’ operator contains the non-orthogonal part of the kinetic energy operator. As a test of this approach, a simple two-dimensional model problem is solved numerically by using so-called parabolic quasi-Sturmian basis representation. Convergence of the solution is achieved as the basis set is enlarged.

Keywords: *Three-body Coulomb system; parabolic coordinates; driven equation; quasi-Sturmians; convergence*

1 Introduction

The three-body continuum Coulomb problem is one of fundamental unresolved problems of theoretical physics. In atomic physics, a prototype example is a two-electron continuum which arises as a final state in electron-impact ionization and double photoionization of atomic systems. Several discrete-basis-set methods for calculations of such processes have been developed recently including a convergent close coupling (CCC) approach [1, 2], a Coulomb–Sturmian separable expansion method [3, 4] and a J -matrix method [5, 6, 7]. In all these approaches (see also [8, 9]), the continuous Hamiltonian spectrum is represented in the context of complete square integrable bases. Despite an enormous progress made so far in discretization and subsequent numerical solutions of three-body differential and integral equations of Coulomb scattering theory, a number of related mathematical problems remain open. Actually, the use of a product of two fixed charge Coulomb waves for two outgoing electrons as an approximation to the three-body continuum state, is typical for these approaches. As a consequence, a long-range potential appears in the kernel of the corresponding Lippmann–Schwinger (LS) equation. Since this integral equation is, in principle, non-compact, its formal solution therefore should be divergent. Note, however, that in the two-body problem this type of definition of the “free particle solution” is not leading to divergent solutions [10]. In addition, in the three-body case, approaches like the exterior complex scaling [11] and generalized Sturmian approaches [8] lead to correct solutions for the driven equation from which the LS equations are derived. One of the aims of this paper is to understand the reason of these differences between the solutions corresponding to the LS type and driven equations.

On the other hand, it is well known [12, 13] that the Schrödinger equation for a three-body Coulomb system at large particle separations, i. e., in the so-called region Ω_0 , is separable in terms of generalized parabolic coordinates $\{\xi_j, \eta_j\}$, $j = 1, 2, 3$ [13, 14]. Moreover, a representation of the corresponding Green’s function operator has been derived in Ref. [15]. Thus, at first glance, one can get an impression that the three-body Coulomb problem can be recast as a Lippmann–Schwinger type equation, where the potential energy operator coinciding with the non-orthogonal part of

the kinetic energy operator, is expressed in terms of second partial mixed derivatives with respect to the parabolic coordinates. No complete studies of the compactness of the kernel of this integral equation can be found in the literature (see discussion in Ref. [16]). Actually, a differential operator of this type seems to be unbounded in the Hilbert space, and therefore finding formal solutions of the corresponding Lippmann–Schwinger equation could be difficult. To avoid these problems, an alternative approach can be used by considering an inhomogeneous Schrödinger equation with a square integrable driven term. In this paper, we formulate a procedure for solving the driven equation using so-called quasi-Sturmian (QS) functions. Unlike Sturmian functions (see, e. g., Refs. [17, 18] and references therein) which are eigensolutions of a Sturm–Liouville differential or integral equation and form a complete set of basis functions, the QS functions are constructed from square-integrable basis functions with the help of an appropriate Coulomb Green’s function operator. In order to test practically the QS approach and the solution of driven type instead of Lippmann–Schwinger equations, we consider a simple two-dimensional model problem on the plane (ξ_1, ξ_3) . Here the total wave operator, aside from the one-dimensional Coulomb wave operators \hat{h}_1 and \hat{h}_3 , contains a ‘perturbation’ term $\frac{\partial^2}{\partial \xi_1 \partial \xi_3}$.

This paper is organized as follows. We introduce notations, recall the generalized parabolic coordinate definition and convert the three-body Coulomb problem into a driven equation in Sec. 2. We present in Sec. 3 a simple two-dimensional model and briefly outline the parabolic QS approach. Calculations of model continuum wave function are also described in Sec. 3. Our aim is to study the rate of convergence as the basis set used to describe the ‘perturbation’ operator is enlarged. The calculations show that the convergence can be achieved on the basis of a reasonable size with appropriately chosen basis parameters. Sec. 4 contains a brief discussion of the overall results. Atomic units are used throughout.

2 Coulomb three-body system in parabolic coordinates

2.1 General considerations

We consider three particles of masses m_1, m_2, m_3 , charges Z_1, Z_2, Z_3 and momenta $\mathbf{k}_1, \mathbf{k}_2, \mathbf{k}_3$. The Hamiltonian of the system after separating out the center-of-mass motion is given by

$$\hat{H} = -\frac{1}{2\mu_{12}}\Delta_{\mathbf{R}} - \frac{1}{2\mu_3}\Delta_{\mathbf{r}} + \frac{Z_1 Z_2}{r_{12}} + \frac{Z_2 Z_3}{r_{23}} + \frac{Z_1 Z_3}{r_{13}}, \quad (1)$$

where \mathbf{r}_{ls} denotes relative coordinates,

$$\mathbf{r}_{ls} = \mathbf{r}_l - \mathbf{r}_s, \quad r_{ls} = |\mathbf{r}_{ls}|, \quad (2)$$

\mathbf{R} and \mathbf{r} are Jacobi coordinates,

$$\mathbf{R} = \mathbf{r}_1 - \mathbf{r}_2, \quad \mathbf{r} = \mathbf{r}_3 - \frac{m_1 \mathbf{r}_1 + m_2 \mathbf{r}_2}{m_1 + m_2}. \quad (3)$$

The reduced masses are defined as

$$\mu_{12} = \frac{m_1 m_2}{m_1 + m_2}, \quad \mu_3 = \frac{m_3 (m_1 + m_2)}{m_1 + m_2 + m_3}. \quad (4)$$

In the Schrödinger equation

$$\hat{H}\Phi = E\Phi, \quad (5)$$

the eigenenergy $E > 0$ is given by

$$E = \frac{1}{2\mu_{12}} \mathbf{K}^2 + \frac{1}{2\mu_3} \mathbf{k}^2, \quad (6)$$

where \mathbf{K} and \mathbf{k} are the momenta conjugate to variables \mathbf{R} and \mathbf{r} . By substituting

$$\Phi = e^{i(\mathbf{K}\cdot\mathbf{R}+\mathbf{k}\cdot\mathbf{r})} \Psi \quad (7)$$

into Eq. (5), we obtain an equation for the reduced wave function Ψ :

$$\left[-\frac{1}{2\mu_{12}} \Delta_{\mathbf{R}} - \frac{1}{2\mu_3} \Delta_{\mathbf{r}} - \frac{i}{\mu_{12}} \mathbf{K} \cdot \nabla_{\mathbf{R}} - \frac{i}{\mu_3} \mathbf{k} \cdot \nabla_{\mathbf{r}} + \frac{Z_1 Z_2}{r_{12}} + \frac{Z_2 Z_3}{r_{23}} + \frac{Z_1 Z_3}{r_{13}} \right] \Psi = 0. \quad (8)$$

Leading-order asymptotic terms of Ψ in the Ω_0 domain are expressed in terms of generalized parabolic coordinates [13]:

$$\begin{aligned} \xi_1 &= r_{23} + \hat{\mathbf{k}}_{23} \cdot \mathbf{r}_{23}, & \eta_1 &= r_{23} - \hat{\mathbf{k}}_{23} \cdot \mathbf{r}_{23}, \\ \xi_2 &= r_{13} + \hat{\mathbf{k}}_{13} \cdot \mathbf{r}_{13}, & \eta_2 &= r_{13} - \hat{\mathbf{k}}_{13} \cdot \mathbf{r}_{13}, \\ \xi_3 &= r_{12} + \hat{\mathbf{k}}_{12} \cdot \mathbf{r}_{12}, & \eta_3 &= r_{12} - \hat{\mathbf{k}}_{12} \cdot \mathbf{r}_{12}, \end{aligned} \quad (9)$$

where $\mathbf{k}_{ls} = \frac{\mathbf{k}_l m_s - \mathbf{k}_s m_l}{m_l + m_s}$ is the relative momentum, $\hat{\mathbf{k}}_{ls} = \frac{\mathbf{k}_{ls}}{k_{ls}}$ and $k_{ls} = |\mathbf{k}_{ls}|$. The operator in square brackets in Eq. (8) denoted by \hat{D} , can be decomposed into two terms [13]:

$$\hat{D} = \hat{D}_0 + \hat{D}_1, \quad (10)$$

where the operator \hat{D}_0 contains the leading term of kinetic energy and the total potential energy:

$$\hat{D}_0 = \sum_{j=1}^3 \frac{1}{\mu_{ls}(\xi_j + \eta_j)} \left[\hat{h}_{\xi_j} + \hat{h}_{\eta_j} + 2k_{ls} t_{ls} \right] \quad (11)$$

for $l < s$ and $j \neq l, s$,

$$\hat{h}_{\xi_j} = -2 \left(\frac{\partial}{\partial \xi_j} \xi_j \frac{\partial}{\partial \xi_j} + ik_{ls} \xi_j \frac{\partial}{\partial \xi_j} \right), \quad (12)$$

$$\hat{h}_{\eta_j} = -2 \left(\frac{\partial}{\partial \eta_j} \eta_j \frac{\partial}{\partial \eta_j} - ik_{ls} \eta_j \frac{\partial}{\partial \eta_j} \right). \quad (13)$$

Here $t_{ls} = \frac{Z_l Z_s \mu_{ls}}{k_{ls}}$ and $\mu_{ls} = \frac{m_l m_s}{m_l + m_s}$. The operator \hat{D}_1 represents the remaining part of kinetic energy [13] which, in the case of the $(e^-, e^-, \text{He}^{++}) = (123)$ system with $m_3 = \infty$, takes the form [19]:

$$\hat{D}_1 = \sum_{j=1}^2 (-1)^{j+1} \left[\mathbf{u}_j^- \cdot \mathbf{u}_3^- \frac{\partial^2}{\partial \xi_j \partial \xi_3} + \mathbf{u}_j^- \cdot \mathbf{u}_3^+ \frac{\partial^2}{\partial \xi_j \partial \eta_3} + \mathbf{u}_j^+ \cdot \mathbf{u}_3^- \frac{\partial^2}{\partial \eta_j \partial \xi_3} + \mathbf{u}_j^+ \cdot \mathbf{u}_3^+ \frac{\partial^2}{\partial \eta_j \partial \eta_3} \right], \quad (14)$$

where

$$\mathbf{u}_j^\pm = \hat{\mathbf{r}}_{ls} \mp \hat{\mathbf{k}}_{ls}. \quad (15)$$

The asymptotic behavior of Ψ is determined by the operator \hat{D}_0 . In particular, there exist solutions of the equation

$$\hat{D}_0 \Psi_{C3} = 0 \quad (16)$$

such that the total wave functions (7) satisfy Redmond conditions [20] in Ω_0 . These solutions are well-known $C3$ wave functions. Ψ_{C3} are expressed in terms of products of three Coulomb waves. For example, Ψ_{C3} with pure outgoing behavior is written as

$$\Psi_{C3} = \prod_{j=1}^3 {}_1F_1(it_{ls}, 1; -ik_{ls}\xi_j). \quad (17)$$

In turn, \hat{D}_1 is regarded as a perturbation which does not violate asymptotic conditions [13, 14].

2.2 Formal solution of the problem

At first glance, given the Green's function operator $\hat{\mathcal{G}} = \hat{D}_0^{-1}$ (see Ref. [15]), one could take into account the non-orthogonal term \hat{D}_1 of the kinetic energy operator by putting it into the kernel of the Lippmann–Schwinger type equation:

$$\begin{aligned} \Psi &= \Psi_{C3} - \hat{\mathcal{G}}\hat{\mathcal{V}}\Psi, \\ \hat{\mathcal{V}} &\equiv \hat{D}_1. \end{aligned} \quad (18)$$

If the kernel $\hat{\mathcal{G}}\hat{\mathcal{V}}$ is compact, the integral equation (18) can be solved by an algebraic method based on the fact that a compact operator may be uniformly approximated by operators of finite rank. For this purpose, e. g., a set of square-integrable parabolic Laguerre basis functions [21]

$$|\mathfrak{N}\rangle \equiv \mathfrak{B}_{\mathfrak{N}}(\xi, \eta) = \prod_{j=1}^3 \phi_{n_j m_j}(\xi_j, \eta_j), \quad (19)$$

$$\phi_{n_j m_j}(\xi_j, \eta_j) = \psi_{n_j}(\xi_j) \psi_{m_j}(\eta_j), \quad (20)$$

$$\psi_n(x) = \sqrt{2b_j} e^{-b_j x} L_n(2b_j x), \quad (21)$$

could be used. The index \mathfrak{N} represents all indexes of the basis function, $\mathfrak{N} = \{n_1, m_1, n_2, m_2, n_3, m_3\}$, and the argument (ξ, η) of the function $\mathfrak{B}_{\mathfrak{N}}(\xi, \eta)$ represents in compact form the dependence on all parabolic coordinates. The basis functions (20), (21) are parametrized by different Coulomb–Sturmian parameters b_j for each pair of $\{\xi_j, \eta_j\}$, $j = \overline{1, 3}$. Thus, the operator $\hat{\mathcal{V}}$ is represented by its projection $\hat{\mathcal{V}}^{\mathcal{N}}$ onto a subspace of basis functions,

$$\hat{\mathcal{V}}^{\mathcal{N}} = \sum_{\mathfrak{N}, \mathfrak{N}'=0}^{\mathfrak{N}_0} |\mathfrak{N}\rangle \langle \mathfrak{N} | \hat{\mathcal{V}} | \mathfrak{N}' \rangle \langle \mathfrak{N}' |, \quad (22)$$

and the solution Ψ of the problem is obtained for $\hat{\mathcal{V}}^{\mathcal{N}}$. Substituting $\hat{\mathcal{V}}$ by $\hat{\mathcal{V}}^{\mathcal{N}}$ in Eq. (18) we obtain a finite matrix equation for the expansion coefficients $[\underline{a}]_{\mathfrak{N}} = \langle \mathfrak{N} | \Psi \rangle$,

$$\underline{a} = \underline{a}^{(0)} - \underline{\mathcal{G}} \underline{\mathcal{V}} \underline{a}, \quad (23)$$

which has a solution

$$\underline{a} = (\underline{\mathbb{1}} + \underline{\mathcal{G}} \underline{\mathcal{V}})^{-1} \underline{a}^{(0)}. \quad (24)$$

Here $[\underline{\mathcal{G}}]_{\mathfrak{N}\mathfrak{N}'} = \langle \mathfrak{N} | \hat{\mathcal{G}} | \mathfrak{N}' \rangle$ and $[\underline{\mathcal{V}}]_{\mathfrak{N}\mathfrak{N}'} = \langle \mathfrak{N} | \hat{\mathcal{V}} | \mathfrak{N}' \rangle$ are the Green's function operator and potential operator matrices of the rank of $\mathfrak{N}_0 + 1$, and $\underline{a}^{(0)}$ is the coefficient vector of Ψ_{C3} , i. e., $[\underline{a}^{(0)}]_{\mathfrak{N}} = \langle \mathfrak{N} | \Psi_{C3} \rangle$. The wave function Ψ is expressed in terms of the solution (24):

$$\Psi = \Psi_{C3} - \sum_{\mathfrak{N}=0}^{\mathfrak{N}_0} [\underline{\mathcal{C}}]_{\mathfrak{N}} \hat{\mathcal{G}} | \mathfrak{N} \rangle, \quad (25)$$

where $\underline{C} = \underline{\mathcal{V}}a$.

We performed various studies of Eq. (18) and found out that its kernel is not compact when expressed in terms of L^2 spaces. Actually, the problem is that any L^2 basis does not possess the appropriate asymptotic behavior. Thus the correct asymptotic behavior is to be implemented and then the perturbation operator \hat{D}_1 [see Eq. (14)] seems to be not bounded. However, if the basis possess already the asymptotic behavior of the problem, \hat{D}_1 turns out to be a short range operator and becomes compact and manageable.

We explore an alternative approach to the problem based on a study of the driven equation

$$\left[\hat{D}_0 + \hat{D}_1 \right] \Psi_{sc} = -\hat{D}_1 \Psi_{C3}, \quad (26)$$

where the wave function Ψ is splitted into outgoing (ingoing) Ψ_{C3} and scattered Ψ_{sc} parts,

$$\Psi = \Psi_{sc} + \Psi_{C3}. \quad (27)$$

Note, the inhomogeneity in Eq. (26) is a square-integrable function. Equation (25) gives a hint on how to construct a solution Ψ_{sc} of Eq. (26) with the help of the square-integrable basis (19). Namely, we suppose that the wave function Ψ can be expressed in the form (25), i. e., we propose to expand Ψ_{sc} as

$$\Psi_{sc} = \sum_{\mathfrak{N}=0} [\underline{c}]_{\mathfrak{N}} |\mathcal{Q}_{\mathfrak{N}}\rangle, \quad (28)$$

where

$$|\mathcal{Q}_{\mathfrak{N}}\rangle \equiv \hat{\mathcal{G}} |\mathfrak{N}\rangle. \quad (29)$$

We call the function $|\mathcal{Q}_{\mathfrak{N}}\rangle$ a *quasi-Sturmian function*. The word ‘quasi’ refers to that there is no need to solve a Sturm–Liouville equation to obtain these functions.

According to the definition (29), the QS functions satisfy a driven equation

$$\hat{D}_0 \mathcal{Q}_{\mathfrak{N}}(\xi, \eta) = \mathfrak{B}_{\mathfrak{N}}(\xi, \eta) \quad (30)$$

and possess the same asymptotic behavior as the kernel $G(E; \xi, \eta, \xi', \eta')$ at large values of ξ, η and finite ξ', η' . We are using here the Laguerre basis functions $\mathfrak{B}_{\mathfrak{N}}(\xi, \eta)$, though any basis sets can be used. However, to preserve the asymptotic behavior of \mathcal{Q} functions, the extension on the configuration state of basis functions has to be finite. A representation of the kernel $G(E; \xi, \eta, \xi', \eta')$ in the basis (19) was given in Ref. [22] and this allows for a closed form expression for QS functions. The right-hand-side of Eq. (30) depends on indexes \mathfrak{N} , thus for each set of values \mathfrak{N} we have a particular function $\mathcal{Q}_{\mathfrak{N}}$. These functions form a complete basis even though they are not orthogonal.

By solving Eq. (26) with the proposition (28) we enforce the solution (27) to possess the correct outgoing asymptotic behavior of scattering function. This is similar to what is observed when generalized Sturmian functions are used [8, 9]. The completeness of the $\mathcal{Q}_{\mathfrak{N}}$ basis, the short range of both the right-hand-side of Eq. (26) and $D_1 \mathcal{Q}_{\mathfrak{N}}$ assure convergence of the expansion. To exemplify this affirmation, we solve in the next section a two-dimensional model problem presented in Ref. [19]. We use a product of QS functions obtained from one-dimensional Green’s function:

$$\mathcal{Q}_n(k, \xi) \equiv \int d\xi' G^{(+)}(k; \xi, \xi') \psi_n(\xi'). \quad (31)$$

This allows us to probe the convergence of expansion of two-dimensional scattering wave function before considering a very elaborate and cumbersome six-dimensional case as required for the full three-body problem.

3 A model problem

3.1 Statement of the problem

A model double continuum electron wave function was presented in 1997 in Ref. [19]. The model used a two-variable hypergeometric function Φ_2 to represent two electrons interacting with a heavy charged nucleus and with each other. An approximate two-electron Schrödinger equation was also numerically solved in Ref. [19]. This equation was associated with very particular kinematic conditions. The model equation is

$$\left[\hat{h}_1(k_1) + \hat{h}_3(k_3) - 8 \frac{k_3}{k_1} \frac{\partial^2}{\partial \xi_1 \partial \xi_3} \right] \Psi(\xi_1, \xi_3) = 0, \quad (32)$$

where a one-dimensional Coulomb wave operator \hat{h} is defined as

$$\hat{h}(k) = \frac{1}{\mu \xi} \left[-2 \frac{\partial}{\partial \xi} \xi \frac{\partial}{\partial \xi} - 2ik\xi \frac{\partial}{\partial \xi} + 2kt \right], \quad kt = \mu Z. \quad (33)$$

We use this model as a starting point of our QS test in this work. This allows us to deal with an equation which contains most of the difficulties of the full three-body problem like a non-separability and scattering type asymptotics of solutions.

We start with splitting the wave function Ψ into two parts,

$$\Psi = \Psi_{sc} + \Psi_{C2}, \quad (34)$$

where

$$\Psi_{C2}(\xi_1, \xi_3) = {}_1F_1\left(i \frac{\mu_1 Z_1}{k_1}, 1, -ik_1 \xi_1\right) {}_1F_1\left(i \frac{\mu_3 Z_3}{k_3}, 1, -ik_3 \xi_3\right). \quad (35)$$

This transforms Eq. (32) into a driven equation

$$\left[\hat{h}_1(k_1) + \hat{h}_3(k_3) - 8 \frac{k_3}{k_1} \frac{\partial^2}{\partial \xi_1 \partial \xi_3} \right] \Psi_{sc}(\xi_1, \xi_3) = 8 \frac{k_3}{k_1} \frac{\partial^2}{\partial \xi_1 \partial \xi_3} \Psi_{C2}(\xi_1, \xi_3). \quad (36)$$

The scattering function Ψ_{sc} is assumed to have a purely outgoing behavior and can be expressed as a finite series in terms of products of QS functions (31):

$$\Psi_{sc}(\xi_1, \xi_3) = \sum_{n_1, n_3=0}^{N-1} c_{n_1 n_3} \mathcal{Q}_{n_1}(p_1, \xi_1) \mathcal{Q}_{n_3}(p_3, \xi_3). \quad (37)$$

Note, p_j is not necessary equal k_j . The one-dimensional Green's function $G^{(+)}$ satisfies the equation

$$\hat{h}(k) G^{(+)}(k; \xi, \xi') = \delta(\xi - \xi'). \quad (38)$$

A detailed description of QS functions (31) will be presented soon elsewhere.

Due to an obvious relation

$$\hat{h}(k) = \hat{h}(p) - \frac{2i}{\mu}(k-p) \frac{\partial}{\partial \xi}, \quad (39)$$

we obtain the following system of linear equations for the unknown coefficients $c_{n_1 n_3}$ after substituting $\Psi_{sc}(\xi_1, \xi_3)$ in Eq. (36) by its expansion (37) and projecting onto $\psi_{m_1}(\xi_1) \psi_{m_3}(\xi_3)$:

$$\begin{aligned} \sum_{n_1, n_3=0}^{N-1} \left\{ \delta_{m_1 n_1} G_{m_3 n_3}^{(3)(+)}(p_3) + G_{m_1 n_1}^{(1)(+)}(p_1) \delta_{m_3 n_3} - \left[\frac{2i}{\mu_1}(k_1 - p_1) C_{m_1 n_1}^{(1)}(p_1) G_{m_3 n_3}^{(3)(+)}(p_3) \right. \right. \\ \left. \left. + G_{m_1 n_1}^{(1)(+)}(p_1) \frac{2i}{\mu_3}(k_3 - p_3) C_{m_3 n_3}^{(3)}(p_3) + 8 \frac{k_3}{k_1} C_{m_1 n_1}^{(1)}(p_1) C_{m_3 n_3}^{(3)}(p_3) \right] \right\} c_{n_1 n_3} \\ = 8 \frac{k_3}{k_1} d_{m_1}^{(1)} d_{m_3}^{(3)}, \quad (40) \end{aligned}$$

where $0 \leq m_1, m_3 \leq N - 1$, and $C_{m,n}^{(j)}$ and $d_m^{(j)}$ are respectively the coefficients of expansion in basis functions ψ_m of derivatives of QS functions (31) and of derivatives of confluent hypergeometric functions which arise in Eq. (36) due to Eqs. (37) and (35).

3.2 Results

We follow Ref. [19] and set $Z_1 = -2$, $\mu_1 = 1$, $k_1 = 1$, and $Z_3 = 1$, $\mu_3 = \frac{1}{2}$, $k_3 = 0.4$. The convergence is intuitively expected if the sum of the first two ('unperturbed') terms in figure brackets in l.h.s. of Eq. (40) is much larger than the ('perturbation') term in square brackets. We hope to affect the ratio of these two contributions to the matrix elements by varying the values of basis parameters p_j .

Our calculations demonstrate that the convergence rate and numerical stability may be significantly improved by taking appropriate values of p_1 and p_2 . The results obtained with parameters $p_1 = 1$ and $p_3 = 0.1$ (the Laguerre scale factors $b_j = p_j$) are shown in Figs. 1–6 where we plot real and imaginary parts of the scattering wave function Ψ_{sc} on the diagonal $\xi_1 = \xi_3$ and on the axes ξ_1 and ξ_3 . The convergence is seen from the figures to be achieved; i. e., the proposed approach is reliable.

4 Conclusions

We presented in this contribution a study of three-body scattering problem expressed in parabolic coordinates. As is well-known, the C3 wave function [14] possesses a correct asymptotic behavior in the Ω_0 region where all particles are far from each other. This is a good starting point for formulating a Lippmann–Schwinger equation or driven type equations. This means that if we consider the C3 function as an asymptotic solution, the scattering part (the remaining part of the solution) should satisfy an equation having a compact kernel or a short range driven term. Due to properties of perturbation corresponding to the C3 function [23], the use of standard L^2 bases is not appropriated. Instead it is necessary to use basis functions possessing the

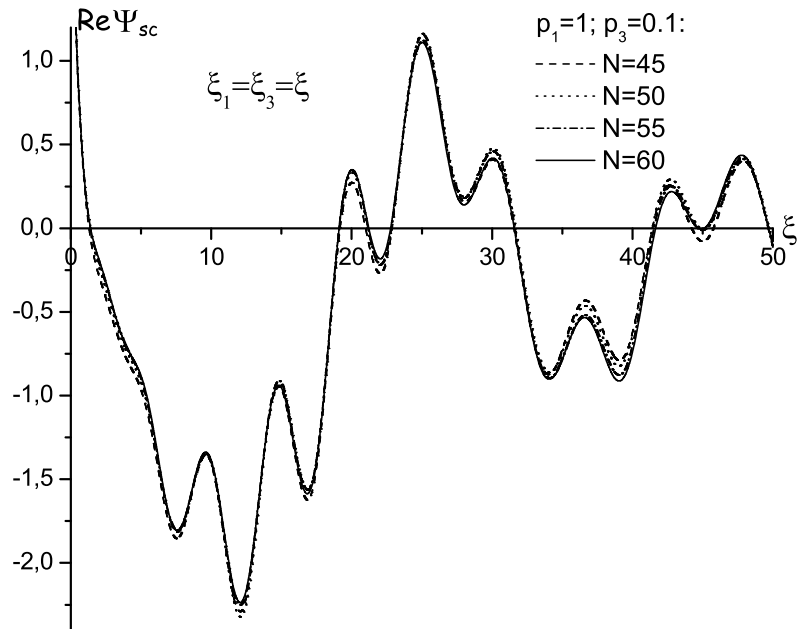


Figure 1: Convergence of the real part of solution vs the number N of basis quasi-Sturmians used in calculation on the diagonal $\xi_1 = \xi_3$.

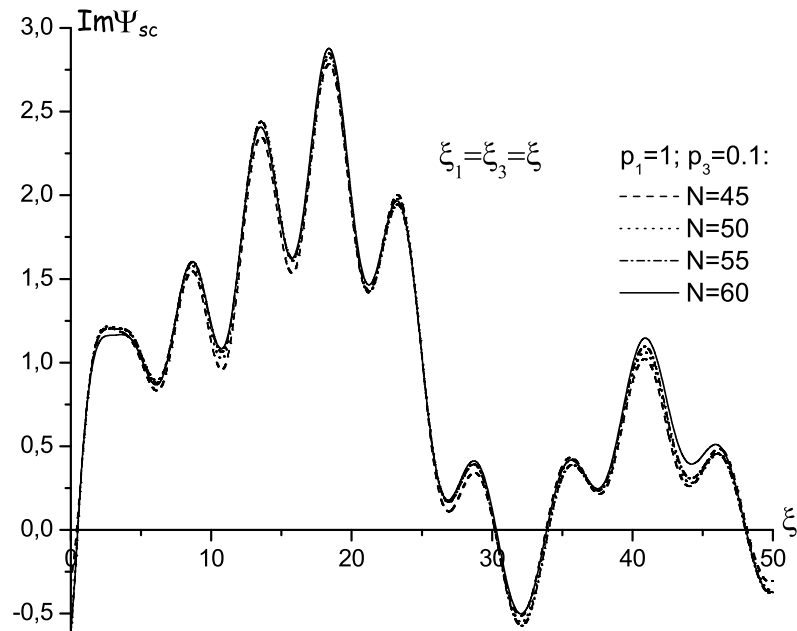


Figure 2: Same as Fig. 1 but for the imaginary part of solution.

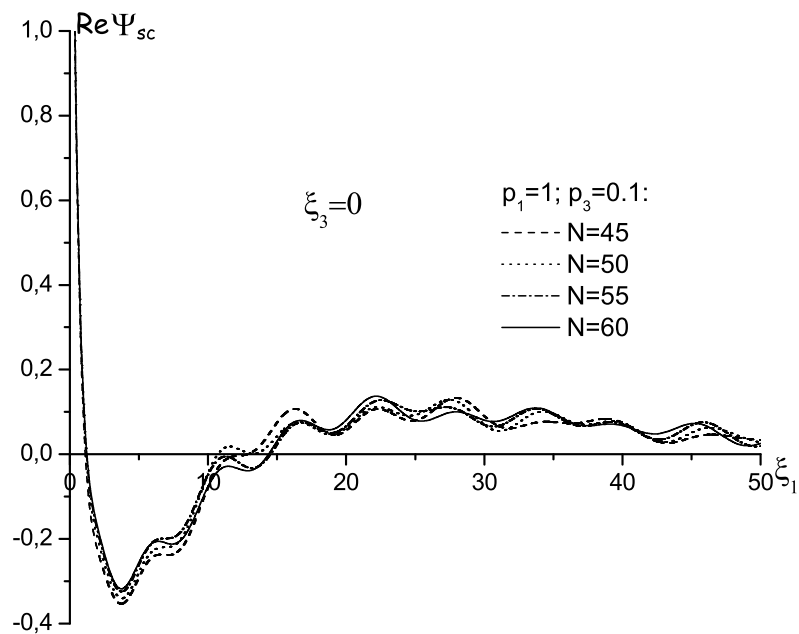


Figure 3: Same as Fig. 1 but on the axis ξ_1 .

asymptotic behavior corresponding to the problem under consideration. Therefore we introduce a set of basis functions that we name quasi-Sturmian functions. They are defined as solutions of a driven differential equation which includes the separable part of the full three-body kinetic energy in generalized parabolic coordinates and also all Coulomb interactions. Any basis set can be used in the right-hand-side of Eq. (30). The choice of a convenient basis depends on the type of the driven term appearing in the full three-body driven equation. The basis in the right-hand-side of Eq. (30) should provide a fast convergence of the driven term. On the other hand, the QS

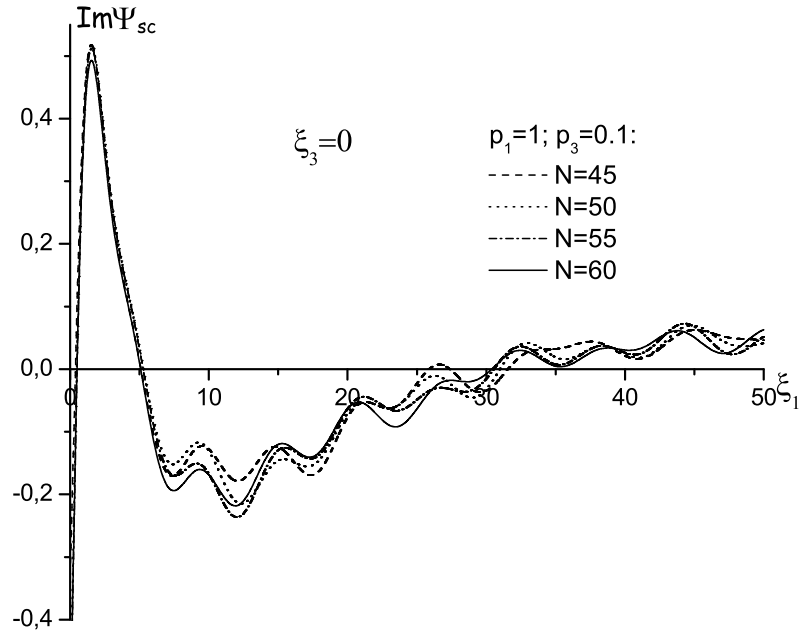


Figure 4: Same as Fig. 2 but on the axis ξ_1 .

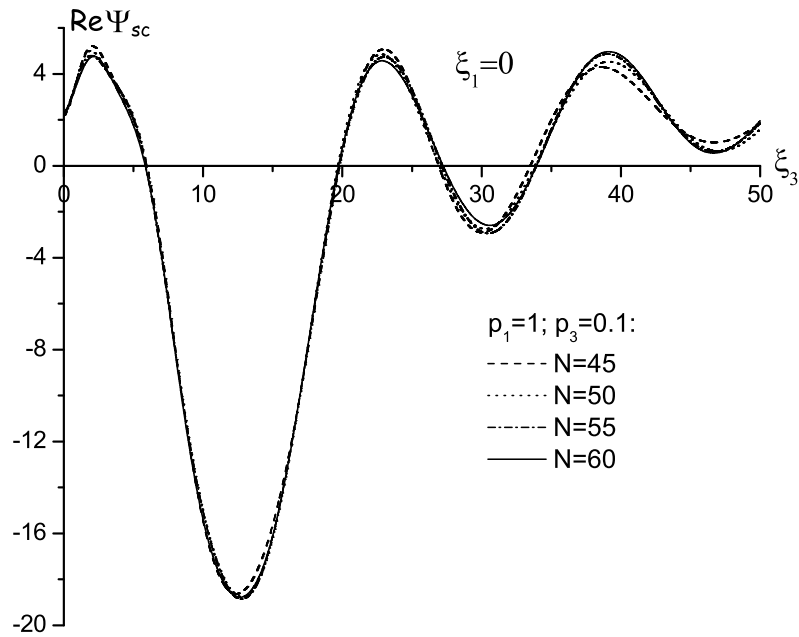


Figure 5: Same as Fig. 1 but on the axis ξ_3 .

functions also form a basis set thus allowing to expand the scattering wave function we are looking for. All QS functions possess the correct asymptotic behavior of the full three-body problem. This means, in principle, that only the inner region where the interaction between all particles takes place, should be expanded.

We demonstrate an efficiency of the proposed method in this contribution by applying it to a two-dimensional problem which possesses most of the full problem difficulties: the non-separability and the scattering type boundary conditions. We probe whether we are able to achieve the convergence of the scattering wave function

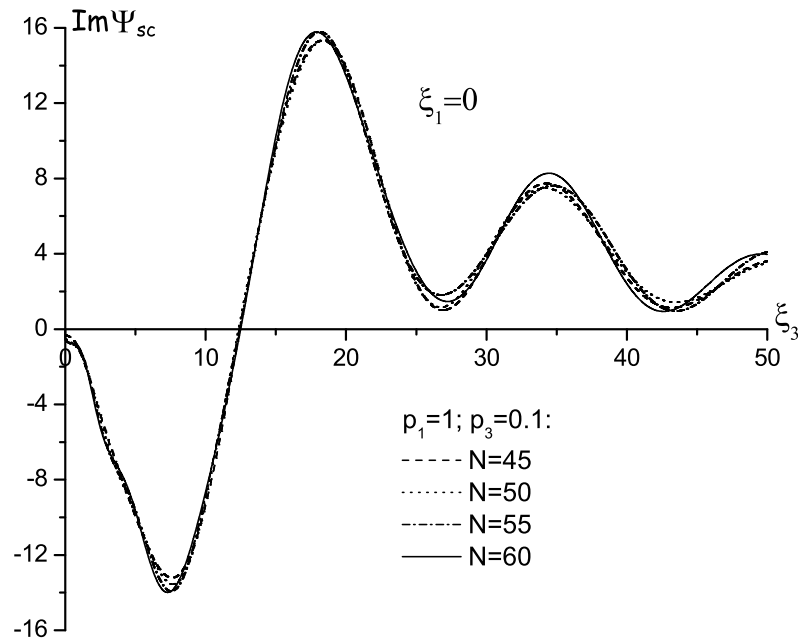


Figure 6: Same as Fig. 2 but on the axis ξ_3 .

by the use of QS functions. A more extensive study of properties of QS functions associated with a different type of basis used to expand the driven term, will be presented soon elsewhere. In this study we shall present a six-dimensional function possessing both incoming and outgoing type boundary conditions.

Acknowledgements

One of the authors (GG) thanks the support by PGI (24/F049) of the Universidad Nacional del Sur. GG acknowledge also the support of ANPCyT (PICT08/0934) (Argentina) and PIP 200901/552 CONICET (Argentina).

References

- [1] I. Bray and A. T. Stelbovics, Phys. Rev. Lett. **70**, 746 (1993).
- [2] I. Bray, D. V. Fursa, A. S. Kheifets and A. T. Stelbovics, J. Phys. B **35**, R117 (2002).
- [3] Z. Papp, Phys. Rev. C **55**, 1080 (1997).
- [4] Z. Papp, C.-Y. Hu, Z. T. Hlousek, B. Kónya and S. L. Yakovlev, Phys. Rev. A **63**, 062721 (2001).
- [5] *The J-matrix method: Developments and applications*, edited by A. D. Alhaidari, E. J. Heller, H. A. Yamani and M. S. Abdelmonem. Springer, 2008.
- [6] S. A. Zaytsev, V. A. Knyr, Yu. V. Popov and A. Lahmam-Bennani, Phys. Rev. A **75**, 022718 (2007).
- [7] M. Silenou Mengoue, M. G. Kwato Njock, B. Piraux, Yu. V. Popov and S. A. Zaytsev, Phys. Rev. A **83**, 052708 (2011).

-
- [8] A. L. Frapiccini, J. M. Randazzo, G. Gasaneo and F. D. Colavecchia, *J. Phys. B* **43**, 101001 (2010).
 - [9] J. M. Randazzo, F. Buezas, A. L. Frapiccini, F. D. Colavecchia and G. Gasaneo, *Phys. Rev. A* **84**, 052715 (2011).
 - [10] G. Gasaneo and L. U. Ancarani, *Phys. Rev. A* **80**, 062717 (2009).
 - [11] C. W. McCurdy, M. Baertschy and T. N. Rescigno, *J. Phys. B* **37**, R137 (2004).
 - [12] L. D. Faddeev and S. P. Merkuriev, *Quantum scattering theory for several particle systems*. Kluwer, Dordrecht, 1993.
 - [13] H. Klar, *Z. Phys. D* **16**, 231 (1990).
 - [14] F. D. Colavecchia, G. Gasaneo and C. R. Garibotti, *Phys. Rev. A* **57**, 1018 (1998).
 - [15] S. A. Zaytsev, *J. Phys. A* **43**, 385208 (2010).
 - [16] J. S. Briggs, *Phys. Rev. A* **41**, 539 (1990)
 - [17] D. M. Mitnik, F. D. Colavecchia, G. Gasaneo and J. M. Randazzo, *Comput. Phys. Comm.* **182**, 1145 (2011).
 - [18] M. J. Ambrosio, J. A. Del Punta, K. V. Rodriguez, G. Gasaneo and L. U. Ancarani *J. Phys. B* **45**, 015201 (2012)
 - [19] P. A. Macri, J. E. Miraglia, C. R. Garibotti, F. D. Colavecchia and G. Gasaneo, *Phys. Rev. A* **55**, 3518 (1997).
 - [20] L. Rosenberg, *Phys. Rev. D* **8**, 1833 (1973).
 - [21] P. C. Ojha, *J. Math. Phys.* **28**, 392 (1987).
 - [22] S. A. Zaytsev, *J. Phys. A* **42**, 015202 (2009).
 - [23] L. U. Ancarani and G. Gasaneo, *Phys. Rev. A* **75**, 032706 (2007).

***J*-Matrix Analysis of Resonant States in the Shell Model**

**A. I. Mazur^a, A. M. Shirokov^{a,b,c}, J. P. Vary^c, P. Maris^c
and I. A. Mazur^a**

^a*Department of Physics, Pacific National University, Khabarovsk 680035, Russia*

^b*Skobeltsyn Institute of Nuclear Physics, Lomonosov Moscow State University, Moscow 119991, Russia*

^c*Department of Physics and Astronomy, Iowa State University, Ames, Iowa 50011, USA*

Abstract

We suggest a method for calculating scattering phase shifts and energies and widths of resonances which utilizes only eigenenergies obtained in variational calculations with oscillator basis and their dependence on oscillator basis spacing $\hbar\Omega$. The validity of the suggested approach is verified in calculations with model Woods–Saxon potentials and applied to calculations of resonances in $n\alpha$ scattering using the no-core shell model.

Keywords: *Shell model; J-matrix approach; resonance energy and width; Breit–Wigner resonance formula; $n\alpha$ scattering*

1 Introduction

To calculate energies of nuclear ground states and other bound states within various shell model approaches, one conventionally starts by calculating the $\hbar\Omega$ -dependence of the energy $E_\nu(\hbar\Omega)$ of the bound state ν in some model space. The minimum of $E_\nu(\hbar\Omega)$ is correlated with the energy of the state ν . The convergence of calculations and accuracy of the energy prediction is estimated by comparing with the results obtained in neighboring model spaces. To improve the accuracy of theoretical predictions, various extrapolation techniques have been suggested recently [1, 2, 3, 4] which make it possible to estimate the binding energies in the complete infinite shell-model basis space.

Is it possible to study nuclear states in the continuum, resonant states in particular, in the shell model using bound state techniques? A conventional belief is that the energies of shell-model states in the continuum should be associated with the resonance energies. It was shown however in Ref. [5] that the energies of shell-model states may appear well above the energies of resonant states, especially for broad resonances. Moreover, the analysis of Ref. [5] clearly demonstrated that the shell model should also generate some states in a non-resonant nuclear continuum. The nuclear resonance properties can be studied in the Gamow shell model, including the *ab initio* no-core Gamow shell model (NCGSM) [6]. Another option is to combine the shell model with resonating group method (RGM). An impressive progress in description of various nuclear reactions was achieved by means of the combined no-core shell model/RGM (NCSM/RGM) approach [7]. Both NCGSM and NCSM/RGM complicate essentially the shell model calculations. Is it possible to get some information about the unbound nuclear states directly from the results of calculations in NCSM or other versions of the nuclear shell model without introducing additional Berggren basis states as in NCGSM or additional RGM calculations as in the NCSM/RGM approach?

A complete study of the nuclear continuum can be performed by extending the nuclear shell model by *J*-matrix formalism in scattering theory. The *J*-matrix formalism

has been suggested in atomic physics [8, 9]. Later it was independently rediscovered in nuclear physics [10, 11] and was successfully used in shell-model applications [12]. However a direct implementation of the J -matrix formalism in modern large-scale shell-model calculations is very complicated: the J -matrix requires calculation of a huge number of eigenstates while modern shell-model codes usually utilize Lanczos algorithm which provides only few lowest Hamiltonian eigenstates. Furthermore, the J -matrix needs also the highest component of wave function of each eigenstate which is usually obtained with a low precision.

On the other hand, the J -matrix formalism can be used for a simple calculation of the scattering phase shift at a single energy $E_\nu(\hbar\Omega)$ which is an eigenstate of the shell-model Hamiltonian. In this case, the phase shift calculation requires only the value of the energy $E_\nu(\hbar\Omega)$ and the basis parameters (the $\hbar\Omega$ value and the basis size). Varying the shell-model parameter $\hbar\Omega$, we generate a variation of $E_\nu(\hbar\Omega)$ and hence we can calculate the phase shifts in some energy range. Calculations of scattering phase shifts at the eigenenergies of the Hamiltonian in the oscillator basis and obtaining the phase shift energy dependence by variation of basis parameters, was recently performed in Ref. [4] using another (not the J -matrix) technique. A detailed study of scattering phase shifts at eigenenergies of the Hamiltonian in arbitrary finite \mathcal{L}^2 basis was performed in Ref. [13]. This study was based on the theory of spectral shift functions introduced by I. M. Lifshitz more than 60 years ago [14] and later forgotten by physicists though used up to now by mathematicians (see Ref. [13] and references therein).

In this contribution, we study the behavior of scattering phase shifts at the eigenenergies $E_\nu(\hbar\Omega)$ of the Hamiltonian in the oscillator basis. Our aim is to formulate criteria for selecting eigenstates associated with resonances and to develop an approach to evaluating energies and widths of these resonances. We are using the J -matrix formalism which provides exact phase shifts in the systems with potential energy described by a finite matrix in oscillator basis, i. e., just in the case of the nuclear shell model.

A brief sketch of the J -matrix theory and examples of phase shift calculations with model interactions are presented in the next Section. Application of the approach to calculations of phase shifts at the eigenenergies $E_\nu(\hbar\Omega)$ of the Hamiltonian in the oscillator basis, comparison with the spectral shift function theory of I. M. Lifshitz and criteria for selecting eigenstates associated with resonances are discussed in Section 3. In Section 4, we discuss the relation between the parameters of the Breit–Wigner resonance formula and the $\hbar\Omega$ dependence of the eigenenergy $E_\nu(\hbar\Omega)$ and give examples of calculating Breit–Wigner parameters with model interactions. An analysis of resonance energies and widths in neutron- α scattering based on NCSM calculations of ${}^5\text{He}$ nucleus is presented in Section 5.

2 J -matrix formalism

We discuss here the simplest version of the J -matrix formalism — a single-channel elastic scattering of an uncharged particle. We use notations of Refs. [15, 16] where one can find more details of the J -matrix theory, the multi-channel version of this approach, a technique of accounting for the long-range Coulomb interaction, etc.

The radial wave function $u_l(k, r)$ describing the relative motion in the partial wave with orbital momentum l is expanded in the J -matrix formalism in infinite series of radial oscillator functions $R_{nl}(r)$,

$$u_l(k, r) = \sum_{n=0}^{\infty} a_{nl}(k) R_{nl}(r), \tag{1}$$

where

$$R_{nl}(r) = (-1)^n \sqrt{\frac{2n!}{r_0 \Gamma(n+l+3/2)}} \left(\frac{r}{r_0}\right)^{l+1} \exp\left(-\frac{r^2}{2r_0^2}\right) L_n^{l+\frac{1}{2}}\left(\frac{r^2}{r_0^2}\right). \quad (2)$$

Here k is the relative motion momentum, $L_n^\alpha(z)$ are Laguerre polynomials and n is the harmonic oscillator radial quantum number. Using expansion (1) we transform the radial Schrödinger equation

$$H^l u_l(k, r) = E u_l(k, r) \quad (3)$$

into an infinite set of linear algebraic equations

$$\sum_{n'=0}^{\infty} (H_{nn'}^l - \delta_{nn'} E) a_{n'l}(k) = 0, \quad (4)$$

where $H_{nn'}^l = T_{nn'}^l + V_{nn'}^l$ are matrix elements of the Hamiltonian H^l in the oscillator basis, and $T_{nn'}^l$ and $V_{nn'}^l$ are kinetic and potential energy matrix elements respectively.

The kinetic energy matrix elements $T_{nn'}^l$ are known to form a tridiagonal matrix, i. e., the only non-zero matrix elements are

$$\begin{aligned} T_{nn}^l &= \frac{1}{2} \hbar \Omega (2n + l + 3/2), \\ T_{n,n+1}^l &= T_{n+1,n}^l = -\frac{1}{2} \hbar \Omega \sqrt{(n+1)(n+l+3/2)}. \end{aligned} \quad (5)$$

These matrix elements are seen to increase linearly with n for large n . On the other hand, the potential energy matrix elements $V_{nn'}^l$ decrease as $n, n' \rightarrow \infty$. Hence the kinetic energy dominates in the Hamiltonian matrix at large enough n and/or n' . Therefore a reasonable approximation is to truncate the potential energy matrix at large n and/or n' , i. e., to approximate the interaction V by a nonlocal separable potential \tilde{V} with matrix elements

$$\tilde{V}_{nn'}^l = \begin{cases} V_{nn'}^l & \text{if } n \leq N \text{ and } n' \leq N; \\ 0 & \text{if } n > N \text{ or } n' > N. \end{cases} \quad (6)$$

The approximation (6) is the only approximation in the J -matrix approach; for separable interactions of the type (6), the J -matrix formalism suggests exact solutions. Note, the kinetic energy matrix is not truncated in the J -matrix theory contrary to conventional variational approaches like the shell model.

The complete infinite harmonic oscillator basis space can be divided into two subspaces according to truncation (6): an internal subspace spanned by oscillator functions with $n \leq N$ where the interaction V is accounted for and an asymptotic subspace spanned by oscillator functions with $n > N$ associated with the free motion.

Algebraic equations (4) in the asymptotic subspace take the form of a second order finite-difference equation:

$$T_{nn-1}^l a_{n-1l}^{ass}(E) + (T_{nn}^l - E) a_{nl}^{ass}(E) + T_{nn+1}^l a_{n+1l}^{ass}(E) = 0. \quad (7)$$

Any solution $a_{nl}^{ass}(E)$ of Eq. (7) can be expressed as a superposition of regular $S_{nl}(E)$ and irregular $C_{nl}(E)$ solutions,

$$a_{nl}^{ass}(E) = \cos \delta_l S_{nl}(E) + \sin \delta_l C_{nl}(E), \quad n \geq N, \quad (8)$$

where δ_l is the scattering phase shift. The solutions $S_{nl}(E)$ and $C_{nl}(E)$ have simple analytical expressions [9, 11, 15]:

$$S_{nl}(E) = \sqrt{\frac{\pi n!}{\Gamma(n+l+3/2)}} q^{l+1} \exp\left(-\frac{q^2}{2}\right) L_n^{l+1/2}(q^2), \quad (9)$$

$$C_{nl}(E) = (-1)^l \sqrt{\frac{\pi n!}{\Gamma(n+l+3/2)}} \frac{q^{-l}}{\Gamma(-l+1/2)} \times \exp\left(-\frac{q^2}{2}\right) \Phi(-n-l-1/2, -l+1/2; q^2), \quad (10)$$

where $\Phi(a, b; z)$ is a confluent hypergeometric function and q is a dimensionless momentum,

$$q = \sqrt{\frac{2E}{\hbar\Omega}}. \quad (11)$$

The solutions $a_{nl}(E)$ of the algebraic set (4) in the internal subspace $n \leq N$ are related to the solutions $a_{nl}^{ass}(E)$ in the asymptotic subspace $n \geq N$:

$$a_{nl}(E) = \mathcal{G}_{nN} T_{N,N+1}^l a_{N+1,l}^{ass}(E). \quad (12)$$

Here matrix elements

$$\mathcal{G}_{nn'} = -\sum_{\nu=0}^N \frac{\langle n|\nu\rangle\langle\nu|n'\rangle}{E_\nu - E} \quad (13)$$

are related to the Green's function of the Hamiltonian H^N which is the Hamiltonian H^l truncated to the internal subspace, and are expressed through eigenenergies E_ν and eigenvectors $\langle n|\nu\rangle$ of the Hamiltonian H^N :

$$\sum_{n'=0}^N H_{nn'}^l \langle n'|\nu\rangle = E_\nu \langle n|\nu\rangle, \quad n \leq N. \quad (14)$$

A relation for calculation of the scattering phase shifts δ_l can be obtained through the matching condition

$$a_{Nl}(E) = a_{Nl}^{ass}(E). \quad (15)$$

Using Eqs. (8), (12) and (15) it is easy to obtain [9, 11, 15]

$$\tan \delta_l(E) = -\frac{S_{Nl}(E) - \mathcal{G}_{NN} T_{N,N+1}^l S_{N+1,l}(E)}{C_{Nl}(E) - \mathcal{G}_{NN} T_{N,N+1}^l C_{N+1,l}(E)}. \quad (16)$$

The scattering phase shifts $\delta_l(E)$ can be calculated using Eq. (16). An acceptable range of *J*-matrix parameters (ARJP) $\hbar\Omega$ and N where the scattering phase shifts $\delta_l(E)$ can be calculated with a reasonable precision, depends on the potential V . The convergence of phase shift calculations can be improved, and hence the ARJP can be enlarged, by 'smoothing' the potential truncation in the oscillator basis space, i. e., by replacing the matrix elements (6) by [17]

$$\mathcal{V}_{nn'} = \sigma_N^n \tilde{V}_{nn'} \sigma_N^{n'}, \quad (17)$$

where

$$\sigma_N^n = \frac{1 - \exp\{-[\alpha(n - N - 1)/(N + 1)]^2\}}{1 - \exp(-\alpha^2)}. \quad (18)$$

We employ the smoothing (17)–(18) with the parameter $\alpha = 5$ in our calculations with model interactions presented below.

We illustrate the *J*-matrix calculations of the phase shifts in the vicinity of resonances in Fig. 1. We use a model Woods–Saxon potential with surface repulsion generating a resonance,

$$V(r) = V_0 \frac{1}{1+z} + V_s \frac{b}{r} \frac{z}{(1+z)^2}, \quad (19)$$

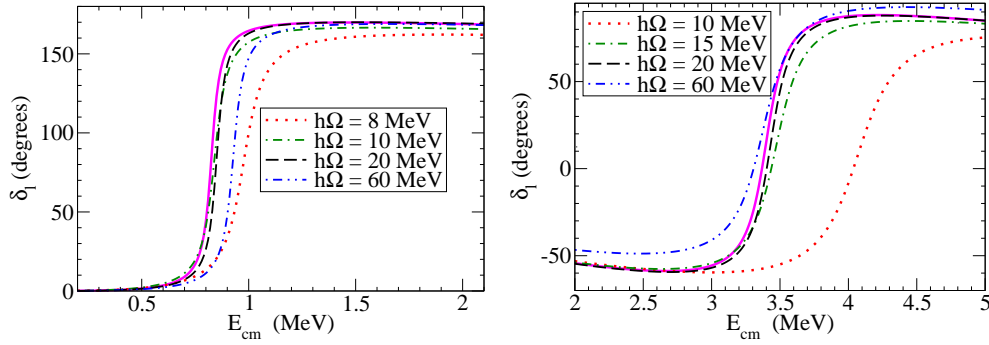


Figure 1: d wave (left) and s wave (right) phase shifts in the vicinity of resonances calculated with model interactions (19) in the J -matrix approach with $N = 5$ and various $\hbar\Omega$ values. The exact phase shifts generated by these interactions are depicted by solid lines.

Table 1: Parameters of the model Woods–Saxon potentials (19) in d and s waves and energies E_r and widths Γ of resonances generated by these potentials.

Partial wave	L	V_0 (MeV)	V_s (MeV)	R (fm)	a (fm)	b (fm)	E_r (MeV)	Γ (MeV)
d	2	-48.0	-20.0	3.08	0.53	3.774	0.8319	0.0612
s	0	-50.0	207.0	3.08	0.53	3.774	3.403	0.2250

where

$$z = \exp\left(\frac{r-R}{a}\right). \quad (20)$$

The reduced mass $m = \frac{4}{5}m_n$ (m_n is a nucleon mass) was used in calculations that corresponds to the scattering of neutron by α -particle. The parameters of the interaction (19) and energies and widths of model resonances generated by it in s and d waves, are presented in Table 1.

The phase shift calculations are well-converged for $N = 5$ in the interval of $\hbar\Omega$ values ranging between 25 and 40 MeV where the J -matrix phase shifts are indistinguishable from the exact results depicted by solid curves in Fig. 1. If $\hbar\Omega$ is taken outside this interval, the J -matrix phase shifts differ from exact as is seen in Fig. 1. The interval of $\hbar\Omega$ values providing excellent description of the phase shifts expands when the truncation boundary N increases. For example, the interval of acceptable $\hbar\Omega$ values starts from approximately 15 MeV in case of $N = 10$.

3 Phase shift and its derivative at $E = E_\nu$

When the energy of relative motion E is equal to one of eigenenergies E_ν of the truncated Hamiltonian H^N , expression (16) for calculation of the phase shifts transforms into

$$\tan \delta_l(E_\nu) = -\frac{S_{N+1,l}(E_\nu)}{C_{N+1,l}(E_\nu)}. \quad (21)$$

The eigenenergy E_ν depends on the size of the internal basis space N and on the value of the oscillator spacing $\hbar\Omega$, $E_\nu = E_\nu(N, \hbar\Omega)$. Therefore one can use Eq. (21) to calculate the phase shifts $\delta(E)$ in some interval of energies E ranging from $E_\nu(\hbar\Omega_1)$ through $E_\nu(\hbar\Omega_2)$ by varying $\hbar\Omega$ within ARJP from $\hbar\Omega_1$ through $\hbar\Omega_2$. The values

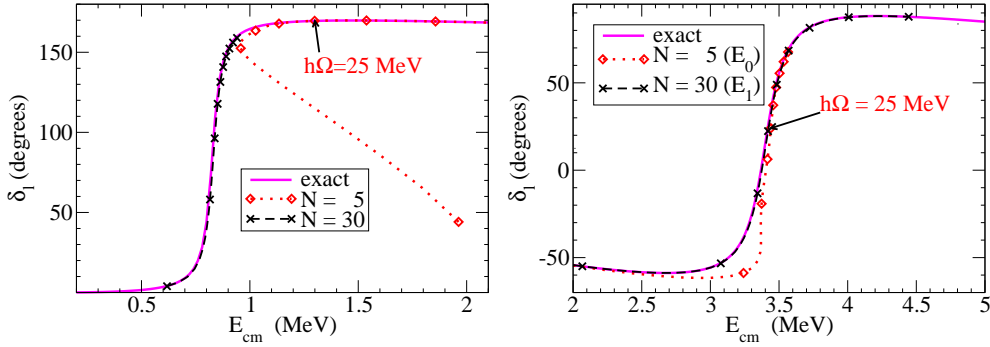


Figure 2: *d* wave (left) and *s* wave (right) phase shifts in the vicinity of resonances calculated with model interactions (19) at the eigenenergies of the truncated Hamiltonian H^N by means of Eq. (21) with $N = 5$ and 30 and various $\hbar\Omega$. The lowest $\hbar\Omega$ value within ARJP in case of $N = 5$ truncation is $\hbar\Omega_1 \approx 25$ MeV, the respective points on the phase shift curves are indicated.

of the lower $\hbar\Omega_1$ and upper $\hbar\Omega_2$ ARJP bounds depend, of course, on N and generally speaking are different for different states $\nu = 0, 1, 2, \dots$. If the ARJP is wide enough and the energy interval $[E_\nu(\hbar\Omega_1), E_\nu(\hbar\Omega_2)]$ covers completely the vicinity of the resonance, the resonance parameters are easily restored from the phase shift behavior in this energy interval. In this case the resonance parameters can be calculated through the $\hbar\Omega$ -dependence of eigenenergy $E_\nu = E_\nu(\hbar\Omega)$ obtained in a standard variational calculation with oscillator basis. However, in some cases the energy interval $[E_\nu(\hbar\Omega_1), E_\nu(\hbar\Omega_2)]$ covers only a fraction, sometimes, a small fraction of the energy range of the resonant behavior of the phase shifts. In those cases, the extraction of the resonance energy and width is more complicated and less accurate. More, sometimes the energy interval $[E_\nu(\hbar\Omega_1), E_\nu(\hbar\Omega_2)]$ corresponds to a non-resonant scattering as was clearly demonstrated in Ref. [5].

We demonstrate in Fig. 2 calculations of phase shifts by means of Eq. (21) in the vicinity of resonances generated in *s* and *d* waves by model interactions (19). In the case of *d* wave, calculations with $N = 5$ and 30 are performed with the lowest eigenstate ($\nu = 0$) obtained with $\hbar\Omega$ ranging from 2.5 to 50 MeV. In the case of *s* wave, varying $\hbar\Omega$ in the same interval from 2.5 to 50 MeV in calculations with $N = 5$, we obtain the variation of the lowest eigenstate energy E_0 between 0.64 and 3.57 MeV covering the vicinity of the resonance. However in calculations with $N = 30$, the lowest eigenstate energy E_0 varies from 0.11 to 3.15 MeV due to variation of $\hbar\Omega$ in the same interval, i. e., E_0 lies below the resonance region. The vicinity of the resonance in this case is completely covered by variation of the energy E_1 of the next state with $\nu = 1$, and we use E_1 for calculations of the phase shifts in the resonance region. We obtain an excellent description of the phase shifts if the *J*-matrix parameters are lying within ARJP. However when $\hbar\Omega$ goes outside ARJP, the obtained phase shifts start deviating from the exact ones. This deviation can be very large when $\hbar\Omega$ is far enough from ARJP and the phase shifts may become ambiguous in some energy interval due to unphysical ‘backbending’ energy dependence (see the left panel of Fig. 2) obtained by variation of $\hbar\Omega$ far outside ARJP.

It is interesting to compare the *J*-matrix approach to calculations of phase shifts at eigenenergies E_ν with the approach utilizing the spectral shift functions of I. M. Lifshitz [14]. We note that the phase shifts at eigenenergies E_ν due to Eq. (21) are equal to

$$\delta_l(E_\nu) = f_{N+1,l}(E_\nu) + m\pi, \tag{22}$$

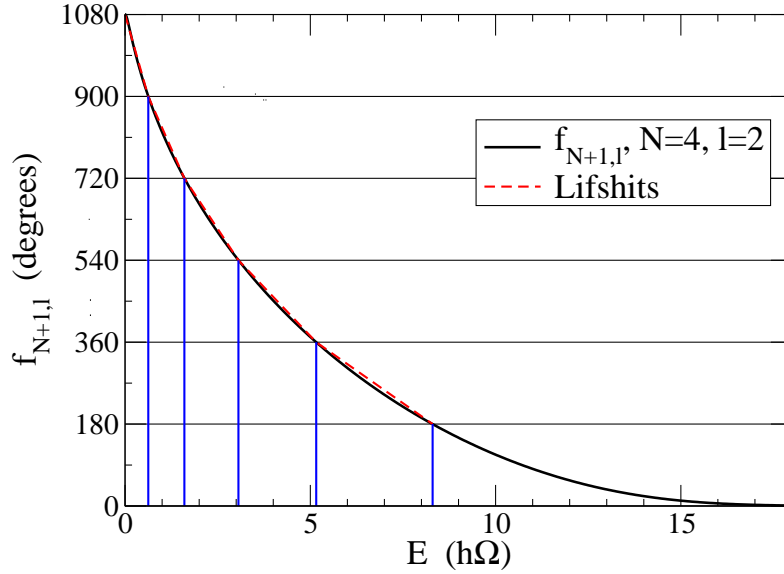


Figure 3: Universal function $f_{N+1,l}(E)$ in case of $N = 4$ and $l = 2$ and its approximation in the Lifshitz spectral shift function method. The vertical solid lines correspond to eigenenergies E_ν^0 of the truncated kinetic energy T^N .

where m can be zero or takes some positive or negative integer value, and the function

$$f_{nl}(E) = -\arctan\left(\frac{S_{nl}(E)}{C_{nl}(E)}\right). \quad (23)$$

Due to Eqs. (9), (10) and (23), it is clear that $f_{nl}(E)$ depends on the energy E and $\hbar\Omega$ only in combination $E/\hbar\Omega$. $f_{nl}(E)$ is a monotonically decreasing function of a dimensionless energy $\varepsilon = E/\hbar\Omega$ which goes down by $(n+1)\pi$ as ε increases from 0 to infinity. An example of this function corresponding to the case $n = 5$ and $l = 2$ is presented in Fig. 3. The values of the function $f_{N+1,l}(E_\nu)$ provide the J -matrix phase shift δ_l at the eigenenergy E_ν for a given $\hbar\Omega$ value as is shown in Fig. 4 where we present in a larger scale a piece of the function $f_{N+1,l}(E)$ shifted to the interval of its values $[0, \pi]$ [the shift of this function by $m\pi$ is of no importance since we can always redefine m in Eq. (22)].

Within the Lifshitz spectral shift function approach [14, 13], the phase shift is calculated as

$$\delta_l(E_\nu) = -\pi \frac{E_\nu - E_\nu^0}{E_{\nu+1}^0 - E_\nu^0}. \quad (24)$$

Here E_ν are the eigenvalues of the truncated Hamiltonian H^N while E_ν^0 are the eigenvalues of the kinetic energy T^N truncated to the matrix of the same size as H^N . We recall that the kinetic energy has a tridiagonal matrix (5) in the oscillator basis, the functions $S_{nl}(E)$ are regular solutions of the respective finite-difference equation (7), and the eigenenergies E_ν^0 of the truncated kinetic energy T^N can be obtained by solving this finite-difference equation with the boundary condition

$$S_{N+1,l}(E_\nu^0) = 0. \quad (25)$$

Therefore, due to Eq. (23), the kinetic energy eigenstates correspond to the energies at which $\tan f_{N+1,l}(E_\nu^0) = 0$ or when the function $f_{N+1,l}(E_\nu^0) = m\pi$, i. e., when the plot of the function $f_{N+1,l}(E)$ crosses the horizontal lines at $\pi, 2\pi, \dots$ as is shown in Fig. 3. We connect these crossing points by straight lines in Fig. 3. A set of these straight lines is seen to provide a good approximation for the function $f_{N+1,l}(E)$.

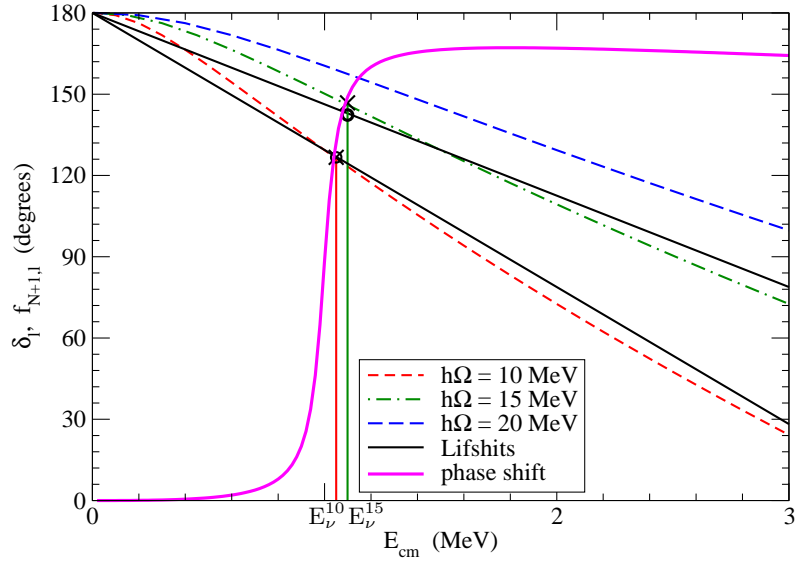


Figure 4: Calculation of phase shifts at eigenenergies E_ν in the J -matrix approach and using Lifshitz spectral shift function method. Dashed lines depict the function $f_{N+1,l}(E)$ for various $\hbar\Omega$ values, solid straight lines depict approximation of this function in the Lifshitz approach. E_ν^{10} and E_ν^{15} are eigenenergies obtained with $\hbar\Omega = 10$ and 15 MeV respectively. Crosses (circles) show the J -matrix (Lifshitz) phase shifts obtained with $\hbar\Omega = 10$ and 15 MeV, solid curve shows the J -matrix phase shifts in a continuous energy interval.

According to Eq. (24), the phase shifts at eigenenergies E_ν in the Lifshitz approach are obtained as the values of this straight-line approximation of the function $f_{N+1,l}(E)$ at energies E_ν as shown in Fig. 4.

It is seen that the J -matrix and Lifshitz approach provide close results for the phase shifts if N is large enough when the straight-line Lifshitz approximation of the function $f_{N+1,l}(E)$ is accurate. In Fig. 4, the difference of $\delta_l(E_\nu)$ values obtained by these approaches is the difference between positions of crosses and circles. It is interesting that the model interaction used to prepare this figure provides exactly the same phase shifts $\delta_l(E_\nu)$ for both methods in calculations with $\hbar\Omega = 10$ MeV. A comparison of results of calculations by means of these two approaches of phase shifts generated by our model interaction (19) in the d wave, is shown in Fig. 5.

It is also interesting to compare our J -matrix approach with the method of Ref. [4]

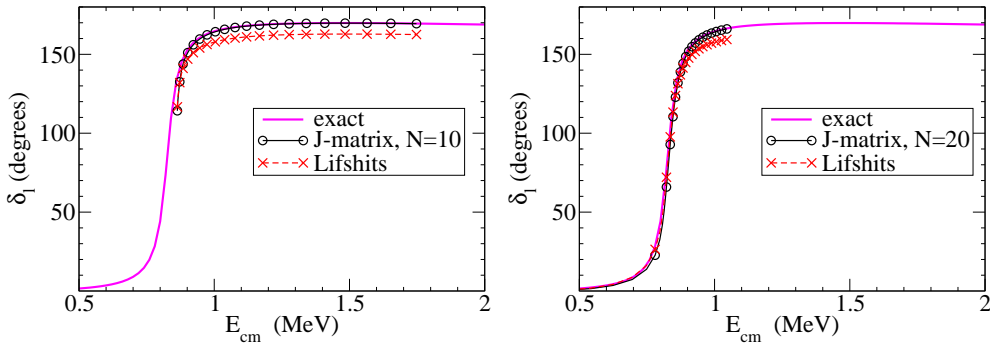


Figure 5: Comparison of d wave phase shifts obtained by J -matrix and Lifshitz methods for the model interaction (19) with $N = 10$ and 20 .

where the phase shifts at the eigenenergies of the Hamiltonian H^N truncated in the oscillator basis was suggested to obtain through the following equation:

$$\tan \delta_l(E_\nu) = \frac{j_l(k_\nu L_i)}{n_l(k_\nu L_i)}. \quad (26)$$

Here $j_l(x)$ and $n_l(x)$ are spherical Bessel and Neumann functions, momentum $k_\nu = \sqrt{2mE_\nu/\hbar^2}$, and for low momenta

$$L_i = \sqrt{2(2N + l + 3/2 + i)} r_0, \quad (27)$$

$$r_0 = \sqrt{\frac{\hbar}{m\Omega}}. \quad (28)$$

The parameter L_i was involved in Ref. [4] in the study of convergence properties of bound states of the Hamiltonian H^N , and the best fit of convergence behavior resulted in $i = 2$.

Equation (26) can be easily obtained from our J -matrix formula (21) in the limit of large N . Asymptotics of functions $S_{nl}(E)$ and $C_{nl}(E)$ were studied in detail in Ref. [18]. In the limit of large n , more precisely, for $n \gg q$, the functions (9) and (10) are well approximated by spherical Bessel and Neumann functions [18, 15]:

$$S_{nl}(E) \approx 2kr_0(n + l/2 + 3/4)^{\frac{1}{4}} j_l\left(2kr_0\sqrt{n + l/2 + 3/4}\right), \quad (29)$$

$$C_{nl}(E) \approx -2kr_0(n + l/2 + 3/4)^{\frac{1}{4}} n_l\left(2kr_0\sqrt{n + l/2 + 3/4}\right). \quad (30)$$

Substituting $S_{nl}(E)$ and $C_{nl}(E)$ in Eq. (21) by their asymptotics (29) and (30), we immediately obtain Eq. (26). The value of $i = 2$ for the parameter L_i unambiguously follows from the fact that $S_{nl}(E)$ and $C_{nl}(E)$ appear in Eq. (21) with $n = N + 1$.

It is easy to conclude from Fig. 3 that eigenvalues E_ν lying in the vicinity of the resonance where the phase shift is rapidly increasing, should change only slightly when the value of $\hbar\Omega$ is changed and hence the derivative $\frac{dE_\nu}{\hbar d\Omega}$ should be small and positive. A wider resonance is associated with a less rapid increase of δ_l and a larger value of the derivative $\frac{dE_\nu}{\hbar d\Omega}$. One should be however accurate with making conclusions about the relative widths of resonances based on comparison of values of derivatives $\frac{dE_\nu}{\hbar d\Omega}$ of respective eigenvalues E_ν . First, the slope of the function $f_{N+1,l}(E)$ decreases with energy E and hence the derivatives $\frac{dE_\nu}{\hbar d\Omega}$ are different for the resonances of the same width but of different energy. Next, the slope of $f_{N+1,l}(E)$ depends also on the orbital momentum l and hence the derivatives $\frac{dE_\nu}{\hbar d\Omega}$ are different for the resonances of the same width and energy but of different l . It is also important to get the eigenvalue E_ν in the vicinity of the resonance: the derivative $\frac{dE_\nu}{\hbar d\Omega}$ decreases when the eigenvalue E_ν is shifted to the edge of the resonance region where the slope of $\delta_l(E)$ decreases; $\frac{dE_\nu}{\hbar d\Omega}$ gets even larger values in the non-resonant region.

Which eigenvalues E_ν are associated with a resonance and which are not? It is important to find a condition able to distinguish these eigenvalues. The phase shift $\delta_l(E)$ is increasing and hence the derivative $d\delta_l/dE$ is positive in the resonance region. We need to find an expression for $\delta_l(E)$ at the energies $E = E_\nu$. Using Eqs. (9) and (10) and expressions for the derivatives of Laguerre polynomials and confluent hypergeometric function [19], we obtain:

$$\frac{dS_{nl}(E)}{dE} = \left(\frac{n + l/2 + 1/2}{E} - \frac{1}{\hbar\Omega} \right) S_{nl}(E) - \frac{\sqrt{n(n + l + 1/2)}}{E} S_{n-1,l}(E), \quad (31)$$

$$\frac{dC_{nl}(E)}{dE} = \left(\frac{n + l/2 + 1/2}{E} - \frac{1}{\hbar\Omega} \right) C_{nl}(E) - \frac{\sqrt{n(n + l + 1/2)}}{E} C_{n-1,l}(E). \quad (32)$$

We note that $S_{nl}(E)$ and $C_{nl}(E)$ are two independent solutions of the second order finite-difference equation (7), and the Casorati determinant of these solutions,

$$\mathcal{K}_n(C, S) \equiv C_{n+1,l}(E) S_{n,l}(E) - C_{n,l}(E) S_{n+1,l}(E), \quad (33)$$

which plays the same role in the theory of linear difference equations as Wronskian in the theory of linear differential equations, differs from zero:

$$T_{n,n+1}^l \mathcal{K}_n(C, S) = \frac{q}{2} \hbar \Omega. \quad (34)$$

Using Eqs. (16), (31)–(34) we obtain

$$\left. \frac{d\delta_l(E)}{dE} \right|_{E=E_\nu} = \frac{q_\nu}{\hbar \Omega} \cdot \frac{1}{S_{N+1,l}^2(E_\nu) + C_{N+1,l}^2(E_\nu)} \times \left[\frac{2}{\langle N|\nu \rangle^2 (N+1)(N+l+3/2)} - \frac{2}{q_\nu^2} \right], \quad (35)$$

where $q_\nu \equiv \sqrt{2E_\nu/\hbar\Omega}$. Expression (35) involves not only the eigenvalue E_ν but also the last component of the eigenvector $\langle N|\nu \rangle$. We would like to eliminate $\langle N|\nu \rangle$ in the expression for the derivative $\frac{d\delta_l(E)}{dE}$ at $E = E_\nu$.

The phase shift δ_l at $E = E_\nu$ in our approach is expressed through the function $f_{N+1,l}$ defined by Eq. (23). The function $f_{N+1,l}$ depends on the eigenenergy E_ν and the oscillator basis parameter $\hbar\Omega$, $f_{N+1,l} = f_{N+1,l}(E_\nu, \hbar\Omega)$. We recall that the value of E_ν depends on $\hbar\Omega$. Suppose that eigenvalue E'_ν is close enough to E_ν and the respective $\hbar\Omega'$ is close enough to $\hbar\Omega$. In this case, we have:

$$f_{N+1,l}(E'_\nu, \hbar\Omega') \simeq f_{N+1,l}(E_\nu, \hbar\Omega) + \frac{\partial f_{N+1,l}}{\partial E}(E'_\nu - E_\nu) + \frac{\partial f_{N+1,l}}{\partial \hbar\Omega}(\hbar\Omega' - \hbar\Omega). \quad (36)$$

The phase shift $\delta_l(E)$ depends only on the energy E and should not depend on $\hbar\Omega$. Therefore

$$\delta_l(E'_\nu) \simeq \delta_l(E_\nu) + \frac{d\delta_l}{dE}(E'_\nu - E_\nu). \quad (37)$$

The partial derivatives $\frac{\partial f_{N+1,l}}{\partial E}$ and $\frac{\partial f_{N+1,l}}{\partial \hbar\Omega}$ entering Eq. (36) can be calculated using Eqs. (23), (9) and (10), and then from Eqs. (35)–(37) we obtain

$$\frac{dE_\nu}{d\hbar\Omega} \simeq \frac{(E'_\nu - E_\nu)}{(\hbar\Omega' - \hbar\Omega)} \simeq \frac{1}{2} \langle N|\nu \rangle^2 (N+1)(N+l+3/2). \quad (38)$$

Using Eq. (38), we rewrite the expression (35) as

$$\left. \frac{d\delta_l(E)}{dE} \right|_{E=E_\nu} \simeq \frac{q_\nu}{\hbar \Omega} \cdot \frac{1}{S_{N+1,l}^2(E_\nu) + C_{N+1,l}^2(E_\nu)} \left(\frac{1}{dE_\nu/d\hbar\Omega} - \frac{\hbar\Omega}{E_\nu} \right). \quad (39)$$

Since the phase shift derivative $\frac{d\delta_l(E)}{dE} > 0$ in the vicinity of resonance, it follows from Eq. (39) that

$$\frac{E_\nu}{\hbar\Omega} > \frac{dE_\nu}{d\hbar\Omega} > 0 \quad (40)$$

in the resonance region. If this inequality is not fulfilled, the eigenvalue E_ν corresponds to a non-resonant phase shift behavior.

One should be careful with using condition (40) for determining which of the Hamiltonian eigenstates obtained in a variational calculation with oscillator basis can be associated with a resonance. In such variational calculations, in the nuclear shell model in particular, each of the obtained eigenenergies usually decreases with $\hbar\Omega$ at small enough $\hbar\Omega$ values, gets a variational minimum at some $\hbar\Omega = \hbar\Omega_0$ and starts

increasing after this minimum. One should use only the increasing part of the function $E_\nu(\hbar\Omega)$ corresponding to $\hbar\Omega > \hbar\Omega_0$ for the analysis by means of inequality (40). The eigenvalues obtained at small $\hbar\Omega < \hbar\Omega_0$ before the minimum of $E_\nu(\hbar\Omega)$ may need strong so-called ultraviolet corrections [2, 3, 4] and thus lie outside ARJP. The $\hbar\Omega$ regions corresponding to large negative $\frac{dE_\nu}{d\hbar\Omega}$ cause the unphysical ‘backbending’ energy dependence of phase shift shown in the left panel of Fig. 2. Note also that in many-body calculations the energies $E_\nu(\hbar\Omega)$ should be calculated relative to the respective threshold. For example, in case of resonance associated with neutron scattered by nucleus AZ , one should calculate the ground state energy $E_0^A(\hbar\Omega)$ and the energy $E_\nu^{A+1}(\hbar\Omega)$ of the state of interest in the nucleus ${}^{A+1}Z$ with respective oscillator quanta of excitations to obtain $E_\nu(\hbar\Omega)$ as

$$E_\nu(\hbar\Omega) = E_\nu^{A+1}(\hbar\Omega) - E_0^A(\hbar\Omega). \quad (41)$$

4 Breit–Wigner resonance

In a variational calculation with the oscillator basis with some truncation boundary N we obtain the energy E_ν of state ν as a function of oscillator parameter $\hbar\Omega$, $E_\nu = E_\nu(\hbar\Omega)$. As was shown above, using the function $E_\nu(\hbar\Omega)$, we can calculate the phase shifts $\delta_l(E)$ in some energy interval $[E_\nu(\hbar\Omega_1), E_\nu(\hbar\Omega_2)]$ where both $\hbar\Omega_1$ and $\hbar\Omega_2$ are within ARJP. Generally the interval $[E_\nu(\hbar\Omega_1), E_\nu(\hbar\Omega_2)]$ shifts down in energy and increases with N . If this energy interval includes a large enough slice of energy in the vicinity of some resonance, we can extract the resonance energy and width.

The phase shifts in the vicinity of resonance are conventionally described by the Breit–Wigner resonance formula [20],

$$\delta_l(E) = \arctan\left(\frac{\Gamma/2}{E_r - E}\right) - \phi_l, \quad (42)$$

where E_r and Γ are resonance energy and width respectively. The background phase ϕ_l is supposed to change only slightly in the resonance region, i.e., we can suppose $\phi_l = \text{const}$ in the vicinity of the resonance to obtain

$$\frac{d\delta_l}{dE} = \frac{\Gamma/2}{(E_r - E)^2 + (\Gamma/2)^2}. \quad (43)$$

The phase shift derivative $\frac{d\delta_l}{dE}$ gets its maximum at $E = E_r$. This maximal value of $\frac{d\delta_l}{dE}$ is related to the resonance width Γ :

$$\Gamma = 2 \left(\frac{d\delta_l}{dE} \right)^{-1} \Big|_{E=E_r}. \quad (44)$$

Combining Eqs. (39) and (43), we obtain

$$\frac{\Gamma/2}{(E_r - E_\nu)^2 + (\Gamma/2)^2} = \frac{q_\nu}{\hbar\Omega} \cdot \frac{1}{S_{N+1,l}^2(E_\nu) + C_{N+1,l}^2(E_\nu)} \left(\frac{1}{dE_\nu/d\hbar\Omega} - \frac{\hbar\Omega}{E_\nu} \right). \quad (45)$$

This equation can be used directly for getting resonance parameters E_r and Γ from the fit to RHS of Eq. (45) where the function $E_\nu(\hbar\Omega)$ is obtained in variational calculations with oscillator basis with $\hbar\Omega$ values from ARJP. Having E_r and Γ one can easily obtain the background phase ϕ_l from Eq. (42) if some of the eigenenergies $E_\nu(\hbar\Omega)$ lie outside the resonance region.

We show in Fig. 6 the phase shifts supported by our model interaction (19) in the vicinities of resonances in s and d waves and their approximation in the vicinities of resonances by the Breit–Wigner formula (42) with parameters fitted using Eq. (45).

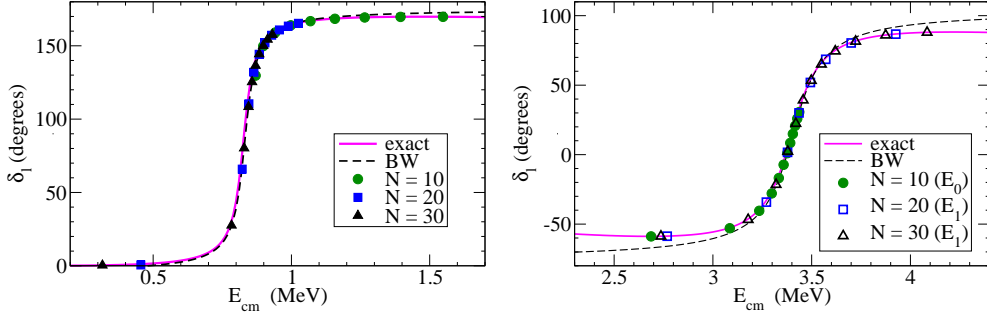


Figure 6: Phase shifts in the vicinity of resonances in d (left) and s (right) waves, resonance description by the Breit–Wigner formula with parameters E_r and Γ obtained by the fit using Eq. (45) and phase shifts used in this fit obtained by our approach [Eq. (21)] at eigenenergies $E_\nu(\hbar\Omega)$ calculated with various $\hbar\Omega$ values and truncations $N = 10, 20$ and 30 . Filled symbols are the phase shifts obtained with the lowest eigenstates $E_0(\hbar\Omega)$, open symbols are the phase shifts obtained with the first excited eigenstates $E_1(\hbar\Omega)$.

The phase shifts at eigenenergies $E_\nu(\hbar\Omega)$ used in this fit are obtained with Hamiltonian truncations $N = 10, 20$ and 30 and are also depicted in Fig. 6. In the case of s wave, the lowest eigenstates $E_0(\hbar\Omega)$ lie below the resonant region, and we use the first excited states $E_1(\hbar\Omega)$ for the resonance parameter fit (the respective phase shifts are shown in Fig. 6 by open symbols). The Breit–Wigner formula is seen to nicely reproduce the phase shifts in the resonance region. The Breit–Wigner parameters obtained by the fit are: $E_r = 0.8315$ MeV, $\Gamma = 0.0602$ MeV and $\phi_l = 5^\circ$ in the d wave and $E_r = 3.405$ MeV, $\Gamma = 0.230$ MeV and $\phi_l = 76^\circ$ in the s wave. The fitted values of the resonance energies E_r and widths Γ reproduce with high precision the exact values given in Table 1.

The highly accurate description of the resonance parameters become possible because we use large enough truncation boundaries in calculations. It is also important to use a ‘global’ fit to a large enough set of eigenvalues $E_\nu(\hbar\Omega)$ covering the whole resonance region as the sets shown in Fig. 6. If we have restrictions in the size of the Hamiltonian, i. e., the values of N are not large enough, or the eigenvalues $E_\nu(\hbar\Omega)$ are available only at the edge of the resonance region, the quality of the fit is reduced.

We illustrate this statement by Fig. 7 where we demonstrate the results obtained with model interaction (19) with various truncations of the Hamiltonian. All results shown in this figure are obtained with eigenvalues $E_\nu(\hbar\Omega)$ fitting inequality (40) which are shown in the upper panels. The middle and lower panels demonstrate ‘local’ fits of resonance energies E_r and widths Γ , i. e., the fits utilizing only three neighboring eigenvalues $E_\nu(\hbar\Omega_{i-1})$, $E_\nu(\hbar\Omega_i)$ and $E_\nu(\hbar\Omega_{i+1})$ obtained with the same truncation N . We see that in the interval of $\hbar\Omega$ values where the eigenstates $E_\nu(\hbar\Omega)$ lie in the resonance region, the locally fitted resonance energies E_r and widths Γ form plateaus well reproducing the exact values. These plateaus are wider for larger N and for the lowest eigenstates $E_0(\hbar\Omega)$ than for excited eigenstates $E_1(\hbar\Omega)$. The plateaus for resonance energies E_r seem to be wider than for widths Γ ; note however very different scales in the middle and lower panels. In the case of the s wave, the plateau for E_r is obtained even with a very small Hamiltonian truncated at $N = 5$. Note that a zigzag in E_r at $\hbar\Omega < 25$ MeV is due to the fact that these $\hbar\Omega$ values are outside ARJP for $N = 5$.

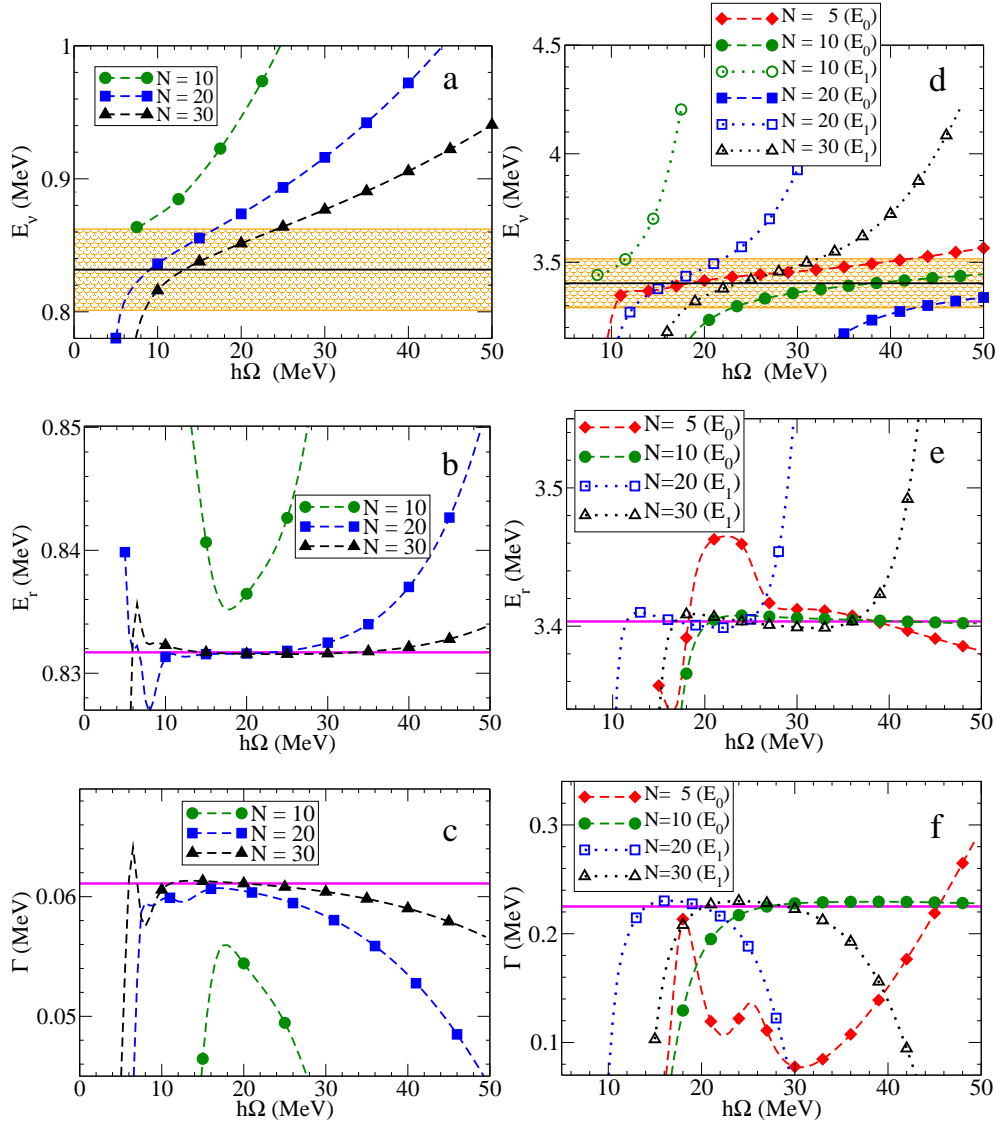


Figure 7: Eigenenergies E_ν (a, d) as functions of $\hbar\Omega$, resonance energies E_r (b, e) and widths Γ (c, f) obtained in ‘local’ fits (see text) with various truncations N for the d (left) and s (right) wave resonances. Solid lines depicts exact values of E_r and Γ , shaded areas in panels a and d show the resonance region. Filled symbols are the results for the lowest eigenstates $E_0(\hbar\Omega)$ while open symbols are the results for the first excited eigenstates $E_1(\hbar\Omega)$.

5 Analysis of resonant states in ${}^5\text{He}$ nucleus based on NCSM calculations

The suggested approach to extracting the resonance energy and width can be applied to any variational calculation with oscillator basis generating a set of eigenvalues $E_\nu(\hbar\Omega)$ forming a function of the oscillator basis spacing $\hbar\Omega$. As an example, we perform calculations of ${}^5\text{He}$ within NCSM [21] and analyze unbound states $3/2^-$ and $1/2^-$ in this nucleus. These states are observed as wide resonances in neutron scattering by α -particles; the $3/2^-$ resonance has an energy $E_r = 0.80$ MeV and width $\Gamma = 0.65$ MeV while the resonance parameters of the $1/2^-$ state

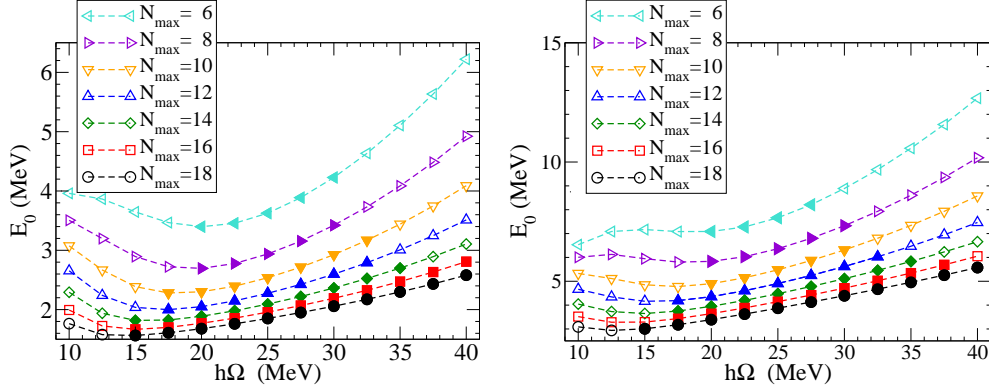


Figure 8: Energies $E_0(\hbar\Omega)$ of $n\alpha$ relative motion associated with $3/2^-$ (left) and $1/2^-$ (right) resonance states in ${}^5\text{He}$ obtained in NCSM calculations of ${}^5\text{He}$ and ${}^4\text{He}$ nuclei with various N_{max} truncations using JISP16 NN interaction. Filled (open) symbols depict eigenstates which fit (do not fit) inequality (40).

are $E_r = 2.07$ MeV and $\Gamma = 5.57$ MeV [22]. We use the JISP16 NN interaction [23] in our NCSM calculations. It is interesting to note that JISP16 and earlier versions of this type of NN interaction, ISTP [24] and JISP6 [25], arise from an application of J -matrix formalism to an inverse scattering treatment of the NN phase shift data.

A very important parameter of NCSM calculations is N_{max} , maximal quanta of oscillator excitations included in the NCSM many-body basis space. It is easy to conclude that relation between the NCSM basis truncation N_{max} and the J -matrix truncation N associated with the principal quantum number of $n\alpha$ relative motion oscillator functions is $N_{\text{max}} = 2N$ in case of $3/2^-$ and $1/2^-$ states in ${}^5\text{He}$.

The $3/2^-$ and $1/2^-$ resonances in ${}^5\text{He}$ are associated with the lowest eigenstates of respective spin-parity $\mathcal{E}_{N_{\text{max}}}^{({}^5\text{He}, J^\pi)}(\hbar\Omega)$ obtained in the NCSM calculations. Note however that we need for the analysis of resonance energy and width the energy $E_0(\hbar\Omega)$ of $n\alpha$ relative motion, i. e., the energy relative to the $n\alpha$ threshold given by Eq. (41) which in our case reads

$$E_0(\hbar\Omega) = \mathcal{E}_{N_{\text{max}}}^{({}^5\text{He}, J^\pi)}(\hbar\Omega) - \mathcal{E}_{N_{\text{max}}}^{({}^4\text{He}, gs)}(\hbar\Omega), \quad (46)$$

where $\mathcal{E}_{N_{\text{max}}}^{({}^4\text{He}, gs)}(\hbar\Omega)$ is the ${}^4\text{He}$ ground state energy obtained in NCSM with the same N_{max} and $\hbar\Omega$. The plots of energies $E_0(\hbar\Omega)$ obtained with various NCSM truncations N_{max} are shown in Fig. 8. Note, some of $n\alpha$ eigenstates $E_0(\hbar\Omega)$ do not fit inequalities (40) and cannot be used for calculations of resonance energy E_r and width Γ (they are shown by open symbols in Fig. 8).

We use only eigenstates $E_0(\hbar\Omega)$ to calculate phase shifts shown in Fig. 9. The borders of ARJP are unknown. We see that some phase shifts values obtained with different N_{max} truncations are in good correspondence and lie on the same curve. However we see that phase shifts calculated using few lowest eigenstates $E_0(\hbar\Omega)$ available for a given small enough basis spaces, i. e., basis spaces characterized by small enough N_{max} values, deviate essentially from the common curve. These smallest eigenstates correspond to lowest $\hbar\Omega$ values which evidently are outside the ARJP. The deviation from the common curve decreases as N_{max} increases. We should use for the calculation of Breit–Wigner parameters E_r and Γ only eigenstates $E_0(\hbar\Omega)$ providing the phase shifts forming the common phase shift curve and fitting inequalities (40), i. e., lying in the resonance region. As a result, we obtain $E_r = 1.41$ MeV and $\Gamma = 0.24$ MeV for the $3/2^-$ resonance and $E_r = 2.55$ MeV and $\Gamma = 0.91$ MeV for the $1/2^-$ resonance. The respective Breit–Wigner phase shifts are also shown in Fig. 9.

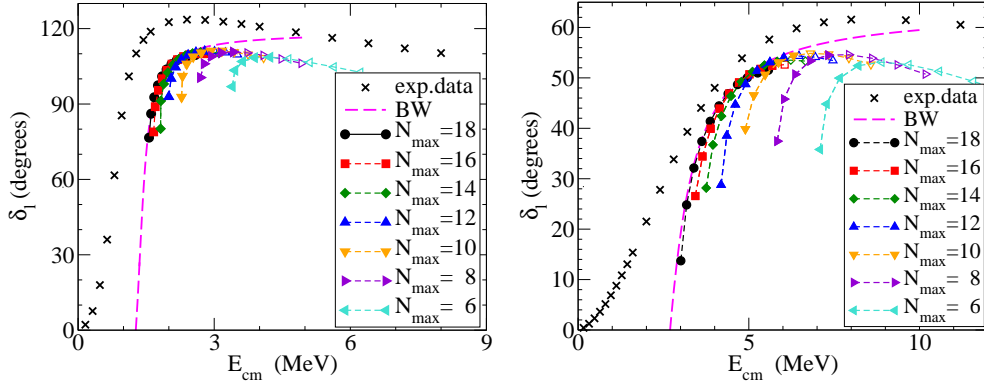


Figure 9: $n\alpha$ phase shifts in $3/2^-$ (left) and $1/2^-$ (right) states obtained by means of Eq. (21) using eigenstates $E_0(\hbar\Omega)$ depicted in Fig. 8 and Breit–Wigner phase shifts (42) calculated with E_r and Γ obtained by the fit. Filled (open) symbols correspond to eigenstates fitting (not fitting) inequality (40). Experimental data are taken from Ref. [26].

Our calculation overestimates resonance energies E_r and underestimates resonance widths Γ for both $3/2^-$ and $1/2^-$ resonances. This is clear from comparison with their experimental values ($E_r = 0.80$ MeV and $\Gamma = 0.65$ MeV for the $3/2^-$ resonance and $E_r = 2.07$ MeV and $\Gamma = 5.57$ MeV for the $1/2^-$ resonance) and from comparison of our phase shifts with experimental data of Ref. [26] shown in Fig. 9. The JISP16 interaction sifts the ${}^5\text{He}$ resonance states up in energy by about 0.5 MeV as compared to experiment. We note that the JISP16 interaction causes also underbinding of both ${}^6\text{Li}$ and ${}^6\text{He}$ nuclei by approximately 0.5 MeV [1]. This seems to be a drawback of the JISP16 interaction in description of nuclei at the beginning of p -shell which can be hopefully eliminated in future versions of this interaction by a more careful fit to experimental data which can include information about resonant states.

6 Conclusions

We formulated a simple method of accurate calculation of phase shifts which uses only eigenenergies E_r obtained by diagonalization of the Hamiltonian in the oscillator basis and their dependence on the oscillator basis parameter $\hbar\Omega$. We analyze the relation of the suggested approach to other methods available in the literature. The method is illustrated by calculations of two-body scattering with model Woods–Saxon potentials.

Next we use this method to formulate an approach for calculating resonance energies and widths which can be applied to the analysis of results for energies above open thresholds obtained in any variational calculation with the oscillator basis, in the nuclear shell model in particular. We illustrate the accuracy of analysis of resonant parameters in calculations with model Woods–Saxon potentials and apply the suggested approach to calculation of resonances in $n\alpha$ scattering in NCSM with the JISP16 NN interaction.

The work was supported in part by the Ministry of Education and Science of Russian Federation through contract No 14.V37.21.1297 and by the US Department of Energy under Grant Nos. DE-FG02-87ER40371 and DESC0008485 (SciDAC-3/NUCLEI). This work was also supported in part by the National Science Foundation under Grant No PHY-0904782. A portion of the computational resources were pro-

vided by the National Energy Research Scientific Computing Center (NERSC), which is supported by the DOE Office of Science. AMS is also supported by the American Physical Society through the International Travel Grant Award Program.

References

- [1] P. Maris, J. P. Vary and A. M. Shirokov, Phys. Rev. C **79**, 014308 (2009).
- [2] S. A. Coon, M. I. Avetian, M. K. G. Kruse, U. van Kolek, P. Maris and J. P. Vary, Phys. Rev. C **86**, 054002 (2012).
- [3] R. J. Furnstahl, G. Hagen, and T. Papenbrock, Phys. Rev. C **86**, 031301(R) (2012).
- [4] S. N. More, A. Ekström, R. J. Furnstahl, G. Hagen and T. Papenbrock, Phys. Rev. C **87**, 044326 (2013).
- [5] A. M. Shirokov, A. I. Mazur, J. P. Vary and E. A. Mazur, Phys. Rev. C **79**, 014610 (2009); A. M. Shirokov, A. I. Mazur, E. A. Mazur and J. P. Vary, Appl. Math. Inf. Sci. **3**, 245 (2009).
- [6] G. Papadimitriou, J. Rotureau, N. Michel, M. Płoszajczak and B. R. Barrett, Phys. Rev. C **88**, 044318 (2013).
- [7] G. Hupin, J. Langhammer, P. Navrátil, S. Quaglioni, A. Calci and R. Roth, arXiv:1308.2700 [nucl-th] (2013); S. Quaglioni, P. Navrátil, G. Hupin, J. Langhammer, C. Romero-Redondo and R. Roth, arXiv:1210.2020 [nucl-th] (2013).
- [8] E. J. Heller and H. A. Yamany, Phys. Rev. A **9**, 1201 (1974); *ibid.* 1209 (1974).
- [9] H. A. Yamany and L. Fishman. J. Math. Phys. **16**, 410 (1975).
- [10] G. F. Filippov and I. P. Okhrimenko, Yad. Fiz. **32**, 932 (1980) [Sov. J. Nucl. Phys. **32**, 480 (1980)]; G. F. Filippov, Yad. Fiz. **33**, 928 (1981) [Sov. J. Nucl. Phys. **33**, 488 (1981)].
- [11] Yu. F. Smirnov and Yu. I. Nechaev, Kinam **4**, 445 (1982); Yu. I. Nechaev and Yu. F. Smirnov, Yad. Fiz. **35**, 1385 (1982) [Sov. J. Nucl. Phys. **35**, 808 (1982)].
- [12] V. A. Knyr, A. I. Mazur and Yu. F. Smirnov, Yad. Fiz. **52**, 754 (1990) [Sov. J. Nucl. Phys. **52**, 483 (1990)]; Yad. Fiz. **54**, 1518 (1991) [Sov. J. Nucl. Phys. **54**, 927 (1991)]; Yad. Fiz. **56**(10), 72 (1993) [Phys. At. Nucl. **56**, 1342 (1993)]; A. I. Mazur and S. A. Zaytsev, Yad. Fiz. **62**, 656 (1999) [Phys. At. Nucl. **62**, 608 (1999)].
- [13] V. I. Kukulin, V. N. Pomerantsev and O. A. Rubtsova, JETP Lett. **90**, 402 (2009); O. A. Rubtsova, V. I. Kukulin, V. N. Pomerantsev and A. Faessler, Phys. Rev. C **81**, 064003 (2010).
- [14] I. M. Lifshitz, Zh. Eksp. Teor. Fiz. **17**, 1017 (1947) (*in Russian*); *ibid.* **17**, 1076 (1947) (*in Russian*); Usp. Mat. Nauk **7**, 171 (1952) (*in Russian*).
- [15] J. M. Bang, A. I. Mazur, A. M. Shirokov, Yu. F. Smirnov and S. A. Zaytsev, Ann. Phys. (NY) **280**, 299 (2000).
- [16] A. M. Shirokov, A. I. Mazur, S. A. Zaytsev, J. P. Vary and T. A. Weber, Phys. Rev. C **70**, 044005 (2004).
- [17] J. Revai, M. Sotona and J. Žofka, J. Phys. G **11**, 745 (1985).

- [18] A. M. Shirokov, Yu. F. Smirnov and S. A. Zaytsev, in *Modern problems in quantum theory*, edited by V. I. Savrin and O. A. Khrustalev. Moscow, 1998, p. 184; Teoret. Mat. Fiz. **117**, 227 (1998) [Theor. Math. Phys. **117**, 1291 (1998)].
- [19] M. Abramowitz and I. A. Stegun (eds.), *Handbook on mathematical functions*. Dover, New York, 1972; NIST Digital Library of Mathematical Functions, <http://dlmf.nist.gov/>.
- [20] A. M. Lane and R. G. Thomas, Rev. Mod. Phys. **30**, 257 (1958).
- [21] P. Navrátil, J. P. Vary and B. R. Barrett, Phys. Rev. Lett. **84**, 5728 (2000); Phys. Rev. C **62**, 054311 (2000).
- [22] A. Csóto and G. M. Hale, Phys. Rev. C **55**, 536 (1997).
- [23] A. M. Shirokov, J. P. Vary, A. I. Mazur and T. A. Weber, Phys. Lett. B **644**, 33 (2007).
- [24] A. M. Shirokov, A. I. Mazur, S. A. Zaytsev, J. P. Vary and T. A. Weber, Phys. Rev. C **70**, 044005 (2004).
- [25] A. M. Shirokov, J. P. Vary, A. I. Mazur, S. A. Zaytsev and T. A. Weber, Phys. Lett. B **621**, 96 (2005); J. Phys. G **31**, S1283 (2005).
- [26] J. E. Bond and F. W. K. Firk, Nucl. Phys. A **287**, 317 (1977).

Witten Parameter and High Performance Calculations on the Lattice

V. A. Goy and A. V. Molochkov

Far Eastern Federal University, 8 Sukhanova st., Vladivostok 690950, Russia

Abstract

The purpose of this article is to study a surface operator in an $SU(2)$ non-Abelian gauge field theory. We analyse an Abelian projection of the $SU(2)$ symmetry on the $U(1)$ group by calculating the Witten parameter by the lattice method. We use multilevel and multi-hit algorithms for the sake of statistical confidence. We demonstrate that the Witten parameter depends on surface area and volume in both phases. Therefore the Witten parameter cannot be considered as an order parameter of confinement-deconfinement phase transition.

Keywords: *Surface operator; $SU(2)$ gluodynamics; phase transition; lattice; multilevel scheme.*

1 Introduction

A vacuum of quantum chromodynamics (QCD) has two phases: a confinement phase where quarks are bound, and a deconfinement phase where quarks are free. Free quarks cannot be observed nowadays. It is possible to see quarks only in bound states such as baryons and mesons.

In electrodynamics, we can take two charged particles and spread them to infinity. However, it is not possible in the QCD confinement phase because quarks are bound by strings. The energy of string tension increases linearly with the distance between the quarks. It is worth mentioning that so far nobody has managed to derive analytically the linear potential between quarks based on the gluodynamics Lagrangian, however the linear potential growth has been clearly demonstrated by supercomputer lattice simulations. This linear growth of the potential can be observed in the asymptotic behavior of large Wilson loop expectation values. The confinement phase is defined through its dependence on the surface area. On the contrary, the deconfinement phase is marked by a dependence on the perimeter. This means that the surface coefficient is the order parameter of phase transition. The Wilson loop is a line operator. It is interesting to learn whether a surface operator can act as an order parameter which can be used to study the structure of vacuum state.

The QCD confinement is a fundamental property of hadron matter which is responsible for explanation of the spectrum of hadrons. One of possible explanations of this property is a condensation of magnetic monopoles in vacuum [1] as a dual superconductor mode. The BCS theory explains superconductivity as a result of condensation of electric chargers as Cooper pairs. In this case, magnetic field lines concentrate in a some analogue of a string between monopoles. In a dual superconductor, an analogous effect occurs through the condensation of magnetic charges (also called magnetic monopoles), and the string connects electrically charged particles. According to 't Hooft [2], the monopoles can appear as a result of partial breaking of the gauge symmetry. In this work, we break the $SU(2)$ symmetry preserving the $U(1)$ group symmetry.

A surface operator [3] is sensitive to the existence of monopoles. This property was first pointed out by Witten [4, 5]. It is manifested as a divergence of the chromomagnetic field flow through a closed surface. We use lattice calculations to study the structure of vacuum in the $SU(2)$ gluodynamics.

In non-Abelian pure gauge theories, the expectation values of large surface operators are difficult to compute via numerical simulation because an increase of surface area results in a very fast decay of the signal-to-noise ratio. We adapt a multilevel scheme [6] introduced for line operators to work with surface operators when the area exceeds 1 fm^2 .

2 Witten parameter

The vector flux of magnetic field through a closed surface in a trivial vacuum, e. g., in electrodynamics, is identical to zero:

$$\oint \mathbf{H} \cdot d\mathbf{S} \equiv 0. \quad (1)$$

In our lattice calculation we use a phase factor $e^{i\varphi}$, therefore the identity (1) acquires the following form:

$$e^{i\kappa \oint \mathbf{H} \cdot d\mathbf{S}} \equiv 1, \quad (2)$$

where κ is a dimensional coefficient. In Abelian theories, this identity works in a simply connected space. If the space topology is non-trivial or the group symmetry is non-Abelian, the identity (2) does not necessarily works. Hence, in lattice quantum chromodynamics we have:

$$e^{i\kappa \sum_k \mathbf{H}_k \cdot \Delta\mathbf{S}_k} \neq 1, \quad (3)$$

where \mathbf{H}_k is the magnetic field vector on the lattice plaquette with index k , $\Delta\mathbf{S}_k$ is a surface area of the plaquette (with the normal vector in the center of the plaquette), and the integral is calculated over a closed surface made up of lattice plaquettes.

Thus we consider the following value as the Witten parameter:

$$W_p(S) = \text{Re} \prod_S e^{i\theta_p}, \quad (4)$$

where θ_p is a plaquette angle. Essentially, the plaquette angle is a quantitative measure of the gauge field impact on an external source moving along the contour of a plaquette. This angle relates to the magnetic field flux through the plaquette surface:

$$\kappa \int_S \mathbf{H} \cdot d\mathbf{S} = \kappa \oint_C \mathbf{A} \cdot d\mathbf{l} = \theta_p, \quad (5)$$

where integration over $d\mathbf{l}$ is carried out on a path surrounding the surface S .

Let us rewrite the magnetic field flux as

$$\int_S \mathbf{H} \cdot d\mathbf{S} = \int_S F_{ik} d\sigma_{ik}, \quad (6)$$

where F_{ik} is the gauge field tensor, $d\sigma_{ik}$ is a surface element (we do not distinguish upper and lower indices because all calculations are performed in the Euclidean space-time after Wick rotation), and $i, k = 1, 2, 3$ are space directions. In this work we consider a pure gauge field theory with $SU(2)$ group symmetry. Thus θ_p is related with $F_{\mu\nu}$ due to the following formula:

$$F_p = \hat{1} \cos \theta_p + i n_i \sigma_i \sin \theta_p, \quad (7)$$

where n_i is a vector on the unit sphere, σ_i is the Pauli matrix, F_p is a value of the gauge field tensor $F_{\mu\nu}$ on the plaquette. Therefore we can define θ_p as

$$\theta_p = \arccos \left(\frac{1}{2} \text{Tr} F_p \right). \quad (8)$$

All phases are calculated on the surface of a cube in four-dimensional space-time. The range of function $\arccos(x)$ is $[0, \pi]$. The range of angle in the gauge group $U(1)$ is $[0, 2\pi]$. Hence the phase on one side of the cube is defined as $+\arccos\left(\frac{1}{2}\text{Tr} F_p\right)$ while on the opposite side it is $-\arccos\left(\frac{1}{2}\text{Tr} F_p\right)$.

The Witten parameter is related not only to the chromomagnetic field but also to an average plaquette correlation function which is defined as

$$C(l) = \left\langle \left(1 - \frac{1}{2}\text{Tr} F_p(x)\right) \left(1 - \frac{1}{2}\text{Tr} F_p(x+l)\right) \right\rangle_x, \quad (9)$$

where $F_p = U_{ij}U_{jk}U_{kl}U_{li}$ and $U_{ij}, U_{jk}, U_{kl}, U_{li}$ are link variables on the plaquette. The correlation between plaquettes located on the opposite planes of the cube decreases when the surface increases. The phase θ_p has the same correlation function which in turn affects the Witten parameter.

3 Witten parameter on lattice

The partition function can be expressed as

$$Z = \int (dU) e^{-S(U)}. \quad (10)$$

We use Wilson formalism of lattice theory [7]. The action in the $SU(2)$ theory can be written as $S(U) = \beta \sum_p \left(1 - \frac{1}{2}\text{Re Tr} F_p\right)$, where $\beta = 4/g_o^2$ and g_o is the gauge coupling constant. We can calculate an observed value of a physical quantity A as

$$\langle A \rangle = Z^{-1} \int (dU) A(U) e^{-S(U)}, \quad (11)$$

where $A(U)$ is a physical quantity calculated on lattice configuration U and the integration is over all configurations with the weight $e^{-S(U)}$.

Within this approach, we need to generate a set of lattice configurations with weights $e^{-S(U)}$. This problem is solved with the use of Monte Carlo algorithm [8]. Next we calculate physical observables on these configurations and average them. To generate configurations, we use the cold start, cyclic boundary conditions and other parameters shown in Table 1. We use the 99% confidence interval in error calculations, therefore errors for 50 configurations are calculated as 2.8σ where σ is a typical dispersion.

We prepare a set of configurations in both phases to study the Witten parameter. We calculate a Polyakov loop to verify the phase state on configurations. This loop is defined as

$$L(T) = \frac{1}{2}\text{Tr} \exp\left(\imath g_o \int_0^{1/T} A_o dt\right), \quad (12)$$

where t is a cyclic variable with period $1/T$, T is a temperature on the lattice. The Polyakov loop is an order parameter of confinement-deconfinement phase transition.

Table 1: Monte Carlo parameters.

Thermalization iterations	2000
Correlation iterations	200
Configurations	50

Table 2: Lattices used to study the volume dependence.

Phase	Lattice size	β	$L(T)$
Deconfinement	$4 \cdot 30^3$	2.55	0.349 ± 0.002
Confinement	41^4	2.55	0.0002 ± 0.0006

It is equal to zero in the confinement phase and differs from zero in the deconfinement phase. The parameters of lattices used in calculations are shown in Table 2. The Polyakov loop on the lattice is a Wilson line composed of lattice links in the direction of time completed by periodic boundary conditions. The Polyakov loop on the lattice is

$$L(\mathbf{x}) = \frac{1}{2} Tr \prod_{t=0}^{N_t-1} U_0(t, \mathbf{x}), \quad (13)$$

where $U_0(t, \mathbf{x})$ is the time direction link.

Within our lattice approach, we select a cube in the 3D subspace (the lattice is defined in the four-dimensional space-time). The phase is calculated on each plaquette on the surface of the cube, the result is obtained by summation of these phases. Next we calculate the Witten parameter at different points in the lattice configuration and average them. The final result is obtained by averaging over the set of configurations.

We consider the cubes with edge length ranging from $1a$ to $13a$ (a is a lattice scale) and surface area ranging from 6 to 1014 plaquettes, respectively. We use the multilevel [6] and multi-hit [9] algorithms for the sake of statistical confidence and the MPI parallelization to speed up the calculations.

3.1 Multilevel scheme

We can fractionize the cube surface into 6 planes. Thus we need to calculate the phases on these planes. We use a multilevel scheme which includes the following calculations performed recursively:

1. If the depth of recursion exceeds some parameter $depth_{\max}$ or the current plane contains only one plaquette, the phase is calculated by the multi-hit algorithm (see below).
2. The current plane is divided into two pieces by a line perpendicular to the longer edge of the plane, see Fig. 1.
3. The multilevel algorithm is used recursively for each piece of the plane to calculate the phase on this plane φ_i ($i = 1, \dots, N_\varphi$ where N_φ is a predefined number of phase calculations on the current plane) as a sum of phases on individual pieces of the plane.
4. When all N_φ calculations of the phases φ_i on the plane are completed, we obtain the phase φ as an average of individual calculations φ_i : $\varphi = Arg\left(N_\varphi^{-1} \sum_i \cos \varphi_i + i N_\varphi^{-1} \sum_i \sin \varphi_i\right)$; otherwise we perform a few Monte Carlo runs to generate new links on the current plane and turn back to the point 3.

To test this scheme, we use a set of recursion depths ranging from 1 to 3 to calculate the dependence of the Witten parameter on a surface area on some set of lattice configurations. The multilevel algorithm applied to calculate the surface operators appears to have very good convergence behavior. The results of calculations for recursive depth equal to two and three are close. The recursion depth is equal to three in all calculations presented below.

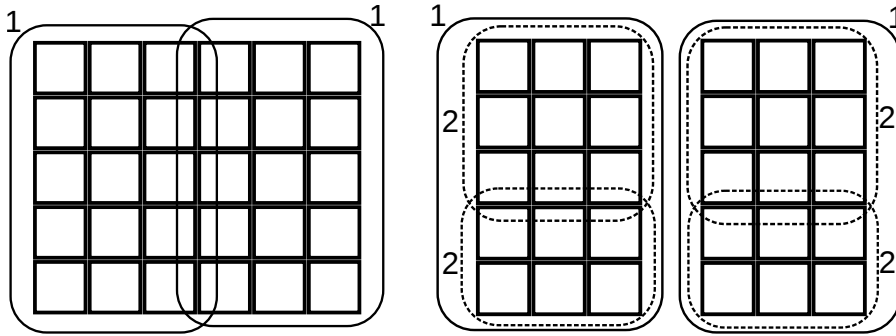


Figure 1: The plane is divided into two pieces at each recursion step. 1 shows surfaces (surrounded by a solid curve) used to calculate phases at the first recursion step, the phases on surfaces 2 are computed at the second recursion step.

3.2 Multi-hit algorithm

The main idea of the multi-hit algorithm is that the phase on the plaquette is defined by boundary conditions. We can substitute the phase calculated on the plaquette by the phase expressed through boundary links. We cannot do it analytically, but we can use the Monte Carlo algorithm to obtain an accurate enough phase value. We perform few Monte Carlo runs on the plaquette to generate boundary links and calculate a set of phases on a single plaquette. The phase is finally obtained by averaging the set of phase factors in the same manner as at the point 4 of the previous subsection.

A combination of these two algorithms makes it possible to improve essentially an accuracy of calculations of the Witten parameter. However, this results in the increase of required computer time. To resolve this problem, we employ an MPI parallelization of calculations.

4 Results

All calculations are performed for 50 lattice configurations at 1000 points on each of them. The results for both phases are shown in Fig. 2. The surface area dependences of the Witten parameter in both phases look the same. To understand better the behavior of the Witten parameter, we fit the obtained dependences as

$$W_p(S, V) = e^{-\sigma S - \gamma V}, \quad (14)$$

where σ is a surface coefficient, γ is a volume coefficient, S is a surface area, and V is the cube volume. The fit is performed by means of the minuit2 library of the ROOT package [10]. We obtain high-quality fits when non-zero values of parameters σ and γ are allowed as is seen in Fig. 2. Therefore the Witten parameter depends on both the cube volume and surface area in each phase.

Regarding the β dependence, the Witten parameter vanishes in the continuum limit corresponding to the $\beta \rightarrow \infty$ limit: as is seen in Fig. 3, the Witten parameter decreases with β . Clearly, the vacuum expectation value is suppressed by the ultra-violet divergence of the self-energy which is proportional to the closed surface area. This means that there is a divergence of the surface coefficient $\sigma = \sigma(a) \xrightarrow{a \rightarrow 0} \infty$, where a is the lattice scale. The scale in the continuum limit tends to zero. This divergence is related to the colored dipole self-energy on the surface. It is analogous

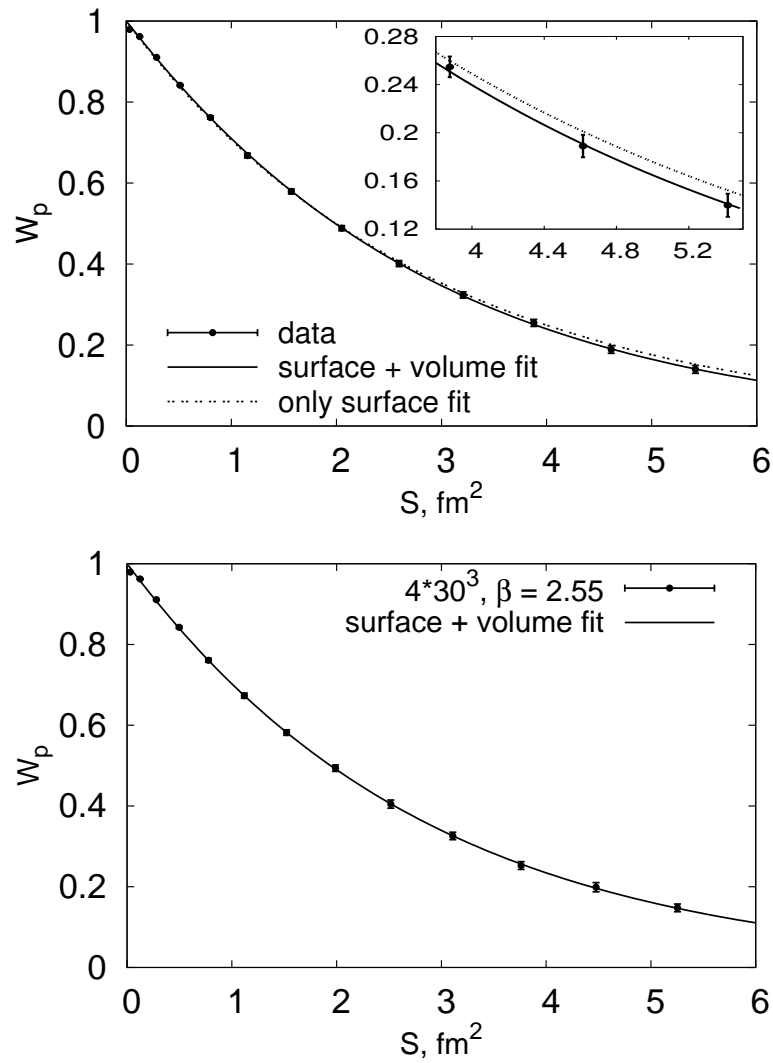


Figure 2: Surface area dependences of the Witten parameter in the confinement (upper panel) and deconfinement (lower panel) phases and comparison of fittings. The confinement phase calculations ('data') were performed with lattice size of 41^4 and $\beta = 2.55$.

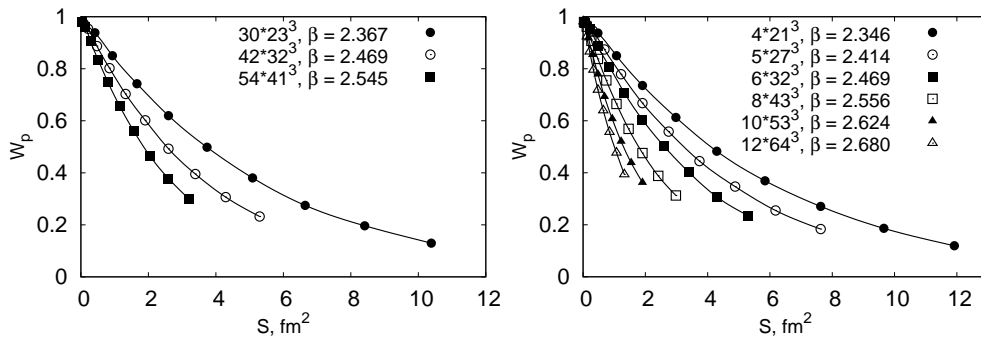


Figure 3: Witten parameter dependences obtained with different β values. Left panel — confinement phase; right panel — deconfinement phase.

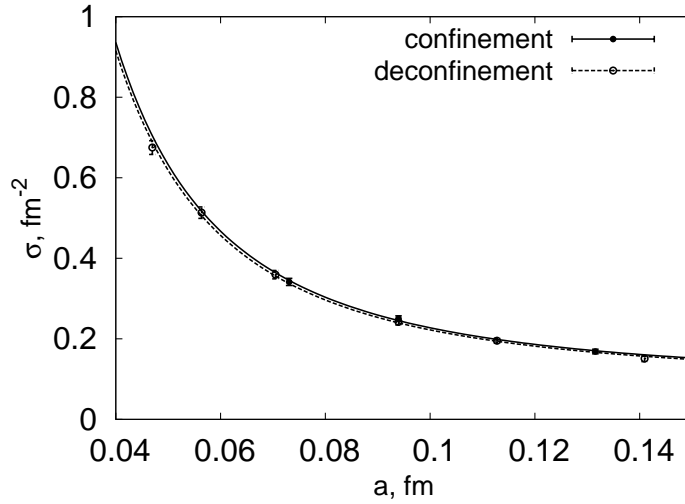


Figure 4: Dependence of σ on lattice spacing a in both phases.

to the divergence of Wilson lines:

$$\left\langle \text{Tr} P \exp \left\{ - \int_C \hat{A}_\mu dx_\mu \right\} \right\rangle \sim \exp \{ - \text{const} g^2 L/a \}, \quad (15)$$

where L is the perimeter of the Wilson line C , a is the lattice spacing, g^2 is a coupling constant, and we keep only the most divergent terms. A description of magnetic degrees of freedom and surface operators may be found in Ref. [11].

Fig. 4 shows the σ dependence on the scale a . σ diverges in the continuum limit while the volume coefficient γ does not depend on lattice scale. Due to Eq. (15), the surface divergence has the following form:

$$\sigma(a) = \sigma_{ph} + \sigma_{div}/a^2, \quad (16)$$

where σ_{ph} is a physical coefficient and σ_{div} is a divergence coefficient. The fit results in $\sigma_{ph} = (0.091 \pm 0.007) \text{ fm}^{-2}$, or $(3.6 \pm 0.3) \cdot 10^3 \text{ MeV}^2$. This approximation is illustrated in Fig. 4.

It is seen that the Witten parameter depends on a surface area and volume in both phases. Consequently, the Witten parameter cannot be considered as an order parameter of the confinement-deconfinement phase transition. This is similar to the behavior of spatial Wilson loops expectation value which is also unrelated to the phase transition. It might be interesting for the study of surface operators to calculate the Witten parameter on the cube with two spatial axis and one temporal axis. In this case the parameter should be sensitive to the phase transition.

Acknowledgments

We are thankful to Dr. M. I. Polikarpov, Dr. P. V. Buividovich, Dr. V. G. Bornyakov, Dr. V. I. Zakharov and Dr. V. V. Braguta for interesting and useful discussions. The authors are obliged to Dr. A. M. Shirokov for useful comments. Many thanks to Miss Nastasiy for the help with English. The work was supported by the Russian Ministry of Science and Education by the federal program “Kadry” through the Contract No 8174. Numerical calculations were performed using the facilities of the Center for Collective Use “Far Eastern Computing Resource” (Vladivostok).

References

- [1] M. N. Chernodub and M. I. Polikarpov, arXiv:hep-th/9710205 (1997).
- [2] G. 't Hooft, Nucl. Phys. B **190**, 455 (1981).
- [3] S. Gukov, “*Phases of gauge theories and surface operators*”, a talk presented at the workshop “Prestrings”, 11-15 August, 2008, Zürich, Switzerland, <http://www.phys.ethz.ch/~mrg/Prestrings/talks/Gukov.pdf>.
- [4] S. Gukov and E. Witten, arXiv:hep-th/0612073v2 (2007).
- [5] S. Gukov and E. Witten, arXiv:0804.1561 [hep-th] (2008).
- [6] M. Lüscher and P. Weisz, JHEP **09(2001)**, 010 (2001); arXiv:hep-lat/0108014 (2001).
- [7] K. Wilson, Phys. Rev. D **10**, 2445 (1974).
- [8] M. Creutz, *Quarks, gluons and lattice*. Cambridge University Press, Cambridge, 1983.
- [9] G. Parisi, R. Petronzio and F. Rapuano, Phys. Lett. B **128**, 418 (1983).
- [10] The ROOT library, <http://root.cern.ch/drupal/>.
- [11] A. Di Giacomo and V. I. Zakharov, Phys. Atom. Nucl. **73**, 711 (2010); arXiv:0806.2938 [hep-th] (2008).

Infrared and Ultraviolet Cutoffs in Variational Calculations with a Harmonic Oscillator Basis

Sidney A. Coon

Department of Physics, University of Arizona, Tucson, Arizona USA

Abstract

I abstract from a recent publication [1] the motivations for, analysis in and conclusions of a study of the ultraviolet and infrared momentum regulators induced by the necessary truncation of the model spaces formed by a variational trial wave function. This trial function is built systematically from a complete set of many-body basis states based upon three-dimensional harmonic oscillator (HO) functions. Each model space is defined by a truncation of the expansion characterized by a counting number (\mathcal{N}) and by the intrinsic scale ($\hbar\omega$) of the HO basis. Extending both the uv cutoff to infinity and the ir cutoff to zero is prescribed for a converged calculation. In [1] we established practical procedures which utilize these regulators to obtain the extrapolated result from sequences of calculations with model spaces. Finally, I update this subject by mentioning recent work on our extrapolation prescriptions which have appeared since the submission of [1]. The numerical example chosen for this contribution consists of calculations of the ground state energy of the triton with the “bare” and “soft” Idaho N³LO nucleon-nucleon (NN) interaction.

Keywords: *No-core shell model; convergence of expansion in harmonic oscillator functions; ultraviolet regulator; infrared regulator*

1 Introduction

The advent of giant nuclear shell-model codes based upon the three-dimensional harmonic oscillator (HO) in the 1970s coincided with the advent of a program to use the HO eigenfunctions as a basis of a finite linear expansion to make a straightforward variational calculation of the properties of light nuclei [2]. At the same time theorems based upon functional analysis established the asymptotic convergence rate of these latter calculations as a function of the counting number (call it \mathcal{N}) which characterizes the size of the expansion basis (or model space) [3, 4]. The convergence rates of these theorems (inverse power laws in \mathcal{N} for “non smooth” potentials with strong short range correlations and exponential in \mathcal{N} for “smooth” potentials such as gaussians) were demonstrated numerically in [3] for the HO expansion and in [5] for the parallel expansion in hyperspherical harmonics. These convergence theorems seem to be known in the hyperspherical harmonic community and are effectively demonstrated in the calculation of the properties of few-nucleon systems “from first principles”; that is, solving the many-body Schrödinger equation with a Hamiltonian containing nucleon-nucleon interactions fitted to scattering data and to properties of the deuteron. The convergence rates of variational calculations using the HO basis have been periodically rediscovered empirically by those who, in the present day, have adapted “giant shell-model codes” or written new codes to perform “*ab initio*” “no-core shell model” (NCSM) calculations of s - and p -shell nuclei. I have never seen a reference to the functional analysis theorems regarding these convergence rates in the NCSM papers. However, the HO expansion basis has an intrinsic scale parameter $\hbar\omega$ which does not naturally fit into an extrapolation scheme based upon \mathcal{N} as discussed by [3, 4, 6]. Indeed the model spaces of these NCSM approaches are characterized

by the ordered pair $(\mathcal{N}, \hbar\omega)$. Here the basis truncation parameter \mathcal{N} and the HO energy parameter $\hbar\omega$ are variational parameters [7, 8, 9]. It is the purpose of this contribution to summarize the properties of another ordered pair which perhaps more physically describes the nature of the model spaces and provides extrapolation tools which use \mathcal{N} and $\hbar\omega$ on an equal footing [1]. This is the pair of ultraviolet (uv) and infrared (ir) cutoffs (each a function of both \mathcal{N} and $\hbar\omega$) induced by the truncation. They were first introduced to the NCSM in [10] in the context of an effective field theory (EFT) approach (for a recent review of this program see [11]). These cutoffs or regulators can usefully be employed in novel extrapolation schemes [1] which are a natural outgrowth of those introduced in the 1970s, rediscovered by the NCSM community, and in current use.

The variational approach alluded to above generates a trial wave function in a completely systematic manner without regard for the details of the Hamiltonian under consideration other than the implementation of exact symmetries. The goal, then, is to define a complete set of states for a few-body system and to construct and diagonalize the Hamiltonian matrix in a truncated basis of these states. The result of the diagonalization is an upper bound to the exact eigenvalue of the complete set. With this method a reliable estimate of the accuracy attained can be made with the variational upper bound [3] provided that the trial function is constructed using the terms of a systematic expansion set and convergence of the diagonalization result (such as a ground-state energy) is observed as the basis is increased. The algebra appropriate to generating and using trial wave functions, based on three dimensional HO eigenfunctions, has been given by Moshinsky [2] and others [12]. The trial functions take the form of a finite linear expansion in a set of known functions

$$\Psi_T = \sum_{\nu} a_{\nu}^{(\mathcal{N})} h_{\nu},$$

where $a_{\nu}^{(\mathcal{N})}$ are the parameters to be varied and h_{ν} are many-body states based on a summation over products of HO functions. The advantage of a HO basis is that it is relatively straightforward to construct a complete set of few-body functions of appropriate angular momentum and symmetry; examples are given in [12, 13]. The trial function must have a definite symmetry reflecting the composition of the bound state: fermions or bosons. This trial function Ψ_T must be quadratically integrable and the expectation value of the Hamiltonian must be finite. The expansion coefficients (known as generalized Fourier coefficients in the mathematical literature) depend on the upper limit (such as an \mathcal{N} defined in terms of total oscillator quanta) and are obtained by minimizing the expectation value of the Hamiltonian in this basis. Treating the coefficients $a_{\nu}^{(\mathcal{N})}$ as variational parameters in the Rayleigh quotient [14], one performs the variation by diagonalizing the many-body Hamiltonian in this basis. This is an eigenvalue problem so the minimum with respect to the vector of expansion coefficients always exists and one obtains a bound on the lowest eigenvalue (and indeed on the higher eigenvalues representing the excited states [15]). The basis functions can also depend upon a parameter (such as the harmonic oscillator energy $\hbar\omega$ which sets a scale) that then becomes a non-linear variational parameter additional to the linear expansion coefficients.

One can view a shell-model calculation as a variational calculation, and thus expanding the configuration space merely serves to improve the trial wave function [16]. The traditional shell-model calculation involves trial variational wave functions which are linear combinations of Slater determinants. Each Slater determinant corresponds to a configuration of A fermions distributed over A single-particle states. If we take any complete set of orthonormal single-particle wave functions and consider all possible A -particle Slater determinants that can be formed from them, then these wave functions form a complete orthonormal set of wave functions spanning the A -particle Hilbert space. The Slater determinant basis of HO single-particle wave function is

often defined in the “ m -scheme”. That is, the single-particle states are labelled by the quantum numbers n , l , j , and m_j , where n and l are the radial and orbital HO quantum numbers, j is the total single-particle spin, and m_j its projection along the z -axis. The many-body basis states have well-defined total spin projection, which is simply the sum of m_j of the single-particle states $M_j = \sum m_j$, hence the name “ m -scheme”. The many-body basis states are limited only by the imposed symmetries — parity, charge and total angular momentum projection (M), as well as by \mathcal{N} . However, in general the many-body basis states do not have a well defined total J . This scheme is simple to implement and in two calculations (for positive and negative parity) one gets the complete low-lying spectrum, including the ground state, even though the spins of the low-lying states are not specified in the trial wave function. The truncation by \mathcal{N} results in finite matrices to be diagonalized, but they are much larger than the matrices of the Moshinsky program which expects the properties of the trial wave function (JT basis in shell model language) to be known. However, because these shell model wave functions do span the space, an expansion in such “ m -scheme” Slater determinants is, in principle, also capable of giving an exact representation of the eigenfunctions of the Hamiltonian.

These early *ab initio* calculations, both of the “no-core” shell model in which all nucleons are active [16] and of the Moshinsky program [17, 18] attempted to overcome the challenges posed by “non-smooth” two-body potentials by including Jastrow type two-body correlations in the trial wave function. Nowadays, the NN potentials are tamed by unitary transformations within the model space [19] or in free space by the similarity renormalization group evolution [20]. In both cases, this procedure generates effective many-body interactions in the new Hamiltonian. Neglecting these destroys the variational aspect of the calculation (and the physics contained in the calculation, of course). We retain the variational nature of our NCSM investigation by choosing a realistic smooth nucleon-nucleon interaction Idaho N³LO [21] which has been used previously without renormalization for light nuclei ($A \leq 6$) [7]. This potential is inspired by chiral perturbation theory and fits the two body data quite well. It is composed of contact terms and irreducible pion-exchange expressions multiplied by a regulator function designed to smoothly cut off high-momentum components in accordance with the low-momentum expansion idea of chiral perturbation theory. The version we use has the high-momentum cutoff of the regulator set at 500 MeV/ c . The Idaho N³LO potential is a rather soft one, with heavily reduced high-momentum components as compared to earlier realistic NN potentials with a strongly repulsive core. Alternatively, in coordinate space, the Yukawa singularity at the origin is regulated away so that this potential would be considered “smooth” by Delves and Schneider and the convergence in \mathcal{N} would be expected to be exponential [3, 4]. Even without the construction of an effective interaction, convergence with the Idaho N³LO NN potential is exponential in \mathcal{N} , as numerous studies have shown [7, 20].

With the HO basis in the nuclear structure problem, convergence has been discussed, in practice, with an emphasis on obtaining those parameters which appear linearly in the trial function (i. e. convergence with \mathcal{N}). Sometimes for each \mathcal{N} the non-linear parameter $\hbar\omega$ is varied to obtain the minimal energy [7, 22] for a fixed \mathcal{N} and then the convergence with \mathcal{N} is examined. Sometimes $\hbar\omega$ is simply fixed at a value which gives the fastest convergence in \mathcal{N} [13]. Other extrapolation schemes have been proposed and used [8]. In all of these schemes, in my opinion, the extrapolation to an infinite basis is effected with the main role played by \mathcal{N} and a secondary role played by $\hbar\omega$. The scheme proposed in [1] gives \mathcal{N} and $\hbar\omega$ equal roles by employing uv and ir cutoffs which which must be taken to infinity and to zero, respectively to achieve a converged result (see Fig. 1).

In section 2 we briefly describe expansion schemes in HO functions. None of the discussion in section 2 is new, but it paves the way for section 3 in which we suggest a convergence analysis based upon the uv and ir cutoffs induced by the truncation

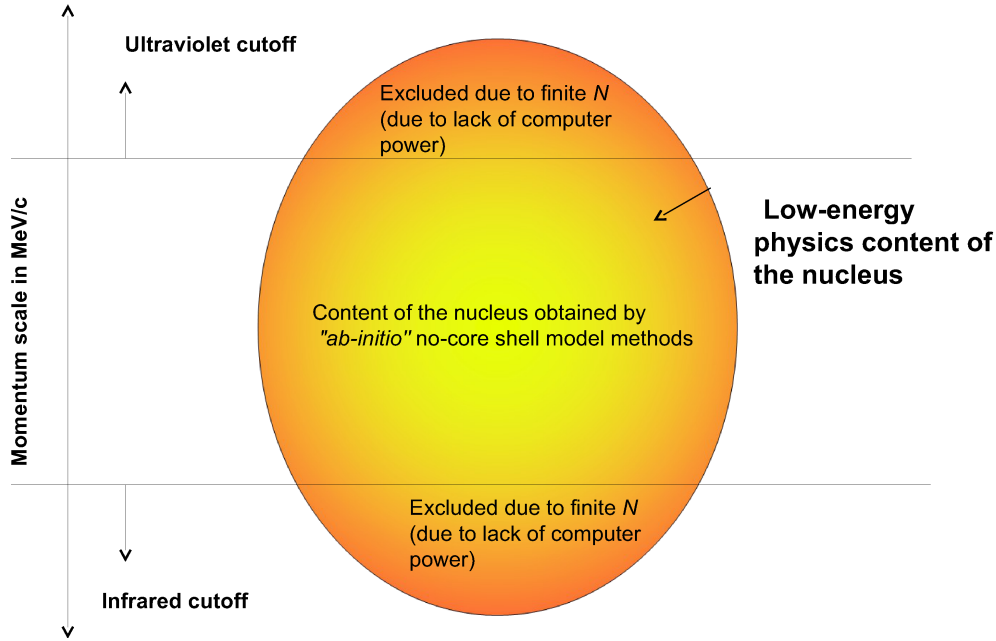


Figure 1: (Color online) Schematic view of a finite model space (limited by the basis truncation parameter N as described in the text), in which the uv and ir momentum cutoffs are arbitrary. To reach the full many-body Hilbert space, symbolized by the complete oval, one needs to let the uv cutoff $\rightarrow \infty$ and the ir cutoff $\rightarrow 0$.

of the model space. Section 4 is devoted to a sampling of tests and examples of this new convergence scheme; for a more extensive discussion with more examples please see Ref. [1].

2 Expansion in a finite basis of harmonic oscillator functions

We briefly indicate the workings of the finite HO basis calculations performed and refer the reader to a comprehensive review article [9] on the no-core shell model (NCSM) for further details and references to the literature. A HO basis allows preservation of translational invariance of the nuclear self-bound system. Translational invariance is automatic if the radial HO wave function depends on relative, or Jacobi, coordinates as was done in Refs. [13, 17, 18, 22]. Antisymmetrization (or symmetrization for the α particle models of [17, 18]) of the basis is necessary and described in Refs. [9] and [23]. Antisymmetrization in a Jacobi basis becomes analytically and computationally forbidding as the number of nucleons increases beyond four or five. For this reason these calculations are alternatively made with antisymmetrized wave functions constructed as Slater determinants of single-nucleon wave functions depending on single-nucleon coordinates. This choice loses translational invariance since, in effect, one has defined a point in space from which all single-particle coordinates are defined. Translational invariance is restored by choosing a particular truncation of the basis: a maximum of the sum of all HO excitations, i. e. $\sum_{i=1}^A (2n_i + l_i) \leq N_{totmax}$, where n_i, l_i are the HO quantum numbers corresponding to the harmonic oscillators associated with the single-nucleon coordinates and N_{totmax} is an example of the generic \mathcal{N} of the Introduction. The gain of this choice is that one can use technology developed and/or adapted for NCSM, such as the shell model code ANTOINE [24], the parallel-

processor codes “Many-Fermion Dynamics — nuclear” (MFDn) [25] and the No-Core Shell Model Slater Determinant Code [26]. These codes set up the many-body basis space, evaluate the many-body Hamiltonian matrix, obtain the low-lying eigenvalues and eigenvectors using the Lanczos algorithm, and evaluate a suite of expectation values using the eigenvectors.

The eigenstates factorize as products of a wave function depending on relative coordinates and a wave function depending on the c. m. coordinates. The precise method of achieving the factorization of the c. m. and intrinsic components of the many-body wave function follows a standard approach, sometimes referred to as the “Lawson method” [27]. In this method, one selects the many-body basis space in the manner described above with $\mathcal{N} = N_{totmax}$ and adds a Lagrange multiplier term to the many-body Hamiltonian $\beta(H_{c.m.} - \frac{3}{2}\hbar\omega)$ where $H_{c.m.}$ is the HO Hamiltonian for the c. m. motion. With β chosen positive (10 is a typical value), one separates the states of lowest c.m. motion ($0S_{\frac{1}{2}}$) from the states with excited c. m. motion by a scale of order $\beta\hbar\omega$. The resulting low-lying states have wave functions that then have the desired factorized form. We checked, for the two cases $A = 3$ and $A = 4$, that the codes *manyeff* [23] which use Jacobi coordinates and No-Core Shell Model Slater Determinant Code [26] based upon single-nucleon coordinates gave the same eigenvalues for the same values of $\mathcal{N} = N_{totmax}$ and $\hbar\omega$, indicating that the Lawson method is satisfactory for the calculations in single-particle coordinates.

Now we return to the truncation parameter \mathcal{N} of the HO basis expansion of the many-body system. Usually, instead of truncating the sum of all HO excitations $\mathcal{N} = N_{totmax}$, one uses the more familiar truncation parameter N_{max} . N_{max} is the maximum number of oscillator quanta shared by all nucleons above the lowest HO configuration for the chosen nucleus. One unit of oscillator quanta is one unit of the quantity $(2n + l)$ where n is the principle quantum number and l is the angular quantum number. For $A = 3, 4$ systems $N_{max} = N_{totmax}$. For the p -shell nuclei they differ, e. g. for ${}^6\text{Li}$, $N_{max} = N_{totmax} - 2$, and for ${}^{12}\text{C}$, $N_{max} = N_{totmax} - 8$. Later on we will want a truncation parameter which refers, not to the many-body system, but to the properties of the HO single-particle states. If the highest HO single-particle state of this lowest HO configuration has N_0 HO quanta, then $N_{max} + N_0 = \mathcal{N}$ identifies the highest HO single-particle states that can be occupied within this many-body basis. Since N_{max} is the maximum of the *total* HO quanta above the minimal HO configuration, we can have at most one nucleon in such a highest HO single-particle state with \mathcal{N} quanta. Note that N_{max} characterizes the many-body basis space, whereas \mathcal{N} is a label of the corresponding single particle space. Let us illustrate this distinction with two examples. ${}^6\text{He}$ is an open shell nucleus with $N_0 = 1$ since the valence neutron occupies the $0p$ shell in the lowest many-body configuration. Thus if $N_{max} = 4$ the single particle truncation \mathcal{N} is 5. On the other hand, the highest occupied orbital of the closed shell nucleus ${}^4\text{He}$ has $N_0 = 0$ so that $\mathcal{N} = N_{max}$.

3 Ultraviolet and infrared cutoffs induced by basis truncation

We begin by thinking of the finite single-particle basis space defined by \mathcal{N} and $\hbar\omega$ as a model space characterized by two momenta associated with the basis functions themselves. In the HO basis, we follow [10] and define $\Lambda = \sqrt{m_N(N + 3/2)\hbar\omega}$ as the momentum (in units of MeV/c) associated with the energy of the highest HO level. The nucleon mass is $m_N = 938.92$ MeV. To arrive at this definition one applies the virial theorem to this highest HO level to establish kinetic energy as one half the total energy (i. e., $(N + 3/2)\hbar\omega$) and solves the non-relativistic dispersion relation for Λ . This sets one of the two cutoffs for the model space of a calculation. Energy, momentum and length scales are related, according to Heisenberg’s uncertainty

principle. The higher the energy or momentum scale we may reach, the lower the length scale we may probe. Thus, the usual definition of an ultraviolet cutoff Λ in the continuum has been extended to discrete HO states. It is then quite natural to interpret the behavior of the variational energy of the system with addition of more basis states as the behavior of this observable with the variation of the ultraviolet cutoff Λ . Above a certain value of Λ one expects this running of the observable with Λ to “start to behave” so that this behavior can be used to extrapolate to the exact answer. However, the truncation of the model space by \mathcal{N} implies a second cutoff, absent in free space; an infrared cutoff. Because the energy levels of a particle in a HO potential are quantized in units of $\hbar\omega$, the minimum allowed momentum difference between single-particle orbitals is $\lambda = \sqrt{m_N\hbar\omega}$ and that has been taken to be an infrared cutoff [10]. That is, there is a low-momentum cutoff $\lambda = \hbar/b$ corresponding to the minimal accessible non-zero momentum (here $b = \sqrt{\frac{\hbar}{m_N\omega}}$ plays the role of a characteristic length of the HO potential and basis functions). Note however that there is *no* external confining HO potential in place. Instead the only $\hbar\omega$ dependence is due to the scale parameter of the underlying HO basis. In [10] the influence of the infrared cutoff is removed by extrapolating to the continuum limit, where $\hbar\omega \rightarrow 0$ with $N \rightarrow \infty$ so that Λ is fixed. Clearly, one cannot achieve both the ultraviolet limit and the infrared limit by taking $\hbar\omega$ to zero in a fixed- N model space as this procedure takes the ultraviolet cutoff to zero.

The calculated energies of a many-body system in the truncated model space will differ from those calculated as the basis size increases without limit ($N \rightarrow \infty$). This is because the system is in effect confined within a finite (coordinate space) volume characterized by the finite value of b intrinsic to the HO basis. The “walls” of the volume confining the interacting system spread apart and the volume increases to the infinite limit as $\lambda \rightarrow 0$ and $b \rightarrow \infty$ with Λ held fixed. Thus it is as necessary to extrapolate the low momentum results obtained with a truncated basis with a given b or $\hbar\omega$ as it is to ensure that the ultraviolet cutoff is high enough for a converged result. These energy level shifts in a large enclosure have long been studied [28]; most recently with the explicit EFT calculation of a triton in a cubic box allowing the edge lengths to become large (and the associated ir cutoff due to momentum quantization in the box going towards zero) [29]. There it was shown that as long as the infrared cutoff was small compared to the ultraviolet momentum cutoff appearing in the “pionless” EFT, the ultraviolet behavior of the triton amplitudes was unaffected by the finite volume. More importantly, from our point of view of desiring extrapolation guidance, this result means that calculations in a finite volume can confidently be applied to the infinite volume (or complete model space) limit. Similar conclusions can be drawn from the ongoing studies of systems of two and three nucleons trapped in a HO potential with interactions from pionless EFT combined with this definition of the infrared cutoff ($\lambda = \sqrt{m_N\hbar\omega}$); see the review [11].

Other studies define the ir cutoff as the infrared momentum which corresponds to the maximal radial extent needed to encompass the many-body system we are attempting to describe by the finite basis space (or model space). These studies find it natural to define the ir cutoff by $\lambda_{sc} = \sqrt{(m_N\hbar\omega)/(N + 3/2)}$ [20, 30]. Note that λ_{sc} is the inverse of the root-mean-square (rms) radius of the highest single-particle state in the basis; $\langle r^2 \rangle^{1/2} = b\sqrt{N + 3/2}$. We distinguish the two definitions by denoting the first (historically) definition by λ and the second definition by λ_{sc} because of its scaling properties demonstrated in the next Section.

The extension in [10] of the continuum ultraviolet cutoff to the discrete (and truncated) HO basis with the definition $\Lambda = \sqrt{m_N(N + 3/2)\hbar\omega}$ seems unexceptional. But, as always when one confidently makes such a statement, there are exceptions. For example, an effective momentum for a HO state can be defined by the asymptotic relation for large n between the radial part $R_{nl}(r)/r$ of the harmonic oscillator functions and the spherical Bessel functions $j_l(kr)$ of radial part of the 3D plane wave [31].

Kallio showed that this relation is very accurate at small r for all n values [32]. The alternate definition, suggested by Vary [33], identifies a uv regulator with the “Kallio momentum” defined by this relation so that $\Lambda_{alternate} = \sqrt{2}\Lambda$. This is a scale change only as is the definition by fiat in [34] which arrives at the same $\sqrt{2}$ factor for their Λ . The more important distinction is the alternate definitions of the ir cutoff which have different functional forms. It is clear that increasing Λ by increasing $\hbar\omega$ in a fixed- N model space is not sufficient; doing so increases both of the putative infrared cutoffs as well because $\Lambda = \lambda\sqrt{N + 3/2} = \lambda_{sc}(N + 3/2)$ and one continues to effectively calculate in an effective confining volume which is getting smaller rather than larger. This confining volume is certainly removed by letting $N \rightarrow \infty$, at fixed $\hbar\omega$, because HO functions form a basis of the complete space. In addition, taking $N \rightarrow \infty$ simultaneously removes the uv cutoff defined by Λ and the ir cutoff defined either by λ or λ_{sc} . But increasing N without limit is computationally prohibitive. Thus there is a practical issue to address: whether one must take the ir cutoff to zero by taking $\hbar\omega \rightarrow 0$ at fixed Λ ($\lambda_{ir} \equiv \lambda$ definition) or whether it is sufficient to allow $\hbar\omega$ be some larger value, perhaps near that used in traditional shell-model calculations, and let an increasing N take λ_{ir} to small values, as it does with the definition $\lambda_{ir} \equiv \lambda_{sc}$.

4 A study of uv and ir cutoffs in the triton

We display in a series of figures the running of the ground-state eigenvalue of a single nucleus, ${}^3\text{H}$, on the truncated HO basis by holding one cutoff of (Λ, λ_{ir}) fixed and letting the other vary. These ${}^3\text{H}$ calculations were made for $N \leq 36$ and values of $\hbar\omega$ as appropriate for the chosen cutoff value. For $N \geq 16$, we used the code *manyeff* [23] which uses Jacobi coordinates and the No-Core Shell Model Slater Determinant Code [26] which use single-particle coordinates for smaller N . We checked that the codes gave the same eigenvalues for overlapping values of N , indicating that the Lawson method satisfactorily restores translational invariance to ground-state energy calculations in single-particle coordinates.

In Fig. 2 and the following figures, $|\Delta E/E|$ is defined as $|(E(\Lambda, \lambda_{ir}) - E)/E|$ where E reflects a consensus ground-state energy from benchmark calculations with this NN potential, this nucleus, and different few-body methods. The accepted value for the ground state of ${}^3\text{H}$ with this potential is -7.855 MeV from a 34 channel Faddeev calculation [21], -7.854 MeV from a hyperspherical harmonics expansion [35], and $-7.85(1)$ from a NCSM calculation [7].

For the choice of Fig. 2, $\lambda_{ir} \equiv \lambda = \sqrt{m_N \hbar\omega}$, $|\Delta E/E|$ decreases exponentially at fixed λ , as Λ increases for the values of Λ achieved in this study. Fixed $\hbar\omega$ implies N alone increases to drive $\Lambda \rightarrow \infty$, $\lambda_{sc} \rightarrow 0$ simultaneously. The linear fit on a semi-log plot is extracted from the data. For fixed Λ , a smaller λ implies a smaller $|\Delta E/E|$ since more of the infrared region is included in the calculation.

In Fig. 3 we hold fixed the uv cutoff of (Λ, λ_{ir}) to display the running of $|\Delta E/E|$ upon the suggested ir cutoff λ . For fixed λ , a larger Λ implies a smaller $|\Delta E/E|$ since more of the uv region is included in the calculation. But we immediately see a qualitative change in the curves between the transition $\Lambda = 700$ MeV and $\Lambda = 800$ MeV; for smaller Λ , $|\Delta E/E|$ does not go to zero as the ir cutoff is lowered and more of the infrared region is included in the calculation. This behavior suggests that $|\Delta E/E|$ does not go to zero unless $\Lambda \geq \Lambda^{NN}$, where Λ^{NN} is some uv regulator scale of the NN interaction itself. From this figure one estimates $\Lambda^{NN} \sim 800$ MeV/ c for the Idaho $N^3\text{LO}$ interaction.

Yet the description of this interaction in the literature says that the version we use has the high-momentum cutoff of the regulator set at $\Lambda_{N^3\text{LO}} = 500$ MeV/ c [21]. This does not mean that the interaction has a sharp cutoff at exactly 500 MeV/ c , since the terms in the Idaho $N^3\text{LO}$ interaction are actually regulated by an exponentially

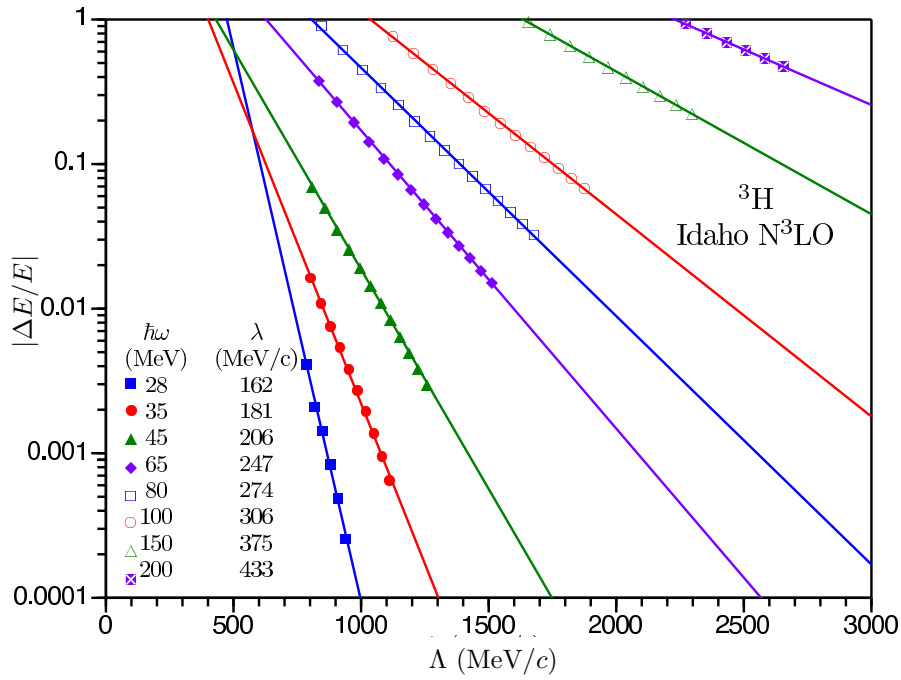


Figure 2: Dependence of the ground-state energy of ${}^3\text{H}$ (compared to a converged value; see text) upon the uv momentum cutoff $\Lambda = \sqrt{m_N(N+3/2)\hbar\omega}$ for different fixed $\lambda = \sqrt{m_N\hbar\omega}$. The curves are a fit to the calculated points.

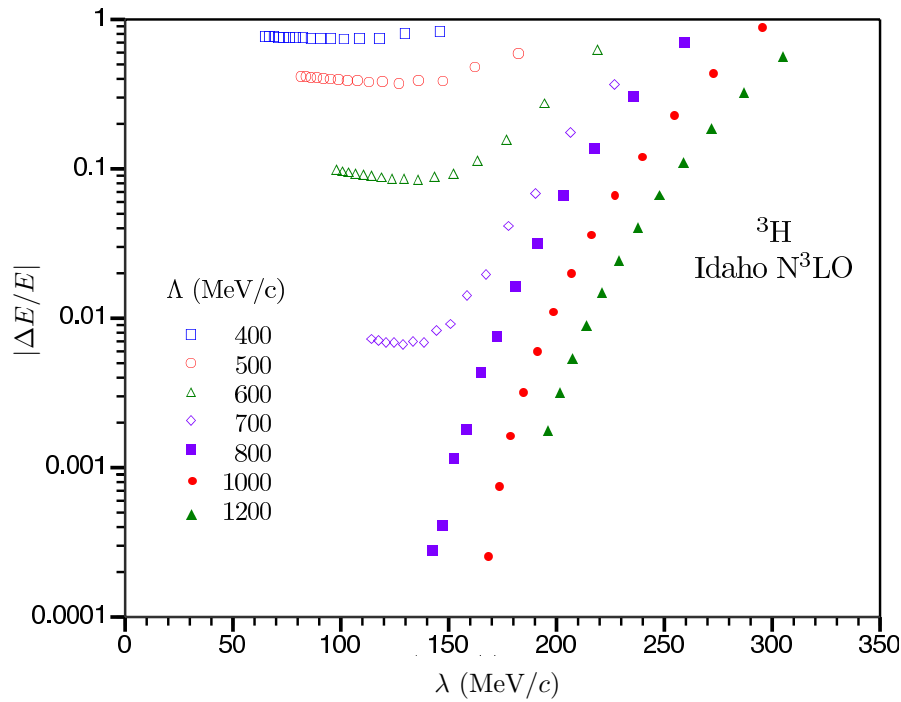


Figure 3: Dependence of the ground-state energy of ${}^3\text{H}$ (compared to a converged value; see text) upon the ir momentum cutoff $\lambda = \sqrt{m_N\hbar\omega}$ for fixed $\Lambda = \sqrt{m_N(N+3/2)\hbar\omega}$.

suppressed term of the form

$$\exp \left[- \left(\frac{p}{\Lambda_{N3LO}} \right)^{2n} - \left(\frac{p'}{\Lambda_{N3LO}} \right)^{2n} \right].$$

In this expression, p and p' denote the magnitude of the initial and final nucleon momenta of this non-local potential in the center-of-mass frame and $n \geq 2$. Because the cutoff is not sharp, it should not be surprising that one has not exhausted the uv physics of this interaction for values of single-particle Λ somewhat greater than 500 MeV/c. Note that this form of the regulator allows momentum transfers ($\vec{p} - \vec{p}'$) to achieve values in the range up to $2\Lambda_{N3LO}$. Can one make an estimate of the uv regulator scale of the Idaho N³LO interaction which is more appropriate to the discrete HO basis of this study? An emulation of this interaction in a harmonic oscillator basis uses $\hbar\omega = 30$ MeV and $N_{max} = N = 20$ [36]. Nucleon-nucleon interactions are defined in the relative coordinates of the two-body system, so one should calculate $\Lambda^{NN} = \sqrt{m(N+3/2)\hbar\omega}$ with the *reduced* mass m rather than the nucleon mass m_N appropriate for the single-particle states of the model space. Taking this factor into account, the successful emulation of the Idaho N³LO interaction in a HO basis suggests that $\Lambda^{NN} \sim 780$ MeV/c, consistent with the figure.

For $\Lambda < \Lambda^{NN}$ there will be missing contributions of size $|(\Lambda - \Lambda^{NN})/\Lambda^{NN}|$, so “plateaus” develop as $\lambda \rightarrow 0$, revealing this missing contribution to $|\Delta E/E|$. We cannot rule out the possibility of a plateau appearing at the level of 0.0001 or less for $\Lambda \geq 800$ MeV/c as $\lambda \rightarrow 0$. This is because the smallest λ available to our calculations is limited by $\lambda = \Lambda/\sqrt{N+3/2}$ and the largest $N = 36$ with our computer resources. That is, the leftmost calculated points of Fig. 3 move to higher values of λ as fixed Λ increases above 800 MeV/c. At fractional differences of 0.001 or less, the development of possible plateaus could be masked by round-off errors in the subtraction of two nearby numbers, each of which may have its own error. Nevertheless, the “plateaus” that we do see are not flat as $\lambda \rightarrow 0$ and, indeed, rise significantly with decreasing $\Lambda < \Lambda^{NN}$. This suggests that corrections are needed to Λ and λ which are presently defined only to leading order in λ/Λ . The authors of [34] take our suggested simile of a truncated basis to a confining region quite seriously and use it to obtain a first order correction to both Λ and λ_{ir} . We hope to learn if higher-order corrections can be directly determined by our data in a future study.

Now we turn to the second pair of cutoffs of (Λ, λ_{ir}) and display in Fig. 4 the analogue of Fig. 2 except that this time $\lambda_{ir} \equiv \lambda_{sc} = \sqrt{m_N \hbar\omega}/(N+3/2)$. For fixed λ_{sc} , $|\Delta E/E|$ does not go to zero with increasing Λ , and indeed even appears to rise for fixed $\lambda_{sc} \geq 35$ MeV/c and $\Lambda \geq 800$ MeV/c. Such a plateau-like behavior was attributed in Fig. 3 to a uv regulator scale characteristic of the NN interaction. Can the behavior of Fig. 4 also be explained by a “missing contributions” argument; i. e. an argument based upon $\lambda_{sc} \leq \lambda_{sc}^{NN}$ where λ_{sc}^{NN} is a second characteristic ir regulator scale implicit in the NN interaction itself? One can envisage such an ir cutoff as related to the lowest energy configuration that the NN potential could be expected to describe. For example, the inverse of the np triplet scattering length of 5.42 fm corresponds to a low-energy cutoff of about 36 MeV/c. The previously mentioned emulation of the Idaho N³LO interaction in a harmonic oscillator basis [36] has $\lambda_{sc}^{NN} \sim 36$ MeV/c. At low Λ and $\lambda_{sc} \leq \lambda_{sc}^{NN}$, $|\Delta E/E|$ does fall with increasing Λ and this behavior can be fitted by a Gaussian as shown for ³H and other s -shell nuclei in [1]. But we will see in the next figure that one has not yet captured the uv region at these low values of Λ .

Fig. 5 is the analogue to Fig. 3: only the variable on the x -axis changes from λ to $\lambda_{sc} = \lambda^2/\Lambda$. For $\Lambda < \Lambda^{NN} \sim 780$ MeV/c the missing contributions and resulting “plateaus” are as evident as in Fig. 3. (Please see discussion of Fig. 3 for an account of possible “plateaus” for larger values of Λ .) The tendency of these plateaus to rise as $\lambda_{sc} \rightarrow 0$ again suggests a refinement is needed to this first-order definition of the

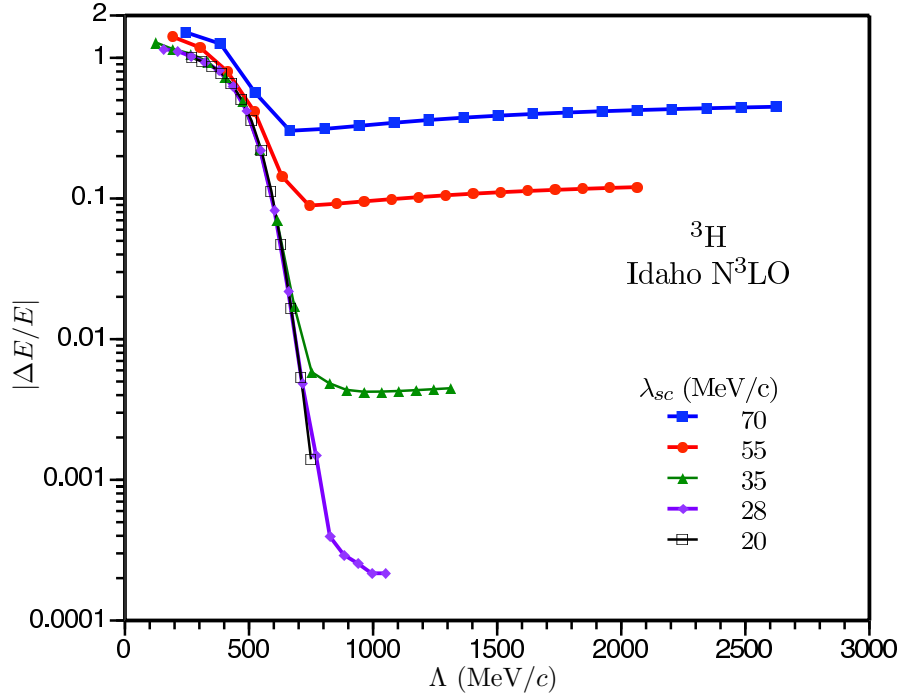


Figure 4: Dependence of the ground-state energy of ${}^3\text{H}$ (compared to a converged value; see text) upon the uv momentum cutoff $\Lambda = \sqrt{m_N(N+3/2)\hbar\omega}$ for different values of the ir momentum cutoff $\lambda_{sc} = \sqrt{(m_N\hbar\omega)/(N+3/2)}$. Curves are not fits but simple point-to-point line segments to guide the eye.

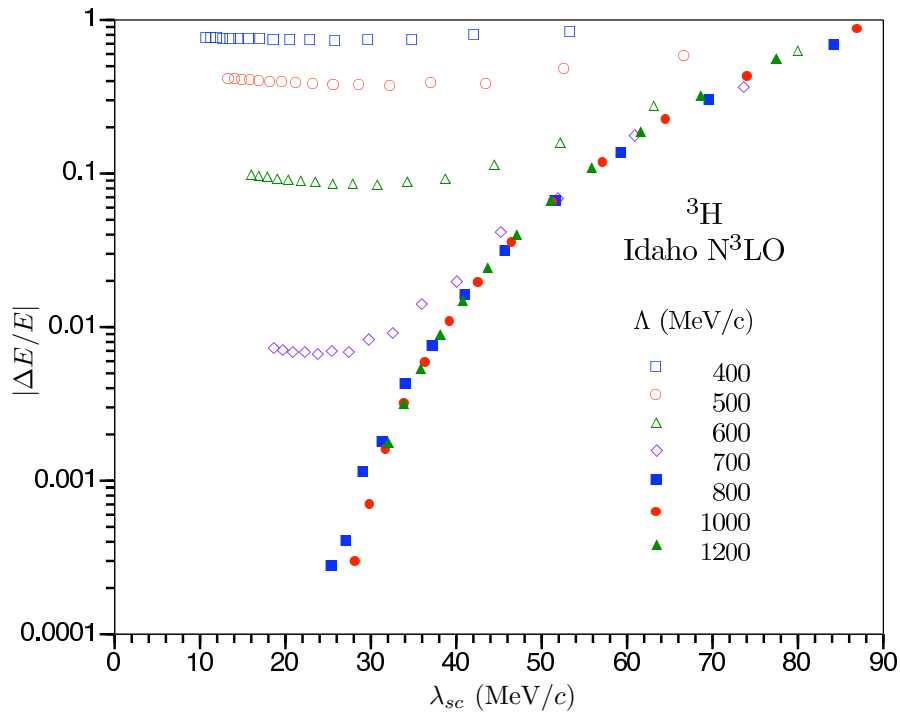


Figure 5: Dependence of the ground-state energy of ${}^3\text{H}$ (compared to a converged value; see text) upon the ir momentum cutoff $\lambda_{sc} = \sqrt{(m_N\hbar\omega)/(N+3/2)}$ for fixed $\Lambda = \sqrt{m_N(N+3/2)\hbar\omega}$.

cutoffs. Around $\Lambda \sim 600$ MeV/c and above the plot of $|\Delta E/E|$ versus λ_{sc} in Fig. 5 begins to suggest a universal pattern, especially at large λ_{sc} . For $\Lambda \sim 800$ MeV/c and above the pattern defines a universal curve for all values of λ_{sc} . This is the region where $\Lambda \geq \Lambda^{NN}$ indicating that nearly all of the ultraviolet physics set by the potential has been captured. Such a universal curve suggests that λ_{sc} could be used for extrapolation to the ir limit, provided that Λ is kept large enough to capture the uv region of the calculation. Fig. 5 is also the motivation for our appellation λ_{sc} , which we read as “lambda scaling”, since this figure exhibits the attractive scaling properties of this regulator.

We now utilize the scaling behavior displayed on Fig. 5 to suggest an extrapolation procedure which we demonstrate in Fig. 6. The extrapolation is performed by a fit of an exponential plus a constant to each set of results at fixed Λ . That is, we fit the ground state energy with three adjustable parameters using the relation $E_{gs}(\lambda_{sc}) = a \exp(-b/\lambda_{sc}) + E_{gs}(\lambda_{sc} = 0)$. The mean and standard deviation of the five values of $E_{gs}(\lambda_{sc} = 0)$ were -7.8511 MeV and 0.0011 MeV, respectively, as suggested by Fig. 7 in which the overlap of the five separate curves cannot be discerned. It should be noted that our five extrapolations in Fig. 7 employ an exponential function whose argument $1/\lambda_{sc} = \sqrt{(N + 3/2)/(m_N \hbar \omega)}$ is proportional to $\sqrt{N/(\hbar \omega)}$. This extrapolation procedure of taking $\lambda_{sc} = \sqrt{m_N \hbar \omega / (N + 3/2)}$ toward the smallest value allowed by computational limitations treats both N and $\hbar \omega$ on an equal basis. The exponential extrapolation in $\sqrt{N/(\hbar \omega)}$ is therefore distinct from the popular extrapolation which employs an exponential in N_{max} ($= N$ for this s -shell case) [7, 8, 9, 20] and provides a refinement to the procedures of the 1970s for dealing with “smooth” potentials.

This extrapolation procedure treats both N and $\hbar \omega$ on an equal basis. For

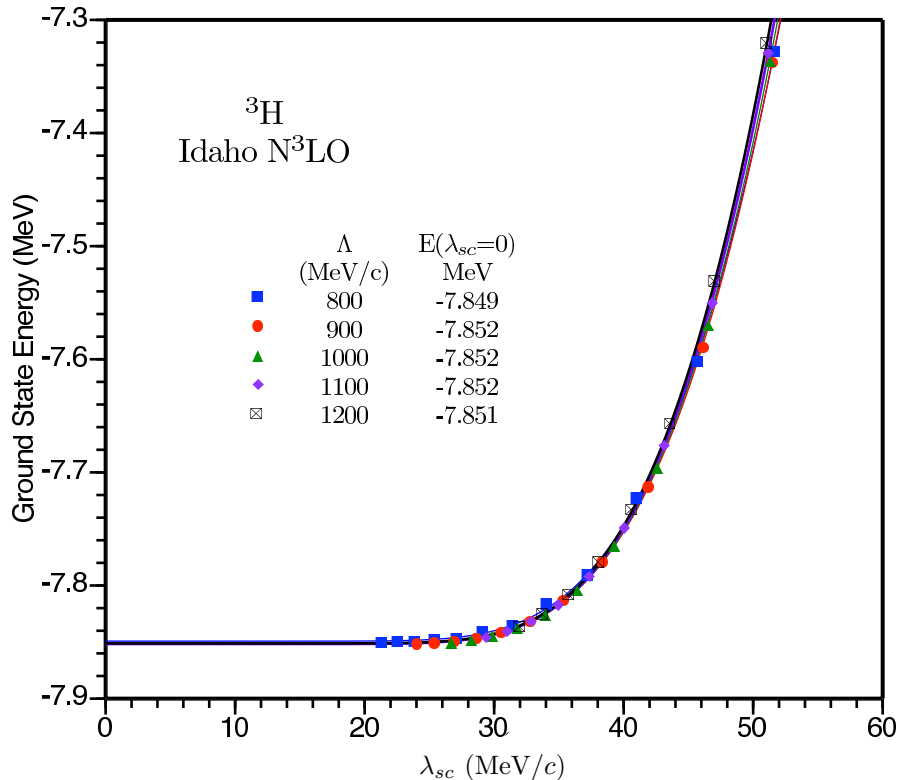


Figure 6: The ground state energy of ${}^3\text{H}$ calculated at five fixed values of $\Lambda = \sqrt{m_N(N + 3/2)\hbar\omega}$ and variable $\lambda_{sc} = \sqrt{(m_N\hbar\omega)/(N + 3/2)}$. The curves are fits to the points and the functions fitted are used to extrapolate to the ir limit $\lambda_{sc} = 0$.

example, the extrapolation at fixed $\Lambda = 1200$ MeV/ c employs values of $\hbar\omega$ from 41 to 65 MeV and $N = 22$ –36. The one at fixed $\Lambda = 800$ MeV/ c employs values of $\hbar\omega$ from 18 to 44 MeV and $N = 14$ –36. The curves of Fig. 6 encompass values of λ_{sc} between 20 and 52 MeV/ c . We attempted to quantify the spread in extrapolated values by fitting only segments of the curves of this figure. Recall that the smallest value of λ_{sc} requires the largest N . Fits to the segment from $\lambda_{sc} = 20$ MeV/ c to $\lambda_{sc} = 40$ MeV/ c (always for the five displayed values of fixed Λ) resulted in a mean of -7.8523 MeV and standard deviation of 0.0008 MeV. Cutting out the left hand parts of the curves and fitting only from $\lambda_{sc} = 30$ MeV/ c to $\lambda_{sc} = 55$ MeV/ c gave a mean of -7.8498 MeV and standard deviation of 0.0022 MeV. For both these trials a rather large N was needed, ranging from 14 to 36 but the extrapolation is quite stable. In contrast, values of λ_{sc} higher than those shown in Fig. 7, namely from $\lambda_{sc} = 50$ MeV/ c to $\lambda_{sc} = 85$ MeV/ c , require fewer computational resources ($N = 8$ –22). The extrapolations have a mean and standard deviation of -7.792 MeV and 0.042 MeV, still not so far away from the accepted value of -7.85 MeV.

Fig. 3 suggests that an extrapolation to the infrared limit could equally well be made by taking $\lambda \rightarrow 0$ for a fixed large Λ . Instead we choose to extrapolate in $\hbar\omega$ with an eye to future exploitation of archival calculations made in the variables $(N_{max}, \hbar\omega)$. In Fig. 7 we fit the ground state energy of ${}^3\text{H}$ with three adjustable parameters using the relation $E_{gs}(\hbar\omega) = a \exp(-c/\hbar\omega) + E_{gs}(\hbar\omega = 0)$ six times, once for each fixed value of Λ . It is readily seen that one can indeed make an ir extrapolation by sending $\hbar\omega \rightarrow 0$ with fixed Λ as first advocated in Ref. [10] and that the five ir extrapolations with $\Lambda > \Lambda^{NN} \sim 780$ MeV/ c are consistent. The spread in the six extrapolated values is about 0.049 MeV or about 1% about the mean of -7.832 MeV. The standard deviation is 0.020 MeV.

Now let us accept the role of the ordered pair (Λ, λ_{ir}) of cutoffs in these variational calculations and examine the ordered pair $(\mathcal{N}, \hbar\omega)$. That is, we take the basis

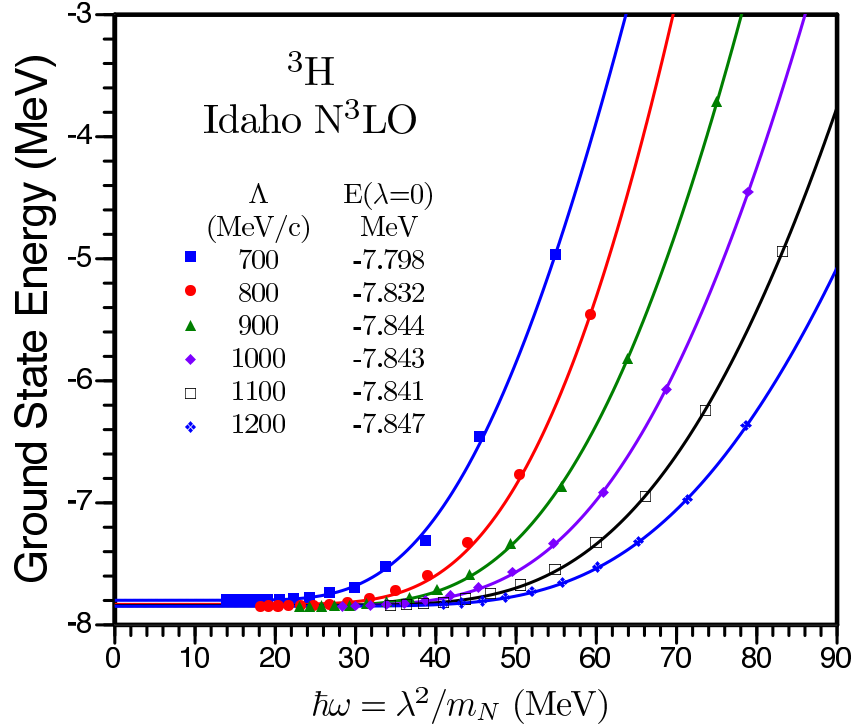


Figure 7: The ground state energy of ${}^3\text{H}$ calculated at six fixed values of $\Lambda = \sqrt{m_N(N + 3/2)\hbar\omega}$. The curves are fits to the points and the functions fitted are used to extrapolate to the ir limit $\lambda = \sqrt{m_N\hbar\omega} = 0$ with fixed Λ as in Fig. 6.

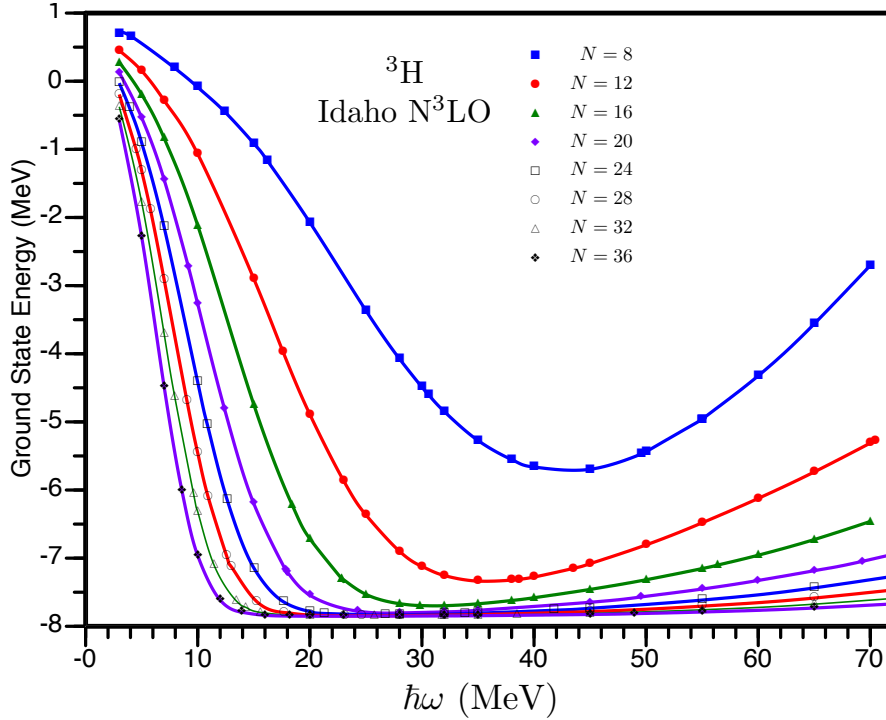


Figure 8: Dependence of the ground-state energy of ${}^3\text{H}$ upon $\hbar\omega = \lambda^2/m_N = \lambda_{sc}^2/[m_N(N + 3/2)]$ for fixed $N = \Lambda^2/\lambda^2 - 3/2 = \Lambda/\lambda_{sc} - 3/2$. Curves are not fits but spline interpolations to guide the eye.

truncation parameter N and the HO energy parameter $\hbar\omega$ to be variational parameters. We now observe convergence as the truncation of the model space is lessened by increasing $N = N_{max}$, where N is the specific truncation parameter N and N_{max} is the total number of energy quanta kept in the basis. Fig. 8 shows a plot of the variational energy of the ground state of ${}^3\text{H}$ plotted in this traditional way, pioneered in Fig. 1 of [2] and continued through [37] to the present day [8, 34]. Optimum values for the parameters that enter linearly can be obtained by solving a matrix eigenvalue problem. But the optimum value of the nonlinear parameter must in principle be obtained by, for example, numerical minimization which could be difficult as the algorithm could easily miss the global minimum and get trapped in a local minima. The plots such as Fig. 8 and others in the nuclear physics literature show that 1) for small bases a change in the non-linear parameter $\hbar\omega$ can have a dramatic change in the variational estimate of the ground state energy and 2) the dependence on the nonlinear parameter decreases as the basis size increases. These observations seem to vitiate the need for an extensive numerical minimization by varying $\hbar\omega$ [38]. For example, in Fig. 8 the minimum of each fixed N curve is easily read off the plot.

From Fig. 8, we see that the variational energy decreases and thus moves away from the converged value -7.85 MeV as $\hbar\omega \rightarrow 0$ at fixed N (for all N considered!). This is readily understood in terms of Fig. 1. At fixed N one captures more infrared physics by lowering the infrared cutoff ($\lambda_{ir} \propto \sqrt{\hbar\omega}$) but misses the ultraviolet physics because lowering $\hbar\omega$ also lowers the ultraviolet cutoff ($\Lambda \propto \sqrt{\hbar\omega}$). The loss of uv physics due to the lower $\hbar\omega$ overwhelms the gain of ir physics and the estimate of the ground state becomes very bad. A similar situation holds as $\hbar\omega$ increases: the uv cutoff increases toward ∞ so that more uv physics is captured but the ir cutoff also rises and more and more of the infrared physics is lost to the calculation.

The approximate minimum of the $N = 8$ curve is at $\hbar\omega \sim 43$ MeV which corresponds to $\Lambda \sim 620$ MeV/ c and $\lambda_{sc} \sim 65$ MeV/ c . From Fig. 5 we realize that for this

small value of $\Lambda < \Lambda^{NN} \sim 780 \text{ MeV}/c$ and large value of $\lambda_{sc} > \lambda_{sc}^{NN} \sim 36 \text{ MeV}/c$, we would expect about a 30% shortfall in the ground state energy and this is what we see in Fig. 8. At the minimum of the $N = 8$ curve the variational parameters are nowhere near their limits in the (Λ, λ_{ir}) regulator picture and the variational energy is not very good. Because $N \propto \Lambda^2/\lambda^2$ or $N \propto \Lambda/\lambda_{sc}$, increasing the truncation parameter N simultaneously increases the uv cutoff and decreases the ir cutoff so that the curves move lower and lower. We observe that, as fixed N increases, the minima of each curve moves to a lower value of $\hbar\omega$, as was previously observed in similar calculations for ${}^4\text{He}$ with this potential [8] and for a variety of nuclei ($A = 2-16$) [8] with another realistic NN potential JISP16 [39]. Maris also observes a monotonic movement to the left with a basis truncation on the single-particle basis so that the truncation parameter \mathcal{N} becomes N_{shell} rather than N_{max} [40]. Apparently another behavior, first a shift to the right and then to the left as fixed N is increased, is noted in [34] and interpreted as first an approach to uv convergence and then, as the uv physics is obtained a further convergence in the ir regulator. We, and other NCSM calculations (including one with a N_{shell} truncation), do not see this behavior.

In Fig. 8, the monotonic movement to a lower $\hbar\omega$ is clear as N increases from 8 to 20, all values corresponding to $\Lambda < \Lambda^{NN} \sim 780 \text{ MeV}/c$, the region in which the uv physics has not yet been captured. As N is increased to $N = 24$ (not yet possible for p -shell nuclei with present day computers and codes) the minimum moves down to $\hbar\omega \sim 24 \text{ MeV}$ which corresponds to $\Lambda \sim 790 \text{ MeV}/c$, $\lambda \sim 150 \text{ MeV}/c$ and $\lambda_{sc} \sim 31 \text{ MeV}/c$. At these values the uv cutoff seems high enough (see Figs. 3 and 5) and the ir cutoff low enough (see Figs. 2 and 4) that one could argue that convergence was nearly reached. As N increases from 24 to 36 the fixed N curves pile up on each other, but an expanded scale (not shown) separates them to demonstrate that the minimum stays near 24 MeV ($\Lambda \sim 920 \text{ MeV}/c$ and $\lambda_{sc} \sim 24 \text{ MeV}/c$) and the curves become somewhat independent of $\hbar\omega$ within a limited range. Even so, any calculation in a finite basis should be examined from the point of view of the more physical regulators (Λ, λ_{ir}) . This calculation should, in principle, always be extrapolated to the uv and ir limits. Independence of $\hbar\omega$ for fixed N is due to a playoff between the uv and ir cutoffs and it should be understood how this playoff affects the calculation. The often heard mantra “look for independence upon the value of $\hbar\omega$ because that means the series of calculations has converged” should be retired, in my opinion.

After submission of [1], Furnstahl, Hagen and Papenbrock posted an investigation of uv and ir cutoffs in finite oscillator spaces [34]. They assume that λ_{sc} (scaled by a factor of $\sqrt{2}$ from the λ_{sc} of this paper) is the ir cutoff. They take our suggested simile of a truncated basis to a confining region quite seriously and use the simile to derive an explicit extrapolation formula in their ir cutoff. The derived formula is the same (exponential in $\sqrt{N/(\hbar\omega)}$) as the one of [1] reviewed here and is used in the same way: establish that the uv cutoff is large enough and then extrapolate in the ir variable. In addition, they suggest a first (higher) order correction to both the uv and ir regulators. The caveat to what they call a “theoretically derived ir formula” is the remark made recently by Lieb *et al.*: “If one fixes the particle number N in a very large box and calculates the shift in energy caused by [a given local one-body potential] V , the answer depends on the box shape and boundary conditions” [41]. But this has always been true [28].

As [34] assumes that (scaled) λ_{sc} is the ir regulator, they took the behavior shown in Fig. 4 for small λ_{sc} to suggest a second extrapolation formula for the uv cutoff. That is, at low Λ and $\lambda_{sc} \leq \lambda_{sc}^{NN}$, $|\Delta E/E|$ falls with increasing Λ and this behavior can be fitted by a Gaussian, as shown for ${}^3\text{H}$ and other s -shell nuclei in [1]. This Gaussian in $\Lambda \propto \sqrt{N(\hbar\omega)}$ then becomes an exponential in $N(\hbar\omega)$. Their final formula assumes relative independence of the uv and ir extrapolations so it is a sum of exponentials with arguments proportional to $N(\hbar\omega)$ from the uv regulator and to $\sqrt{N/(\hbar\omega)}$ from their ir

regulator. These results are a useful advance on the exponential form of convergence in N (with no mention of the role of the scale parameter $\hbar\omega$) shown less concretely by the forty-year-old theorems of [3] and [4]. The authors of [34] caution, as have we, that results such as these should be expected only for the “smooth” potentials of [3] and [4] (or in their momentum space characterization: “super-Gaussian falloff in momentum space”) such as those inspired by chiral EFT or obtained by renormalization group transformations. The extrapolation formulae appear to be successful in calculations of open shell medium to heavy nuclei ($A = 74$) with nuclear interactions inspired by chiral EFT [42].

There has been a recent turn to consider other bases for expanding the trial wave function; bases which have a presumed better behavior at large distances than the HO basis which has a Gaussian falloff [43]. The most effective basis used in few-nucleon physics [44], in nucleon-nucleus scattering [45] and in nuclear reactions [46] are the Coulomb–Sturmians. This is a complete and discrete set of the eigenfunctions of a Sturm–Liouville problem associated with the Coulomb potential [47]. Caprio *et al.* have recently used this basis to make NCSM calculations of light nuclei [48]. They found it beneficial to link the length scale parameter b_l of the Sturmian with the length scale b of the HO eigenfunction so as to provide a closer alignment of the low- n Coulomb–Sturmian basis functions with the harmonic-oscillator basis functions. They choose to *formally* truncate the Coulomb–Sturmian basis with an N_{max} counting number. Thus they end up with the same ordered pair $(\mathcal{N}, \hbar\omega)$ as with the HO basis. However, the $\hbar\omega$ value quoted for the Coulomb–Sturmian basis is simply the $\hbar\omega$ of the reference oscillator length, from which the actual l -dependent length parameters b_l are chosen to align the low- n Coulomb–Sturmian basis functions with the harmonic-oscillator basis functions. It therefore has no direct significance as an energy scale for the problem. Moreover, the N_{max} truncation is difficult to interpret as an “energy cut” as it is for the HO basis. Caprio *et al.* extrapolate to an infinite basis in the following way: the non-linear parameter $\hbar\omega$ is varied to obtain the minimal energy for the highest \mathcal{N} available, $\hbar\omega$ is then fixed at that value and the convergence with \mathcal{N} is assumed to be exponential (extrapolation B of [8]). This is basically the procedure of Delves [3], rooted in theorems of functional analysis, and is not directly related to the EFT inspired cutoffs discussed here. Given that neither \mathcal{N} nor $\hbar\omega$ are given an energy interpretation in this paper, it is problematic that one can simply take over the arguments of [1] or [34] to define new dimensionful uv or ir cutoffs for use in extrapolation. Yet the savings in computation and increase in physical understanding should motivate such an effort in the future.

In summary, we have introduced a practical extrapolation procedure with $\Lambda \rightarrow \infty$ and $\lambda_{ir} \rightarrow 0$ which can be used when the size of the HO basis needed exceeds the capacity of the computer resources as it does for ${}^4\text{He}$ and ${}^6\text{He}$ and certainly will for any more massive nuclei. Unlike other extrapolation procedures the ones advocated in this paper treat the variational parameters \mathcal{N} and $\hbar\omega$ on an equal footing to extract the information available from sequences of calculations with model spaces described by $(\mathcal{N}, \hbar\omega)$. We have established that Λ does not need to be extrapolated to ∞ but if $\Lambda > \Lambda^{NN}$ set by the potential one can make the second extrapolation to zero with either ir cutoff λ_{sc} (see Fig. 6) or λ (see Fig. 7). The choice of the scaling cutoff λ_{sc} is especially attractive as Λ need not be held constant but *any* Λ large enough can be used in the ir extrapolation. The traditional plots in the variables $(\mathcal{N}, \hbar\omega)$ can be understood by considering the uv and ir cutoffs as primary.

Acknowledgements

The study culminating in [1] was conceived and initiated at the National Institute for Nuclear Theory’s program *Effective field theories and the many-body problem* in the spring of 2009. This contribution was written while I was enjoying the stimulating

hospitality of the fall 2012 INT program *Light nuclei from first principles* (INT-PUB-12-052). I am grateful to my collaborators Michael Kruse and Matthew Avetian for the numerical aspects of the study and include them as well as U. van Kolck and James Vary for much effort in the interpretive aspects. I thank Sigurd Kohler for emphasizing to me the importance of the early studies of many-body systems confined to a finite coordinate space volume.

We are grateful to Petr Navrátil for generously allowing us to use his No-Core Shell Model Slater Determinant Code and his *manyeff* code for the calculations cited. The calculations cited were done with allocations of computer time from the UA Research Computing High Performance Computing (HPC) and High Throughput Computing (HTC) at the University of Arizona and from the LLNL institutional Computing Grand Challenge program. Numerical calculations have been performed in part at the LLNL LC facilities supported by LLNL under Contract No. DE-AC52-07NA27344. This contribution was supported in part by USDOE Division of Nuclear Physics grant DE-FG02-04ER41338 (Effective Theories of the Strong Interaction) and NSF award 0854912 (New Directions in Nuclear Structure Theory).

References

- [1] S. A. Coon, M. I. Avetian, M. K. G. Kruse, U. van Kolck, P. Maris and J. P. Vary, *Phys. Rev. C* **86**, 054002 (2012).
- [2] M. Moshinsky, *The harmonic oscillator in modern physics: from atoms to quarks*. Gordon and Breach, New York, 1969.
- [3] I. M. Delves, in *Advances in Nuclear Physics, Vol. 5*, edited by M. Baranger and E. Vogt. Plenum Press, New York, 1972, p. 1.
- [4] T. R. Schneider, *J. Math. Phys.* **12**, 1508 (1971); *Phys. Lett. B* **40**, 439 (1972).
- [5] M. Fabre de la Ripelle, *Ann. Phys. (NY)* **147**, 281 (1983).
- [6] S. Kvaal, *Phys. Rev. B* **80**, 045321 (2009).
- [7] P. Navrátil and E. Caurier, *Phys. Rev. C* **69**, 014311 (2004).
- [8] P. Maris, J. P. Vary and A. M. Shirokov, *Phys. Rev. C* **79**, 014308 (2009).
- [9] P. Navrátil, S. Quaglioni, I. Stetcu and B. R. Barrett, *J. Phys. G* **36**, 083101 (2009).
- [10] I. Stetcu, B. R. Barrett and U. van Kolck, *Phys. Lett. B* **653**, 358 (2007).
- [11] I. Stetcu and J. Rotureau, arXiv:1206.0234 [nucl-th] (2012), to appear in *Progr. Part. Nucl. Phys.*
- [12] V. C. Aguilera-Navarro, M. Moshinsky and W. W. Yeh, *Rev. Mex. Fisica* **12**, 241 (1968); D. A. Agrelo, V. C. Aguilera-Navarro and J. N. Maki, *Rev. Brasileira de Fisica* **11**, 163 (1981).
- [13] A. D. Jackson, A. Lande and P. U. Sauer, *Nuc. Phys. A* **156**, 43 (1970); *Phys. Lett. B* **35**, 365 (1971); M. R. Strayer and P. U. Sauer, *Nucl. Phys. A* **231**, 1 (1974).
- [14] M. K. G. Kruse, J. M. Conroy and H. G. Miller, arXiv:1112.0292 [nucl-th] (2011).

- [15] J. K. R. McDonald, Phys. Rev. **43**, 830 (1933). For recent discussions in the physics literature of this well known result see J. L. Friar, B. F. Gibson and G. L. Payne, Phys. Rev. C **24**, 2279 (1981) and N. C. Bacalis, arXiv:0809.3826 [physics.chem-ph] (2008).
- [16] J. M. Irvine, G. S. Mani, V. F. E. Pucknell, M. Vallieres and F. Yazici, Ann. Phys. (NY) **102**, 129 (1976).
- [17] C. Ciofi degli Atti and S. Simula, Phys. Rev. C **32**, 1090 (1985).
- [18] O. Portilho, J. Phys. G **28**, 2409 (2002).
- [19] S. Okubo, Prog. Theor. Phys. **12**, 603(1954); K. Suzuki and S. Y. Lee, Prog. Theor. Phys. **64**, 2091 (1980).
- [20] E. D. Jurgenson, P. Navrátil and R. J. Furnstahl, Phys. Rev C **83**, 034301 (2011).
- [21] D. R. Entem and R. Machleidt, Phys. Rev C **68**, 041001(R) (2003).
- [22] S. A. Coon and O. Portilho, Lect. Notes Phys. **273**, 219 (1987).
- [23] P. Navrátil, G. P. Kamuntavičius and B. R. Barrett, Phys. Rev. C **61**, 044001 (2000).
- [24] E. Caurier, G. Martinez-Pinedo, F. Nowacki, A. Poves and A. P. Zuker, Rev. Mod. Phys. **77**, 427 (2005).
- [25] J. P. Vary, *The many-fermion-dynamics shell-model code*. Iowa State University, 1992 (unpublished); J. P. Vary and D. C. Zheng, *ibid.*, 1994 (unpublished); P. Maris, M. Sosonkina, J. P. Vary, E. G. Ng and C. Yang, Procedia CS **1**, 97 (2010).
- [26] P. Navrátil, *No-Core Shell Model Slater Determinant Code*, 1995 (unpublished).
- [27] D. H. Gloeckner and R. D. Lawson, Phys. Lett. B **53**, 313 (1974).
- [28] For examples, see N. Fukuda and R. G. Newton, Phys. Rev. **103**, 1558 (1956); B. S. DeWitt, Phys. Rev. **103**, 1565 (1956); P. W. Anderson, Phys. Rev. Lett. **18**, 1087 (1967); M. Luscher, Commun. Math. Phys. **105**, 153 (1986); Nucl. Phys. B **354**, 531 (1991); D. Lee and M. Pine, Eur. Phys. J. A **47**, 41 (2011).
- [29] S. Kreuzer and H.-W. Hammer, Phys. Lett. B **694**, 424 (2011).
- [30] G. Hagen, T. Papenbrock, D. J. Dean and M. Hjorth-Jensen, Phys. Rev. C **82**, 034330 (2010).
- [31] A. Erdélyi, *Higher Transcendental functions, Vol. II*. McGraw-Hill, New York, 1953, p. 199; available online at <http://apps.nrbook.com/bateman/Vol2.pdf>.
- [32] A. Kallio, Phys. Lett. **18**, 51(1965).
- [33] J. P. Vary, *Lectures at DST-SERC school Modern trends in nuclear structure and dynamics, Roorkee, India, February 2012*.
- [34] R. J. Furnstahl, G. Hagen and T. Papenbrock, Phys. Rev. C **86**, 031301(R) (2012).
- [35] A. Kievsky, S. Rosati, M. Viviani, L. E. Marcucci and L. Girlanda, J. Phys. G **35**, 063101 (2008).
- [36] N. Barnea, W. Leidemann and G. Orlandini, Phys. Rev. C **81**, 064001 (2010).

- [37] R. M. Mendez-Moreno, M. Moreno and T. H. Seligman, Nucl. Phys. A **221**, 381 (1974).
- [38] One should be aware that the variational principle guarantees only an extremum which could be a stationary point rather than a minimum. Examples of cases in which the ground state energy does not increase with an increase in \mathcal{N} for a limited range of $\hbar\omega$ are discussed by L. Majling, J. Řízek, Z. Pluhaur and Yu. F. Smirnov, J. Phys. G **2**, 357 (1976). The odd-even effect of Fig. 1 of [2] and of [8] is related and all three articles should serve as a warning against arbitrary assumptions about convergence in \mathcal{N} .
- [39] A. M. Shirokov, J. P. Vary, A. I. Mazur and T. A. Weber, Phys. Lett. B **644**, 33 (2007).
- [40] P. Maris, arXiv:1209.6573 [nucl-th] (2012).
- [41] R. L. Frank, M. Lewin, E. H. Lieb and R. Seiringer, Phys. Rev. Lett. **106**, 150402 (2011).
- [42] V. Somá, *Open-shell nuclei from first principles, Seminar at INT program 12-3 Light nuclei from first principles, October 18, 2012.*
- [43] M. De Sanctis, Electronic J. Theor. Phys. **7**, 137 (2010).
- [44] Z. Papp and S. Moskowski, Mod. Phys. Lett. B **22**, 2201 (2008) and references therein; E. Smith, R. Woodhouse and Z. Papp, arXiv:1209.0529 [nucl-th] (2012).
- [45] K. Amos, L. Canton, G. Pisent, J. P. Svenne and D. van der Knijff, Nucl. Phys. A **728**, 65 (2003); P. Fraser, K. Amos, L. Canton, S. Karataglidis, G. Pisent, J. P. Svenne and D. van der Knijff, Phys. Rev. Lett. **101**, 242501 (2008).
- [46] A. Laid, J. A. Tostevin and R. C. Johnson, Phys. Rev. C **48**, 1307 (1993); F. M. Nunes and A. Deltuva, Phys. Rev. C **84**, 034607 (2011).
- [47] S. Weinberg, in *Lectures on Particles and Field Theory, Brandeis Summer Institute in Theoretical Physics, Vol. 2*. Prentice-Hall, Englewood Cliffs, NJ, 1965, p. 289.
- [48] M. A. Caprio, P. Maris and J. P. Vary, Phys. Rev. C **86**, 034312 (2012).

Overview on the Rare Isotope Science Project in Korea

Y. Kim, B. H. Choi, C. J. Choi, Y. S. Chung, J. E. Han,
I. S. Hong, W. J. Hwang, D. Jeon, J. Joo, H. C. Jung,
B. H. Kang, B. C. Kim, D. G. Kim, G. D. Kim, H. J. Kim,
H. J. Kim, M. J. Kim, S. K. Kim, Y. K. Kim, Y. J. Kim,
Y. K. Kwon, J. H. Lee, S. J. Park, Y. H. Park, C. S. Seo,
H. J. Woo and C. C. Yun

Institute for Basic Science, Daejeon 305-811, Korea

Abstract

In this write-up, we briefly summarize the Rare Isotope Science Project in Korea.

Keywords: *Rare Isotope Science Project; neutron rich rare isotope beams*

1 Introduction

With the goal of creating world-class institute in basic sciences, Institute for Basic Science (IBS) has been launched in November of 2011 [1]. IBS is located in Daejeon, Korea. The core project of IBS is “Research Group Configuration” and “Rare Isotope Accelerator.” IBS will host about fifty research centers and affiliated institutes. The rare isotope accelerator is one of key research facilities to secure innovative successes in basic sciences such as nuclear physics, astrophysics, and atomic physics. The rare isotope accelerator will be designed and constructed under Rare Isotope Science Project (RISP) of IBS. Currently RISP is a project team in IBS. Later, RISP will become an affiliated institute of IBS. The accelerator of RISP/IBS is officially named RAON, previously it was called KoRIA. RAON is a pure Korean word, meaning *delightful*. This name implicates a wish that the rare isotope accelerator of RISP/IBS would be a delightful gift for scientists all over the world and for the bright future of mankind.

In this briefing, we present a bit on the history of RISP, its present status, and its future plans. For more details on RISP, we refer to [2]. Some overviews on rare isotope physics are given in [3, 4, 5].

2 Rare Isotope Science Project

We start with a brief history of RISP and its future plan. RISP of IBS started in December of 2011 to perform technical design of RAON and to construct it. Currently, RISP consists of five divisions: Experimental Systems, Accelerator Systems, Construction, Theory, and Administration. The division of experimental systems consists of three teams: ISOL system, Spectrometer and Detector development, and Application facility teams. The division of accelerator system is composed of three teams: Injector and beam Physics, Superconducting Linac (SCL), In-flight Fragmentation (IF) and RF (Radio Frequency) teams. The theory division contains nuclear physics and particle/astrophysics teams. At the beginning stage, the utmost goals of RISP were to determine main scientific research fields at RISP, to establish the concept of the accelerator, and to review/revise/improve the Conceptual Design report (CDR) of RAON [6] made from March 2010 to February 2011. The Baseline Design

Summary [7], which is an upgraded version of the CDR summary, was completed in June 2012.

Below is the development plan of RISP for RAON:

- The Technical Design Report of RAON will be completed by 2013.
- Main component production will start from 2014.
- Installation will start from 2016.
- Day-1 experiments are expected to be embarked in 2017.

Now we touch a bit on accelerator systems.

RAON is planned as a world class multi-purpose accelerator facility to provide exotic rare isotope beams of various energies. The accelerator complex has three accelerators: two heavy ion linear accelerators (Driver Linac, Post Linac) and one cyclotron. The main heavy ion accelerator, Driver Linac, is designed to accelerate ions from proton to Uranium to be used as the driver for 400 kW in-flight (IF) system and for 400 kW isotope separation on-line (ISOL) system with the proton beam. In addition, it can be used as a post accelerator for isotopes, which will be accelerated up to 250 MeV/u, produced by the ISOL system.

As to rare isotope productions, RAON utilizes the IF system for fragmentation and the ISOL system for target spallation and fission. To produce more exotic rare isotope beams, a unique method, a combination of ISOL and IF systems in which the RI beams generated by the ISOL facility will be accelerated to a higher energy by the in-flight fragmentation Linac, will be also used.

Before we move onto experimental systems, we sketch main research fields and subjects at RISP. A variety of basic and applied science can be studied with RI beams. Especially high intensity RI beams with high purity near the drip lines offer much opportunities to explore every facet of our universe. The research at RISP is categorized into four science fields: Nuclear Science, Atomic and Molecular Science, Material Science, and Medical and Bio Science.

Major scientific research fields at RISP are:

- Nuclear astrophysics and nucleosynthesis;
- Nuclear structure and matter;
- Nuclear data;
- Nuclear theory;
- Precision mass measurements and laser spectroscopy;
- RI material research;
- Medical and Bio applications.

The highest priority research subjects of RISP are:

- Nuclear reaction experiments important to nuclear astrophysics;
- Search for super heavy elements: $Z > 113$;
- Nuclear structure of n -rich RI near $N = 126$;
- Nuclear symmetry energy at sub-saturation density,

and its important scientific applications are:

- Precision mass measurement and Laser spectroscopy;
- Material science: β -NMR, μ SR;
- Medical and bio science;
- Nuclear data for Gen-IV NPP and nuclear waste transmutation.

Now, we have a glance over the experimental systems of RAON.

The Korea Recoil Spectrometer (KRS) is a main facility for nuclear structure, nuclear astrophysics, and super heavy elements search.

The Large Acceptance Multipurpose Spectrometer (LAMPS) is designed to explore the nuclear symmetry energy and equation of state (EOS) of nuclear matter with various neutron-proton asymmetries.

For the super heavy element research, we plan to use two types of separators: gas-filled separator such as FLNR at Dubna and GARIS at RIKEN and vacuum type separator such as SHIP at GSI.

Ion trap and laser spectroscopy are to do precise mass measurements and offer spectroscopic information of rare isotopes.

In addition, the experimental apparatus of RAON includes β -NMR facility, μ SR facility, and neutron Time-of-Flight (n -ToF).

In a nutshell, essential experimental systems for the main scientific research fields could be summarized as:

- Nuclear physics \Rightarrow Large Acceptance Spectrometer;
- Nuclear astrophysics \Rightarrow Korea Recoil Spectrometer (KRS), Gas filled Separator for SHE;
- Atomic physics \Rightarrow Atom and Ion Trap System;
- Nuclear data by fast neutrons \Rightarrow neutron Time-of-Flight (n -ToF);
- Material science \Rightarrow β -NMR/NQR, μ SR, Laser Selective Ionizer;
- Medical and Bio sciences \Rightarrow Heavy Ion Therapy research, Irradiation Facility.

Finally, we show the selected rare isotope beams that are summarized on the Baseline Design Summary in Table 1.

3 Summary

RISP will be establishing rare isotope accelerator, RAON, experimental systems, and the theoretical foundation for basic sciences. The Technical Design Report for the accelerator and experimental apparatus will be published by the end of 2013.

Acknowledgement

This work was supported by the Rare Isotope Science Project funded by the Ministry of Education, Science, and Technology (MEST) and National Research Foundation (NRF) of KOREA.

Table 1: Selected RI beams in the Baseline Design Summary. Here, NS — nuclear structure; NA — nuclear astrophysics; MS — material science; SE — symmetry energy; NSPT — nuclear study with polarized target; NSPRI — nuclear study with polarized RI beam; SHE — super heavy elements; AP — atomic physics; MBS — medical and bio science.

RI beam species	Energy range	Desired intensity [pps]	Research fields
$^{132}\text{Sn}, ^{144}\text{Xe}$	> 100 A MeV	$10^8, 10^6$	NS
^{15}O	< 10 A MeV	10^{10}	NA
^{15}O	< 30 keV	10^8	MS
^{26m}Al	< 15 A MeV	10^7	NA
^{45}V	0.6–2.25 A MeV	10^7 – 10^9	NA
$^{68}\text{Ni}, ^{106}\text{Sn}, ^{132}\text{Sn}, ^{140,142}\text{Xe}$	10–250 A MeV	10^9	SE
$^{6,8}\text{He}, ^{12}\text{Be}, ^{24-30}\text{O}$	50–100 A MeV	10^9	NSPT
$^{17}\text{N}, ^{17}\text{B}, ^{12}\text{B}, ^{14-15}\text{B}, ^{31-32}\text{Al}, ^{34}\text{K}$	50–100 A MeV	10^9	NSPRI
$^{64}\text{Ni}, ^{58}\text{Fe}$ (stable)	a few MeV/A	10^{12}	SHE
$^8\text{Li}, ^{11}\text{Be}, ^{17}\text{Ne}$	< 30 keV	10^8	MS
$^{133-140}\text{Sn}$	< 60 keV	1	AP
$^8\text{B}, ^{9-11}\text{C}, ^{15}\text{O}$	≥ 200 A MeV	10^7 – 10^9	MBS

References

- [1] <http://www.ibs.re.kr/>.
- [2] J.-W. Kim *et al.*, in *Proc. 26th International Linear Accelerator Conference, LINAC12, Tel Aviv, Israel, 9–14 September, 2012*; Y. K. Kwon *et al.*, in *Proc. 20th International IUPAP Conference on Few-Body Problems in Physics (FB20), Fukuoka city, Japan, 20–25 August, 2012*.
- [3] D. F. Geesaman, C. K. Gelbke, R. V. F. Janssens and B. M. Sherrill, *Ann. Rev. Nucl. Part. Sci.* **56**, 53 (2006).
- [4] W. Nazarewicz, *Physics with Rare Isotope beams, an overview*, lecture given at *Exotic Beam Summer School 2011, National Superconducting Cyclotron Laboratory (NSCL), Michigan State University, 25–30 July, 2011*.
- [5] F. M. Nunes and N. J. Upadhyay, arXiv:1209.2691 [nucl-th] (2012).
- [6] *Conceptual Design Report: Korea Rare Isotope Accelerator*, KoRIA Conceptual Design Project, Ministry of Education, Science and Technology, Korea, 2011.
- [7] *Baseline Design Summary*, RISP, IBS 2012.

List of participants

- **Takashi Abe**, University of Tokyo, Japan
tabe@cns.s.u-tokyo.ac.jp
- **Maxim S. Aleshin**, Pacific National University, Russia
aleshin.m.s@gmail.com
- **Leonid D. Blokhintsev**, Moscow State University, Russia
blokh@srd.sinp.msu.ru
- **Corrado Campigotto**, Swiss Federal Office for Informatics and Telekom,
Switzerland
corrado.campigotto@gmail.com
- **Tatjana V. Chuvilskaya**, Moscow State University, Russia
tatchuv@anna19.sinp.msu.ru
- **Sidney A. Coon**, University of Arizona, USA
coon@physics.arizona.edu
- **Tomas Dytrych**, Louisiana State University, USA
tdytrych@phys.lsu.edu
- **Vladimir A. Goy**, Far East Federal University, Russia
vovagoy@gmail.com
- **Konstantin A. Gridnev**, St. Petersburg State University, Russia
kgridnev@yahoo.com
- **Youngman Kim**, Institute for Basic Science, Korea
ykim@apctp.org
- **Vasiliy A. Kulikov**, Moscow State University, Russia
qulikov@gmail.com
- **Alexander I. Mazur**, Pacific National University, Russia
mazur@khhb.ru
- **Evgeniy A. Mazur**, Pacific National University, Russia
Evgeniy.Mazur@mail.khstu.ru
- **Igor A. Mazur**, Pacific National University, Russia
mazuri@mail.ru
- **Andrey M. Shirokov**, Moscow State University, Russia
shirokov@nucl-th.sinp.msu.ru
- **Yurii M. Tchuvil'sky**, Moscow State University, Russia
tchuvl@nucl-th.sinp.msu.ru
- **Yutaka Utsuno**, Japan Atomic Energy Agency, Japan
utsuno.yutaka@jaea.go.jp
- **James P. Vary**, Iowa State University, USA
jvary@iastate.edu
- **Victor Vasilevsky**, Bogolyubov Institute for Theoretical Physics, Ukraine
VSVasilevsky@gmail.com

- **Sergey L. Yakovlev**, St. Petersburg State University, Russia
sl-yakovlev@yandex.ru
- **Sergey A. Zaytsev**, Pacific National University, Russia
zay1962@mail.ru

Contents

J. P. Vary, <i>Preface</i>	3
<u>James P. Vary</u> , <i>Ab initio nuclear structure — recent developments</i>	7
<u>Y. Utsuno</u> , <i>Monte Carlo shell model and its applications to exotic nuclei</i>	26
<u>T. Abe</u> , P. Maris, T. Otsuka, N. Shimizu, Y. Utsuno and J. P. Vary, <i>Application of the Monte Carlo shell model to ab initio no-core calculations</i>	33
<u>V. A. Kulikov</u> , A. M. Shirokov, A. I. Mazur, J. P. Vary and P. Maris, <i>Deuteron-equivalent phase-equivalent transformation and its manifestation in many-body systems</i>	40
<u>T. Dytrych</u> , J. P. Draayer, K. D. Launey and D. Langr, <i>Symmetry-guided ab initio approach to light and medium-mass nuclei</i>	50
<u>L. D. Blokhintsev</u> , <i>Analytic continuation methods in nuclear reaction theory and indirect approaches in nuclear astrophysics</i>	58
<u>V. S. Vasilevsky</u> , F. Arickx, W. Vanroose and J. Broeckhove, <i>On nature of bound and resonance states in ^{12}C</i>	73
S. Yu. Igashov and <u>Yu. M. Tchuvil'sky</u> , <i>Composite-particle interaction</i>	92
<u>K. A. Gridnev</u> , V. N. Tarasov, D. K. Gridnev, D. V. Tarasov, X. Viñas and W. Greiner, <i>Extreme neutron rich sector of the nuclear chart: new horizons!</i> .	105
<u>A. M. Shirokov</u> , <i>Scattering and nuclear structure with oscillator basis</i>	113
P. A. Belov, E. R. Nugumanov and <u>S. L. Yakovlev</u> , <i>Computing binary scattering and breakup in three-body system</i>	121
<u>S. A. Zaytsev</u> and G. Gasaneo, <i>Quasi-Sturmian approach to the three-body continuum Coulomb problem</i>	135
<u>A. I. Mazur</u> , A. M. Shirokov, J. P. Vary, P. Maris and I. A. Mazur, <i>J-matrix analysis of resonant states in the shell model</i>	146
<u>V. A. Goy</u> and A. V. Molochkov, <i>Witten parameter and high performance calculations on the lattice</i>	163
<u>Sidney A. Coon</u> , <i>Infrared and ultraviolet cutoffs in variational calculations with a harmonic oscillator basis</i>	171
<u>Y. Kim</u> , B. H. Choi, C. J. Choi, Y. S. Chung, J. E. Han, I. S. Hong, W. J. Hwang, D. Jeon, J. Joo, H. C. Jung, B. H. Kang, B. C. Kim, D. G. Kim, G. D. Kim, H. J. Kim, H. J. Kim, M. J. Kim, S. K. Kim, Y. K. Kim, Y. J. Kim, Y. K. Kwon, J. H. Lee, S. J. Park, Y. H. Park, C. S. Seo, H. J. Woo and C. C. Yun, <i>Overview on the Rare Isotope Science Project in Korea</i>	189
List of participants	193

**NUCLEAR THEORY
IN THE SUPERCOMPUTING ERA**

International Workshop Proceedings

Khabarovsk
June 18–22, 2012

Printing date: December 02, 2013. Format 70x108 1/16.

Writing paper. “Computer modern” font. Digital printing.

Quire 17.2. Number of copies 70. Order number 320.

Publisher: Pacific National University,
136 Tikhookeanskaya street, Khabarovsk 680035, Russia.